Métabolisme cérébral et olfaction : Étude des réponses olfactives et leur consommation d'énergie dans le bulbe olfactif du rat anesthésié

Jérôme Lecoq

THESE DE DOCTORAT

UNIVERSITE PARIS VI

Spécialité : Neurosciences

École doctorale Cerveau-Cognition-Comportement

Présentée par **Jérôme LECOQ**

Sujet de la thèse :

Métabolisme cérébral et olfaction : Étude des réponses olfactives et leur consommation d'énergie dans le bulbe olfactif du rat anesthésié.

Pour obtenir le grade de

DOCTEUR de l'UNIVERSITE PIERRE ET MARIE CURIE

Sous la direction de **Serge CHARPAK**

Soutenue le 26 septembre 2008

Devant un Jury composé de :

Pr. **Serge CHARPAK** (directeur de thèse)

Pr. **Pierre MAGISTRETTI** (rapporteur)

Pr. **Martin LAURITZEN** (rapporteur)

Pr. **Ann LOHOF** (examinateur)

THESE DE DOCTORAT

UNIVERSITE PARIS VI

Spécialité : Neurosciences

École doctorale Cerveau-Cognition-Comportement

Présentée par **Jérôme LECOQ**

Sujet de la thèse :

Métabolisme cérébral et olfaction : Étude des réponses olfactives et leur consommation d'énergie dans le bulbe olfactif du rat anesthésié.

Pour obtenir le grade de

DOCTEUR de l'UNIVERSITE PIERRE ET MARIE CURIE

Sous la direction de **Serge CHARPAK**

Soutenue le 26 septembre 2008

Devant un Jury composé de :

Pr. **Serge CHARPAK** (directeur de thèse)

Pr. **Pierre MAGISTRETTI** (rapporteur)

Pr. **Martin LAURITZEN** (rapporteur)

Pr. **Ann LOHOF** (examinateur)

Métabolisme cérébral et olfaction : Étude des réponses olfactives et leur consommation d'énergie dans le bulbe olfactif du rat anesthésié

Résumé: Les techniques modernes d'imagerie fonctionnelle du cerveau utilisent le métabolisme cérébral comme marqueur d'activité neuronale. En effet le cerveau dépend intimement des apports sanguins en métabolites pour son fonctionnement. Cependant les mécanismes de régulation du métabolisme sont encore mal connus. Dans cette étude nous avons utilisé le modèle du bulbe olfactif chez le rat anesthésié pour caractériser la consommation d'oxygène en réponse à une stimulation physiologique. La quantification précise de la vascularisation du bulbe olfactif a pu mettre en évidence que la couche glomérulaire, très dense en synapses, est l'une des zones les plus vascularisées du cerveau. Cette couche est aussi le lieu d'une intense consommation d'oxygène lors du traitement de l'information olfactive. Par contraste, la couche du nerf, complètement dénuée d'interactions synaptiques et très peu vascularisée, consomme peu d'oxygène. L'étude pharmacologique de ces réponses métaboliques nous a permis de montrer que le compartiment post-synaptique du glomérule est le siège de cette intense activité métabolique. Cette dernière est aussi dépendante du traitement de l'information olfactive qui est effectué à la fois dans le bulbe olfactif et à la périphérie, dans la cavité nasale. Ceci nous a permis de caractériser l'effet de l'adaptation périphérique sur la consommation d'oxygène et le traitement local de l'information olfactive. Enfin, nous avons décrit en détail l'importance des phénomènes de diffusion au niveau du réseau microvasculaire dans le rééquilibrage transitoire du taux d'oxygène local.

Mots-clés: Olfaction, métabolisme cérébral, couplage neurovasculaire, oxygène, in vivo, deux photon, imagerie, diffusion, microcirculation

Laboratoire: Laboratoire de Neurophysiologie et Nouvelles Microscopies - INSERM U603 - CNRS UMR 8154 - 45 rue des Saints Pères - 75006 Paris - France

Brain metabolism and olfaction : a study on olfactory responses and their energy usage in the olfactory bulb of anesthetized rats.

Abstract: The relationship between metabolism of neuronal activity, microvascular organization and blood flow dynamics is critical for interpreting functional brain imaging. Here we used the rat dorsal olfactory bulb as a model to determine *in vivo* the correlation between action potential propagation, synaptic transmission, oxygen consumption and capillary density during odor stimulation. We find that capillaries are extremely dense in layers of intense synaptic interactions like the glomerular layer while it is very low in the overlying nerve layer, devoid of capillaries. In glomeruli, odor triggers a local early decrease in tissue oxygen partial pressure that results principally from dendritic activation rather than from firing of axon terminals, transmitter release or astrocyte activation. In the nerve layer, action potential propagation does not generate local changes in tissue oxygen partial pressure. We also show that under strong peripheral stimulation, i.e. high odor concentration, glomerular neuronal and metabolic responses are shaped by peripheral adaptation of olfactory sensory neurons. Eventually, we show the importance of oxygen diffusion processes from brain capillaries to neuronal tissue. We characterize how transient changes in blood flow are precisely influencing the oxygen tissue level.

Keywords: Olfaction, brain metabolism, neurovascular coupling, oxygen, in vivo, two photon, imaging, diffusion, microcirculation

Laboratory: Neurophysiology and New Microscopies Laboratory - INSERM U603 - CNRS UMR 8154 - 45 rue des Saints Pères - 75006 Paris - France

Résumé détaillé

Nos connaissances des mécanismes au cœur du métabolisme cérébral sont encore incomplètes. Nous avons dans cette étude tiré profit des particularités du bulbe olfactif afin d'étudier la consommation d'oxygène des différents compartiments neuronaux. En effet, les deux premières couches du bulbe, la couche glomérulaire et la couche du nerf sont remarquablement distinctes. La première est extrêmement dense en synapses alors que la seconde en est complètement dénuée. En utilisant un algorithme de reconstruction tridimensionnel à partir des données d'imagerie obtenues en microscopie biphotonique, nous avons pu quantifier de manière très précise la vascularisation des deux couches. La densité des capillaires dans la couche glomérulaire s'élève à 1056 mm/mm^3 alors que dans la couche du nerf, elle est plus de 10 fois inférieure (45 mm/mm^3). Nous avons pu comparer ces valeurs avec la densité des capillaires dans d'autres régions du cerveau et la couche glomérulaire s'est révélée être une des zones les plus élevées jamais mesurées dans le cerveau.

En couplant la microscopie biphotonique avec des enregistrements electrophysiologiques et polarographiques, nous avons mesuré, de manière simultanée, le flux sanguin, le taux d'oxygène et l'activité neuronale. Nous avons effectué ces enregistrements en réponse à une stimulation olfactive à la fois dans la couche glomérulaire et dans la couche du nerf chez le rat anesthésié. Dans la couche glomérulaire, ces mesures ont démontré que l'activation neuronale d'un glomérule par une odeur induit une décroissance très rapide du taux d'oxygène local (en moins de 200ms). Cette décroissance est suivie d'une augmentation du flux sanguin environ une seconde plus tard qui se traduit par un rééquilibrage du taux d'oxygène. Des mesures dans la couche du nerf ont révélé que cette dernière présente aussi une chute d'oxygène locale. Cependant cette chute est retardée et résulte de phénomènes de diffusion à partir de la couche glomérulaire. Nous en avons conclu que la couche du nerf, où seuls des potentiels d'actions se propagent, ne dépend pas d'une production d'énergie aérobie pour rééquilibrer la quantité d'ATP consommée pendant une stimulation olfactive.

L'injection local d'antagonistes aux récepteurs au glutamate a mis en évidence que le compartiment post-synaptique du glomérule est responsable de la majorité du signal de consommation.

Au cours de cette thèse, nous avons aussi pu caractériser l'effet d'un mécanisme d'adaptation périphérique sur le codage de l'information olfactive dans le bulbe. Nous avons tout d'abord mis en place des enregistrements simultanés des compartiments pré-synaptiques (imagerie calcique des terminaisons axonales) et post-synaptiques (mesure de potentiel de champ) glomérulaires. Nous avons ensuite observé qu'à de très fortes concentrations, les odeurs modifient

les cartes d'activation glomérulaire en entraînant des diminutions sensibles des réponses des glomérules spécifiques. Ce phénomène d'adaptation glomérulaire résulte d'une diminution du glutamate libéré par les afférences. Cette diminution est secondaire non pas d'un phénomène d'inhibition présynaptique mais plutôt d'une adaptation périphérique des récepteurs sensoriels indiquant que ce phénomène joue un rôle essentiel dans le codage des fortes concentrations d'odeur.

Enfin, nous avons tiré profit des fluctuations spontanées du flux des capillaires cérébraux pour étudier les phénomènes de diffusion à l'échelle micrométrique. Le taux d'oxygène tissulaire s'est révélé extrêmement corrélé avec le flux sanguin du capillaire le plus proche. Les phénomènes de diffusion se traduisent par l'existence d'un délai entre ces deux signaux qui peut être extrait en utilisant des algorithmes de cross-corrélation. L'étude de l'évolution de ces délais avec la distance au centre des capillaires a mis en évidence, comme attendu, qu'ils augmentent avec la distance. Cependant, leur valeur absolue est beaucoup plus élevée dans les cas où le taux d'oxygène tissulaire basal est faible. Ces résultats suggèrent l'existence d'un tampon de l'oxygène dans le tissu neuronal.

Table of Contents

"*A fact is a simple statement that everyone believes. It is innocent, unless found guilty. A hypothesis is a novel suggestion that no one wants to believe. It is guilty, until found effective*."

Edward Teller

Forewords & Acknowledgments

Doing a PhD has been quite an adventure. As my studies moved from physic to experimental biology, this proved to be particularly adventurous to me. I painfully discovered the underlying meaning of the letter N which I hadn't appropriately considered while I was doing my engineer degree. In physic, a single and well-design experiment is enough to justify using the letter O for Obvious.

I also discovered that *in vivo* experiments can't be stopped whenever you want which had a significant effect on my evening time. I am especially grateful to Jacqueline Hicks who also discovered this particular aspect of my thesis and supported me in every possible way. She also went through this thesis manuscript in details to correct my English and I am particularly thankful for this.

Overall, during these four years, I have learned a lot both about science and myself. Applying what I had learned during the previous years to try to actually create new knowledge was a very exciting and rewarding task.

I wish to thank all the members of the laboratory. They have had to handle my ups and downs throughout these years. Lunch times were always one of the best times of the day and I hope it will always be. Elena Avignone deserves a special note regarding the numerous ice creams we shared.

Pascale, with whom I extensively worked during this thesis, also had to cope with my alternating moods during the course of our experiments. I wish to thank her for her patience.

I am wholeheartedly thankful to Serge Charpak who directed this thesis and helped me discover the beauty of the brain and its metabolism.

I thank Pierre Magistretti and Martin Lauritzen who have given me the true honor of coming to Paris to be reporters of my thesis. Many thanks to Ann Lohof for accepting at the last minute to be part of this thesis examining board.

Bénédicte Rossi gave me the courage to work on this manuscript during a very sunny summer and has even postponed her holidays for me. I can just hope to be as supportive during her own thesis defense.

Eventually, I want to thank Boulinier, the local bookstore, for staying open so late at night.

Chapter 1 : Forewords & Acknowledgments

Introduction

Here, I will review some of the knowledge involved in this study. As I had to deal with numerous fields during my thesis (Namely olfaction in the olfactory bulb and epithelium, brain imaging, neurovascular coupling, brain metabolism and oxygen diffusion), I have decided to give an outline which focuses on the notions required to understand this manuscript. Once in a while, you'll see references to some good reviews which I recommend if you want to look into more details at a specific subject.

Chapter 2 : Introduction

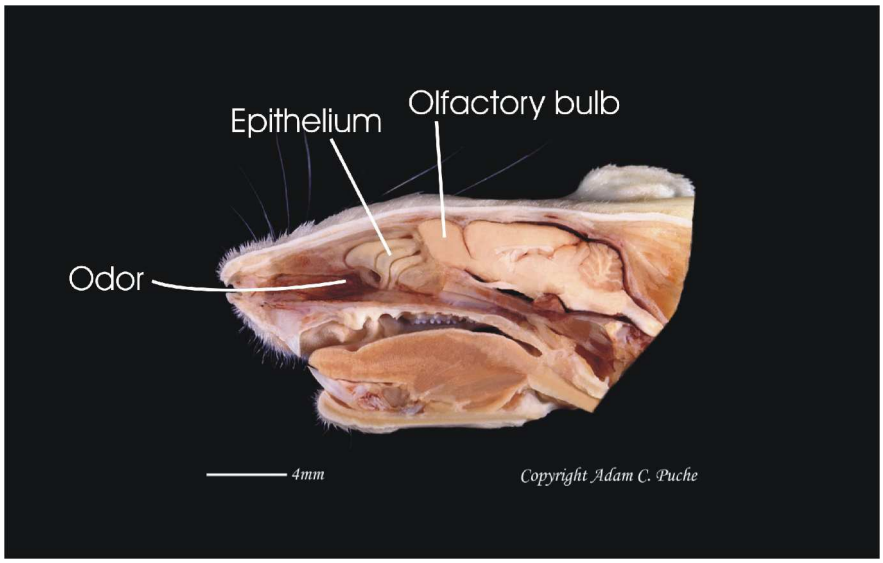

Illustration 1: Medial view of a dissection of an adult rat head showing the olfactory epithelium and bulb in situ. Photograph by Adam C. Puche

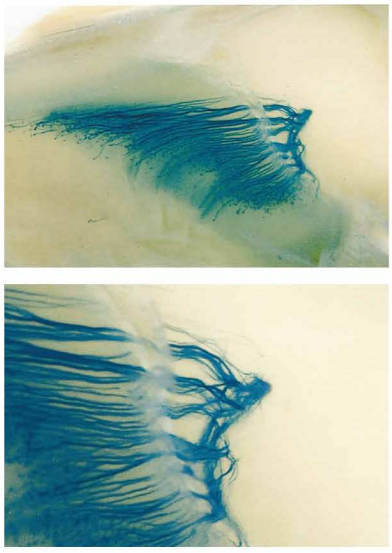

Illustration 2: ORNs expressing a given receptor type project their axons to a pair of glomeruli : an X-gal-stained view of the nasal septum and bulb of a transgenic mouse expressing tau-LacZ together with the P2 receptor. (Mombaerts and coll, 1996)

2.1 Odor's transduction and its underlying neuronal circuit

Although the human sense of smell is limited compared to other mammals, we can still distinguish a wide variety of odors. The mechanism responsible for odor perception first relies on the consecutive action of the two structures which are shown in Illustration 1. In the olfactory system, the sensory cells responsible for the conversion of an odor into electrical activity are located in the olfactory epithelium in the back of the nasal cavity (see Illustration 1). The axons of those olfactory sensory neurons cross a small plate of bone called the cribriform plate. Then they reach the first relay of olfactory information in the olfactory bulb.

It was found that approximately 1000 different receptors are expressed in the olfactory epithelium of the rat. This constitutes an extremely large family of genes, which were discovered in 1991 (Buck and Axel 1991).

Interestingly, those receptors are expressed in quite large and overlapping zones in the olfactory epithelium (Ressler, Sullivan, and Buck 1993). Furthermore, a given olfactory sensory neuron expresses a unique receptor (Malnic et al. 1999).

The olfactory bulb receives the input from the olfactory sensory neurons in spherical like structures called glomeruli (see Illustration 6). The projections of these olfactory sensory neurons are remarkably organized. In fact using transgenic mice, Mombaerts et al. were able to show that olfactory sensory neurons expressing a given receptor send their axons towards only two precise locations in the olfactory bulb (see Illustration 2) (Mombaerts et al. 1996). Therefore, for each bulb, the two glomeruli receive the input from a unique type of receptor and are always situated in a similar location for animals of the same species (Schaefer, Finger, and Restrepo 2001; Nagao et al. 2002). Using this, it is hence possible to record maps of activated glomeruli for each odor.

2.1.1 Odor transduction in the epithelium

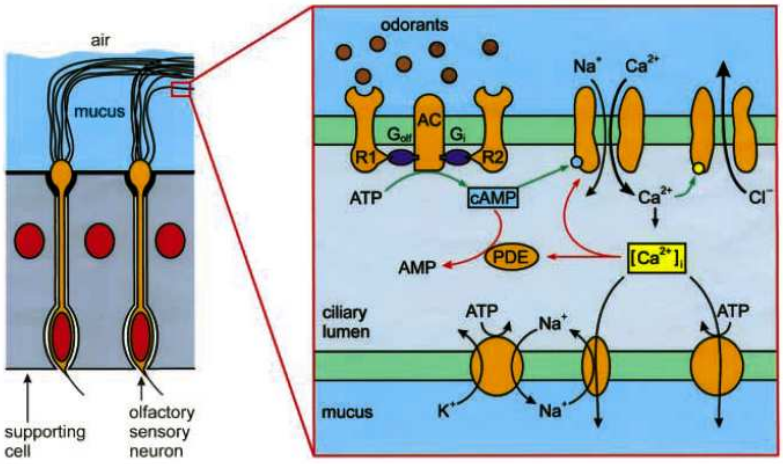

Illustration 3: (Left) Position of olfactory sensory neurons and epithelial supporting cells in the olfactory neuroepithelium. (Right) Schematic representation of the cAMP mediated transduction pathway operating in the sensory cilia. Generation of the receptor current is indicated by green arrows, termination by red arrows. AC, adenylyl cyclase; Golf/Gi, GTP-binding proteins; PDE, phosphodiesterase; R1/R2, odorant receptor proteins. (Frings 2001)

Since David Ottoson elegantly recorded olfactory responses in the frog epithelium (Ottoson 1955), much insight has been gained into the molecular basis of odor detection in the olfactory sensory neurons (for a good review see (S. Frings 2001)). A schematic representation of those pathways is presented in the Illustration 3. The main mechanism of odor transduction relies on the activation of the adenylyl cyclase and the subsequent increase in intracellular Adenosine 3,5-

cyclic monophosphate (cAMP). Odorants bind with membrane receptor R1 and activate adenylyl cyclase through a GTP-binding protein called Golf. Adenylyl cyclase then synthesizes cAMP from ATP. The increase in intracellular cAMP causes the activation of a cyclic nucleotide-gated channel (CNG) permeable to both Ca^{2+} and Na^{+}. They are also slightly less permeable to K+. This process initiates the depolarization of the cell which is further enhanced by Ca^{2+} activated Cl^{-} channels. Since Cl^{-} concentration in the mucus is lower than in olfactory sensory neurons cytosol, activation of ciliary Cl^{-} channels causes a depolarizing inward current (Reuter et al. 1998). All together, these cationic and anionic currents generate a depolarization that spreads from the cilia to the cell body, triggering action potentials.

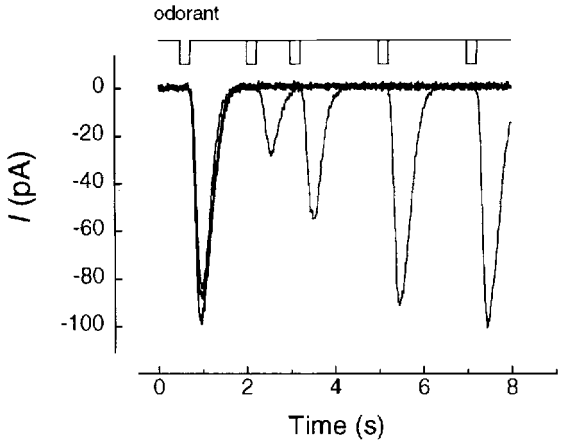

Illustration 4: Currents evoked in a solitary olfactory receptor cell hold at -50mV by brief repeated odorant stimulation. Pulses of amyl acetate were applied at different intervals (1.5, 2.5, 4.5 and 6.5 s) (Kurahashi and Menini, 1997).

2.1.2 Odor adaptation

Several mechanisms can bring about the termination of the response. A decrease in extracellular odorants can naturally stop the response as it reduces the rate of the initial activation of adenylyl cyclase.

Nevertheless, as early as 1955, Ottoson (Ottoson 1955) described an adaptation of odor responses during sustained activation. Later research used recordings from sensory neurons to show a marked reduction in the odor invoked currents during repeated stimulation (see Illustration 4, (Kurahashi and Menini 1997)).

Single unit recordings in the olfactory epithelium *in vivo* showed that this adaptation process has an effect on the output (see Illustration 5) of olfactory sensory neurons (Duchamp-Viret, Chaput, and Duchamp 1999; Duchamp-Viret, Duchamp, and Chaput 2000). The potential pathway involved in the adaptation is still a matter for debate. Three possible mechanisms have been proposed. Each of these identifies a different location in the cascade of odor transduction events for the occurrence of adaptation. They are depicted in the Illustration 3 with red arrows.

- Opening of the CNG leads to high intracellular calcium concentration

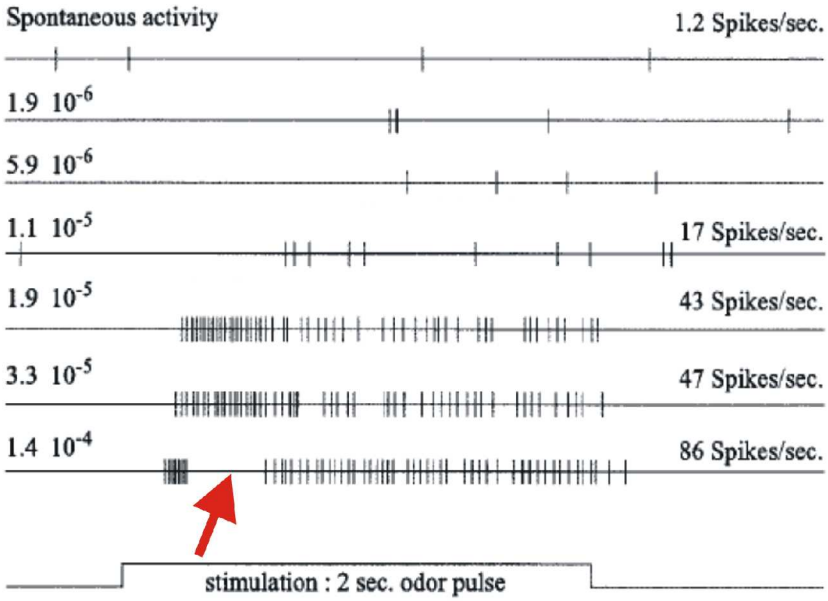

Illustration 5: Spontaneous and odor-evoked single-unit responses of olfactory sensory neurons in the rat in vivo to increasing concentrations of limonene (expressed in mol/liter). Note the adaptation triggered at higher frequencies (red arrow) (Duchamp-Viret, Chaput and Duchamp, 1999).

which was shown to be a possible basis for adaptation (Kurahashi and Menini 1997). The calcium binds to calmodulin onto CNG channels, reducing its cAMP sensitivity. Bradley et al. (Bradley et al. 2004) showed that, even in the absence of calcium, calmodulin is bound to the CNG channel but is inactive. When Ca^{2+} concentration rises in the cell, it binds to Calmodulin. The combined effect of Ca^{2+}/Calmodulin reduces the cAMP sensitivity of the CNG channel.

- The rat olfactory sensory neurons are highly enriched in phosphodiesterase (PDE) (Yan et al. 1995). Similarly to the CNG channels, those PDEs are Ca^{2+}/Calmodulin sensitive. The increase in intracellular calcium promotes the hydrolysis of cAMP by the PDE which terminate the odor response.

- Some other studies have also showed that an increase in calcium triggers the phosphorylation of the adenylyl cyclase directly, again through calmodulin (J Wei et al. 1998). This directly reduces the cAMP production as there is a lower concentration of active adenylyl cyclase.

2.1.3 Olfactory bulb circuitry

As a model for brain metabolism, the olfactory bulb is a very valuable structure due to some particular features it possesses. Firstly, part of the olfactory

bulb is dorsal and therefore accessible for in vivo two photon imaging. Secondly, as previously mentioned, it receives its inputs directly from the olfactory epithelium, without any thalamic relay.

The laminar organization is also advantageous in addressing the relative contribution of the pre and postsynaptic processes to various responses (see Illustration 6).

Here, we will give a brief overview of the different cell types involved in the olfactory bulb. For a more detailed description of them, see (G. M. Shepherd 2003).

The Olfactory Nerve Layer (ONL) contains mainly the axons from the epithelium along with a particular type of glial cell, specific to the olfactory bulb, named olfactory ensheating cells. The Glomerular Layer (GL) contains the axon terminals from the olfactory sensory neurons, the apical dendrites of the principal cells of the olfactory bulb, the Mitral Cells (MC), the Tufted Cells (TC), and some local interneurons. These interneurons make up a local network made of PeriGlomerular Cells (PGCs which are GABAergic) and Short Axons cells (SA which are glutamatergic). These are subclasses of the JuxtaGlomerular Cells. Glomeruli can therefore be interconnected either through the axons of SAs or through PGCs.

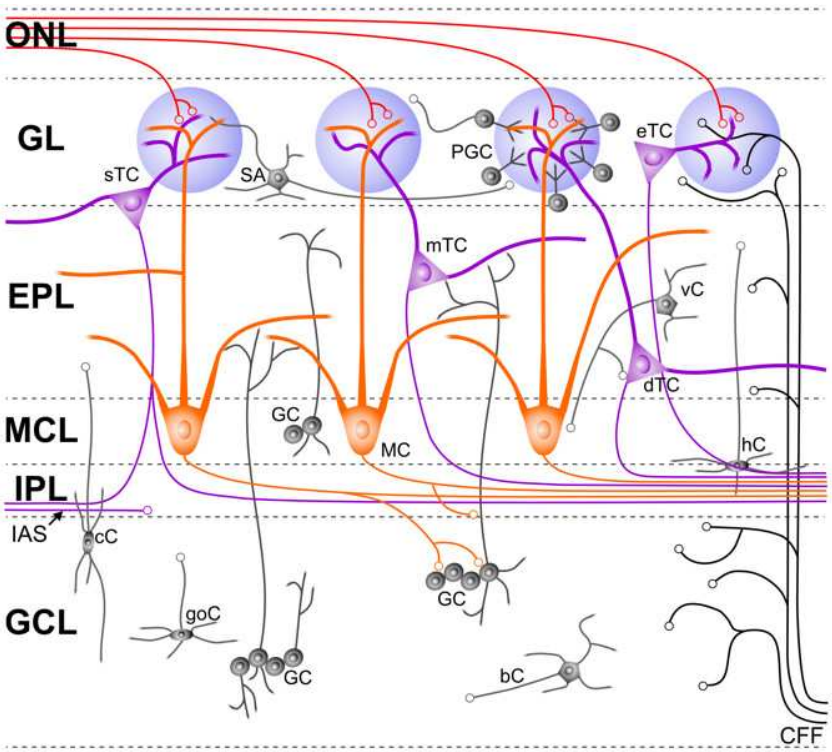

Illustration 6: Circuit diagram showing all major and minor cell types present in the main olfactory bulb. Drawing by Adam C. Puche

Deeper in the bulb is the External Plexiform Layer (EPL), made of the secondary dendrites from the MCs and the cell bodies of the TCs. The Mitral Cell Layer (MCL) is at the limit of two-photon imaging capabilities, just above the Internal Plexiform Layer (IPL) made of the axons from the MCs and the TCs to the olfactory cortex and above the Granule Cell Layer (GCL) where the small granule cells are located.

Interestingly, the glomerulus as a function module is peculiar in regards to its very high convergence. Approximately 11 000 sensory axons converge on one glomerulus and make contact with about 50 mitral cells and tufted cells and 1000 periglomerulars cells (G. M. Shepherd 2003).

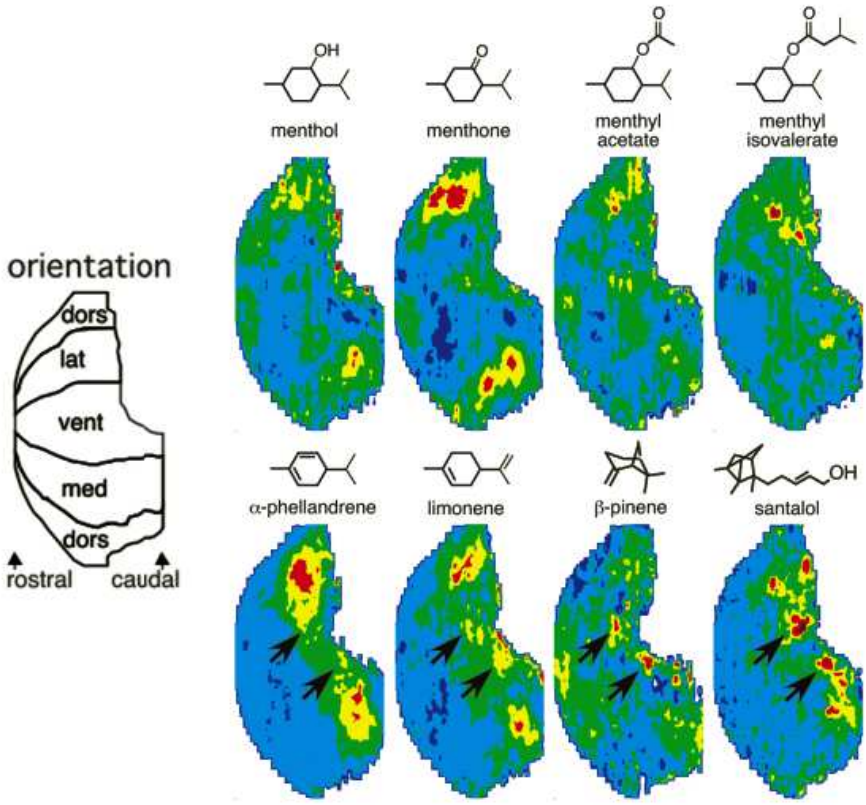

Illustration 7: Glomerular activity pattern extracted from 2DG uptake in response to various odorants. Arrows indicate ventral activated regions. The bulb is opened dorsally and rolled out as on the left figure (Johnson et al., 2002).

2.1.4 Odor maps

This high convergence ratio together with the specificity of glomeruli to a

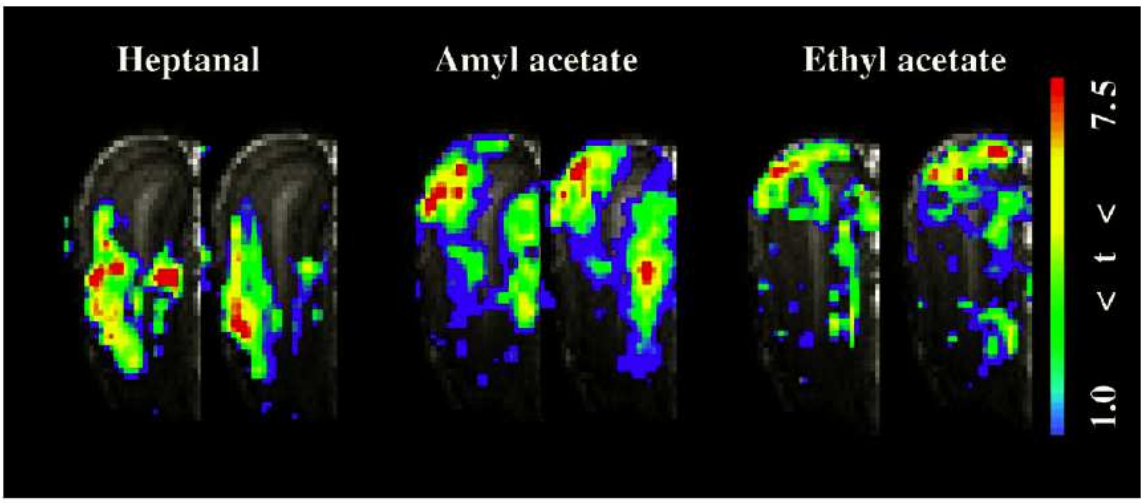

Illustration 8: BOLD signal allow to study the increase in blood supply in relation to odor maps in rat olfactory bulb. Different colors indicate different values of student t-test. (Schafer and coll, 2006)

receptor indicates that the pattern of odorant-evoked activation in the Glomerular Layer is reflecting the activation of odor receptors in the nose. This was confirmed by numerous studies using a variety of techniques.

- Odor stimulation triggers a transient increase in gene expression in activated regions which can be mapped ex vivo. Several studies have looked at the increase in the expression level of transcription factors like c-Jun (Baba et al. 1997) or c-Fos (Guthrie et al. 1993). While their stimulation protocol consisted of a long exposure to odor (≈5 to 30 min), they showed a marked increase both in the periglomerulars cells of activated glomeruli and in cells from deeper layers. They also observed a marked difference between odors in the Glomerular Layer staining. Interestingly, this staining was sparser in the Glomerular Layer compared to the mitral cell layer and the granule cell layer. This is in agreement with the idea that deeper network are more widely activated in response to odor.

- As we will see later (see chapter 2.2.2), increased neuronal activity induces an increase in glucose consumption which can be revealed through radioactive 2-DG. This was first used by Shepherd and Greer to compare the consumption of the different neuronal layers (C. A. Greer et al. 1981; F. R. Sharp, J. S. Kauer, and G. M. Shepherd 1975) and then by Leon and Johnson in a large number of publications where they looked at the effect of changing the odorant molecular features on the odor maps (B. A. Johnson et al. 2002; B. A. Johnson, Woo, and M. Leon 1998; C. Linster et al. 2002; Cleland et al. 2007). They eventually created a database of those maps which they made freely available on the web called the **Glomerular Activity Response Archive** (http://leonserver.bio.uci.edu/). They showed

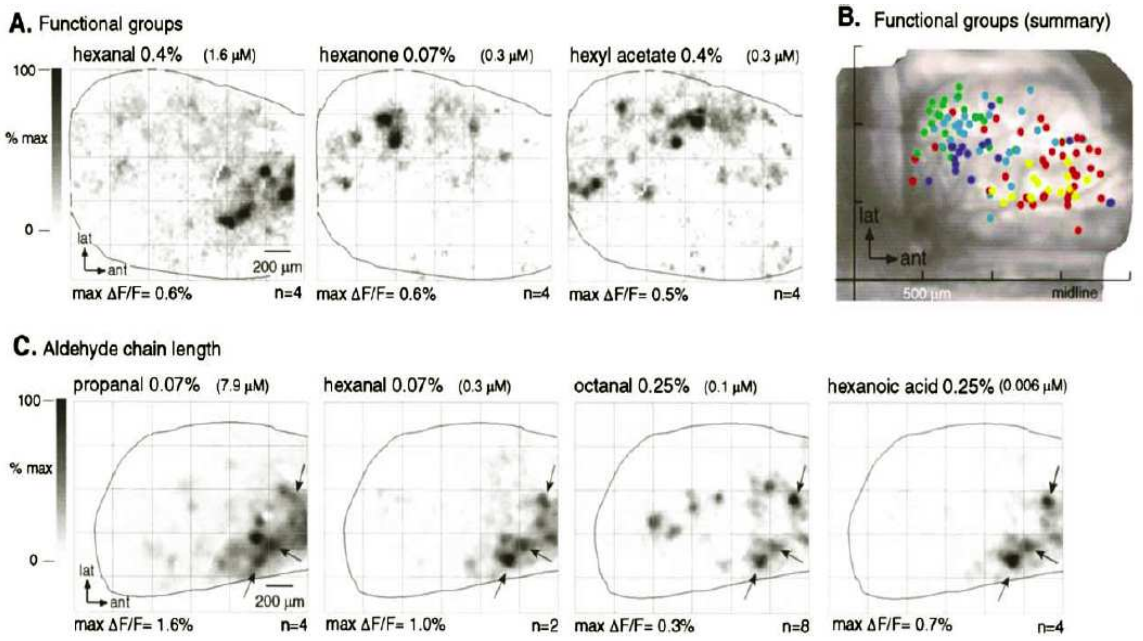

Illustration 9: Effect of varying odorant features on odor maps recorded through in vivo calcium imaging in the mice (Wachowiak and Cohen 2001)

that molecular features like carbon chain length and chemical functions were key parameters in the shape of odors maps as shown on Illustration 7 (B. A. Johnson, Woo, and M. Leon 1998). To date, they have tested 365 odorants and released more than 500 maps. However, it is important to note that this technique has important drawbacks. It requires long odor exposure time (they routinely use 45 min) and it cannot be used to map several odorants in the same animal.

- fMRI offers a very attractive tool to take a non-invasive look at the brain because it can monitor the change in the BOLD directly in the different layers of the olfactory bulb (see chapter 2.4.5) (Yang et al. 1998). The best spatial resolution achieved today is a voxel size of 110x110x250 μm^3 which still requires repeated odor exposures at 2 minutes intervals in order to improve the signal to noise ratio (Kida et al. 2002). A recent study (C. Martin et al. 2007) has used odor stimulation of 5 seconds with a larger voxel (twice as large). The responses were averaged over 15 trials. While the volume of these voxels is slightly larger than the volume of a glomerulus, it is now possible to look at odor maps in response to several odorants. Illustration 8 shows an example of those blood flow maps and their relation to different odors (Schafer et al. 2006). Using this technique, Kida et al. showed a great variability in the activation pattern between subjects for the same odor. They couldn't conclude whether it was due to variation in neuronal activity or to other factors like vessel anatomy.

- Fluorescence *In vivo* imaging of the olfactory bulb was made possible

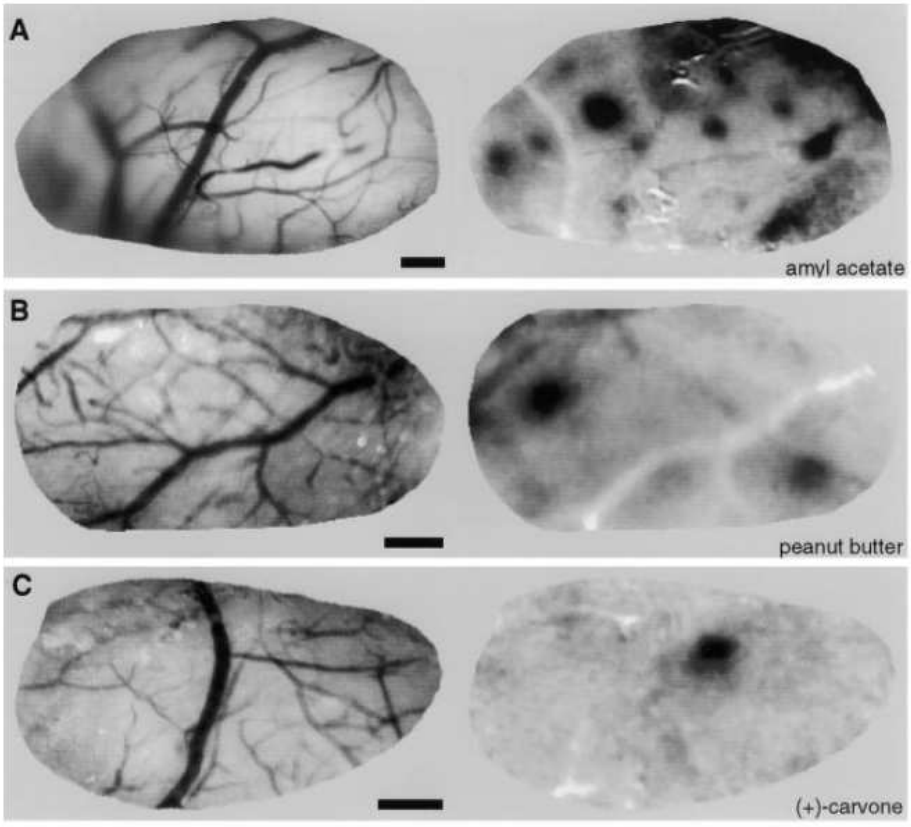

Illustration 10: Optical imaging of Intrinsic signals in response to odorants in the rat olfactory bulb (Rubin and Katz 1999)

thanks to the invention of a new loading protocol by Friedrich et al. (Friedrich and Korsching 1997). It consisted of simply injecting the dye directly in the nasal cavity of the zebrafish. They were then able to image glomeruli with a very good spatial and time resolution. This technique was first transferred to the mouse (Matt Wachowiak and L. B. Cohen 2001) and then to the rat (Verhagen et al. 2007) by Wachowiak et al.. While they only recorded dorsally for obvious technical reasons, they were able to show responses at very low concentration and confirmed that different odorants activate different sets of glomeruli (see Illustration 9). They also showed that each glomerulus responds to a large variety of odors which depends on the affinity of its receptor to the odorant molecule.

- Intrinsic imaging was first used in the visual system and in the barrels to record activity without the use of any dyes (Grinvald et al. 1986), see chapter 2.4.2 for a more detailed description. Later on, this technology was transferred to the olfactory bulb to show, for the first time, odor maps recorded directly *in vivo* (Rubin and Katz 1999). This pioneering work showed similar results to the 2DG uptake method, namely odor maps which

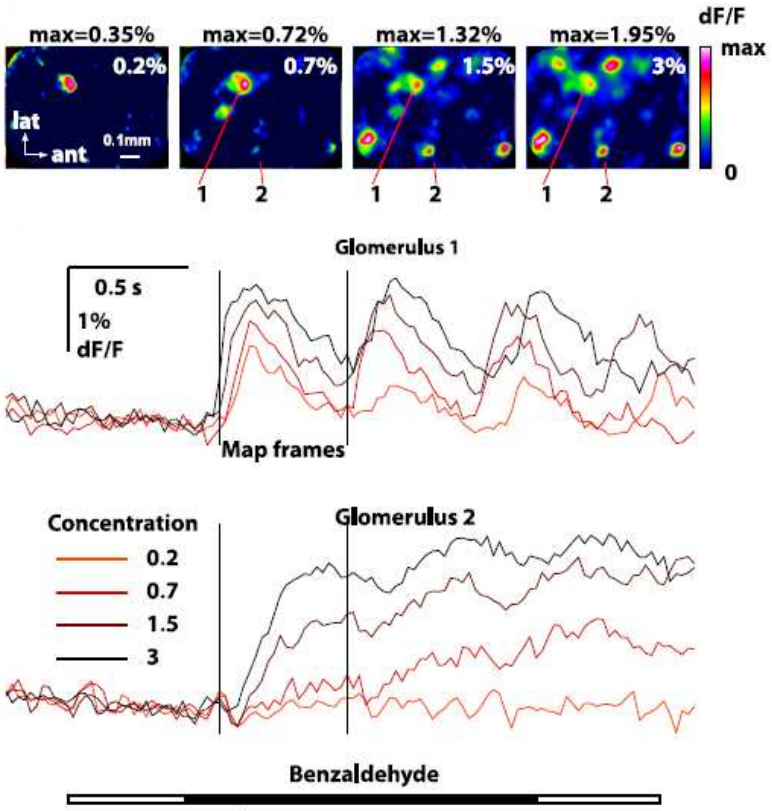

Illustration 11: Effect of odor concentration on presynaptic calcium responses (Spors et al. 2006).

related to the molecular features of each odorant (see Illustration 10). However, some discrepancies between calcium recordings and intrinsic imaging were found in the following years due to the complex underlying mechanisms of intrinsic imaging. These differences were highlighted by a study undertaken by Wachowiak et al. (Matt Wachowiak and Lawrence B. Cohen 2003). It has only been quite recently that a more thorough examination of the intrinsic signal in the olfactory bulb has been conducted (Gurden, Uchida, and Mainen 2006). Nevertheless dependence of the odor concentration on this signal, as shown by Wachowiak et al. (Matt Wachowiak and Lawrence B. Cohen 2003), has not yet been clarified.

- Voltage sensitive dyes have been used several times in the olfactory bulb, notably in a valuable study by Spors et al. (Spors and Grinvald 2002). The results were very similar to those with calcium imaging experiments even if the signal to noise ratio was smaller. They “bath-applied” the dye onto the olfactory bulb. The resultant staining was therefore relatively sparse in comparison to the nasal injected protocol and they couldn't determine the glomerular compartment. Collectively, these arguments

contribute to explain why the same authors have then moved on to calcium imaging (Spors et al. 2006).

2.1.5 Effect of increasing odor concentration on odor maps

Varying odor concentration has been shown to alter the odor maps in a number of ways (see Illustration 11). Firstly the number of recruited glomeruli has been shown to increase with concentration (Matt Wachowiak and Lawrence B. Cohen 2003; B A Johnson and M Leon 2000). In addition, the amplitude of responses of those glomeruli which are already responding increases unless it has reached saturation (Spors et al. 2006; Friedrich and Korsching 1997). This suggests that the governing process is the affinity of the olfactory sensory neuron receptor to the odorant.

Finally, it has been found that the onsets of the responses are shorter for higher concentration (Spors et al. 2006; Spors and Grinvald 2002).

However, while odor adaptation in the epithelium is a matter of intense debate and has been shown to be prominent for higher odor concentration, only one study focused on its effect on the olfactory bulb (Schafer et al. 2005). Since they used fMRI, they were limited by the time resolution of their technical apparatus and they could only look at the indirect effect on blood flow responses.

2.2 General brain metabolism

In the field of brain metabolism, it is now widespread knowledge that, while the brain weight is only 2% of the whole body mass, it consumes about 20% of its energy. To look into more details at the dramatic consumption of the brain, we can compare the absolute inflow of oxygen into the brain and its consumption.

Brain oxygen solubility is low, around $3x10^{-8}$ L per mL of brain and per mmHg (Leniger-Follert 1977), so if one takes an average brain oxygen level of pressure of 20mmHg (Ndubuizu and LaManna 2007), this leads to the final concentration of about $3x10^{-12}$ moles of oxygen per mm^3 of brain.

A typical value of brain consumption is around 0.010L per 100g of brain per minute (Leniger-Follert 1977; Secomb et al. 2000) which after proper conversion lead to $7.5x10^{-11}$ moles of oxygen per mm3 per second, given an average brain density of 1 mg/mm^3 (brain density is close to value for water).

So in 1 second, the brain consumes about 20 times more oxygen than what is available if there was no blood supply. This simple statement shows how important blood supply is to brain activity. As a result, the different mechanisms regulating blood flow and brain metabolism were all designed to face with this huge consumption. The link between the vasculature and neuronal activity must be so intimate that it seems impossible to address the issue of the work done by the brain without understanding how brain metabolism is regulated and appropriately supplied in metabolites. This aspect is of particular importance since most modern brain-imaging techniques, such as functional Magnetic Resonance Imaging (fMRI, see chapter 2.4.5) or Positron Emission Tomography (PET, see chapter 2.4.4), use this tight coupling to have access to neuronal activity.

Now, we will explain why and how the brain consumes such a large amount of energy.

2.2.1 Energy requirements of the brain

Storing energy is one of the main dilemmas of modern society. It is interesting to see how biological systems have dealt with this challenge. Nature chose a very peculiar approach to energy storage in the form of electrochemical gradients. Every cell maintains a gradient of chemical concentration between the intra and extracellular compartment. This is used as a driving force when energy is required for any process. As a consequence, action

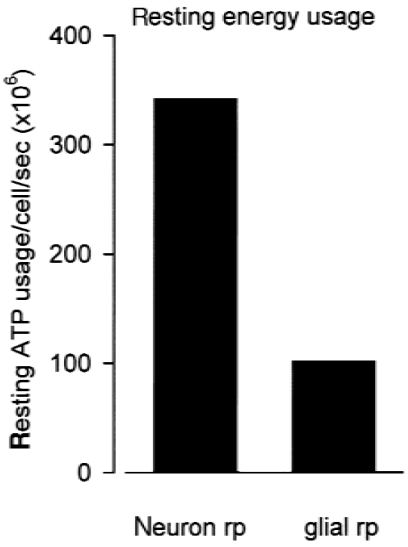

Illustration 12: Brain energy budget, glia vs neurons resting potential consumption (Attwell and Laughlin 2001)

potential propagation, synaptic transmission and postsynaptic currents generate ionic movements which have to be restored through ionic pumps. These pumps like the Na^+/K^+-ATPase pump, the Ca^{2+}-ATPase pump and so on use the chemical energy stored in ATP. Therefore, it is possible to restrict the energy budget to the usage of ATP. Based on this assumption, an energy budget for brain work was proposed several years ago (Attwell and Laughlin 2001). They estimated the resting potential usage between glial cells and neurons based on their input resistance (basically looking at the ion currents the Na^+/K^+-ATPase pump has to compensate at resting potential). The result, depicted in the Illustration 12, highlights the fact that neurons at resting potential consume three times more energy than glial cells.

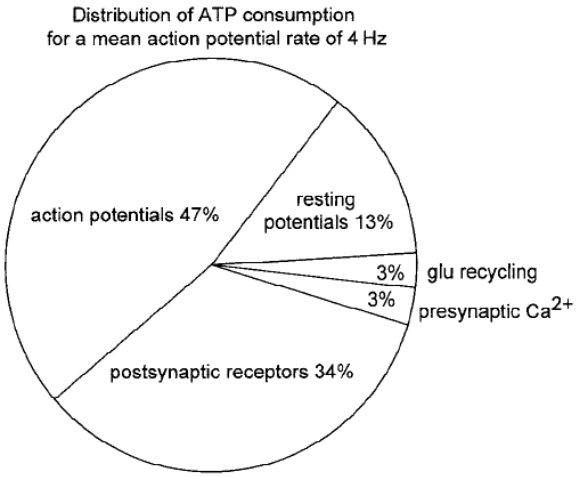

Illustration 13: Brain energy budget of an activated neuron (Attwell and Laughlin 2001)

They next look into the requirements of neurons to sustain activity. To do so, they had to make several major assumptions. Firstly, they created a single averaged neuron as a representative of the whole neuronal brain population. As a result, only glutamatergic transmission was considered and a very simple geometry was postulated for this neuron (for instance a 4cm long axon), Then they estimated the usage of ATP for every processes involved in neuronal activity. The result is shown in the Illustration 13. Clearly, action potential and postsynaptic receptors account for two thirds of the overall budget. This shows that it is indeed neuronal activity itself that is responsible for the huge consumption of the brain. Moreover, they attributed the major consumption to action potentials propagation along the unmyelinated axons. This publication was largely debated in the field of brain metabolism, due to its extensive simplification of the studied phenomena. The contribution of astrocyte to the energy budget is probably underestimated (Hertz, Peng, and Gerald A Dienel 2006), no energy transfer between neurons and astrocytes is assumed except for glutamate recycling and the action potential propagation is probably also overestimated as we will see. However, this model is frequently quoted as a numerical “tour de force” which tries to put numbers on physiology. Ultimately, this approach will greatly help us to obtain a precise energy budget.

An extension of this model has recently been proposed (Nawroth et al. 2007). Fortunately to us, they chose to go into detail for the olfactory bulb. Indeed, the precise known anatomy (see chapter 2.1.3) and the extensive quantitative

information which has been accumulated in the last 20 years on the olfactory bulb make it a very fine candidate to describe a more precise energy budget. However, they tried this time to include as much geometrical information on every neuronal, glial and vascular compartment as possible in the model. The results, depicted in the Illustration 14, predict the ATP consumption of every single processes evolved in odor transduction. We will see later on how this model will fit with our own results.

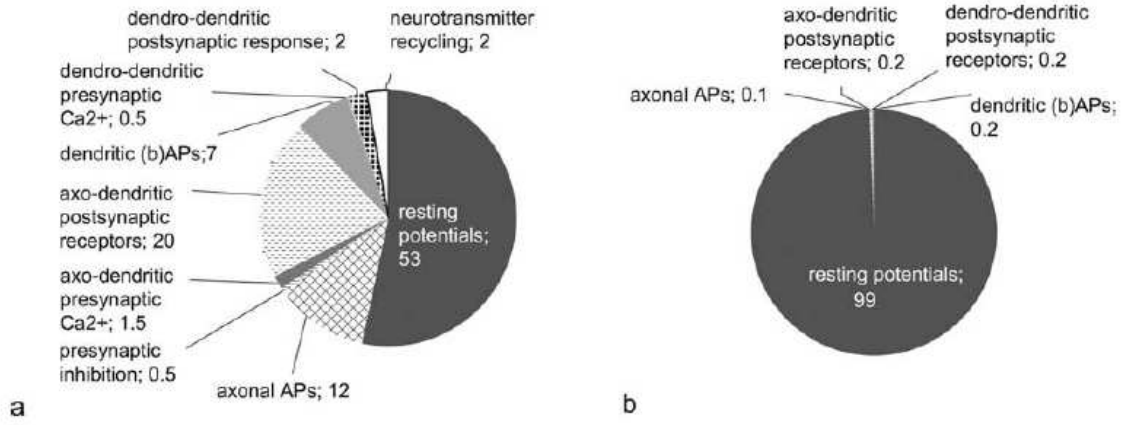

Illustration 14: Energy demands of the activated glomerulus after electrophysiological stimulation of the olfactory nerve bundle. a,Distribution of ATP usage in the glomerulus for an activation of 100% of the olfactory receptors axons. b, Distribution of ATP usage in the glomerulus for an activation of 1% of the axons (Nawroth et al. 2007)

Structure	Local cerebral glucose utilization (μmol/100 g/min)
	Gray matter
Visual cortex	111 ± 5
Auditory cortex	157 ± 5
Parietal cortex	107 ± 3
Sensory-motor cortex	118 ± 3
Lateral geniculate body	92 ± 2
Medial geniculate body	126 ± 6
Thalamus: lateral nucleus	108 ± 3
Thalamus: ventral nucleus	98 ± 3
Hypothalamus	63 ± 3
Caudate-putamen	111 ± 4
Hippocampus: Ammon's horn	79 ± 1
Amygdala	56 ± 4
Cochlear nucleus	124 ± 7
Lateral lemniscus	114 ± 7
Inferior colliculus	198 ± 7
Superior olivary nucleus	141 ± 5
Superior colliculus	99 ± 3
Vestibular nucleus	133 ± 4
Pontine gray matter	69 ± 3
Cerebellar cortex	66 ± 2
Cerebellar nucleus	106 ± 4
	White matter
Corpus callosum	42 ± 2
Genu of corpus callosum	35 ± 5
Internal capsule	35 ± 2
Cerebellar white matter	38 ± 2

* Determined at 30 min following pulse of [^{14}C]deoxyglucose.

Table 1: Local cerebral glucose utilization in different areas of the albino rat (Sokoloff 1977)

2.2.2 Glucose is the main source of energy

To produce such a quantity of ATP, neurons heavily rely on glucose provided by cerebral blood flow. This was clearly shown by Sokoloff thirty years ago using a very ingenuous combination of techniques (Sokoloff 1977). Deoxyglucose and glucose are very competitive substrates for both blood-brain transport and cell metabolism. However contrary to glucose, deoxyglucose is not processed further in the cell and is eventually trapped in neuronal tissue in the form of deoxyglucose-6-phosphate (instead of being converted to CO_2 as for glucose). Therefore, if you label deoxyglucose in the form of 2-deoxy-D-[14C]glucose and inject this tracer in the blood, you can track the usage of its cousin glucose via autoradiography.

Sokoloff et al. were able to show huge increases in uptake of glucose after functional activation. They quantified the glucose consumption of several areas of the brain. Their results are resumed in the Table 1. The first thing to note is that

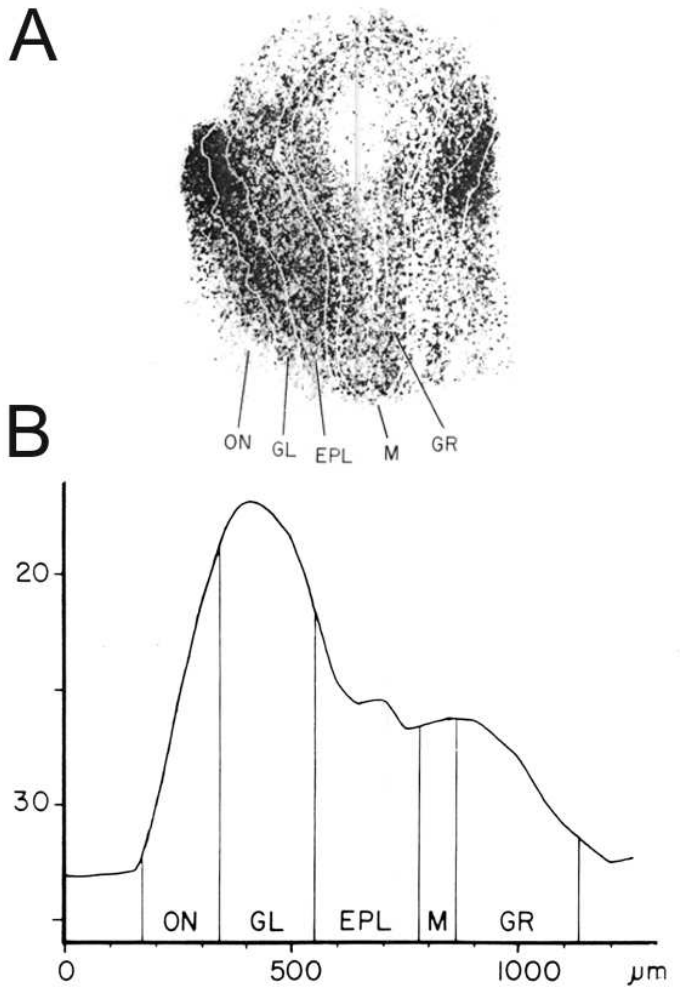

Illustration 15: Rat stimulated with amyl acetate. The autoradiogram in A shows the relative 2DG uptake of different layers of the olfactory bulb. The intense spot correspond to a glomerulus. This uptake is quantified on the panel B in an activated region. (Sharp et al., 1977)

white matter, made of myelinated axons, consumes very little glucose. The most demanding regions of the brain are the inferior colliculus and the auditory cortex. Interestingly these regions are involved in sound processing where neurons have very high firing rates in order to be able to code high frequency sound.

Notably, the calyx of held, one of the largest synapses in the brain is located in the mammalian auditory brainstem, in the superior olivary nucleus.

2DG uptake experiments in the olfactory bulb have also been done. The intense uptake of the Glomerular Layer is used as an indirect method to study odor maps as we have already shown (see chapter 2.1.4). In the Illustration 15, you can see a quantification of the relative uptake of the different neuronal layers

(F R Sharp, J S Kauer, and G M Shepherd 1977). The Glomerular Layer is the most demanding region during odor stimulation while a significant uptake can also be seen in the nerve layer. This result was confirmed by another group later on (Jourdan et al. 1980).

2.2.3 Metabolic pathways of glucose

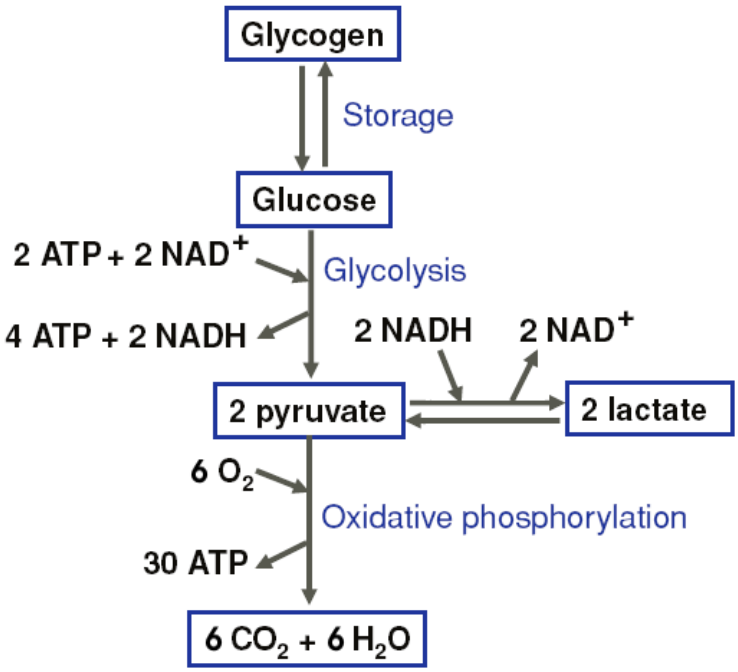

Illustration 16: A schematic representation of the metabolism of glucose from glycolysis to oxidative phosphorylation (modified from Raichle and Mintun 2006).

As an energy substrate, glucose is involved in several pathways (for a good review, see (Edvinsson and Krause 2001)). As shown in the Illustration 16, this catabolic process contains a nonoxidative (glycolysis) and an oxidative branch (oxidative phosphorylation). The oxidative branch takes place in the mitochondria while glycolysis occurs in the cytoplasm. The oxidative branch starts with pyruvate given by glycolysis and involves the Tricarboxylic Acid Cycle (TCA) and oxidative phosphorylation in the mitochondria membrane through electron transport.

They both produce ATP but by far, the largest amount of ATP is generated using oxygen during oxidative phosphorylation (30 ATP molecules versus 2 for glycolysis). If the two NADHs derived from glycolysis are shuttled into the mitochondria, an additional six molecules of ATP can be produced. Nevertheless, these NADHs can also be used to produce lactate from pyruvate via the Lactate

DeHydrogenase (LDH).

Glycogen, at the top of the Illustration 16, is a form of energy storage for the brain, and was somehow neglected until recently due to its low content in the brain compared to the liver or muscles (by a factor of approximately 50) (Angus M Brown and Ransom 2007), but we will revisit this matter later in the thesis.

2.2.4 Monitoring oxidative phosphorylation

Since oxidative phosphorylation produces the largest amount of ATP, it was long thought that the brain always relies on the full oxidation of glucose. Indeed Wong-Riley et al. used the cytochrome oxidase as a marker of activity to see whether oxidative phosphorylation was predominant in the brain (Wong-Riley 1989; Hevner and Wong-Riley 1989; Hevner, S. Liu, and Wong-Riley 1995). Cytochrome oxidase is a protein of the inner mitochondria membrane which catalyzes the transfer of electrons from cytochrome c to oxygen to form water. As a result, cytochrome oxidase is an endogenous metabolic marker for oxidative phosphorylation.

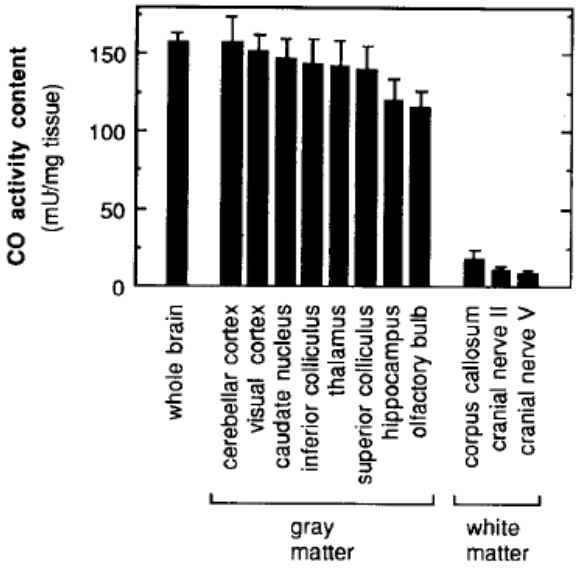

Illustration 17: Cytochrome Oxidase (CO) activity in the whole brain and in eight large regions of gray matter and three white matter areas (Hevner, Liu, and Wong-Riley 1995)

The results, depicted in Illustration 17, were strikingly similar to the results from Sokoloff et al. on glucose consumption (Table 1). They confirmed that white matter had low energy requirements compared to gray matter.

Nevertheless, some clear differences were found. Firstly, there was a twelve fold increase between white and gray matter, compare to the three fold increase in the Table 1. They attributed these discrepancies to technical differences between the two methods. It could, however, also have been related to the different relative contribution of glycolysis versus oxidative phosphorylation. Secondly, the absolute values of the different gray matter areas didn't perfectly match, in particular the inferior colliculus.

In the olfactory bulb, the Glomeruli Layer and the External Plexiform Layer were intensively stained, as can be seen in the Illustration 18. The Mitral Cell Layer, the Granule Cell Layer as well as the Nerve Layer were poorly stained.

As you did for the whole brain tables, you can now compare the Illustration 15 and Illustration 18: clearly glomeruli are intensively stained in both pictures which confirm that the glomerulus is consuming a very substantial quantity of energy. However, please also note that the staining in the Olfactory Nerve Layer in the Illustration 18 is low, while it is quite strong in the Illustration 15. This already suggests a different energy balance in glucose and oxygen consumption as we will see.

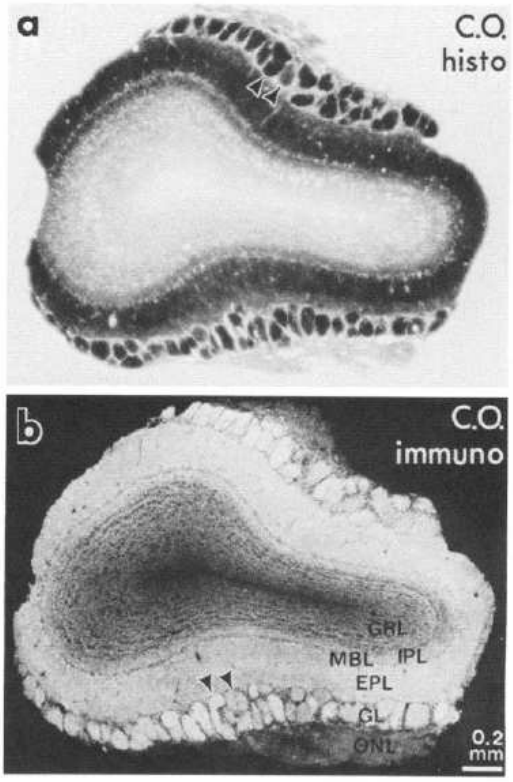

Illustration 18: Cytochrome oxidase activity (a) and amount (b) in the mice olfactory bulb. High level of activity (a) are in dark while large amount (b) are white. Arrows point at stained glomeruli. (Hevner and Wong-Riley 1989)

2.2.5 Glucose/Oxygen ratio

We have seen that if glucose undergoes the complete metabolic pathway of glycolysis and oxidative phosphorylation, then six molecules of oxygen are used per molecule of glucose. This ratio is very easy to verify and numerous groups in the last 20 years tried to see whether functional activation of the brain changes this ratio. In practice, at rest (without any particular brain work involved, as the brain is never completely at rest), this ratio is either 6 (P. L. Madsen et al. 1999) or slightly inferior, in the vicinity of 5.6 measured in PET (see chapter 2.4.4) (Baron et al. 1982). This is probably due to other pathways consuming glucose at rest, like glycogen storage and the pentose phosphate pathway, which we will describe in more detail later on.

However, the first report to point at discrepancies in these results in comparison to the dogma came 20 years ago (P T Fox et al. 1988). Fox et al. reported that through PET in human upon visual stimulation, there was a strong consumption of glucose without a corresponding increase in oxygen consumption. In fact, their ratio fell from 4 to 0.4 after stimulation, lasting for minutes suggesting that glucose consumption increased at a much higher rate than oxygen consumption. Their baseline ratio of 4 was lower than a previous study using PET (Baron et al. 1982) and others using various techniques (P. L. Madsen et al. 1999). Some authors suggested that $CMRO_2$ is probably underestimated in PET due to its limited spatial and time resolution (Hoge and Pike 2001). Even so, this result was

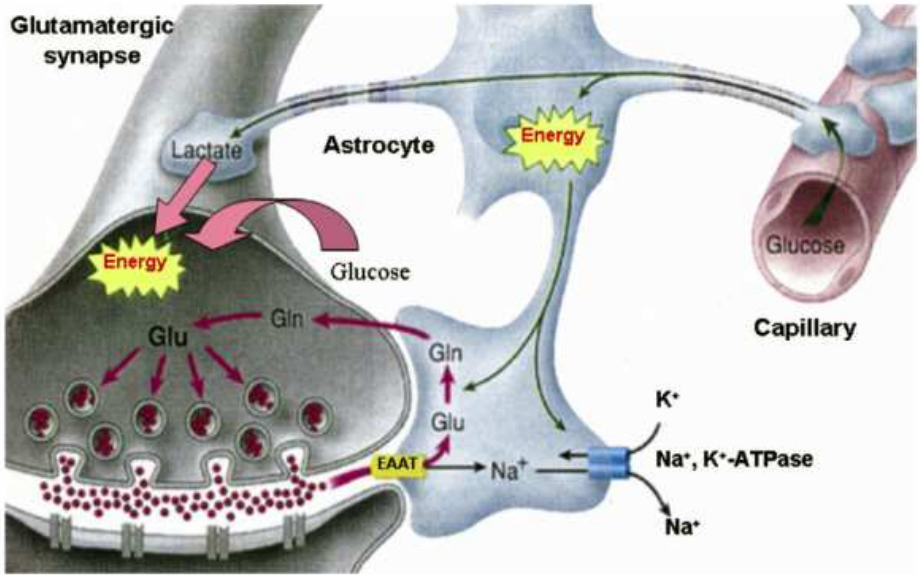

Illustration 19: Model for neuron-glia metabolic coupling (Magistretti 2006)

confirmed by other groups including those with other techniques in the following decade (P. L. Madsen et al. 1999; P L Madsen et al. 1995; Frahm et al. 1996; Fujita et al. 1999). Hence, upon stimulation, in some conditions, there is a transient increase in glucose uptake which is in excess of oxygen consumption.

2.2.6 Astrocyte-neuron lactate shuttle hypothesis

Two phenomenons can account for this change in the oxygen/glucose ratio:

- A fast increase in glycolysis rate without the concomitant uptake of the TCA cycle, leading to lactate overproduction. This was called **aerobic glycolysis** to account for a favored glycolysis in the presence of oxygen.
- An increase in the usage of glucose by paralleled pathways like glycogen storage.

In the light of these discrepancies and of their own results in cultured neurons, Pellerin and Magistretti proposed in 1994 a cellular basis to explain this transient uncoupling (L Pellerin and P J Magistretti 1994).

Glutamate released by neurons is removed from the synaptic cleft by astrocytes both to avoid its toxic effect on neurons and to recycle the glutamate pool through the glutamate-glutamine pathway (see Illustration 19). Failure of this uptake leads to excitotoxicity (Rossi, Oshima, and Attwell 2000).

Pellerin and Magistretti showed that glutamate uptake was also a potent stimulator of glycolysis (see Illustration 19). Indeed, glutamate transporter EAAT (for Excitatory Amino Acid Transporter) co-transports glutamate with 3 Na^+. For this

reason, activated presynaptic compartments will increase glutamate concentration in the synaptic cleft which in turn will increase sodium concentration in the astrocyte. This sodium is then pumped out of the cell through the Na^+/K^+-ATPase which consumes ATP (as the glutamate-glutamine pathway). As a consequence glycolysis is locally activated and stimulates glucose uptake from the nearby capillary to the astrocyte.

The two molecules of lactate produced per glucose can either be further oxidized in the astrocyte or shuttled to the neurons via MonoCarboxylate Transporter (MCT) channels.

Several lines of evidence lead to the idea that astrocytes can sustain neuronal activity through this pathway. For a more precise review, see (Edvinsson and Krause 2001).

- *In vitro*, neurons can use lactate as their sole energy source (A Schurr, West, and Rigor 1988).
- Neurons express a form of lactate dehydrogenase (LDH1) which is more likely to consume lactate than to produce it. This is contrary to astrocytes, which express LDH5 having opposite properties.
- Neurons and astrocytes also express different MCT channels, MCT1 and 4 for astrocytes and MCT2 for neurons (Pierre and Luc Pellerin 2005).

This collaboration between neurons and astrocytes is commonly called the Astrocyte-Neuron Lactate Shuttle Hypothesis (ANLSH).

Numerous works have confirmed the transient increase in lactate production following neuronal activity (P. L. Madsen et al. 1999; Peter L Madsen et al. 1998; Frahm et al. 1996).

The relative contribution of astrocytes and neurons has given rise to a very intense debate during the last decade. The most important articles concerning the importance of astrocyte in brain energy consumption triggered numerous published commentaries (Luc Pellerin and Pierre J. Magistretti 2004) and even initiated a debate on the role of hypothesis in Science (Luc Pellerin and Pierre J Magistretti 2004; Kimelberg 2004).

While the debate opposes several groups on the relative role of astrocyte and neurons in energy production, it is now clear that astrocytes play a key role and are activated by neuronal activity.

2.2.7 Other pathways for glucose consumption

- **Glycogen**

As shown in the Illustration 16, glucose is also stored as glycogen in the brain. This pathway, until recently, didn't receive the same interest as the Glycolysis/Oxidative phosphorylation pathway, probably because, as already mentioned, glycogen is 50 times less concentrated in the brain than in the liver or

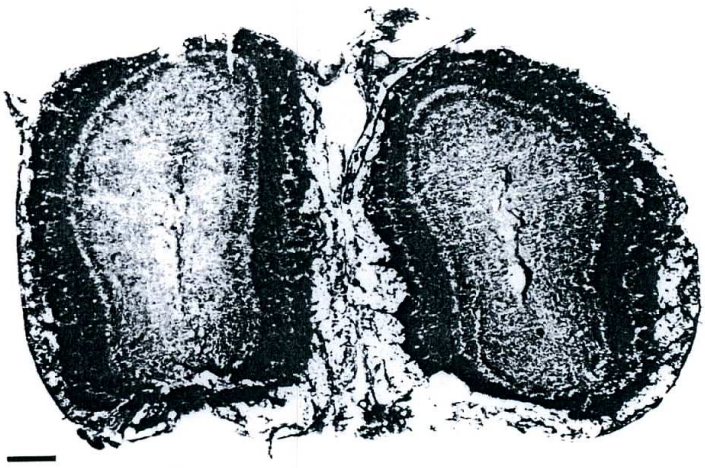

Illustration 20: Glycogen a and b phosphorylase activity in the olfactory bulb. The Glomeruli Layer and the External Plexiform Layer are strongly stained. (Coopersmith and Leon, 1987)

the muscle.

While it has been shown that neurons store glycogen during development, notably in the olfactory bulb (Robert Coopersmith and Michael Leon 1995), in the adult glycogen is mainly located in astrocytes (Pellegri et al. 1996). Neurons have the biological machinery to produce glycogen, but they silence it to avoid apoptosis, as has recently been shown (Vilchez et al. 2007; Pierre J Magistretti and Allaman 2007). As a result the main local source of glycogen for neurons resides in astrocytes.

If glycogen is not concentrated enough to account for significant energy storage, then what is it for? The answer can be considered through the examination of several important studies.

A very nice study on the effect of barbiturate, an anesthetic, showed a strong accumulation of glycogen in astrocytes after reduction of neuronal activity, suggesting that indeed glycogen is in equilibrium with neuronal activity (Creighton H. Phelps 1972). Phelps added that the accumulation of glycogen was stronger in the area of high synaptic density as would be expected from the cytochrome oxidase activity studies (see Illustration 17).

Later on, Madsen et al. Showed by freezing the brain at different times after stimulation, that glycogen decreased transiently after stimulation (Gerald A Dienel, Robert Y Wang, and Nancy F Cruz 2002; P. L. Madsen et al. 1999) and recovered later on.

Interestingly, the level of glycogen phosphorylase activity, the enzyme responsible for the glycogen breakdown, is very high in the olfactory bulb (R

Coopersmith and M Leon 1987), particularly in the Glomerular Layer, which was the highest expression of this enzyme in the brain and where intense oxygen consumption also occurs (see below).

These results showed that glycogen is a key actor in the transient response of the brain to sensory stimulation.

Recent studies have shown that during intense exercise, muscles also break their glycogen leading to the accumulation of lactate in the blood and the brain takes some of this lactate for its own metabolism (Dalsgaard 2005), leading to an interesting interaction between the periphery and the central nervous system.

- **Pentose phosphate pathways**

Glycolysis and oxidation phosphorylation are powerful pathways to produce ATP. While ATP releases its energy through hydrolysis, some biological reactions require energy in the form of reducing power. This is provided by the reduced form of nicotinamide adenine dinucleotide phosphate (NADPH).

NADPH is required to produce fatty acids for myelin as well as for the scavenging of Reactive Oxygen Species (ROS) produced by a variety of cellular processes. ROS are highly reactive due to the presence of unpaired valence shell electrons. As a result they are damaging for cells.

To produce this NADPH, there is the pentose phosphate pathway which starts with glucose and gives back fructose-6-phosphate or glyceraldehyde-3-phosphate to glycolysis. As a result the pentose phosphate pathway is essentially a derivation of glucose from glycolysis which is activated when NADPH level is low. The first and limiting reaction of this pathway is controlled by the enzyme glucose-6-phosphate dehydrogenase.

Interestingly the activity of glucose-6-phosphate dehydrogenase is again very high in the olfactory bulb, seemingly one of the highest in the brain, see Illustration 21, particularly in the Olfactory Nerve Layer and in the Glomerular Layer (Miller, Robert Coopersmith, and Michael Leon

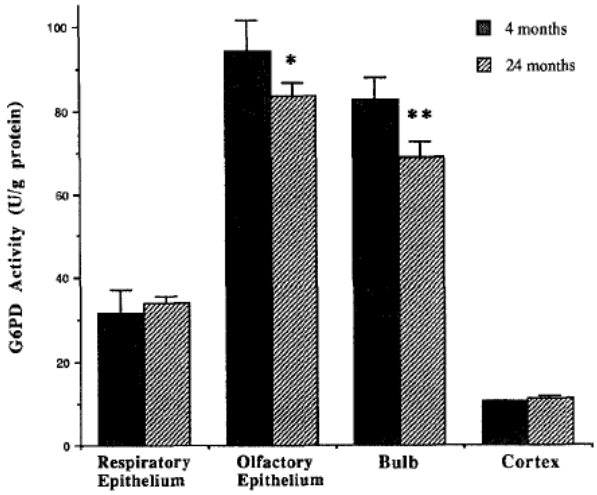

*Illustration 21: glucose-6-phosphate dehydrogenase activity ± SEM in respiratory epithelium (RE, n=5), olfactory epithelium (OE, n =5), olfactory bulb (n=5), and occipital cortex (n = 6) of male Fisher 344 rats at 4 and 24 months of age.*p<0.05, **p<0.01. (Miller and Collab. 1991)*

1991; Enrica Biagiotti et al. 2005). This is probably due to the high glutathione reductase activity, an enzyme involved in scavenging reactive oxygen species and has also been shown to be highly expressed in the olfactory bulb (Enrica Biagiotti et al. 2005). It has been suggested that this is related to the particular position of the olfactory epithelium and its axonal projection in the bulb, in direct contact with the external environment (and to high levels of oxygen compared to neuronal tissue, see chapter 2.5.1). It could also be related to the high levels of neurogenesis which occurs in the olfactory epithelium. Interestingly glucose-6-phosphate dehydrogenase is also high in the tongue, which is also in direct contact with the air (E Biagiotti et al. 2000).

As far as we know, no study has looked yet at the transient activation of glucose-6-phosphate dehydrogenase upon odor stimulation.

- **Amino Acid metabolism**

Several entry points exist in the glycolysis pathway and TCA cycle for amino acid production like glutamate or glycine. For a good review, see (Edvinsson and Krause 2001), their contribution to glucose consumption in the light of the oxygen/ glucose ratio at rest is presumably small compared to ATP production.

2.2.8 Summary

We have shown that the brain is consuming a substantial amount of energy compared to other organs. Because of this high energy requirement, brain metabolism is highly regulated. When a particular brain region is activated, ATP levels in both neurons and astrocytes drop. To refurnish their ATP stock, neurons and astrocytes rely on complex cellular machinery which involves glucose, oxygen, lactate and glycogen as key players. The contribution of these players in ATP production evolves with time after neuronal activity. An increase in oxidative phosphorylation in the neuronal compartment is followed by an increase of both glycolysis and glycogen breakdown in the astrocytic compartment. The relative timing (on the order of seconds) and importance of these events in vivo in response to a physiological stimulus still remain to be precisely determined, even if some *in vitro* work has already clarified this matter (Kasischke et al. 2004).

2.2.9 Perspective

The strong debate that followed the proposal of the Astrocyte Neuron Lactate Shuttle Hypothesis (C P Chih, Lipton, and Roberts 2001; C. P. Chih and Roberts Jr 2003; P. L. Madsen et al. 1999; Peter L Madsen et al. 1998; P L Madsen et al. 1995; Luc Pellerin and Pierre J Magistretti 2003; Luc Pellerin and Pierre J Magistretti 2004; A Gjedde and Marrett 2001; Luc Pellerin and Pierre J. Magistretti 2004; Korf 2006; A. Schurr 2006; Kimelberg 2004) arises probably from the difficulty to draw a general rule for the whole brain. Indeed, as we have shown, brain consumption is highly variable between brain regions (see Table 1). The auditory cortex, for instance, consumes a substantial amount of glucose, while

white matter made of myelinated axons is less demanding. Even between gray matter regions, glucose consumption can double, the highest consumption rates being in the regions where synaptic densities are elevated. As a result different brain regions will probably modulate their energy usage and production differently. This means we now have to change our strategy to study brain metabolism in order to correlate the local energy need of each region with the different ways each region chooses to produce its energy.

The olfactory bulb, in particular the Glomerular Layer, with its well defined neuronal anatomy and high synaptic density is seemingly one of the most energy demanding regions of the brain. As a result, probably all of the potential pathways involved in energy production are locally involved and we could benefit from a systematic study of this particular region.

The known features of the olfactory bulb have made it possible to recently build a local theoretical energy budget (Nawroth et al. 2007) which, contrary to a more general older model (Attwell and Laughlin 2001), makes precise predictions on the energy needs of a glomerulus (see Illustration 14).

On the experimental side, glucose consumption in the olfactory bulb have been extensively studied through 2DG uptake experiments ((B. A. Johnson, Woo, and M. Leon 1998; F. R. Sharp, J. S. Kauer, and G. M. Shepherd 1975; Jourdan et al. 1980). Glycogen breakdown has also been characterized in this same structure (Robert Coopersmith and Michael Leon 1995; R Coopersmith and M Leon 1987) as well as the pentose phosphate pathway (Miller, Robert Coopersmith, and Michael Leon 1991).

However, no study, except for indirect measurements through intrinsic imaging (see chapter 2.1.4), have quantified the precise oxygen consumption in space and time that occurs upon odor stimulation in the olfactory bulb. These results could help delineate the local metabolic events that happen following odor stimulation in order to build a local energy need and production budget in the near future.

2.3 Cerebral blood flow regulation

We have previously shown that the brain heavily relies on cerebral blood flow to maintain its function. Indeed only 15 seconds of cardiac arrest is enough to lose

Regional Capillary Network in Rat Brain (Mean ± SEM)

Regions	Capillary length (mm/mm^3) (n = 5)
Subcortical white matter	98 ± 9
Spinal tract IV	108 ± 7
Pyramidal tract	157 ± 8
Hippocampus Stratum radiatum	170 ± 12
Cerebellum White matter	173 ± 11
Ventral tegmental area	195 ± 16
Hippocampus Stratum oriens	265 ± 33
Dentate gyrus— outer blade Molecular layer	290 ± 17
Periaqueductal gray matter	318 ± 6
Dentate gyrus— inner blade Outer molecular layer	323 ± 23
Substantia nigra, pars reticulata	350 + 21
Hippocampus Stratum lacunosum-moleculare	363 ± 26
Cerebellum molecular layer	376 ± 25
Frontal cortex Layer I	380 ± 10
Retrosplenial cortex Layers II–V	419 ± 18
Superior colliculus Stratum griseum superficiale	422 ± 11
Spinal nucleus V	438 ± 30
Medial geniculate	454 ± 35
Red nucleus	516 ± 35
Cerebellum Granular layer	589 ± 24
Interpeduncular nucleus	625 ± 56
Vestibular nucleus	635 ± 38
Inferior colliculus	811 ± 22

Table 2: Capillaries densities in various part of the rat brain (Borowsky and Collins, 1989)

consciousness (M. E. Raichle and M. A. Mintun 2006). As a result, the brain is so much protected from shortage in metabolites that blood flow is regulated in many ways in the brain.

2.3.1 Vasculogenesis and angiogenesis

It is not common in the handbooks of neurovascular coupling to introduce angiogenesis as part of the link between neurons and blood flow. However it has been known for decades that blood vessels densities tightly match the needs in energy. Already in 1920, Craigie (Craigie 1920) observed that gray matter was a lot richer in capillaries than white matter. This was refined a few years later by Dunning et al. (Dunning and Wolff 1937) where they postulated that “impulse from neuron to neuron is more richly supplied with blood than nervous tissue involved in conduction only within the neurons”. More recently Borowsky et al. showed that capillary density paralleled the use of glucose (Borowsky and Collins 1989) as can be seen on the Table 2. A quick comparison with the Table 1 obtained a decade earlier will easily convince you that glucose usage is highly correlated with capillaries density.

Borowsky et al. also analyzed the density in the olfactory bulb and showed, qualitatively, that the Glomerular Layer was more densely filled with capillaries than the others layers. While the density in the External Plexiform Layer has been

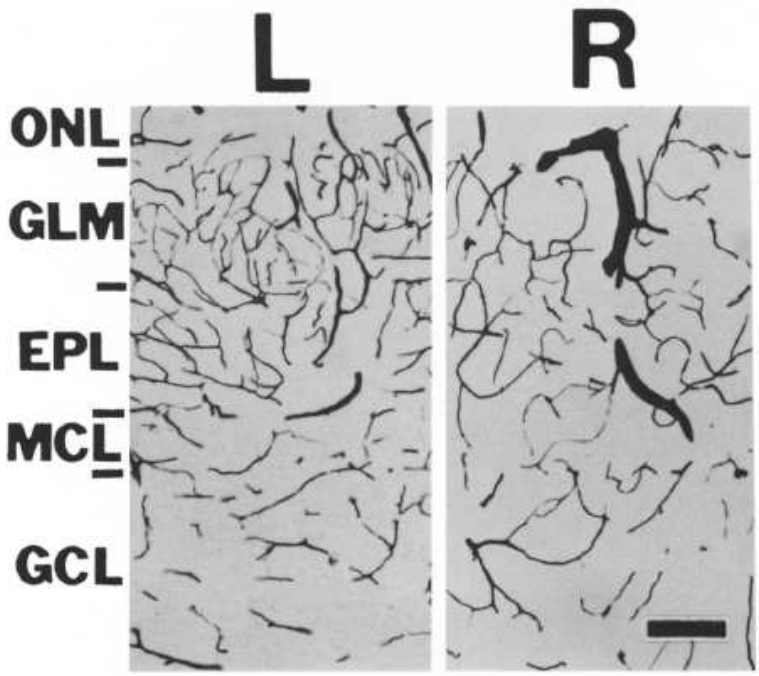

Illustration 22: Photomicrographs of bulbs from a P20 animal occluded on PI. L, left "control" bulb; R, right"deprived" Scalebar = 0.1 mm. GLM stands for Glomerular Layer. (Korol and Brunjes, 1992)

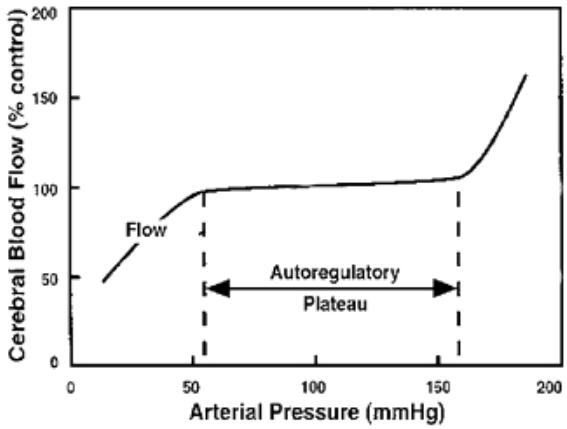

Illustration 23: Cerebral blood flow versus arterial pressure. Autoregulation ensures a relatively constant level of cerebral blood flow over broad range of arterial pressure.

quantified with age (Hinds and McNelly 1982), no precise quantification of the Glomerular Layer and the Nerve Layer has been done.

In addition, blood vessel anatomy is known to be highly variable between animals, as can be seen on the surface of the olfactory bulb of different animals (Illustration 10) and this is a demonstration of the fact that angiogenesis is not fully preprogrammed by genes and that neuronal activity controls it. This result was confirmed using unilateral naris closure (Korol and Brunjes 1992) as shown in the Illustration 22. Note the striking difference between the deprived and the control bulb.

A very complete description of vascular system of the cerebral cortex and its development can be found in a publication by Bar (Bar 1980).

2.3.2 Autoregulation

Autoregulation refers to the capacity of cerebral blood flow to remain relatively constant despite variations in perfusion pressure. Indeed in our everyday life, blood pressure in the brain varies (between when we stand up and when we lie down for instance). To counteract these variations (and avoid cerebral ischemia or edema), cerebral arteries and arterioles dilate when pressure drops and contract when it increases. This mechanism involves several populations of vessels depending on their diameter (Kontos et al. 1978). As a result, an autoregulatory plateau ensures constant cerebral blood flow in the brain roughly between 50 and 160 mmHg (see Illustration 23). However this effect has its limits. In the upper range of pressure, blood vessels fail to counteract the huge increase in pressure and their diameter start to increase, eventually leading to edema. In the lower range, the pressure is too low for the blood vessel to maintain a constant blood supply and this time their diameter decreases, eventually leading to ischemia. Many factors, arterial CO_2 (see Illustration 26), chronic hypertension, sympathetic nerve activity or other pharmacologic agents affect the autoregulation curve.

2.3.3 Gas tension responses

It has long been known that abnormal arterial CO_2 and oxygen tension affect

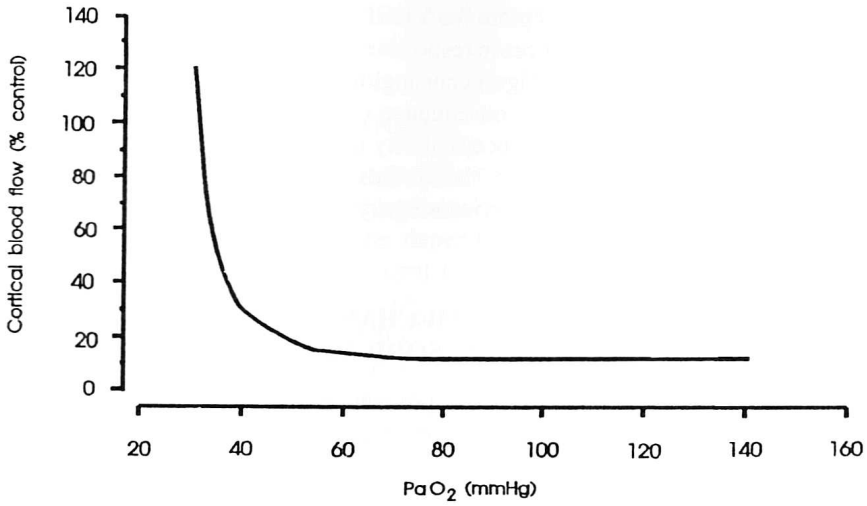

Illustration 24: Effect of alterations in arterial Pa_{O_2} on cortical blood in dogs while maintaining Pa_{CO_2} within physiologic limits (Edvinsson and Krause 2001)

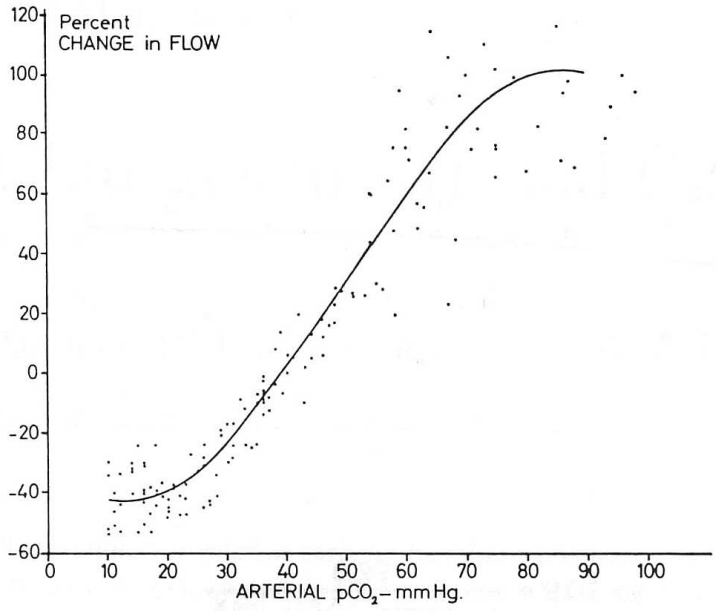

Illustration 25: Effect of alterations in arterial Pa_{CO_2} on cortical blood in dogs (Edvinsson and Krause 2001).

cerebral blood flow (for a good review see (Edvinsson and Krause 2001)). Increasing the inhaled partial pressure of CO_2 (hypercapnia) induces consistent and reproducible vasodilatory responses. Clark, who developed the famous oxygen electrode (Clark et al. 1953), already observed in 1958 an effect of altered gas tension on basal oxygen levels in the brain (Clark, Misrahy, and R. P. Fox 1958).

As opposed to altered partial pressure of oxygen (see Illustration 24), increasing Pa_{CO_2} increases cerebral blood flow quite rapidly (Illustration 25) and this effect is mediated through vasodilatory responses. For the oxygen to have an effect on cerebral blood flow, you need to decrease Pa_{O_2} below 50 mmHg (see Illustration 24). The effect increases then sharply for lower values.

Since basal arteriole diameter is changed, one can expect autoregulation to be affected by changes in Pa_{CO_2}. Indeed as seen on Illustration 26, hypercapnia decreases the upper limit of the autoregulatory plateau while hypocapnia

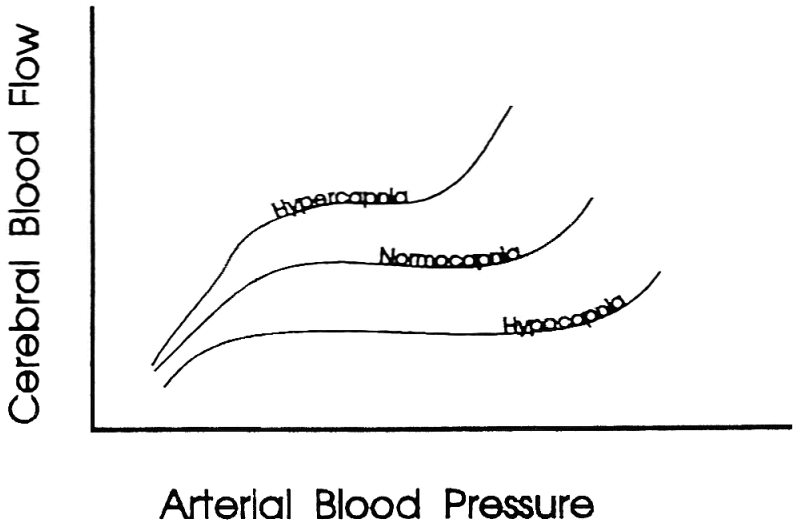

Illustration 26: Effect of P_{CO_2} on autoregulation of cerebral blood flow (Edvinsson and Krause 2001).

increases it.

2.3.4 Functional hyperemia

Neuronal activity is intimately coupled with blood flow as expected from the intimate link between neuronal activity and brain consumption (see Table 1). The first evidence of such a link is commonly attributed to Angelo Mosso (M E Raichle 1998). He recorded in 1881 the pulsation of the human cortex in patients with skull defects. Mental activity increased regionally these pulsations, suggesting that

brain circulation changes with neuronal activity. A large number of studies followed and showed that, without a doubt, Mosso was right (for a good review, see (M E Raichle 1998)).

This local increase in blood flow was named **functional hyperemia** because that it relates a change in **function** with a change in **blood flow** (-emia comes from the Greek haima, blood).

The advent of modern imaging techniques (see chapter 2.4.4) 30 years ago renewed the interest in functional hyperemia. An extensive number of studies started to show what type of neuronal activity is most correlated with blood flow responses. Is it spikes? Is it postsynaptic depolarization? Is it somata depolarization?

Answering this question is difficult because all three of these phenomenons are the results of one another. One way to look at it is to determine correlations and look at the correlation coefficient between the different recordings. Logothetis et al followed this idea and combined BOLD, Local Field Potential (LFP) and Multi-Unit Activity (MUA) in the same monkey (Logothetis et al. 2001). They showed that LFP, which mainly reflects synaptic activity, was better correlated with the BOLD signal than MUA, which mainly reflects action potential activity. While their estimated correlation were close (LFPs and BOLD, $r^2 = 0.521$ and BOLD and MUA, $r^2 = 0.445$), several other studies confirmed this result (for a review see (Martin Lauritzen and Lorenz Gold 2003)). For this reason, we decided to record LFP in the olfactory bulb.

Since the synapse is probably a key actor in this coupling, we still need to know to what extent the presynaptic and the postsynaptic compartments contribute to this coupling. This is essentially the subject of the publication in the Annex.

2.3.5 Mechanisms

While it was possible a few decades ago to say that the mechanisms involved in cerebral blood flow regulation were not precisely known, now the problem is opposite, because there simply are too many possibilities. Reviewing all of these is beyond the scope of this thesis and would require an additional hundred pages.

These mechanisms can be divided in two classes. There are those which involve neurons and those which don't. The first class of mechanisms concern neurovascular coupling and are at the heart of functional hypermia. The second class only involves members of the vascular wall: smooth muscles cells, pericytes and endothelial cells. These mechanisms serve for autoregulation, gas tension responses or even angiogenesis. In the next paragraph, I will only focus on the first class. For a complete and detailed description of both classes, I would recommend the excellent work of Lars Edvinsson (Edvinsson and Krause 2001).

For this manuscript, suffice it to say that neurons potentially act on vessels

through several possible pathways.

- Neurons directly innervate arterioles (Hamel 2006). These projections either come from local interneurons or from specific nuclei such as Raphe Nucleus. Interestingly large extra-cerebral vessels running at the surface are differentially innervated than intra-cerebral microvessels.

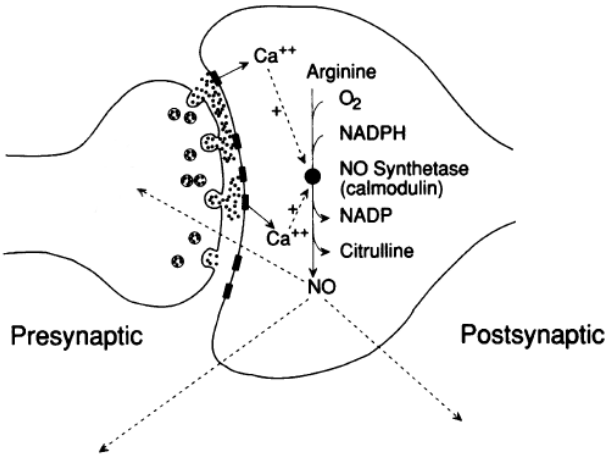

Illustration 27: NO is produced in the postsynaptic compartment upon calcium entry through the NMDA channels. The enzyme NO Synthetase uses Arginine, O_2 and NADPH in this process. (Gally et al., 1990)

- Neurons can act directly on smooth muscle cells in the arteriole walls through the release of a mediator in the extracellular space. Among the numerous potential mediators, Nitric Oxide (NO) is of particular interest as it is a vasodilator transiently released upon activation by the postsynaptic compartment (see Illustration 27) (Gally et al. 1990).

- Neuronal activity can act on astrocytes which in turn control blood flow. This idea is today particularly popular because astrocytes are already in place for such a role. They both contact synaptic buttons and cover endothelial cells on blood vessels (Kacem et al. 1998). Neurotransmitter can directly acts on astrocytes and increase astrocytic intracellular calcium. Among these, Glutamate, as the main neurotransmitter in the brain is of a particular interest because the metabotropic receptor mGlur located in the astrocyte membrane helps the astrocyte sense local glutamate levels. Moreover an increase in intracellular calcium activates the synthesis of several potential vasodilators (for a review see (Iadecola and Nedergaard 2007)).

2.4 Techniques to record oxygen in the brain

Various techniques have been used in the past to record oxygen levels in the brain and in the periphery (for a good review, see (Tsai, P. C. Johnson, and M. Intaglietta 2003) and (Ndubuizu and LaManna 2007)). Monitoring oxygen in the brain is crucial in order to understand two important phenomena. The first phenomenon is obviously the consumption of oxygen by the neuronal tissue which is triggered by neuronal activity. The second phenomenon is the diffusion of oxygen in brain tissue. These two topics are linked and have strongly been debated since it became possible to record oxygen reproducibly in the 1950s.

2.4.1 Microelectrode

Clark electrodes were invented in 1958 by Leland C. Clark as an evolution of the already widely used oxygen polarographic electrodes. Previous polarographic electrodes were highly unstable in biological tissues due to the membrane of red blood cells or of others cells interfering with the operation of the cathode. Clark's idea was to isolate the cathode with a cellophane membrane permeable to oxygen (Clark et al. 1953). As a result he obtained very stable recordings and he even managed to chronically implant them in the cat brain for as long as two years (Clark, Misrahy, and R. P. Fox 1958). His work triggered a large amount of research based on oxygen recordings in the periphery or in the brain. All commercially available blood samplers are now based on his electrode. Its principle is detailed in the Methods (chapter 3.2.1) of this thesis. They provide a direct access to oxygen partial pressure at a precise point in the tissue (tip diameter from 1 to 5 µm) with a time resolution inferior to the second.

2.4.2 Spectrophotometric methods

Hemoglobin changes color when it is bound to oxygen. Looking at blood color is still the simplest method to distinguish arterioles and veinules. Therefore one can determine the oxygen content of a vessel from its spectral properties.

Two powerful techniques derived from this simple statement are: Near Infrared Spectroscopy (NIRS) and intrinsic optical imaging.

- NIRS was first introduced in 1977 (Jöbsis 1977) as a non invasive technique to monitor changes in oxygenation. Typical used wavelengths range from 800 to 1000nm. Both hemoglobin and cytochrome oxidase have been shown to alter significantly the spectrum in this near infrared region. Cytochrome oxidase absorption is smaller than hemoglobin but can be extracted from hemoglobin using double wavelength recordings. Extracting quantitative information is difficult due to contributions from numerous unknown parameters. Nevertheless, NIRS can be used clinically and allows to monitor quick change in cerebral oxygen saturation (for a good review, see (P L Madsen and Secher 1999).
- Shorter wavelengths, between 500 and 700 nm, also carry a

significant amount of information on intrinsic activity of the neuronal tissue. Intrinsic optical imaging was drastically improved by Grinvald et al. in 1986 (Grinvald et al. 1986) as a new powerful indicator of cortical activity (R D Frostig et al. 1990). The principle is to illuminate the surface of the brain with a specific wavelength and examine the reflected signal over time. Between 500 and 600 nm, hemoglobin and deoxyhemoglobin absorption dominates, while above 600 nm a third component called the “Light scattering component” corresponds to 70% of the signals (Malonek and Grinvald 1996). The third component presumably reflects the change in the extracellular space volume which follows neuronal activity. A recent study in the olfactory bulb has shown that astrocytes play a major role in this regard (Gurden, Uchida, and Mainen 2006). Hence, this technique doesn't provide absolute values of oxygen partial pressure (during neuronal activity); however it does present a relative indication.

2.4.3 Fluorescence methods

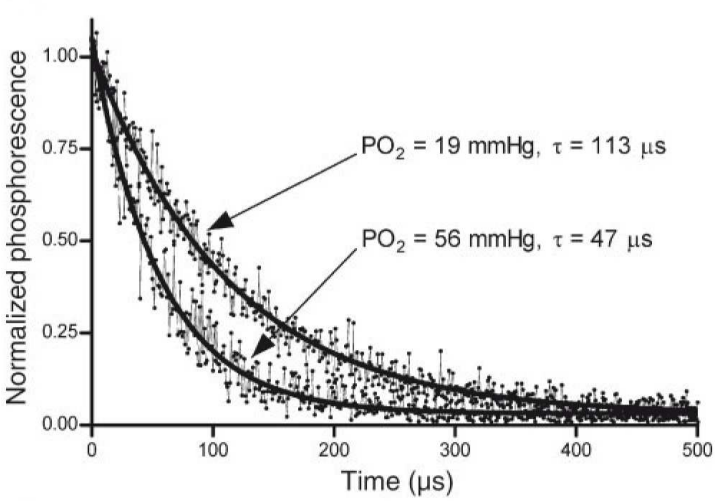

Illustration 28: Two-photon excitation phosphorescence lifetime measurements in vitro. 2 examples of phosphorescence traces recorded at different oxygen levels. Traces are the average of 64 laser pulses (Mik et al. 2004).

Fluorescence-based methods of oxygen detection depend on the sensitivity of a dye to oxygen. A very powerful and promising approach uses a derivative of porphyrins. Pd-porphyrins can be excited with blue or green light to produce phosphorescence. The time constant of this decay is related to the local partial pressure of oxygen (see Illustration 28). For this reason, this technique yields quantitative values. Until recently, a major drawback of this technique was a poor penetration depth due to its low signal to noise ratio. Furthermore, it was

necessary to average such a large number of trials that the time resolution would be low. Nonetheless, two-photon imaging of this dye (Mik et al. 2004) has recently been achieved and the time resolution has substantially been improved (Estrada et al. 2008; Golub and Pittman 2005).

2.4.4 Positron Emission Tomography (PET)

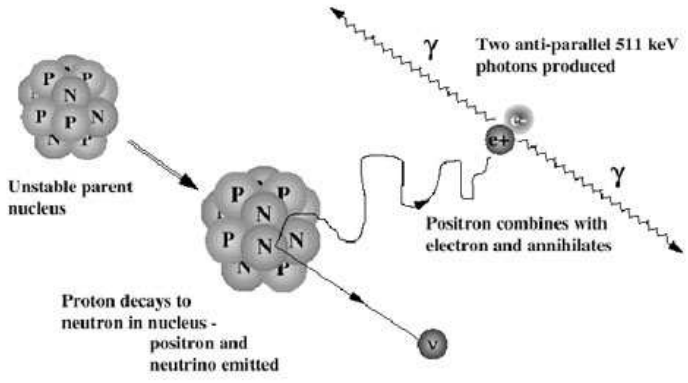

Illustration 29: PET principle is based on the detection of photons emitted during the radioactive decay of a tracer.

(source : http://www.petnm.unimelb.edu.au/pet/)

Positron Emission Tomography relies on the detection of positrons from a radioactive tracer which is injected in the body. These tracers have short half-life (in the minutes range) and their decay emits a positron, which is the antimatter counterpart of the electron (see Illustration 29). The instant that the positron meets or contacts an electron (which is normally after a trajectory of about 1 mm through the tissue (Sá et al. 2004)), they annihilate and two photons are emitted in precise opposite directions to each other. These photons can be detected using an array of sensors. PET can therefore monitor any molecule provided that a radioactive tracer is attached to it. To monitor glucose consumption (the most common application of this technique in current practice), ^{18}F-fluorodeoxyglucose (18F-DG) is used the same way Sokoloff et al. (Sokoloff 1977) mapped glucose usage in the brain (see chapter 2.2.2). PET can also monitor oxygen consumption using the consecutive recordings of $^{15}O_2$ (inhaled by the subject), $H_2{}^{15}O$ (injected in the blood) and ^{11}CO (inhaled) decay.

$H_2{}^{15}O$ measurements are related to Cerebral Blood Flow (CBF). Indeed water in the blood is permanently being exchanged with water in the brain tissue. The flow of water between from the blood stream to the tissue is a function of time. So at a certain time, the quantity of $H_2{}^{15}O$ in the tissue is the integral of the flow of blood at a location in the brain. By determining the time since the tracer was

injected, the definite integral (which is the accumulation of the tracer) can be established. Differentiating this value yields the CBF (Herscovitch, Markham, and M E Raichle 1983).

^{11}CO stays in the blood and forms carboxyhemoglobin. It is therefore useful to monitor Cerebral Blood Volume (CBV) with a good accuracy (M E Phelps et al. 1979).

Inhaled $^{15}O_2$ follows a complex path in the brain. Some is converted into $H_2{}^{15}O$ in neuronal tissue and is redistributed between vessels and neuronal compartment while the rest stays in the blood. However using a comprehensive model, Mintun et al. (M A Mintun et al. 1984) used the consecutive measurement of CBV with ^{11}CO, CBF with $H_2{}^{15}O$, and the results from inhaled $^{15}O_2$ to determine the local extraction of oxygen from the blood, which we have denoted E, and the arterial content in oxygen C_aO_2. They could compute the local consumption of oxygen, $CMRO_2$, using the following formula:

$$CMRO_2 = E \times CBF \times C_a O_2 \quad (1)$$

The whole process (consecutive recordings of the three parameters) takes less than one hour and it produces consumption maps with a spatial resolution in the millimeter range and a temporal resolution in the order of tens of seconds. Interestingly, PET can provide a good measure of CMRO2 but it doesn't provide information on the partial pressure of oxygen PO_2.

2.4.5 functional Magnetic Resonance Imaging (fMRI)

When a strong magnetic field is applied to matter, particles which have a

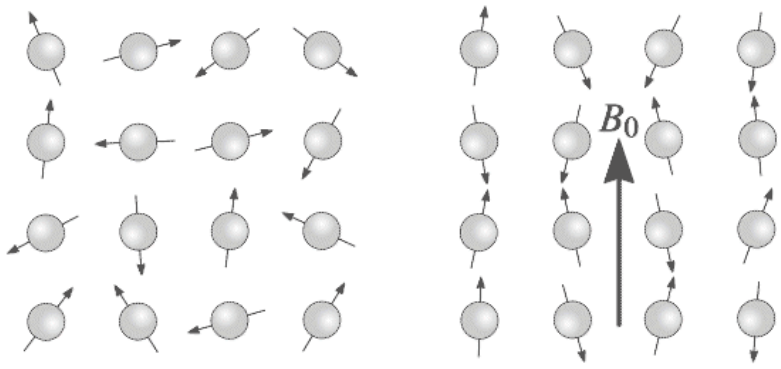

Illustration 30: Magnetic resonance imaging principle. A collection of 1H nuclei (spinning protons) in the absence of an externally applied magnetic field are shown on the left. Their magnetic moments have random orientations. An external magnetic field B0 is applied which causes the nuclei to align themselves B0.

(Source : http://www.easymeasure.co.uk/principlesmri.aspx)

magnetic spin will align as magnets with the field direction (see Illustration 30). However, under certain conditions, they can also rotate around the strong magnetic field axis, just as a spinning top would do (see Illustration 31). This rotation can be induced by a second perpendicular oscillating magnetic field at a set frequency. The frequency required to make a particle with a particular spin rotate around its axis is dependent on the intrinsic properties of the involved nucleus. Since these rotations can be detected, it provides access to information on the density of a particular element in space. This is the basic principle of Magnetic Resonance Imaging (MRI).

Water protons have a small but significant tendency to align with the field. Since water is predominant in biological tissue, it is possible to extract an image of water distribution in the tissue, Using this technique, one can therefore non invasively gain access to the anatomy of a body. An example is accessing the distribution of gray and white matter as they have different water content.

It was then discovered that oxyhemoglobin is diamagnetic (which means it doesn't react with the magnetic field) while deoxyhemoglobin is paramagnetic (as protons). This simple finding is at the base of functional Magnetic Resonance Imaging (fMRI) which was invented in 1990 (Ogawa et al. 1990). As a matter of fact, the presence of deoxyhemoglobin modifies the susceptibility of nearby protons, which modifies the local contrast of MRI pictures or Blood Oxygenation Level-Dependent (BOLD) contrast. Since it had already been shown using PET (P T Fox and M E Raichle 1986) (see chapter 2.2.5) that blood flow responses were largely in excess of oxygen consumption, the major effect is a large increase of oxyhemoglobin concentration upon stimulation, or positive BOLD. Now fMRI offers a temporal resolution of about one second with a typical spatial resolution of few hundreds of microns (see chapter 2.1.4).

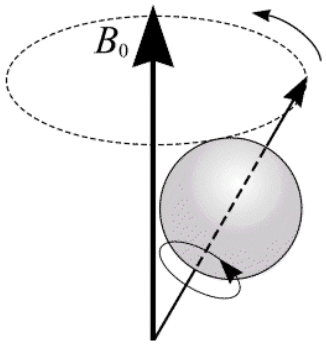

Illustration 31: The magnetic moment of a nuclei processes around the magnetic field B0. Its path describes the surface of a cone.

(Source : http://www.easymeasure.co.uk/principlesmri.aspx)

As for PET, fMRI provides very insightful information on changes of oxygen in blood but it cannot quantitatively measure PO_2.

2.4.6 Electron Paramagnetic Resonance (EPR)

In a similar fashion to the use of magnetic fields for MRI, it is possible to look at electron behavior in an electromagnetic field. However, since most electrons associate in pairs of opposite field direction, only strongly isolated electron (unpaired) can be used for detection. Oxygen can be monitored by looking at its effect on an EPR probe which can be distributed in several locations at the same time (Jeff F. Dunn and Swartz 2003) and this yields quantitative oxygen values.

Either implants of lithium phthalocyanine (LiPc) (Hou et al. 2003; Jeff F. Dunn and Swartz 2003) in small dots or soluble materials are used as the probe for oxygen levels.

The implants are small in size (0.2 mm) (Shimin Liu et al. 2004) and can be distributed in several locations providing reproducible access to multiple oxygen recordings in awake and anesthetized rats. Imaging can be performed using soluble materials as nitroxides but the spatial (millimeter) and time (20 minutes per image) resolutions are still poor. Nevertheless, it still rests a very promising technique (Elas et al. 2003).

2.5 Oxygen regulation in the brain

2.5.1 Oxygen level in the brain

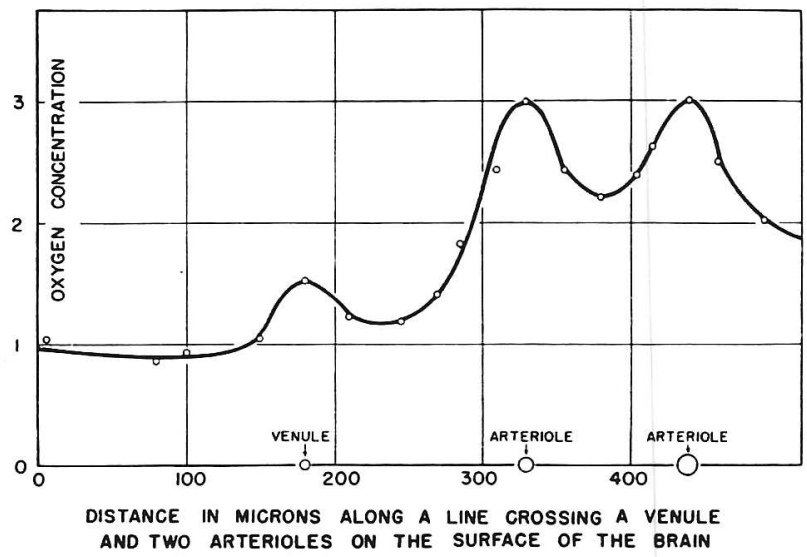

Illustration 32: Oxygen level in the brain at different distances of major vessels on the brain surface (Davies and Bronk, 1957)

Basal oxygen level in the brain is low, it has been known since the very beginning of oxygen microelectrode recordings. While the partial pressure of oxygen in the air we breathe is around 180 mmHg, a typical value of oxygen partial pressure in the brain is between 10 mmHg and 40 mmHg with quite an extensive variability on the microregional level. At any given location, oxygen tissue tension depends on the local respiration of the tissue, the oxygen level in the nearby vessels, the proximity of these vessels and the diffusion coefficient.

As early as 1957, Davies and Bronk showed such a variability in the visual system of the cat (Davies and Bronk 1957) as can be seen in the Illustration 32. Locations closer to major vessels have higher levels of oxygen while parenchymal tissue located at a distance from blood vessels have lower tensions of oxygen (Sharan et al. 2008).

It has been shown that myelinated white matter has lower levels of basal oxygen tension compared to gray matter (Feng et al. 1988).

As can be assessed from the distribution of vessels (see Table 2) and the consumption of neuronal compartments (see Table 1), the basal oxygen level is tightly regulated to avoid hypoxic regions in regions of intense activity.

2.5.2 Transient oxygen consumption in the brain

The development of fMRI in the last 20 years has brought the field of brain oxygen consumption into the spotlight (for a good review, see (Buxton 2001)). Several studies have shown that prior to the widely described positive and large BOLD signal (see chapter 2.4.5), there is a small decrease in oxyhemoglobin which can be observed (Ernst and Hennig 1994). It was termed “the initial dip” in reference to its appearance in the early phase of BOLD responses. It reflects the local increase in oxidative activity due to neuronal activity. Nevertheless, the acceptance of such an event was controversial because some research groups failed to observe this (Lindauer et al. 2001). PET studies also showed that glucose consumption was largely in excess of oxygen consumption as we mentioned previously (see chapter 2.2.5). In addition a study from Lenigert-Follert et al., using direct oxygen measurements didn't show any initial decrease in oxygen following electrical stimulation of the cortex. However they routinely used combined electrodes for oxygen and microflow measurements whose diameter was 2 mm (Leniger-Follert, Wrabetz, and Lubbers 1976).

As a consequence, direct measurements with improved spatial and time resolution were required to establish a more precise picture of the evolution of the oxygen field following neuronal activation. Recent insight has come from polarographic, spectrophotometric, and fluorescent methods.

Due to the fact that the controversy started in the visual cortex (P T Fox et al. 1988), most recordings were performed in this particular area. Grinvald et al. were particularly active on this regard. They showed using both spectroscopic (Malonek and Grinvald 1996) and fluorescent methods (Vanzetta and Grinvald 1999) the appearance of an initial decrease in oxygen tension occurring rapidly after visual stimulation in the cat.

As yet, no combined recording of local neuronal activity and oxygen partial pressure had been done to show that the oxygen decrease was restricted to the area

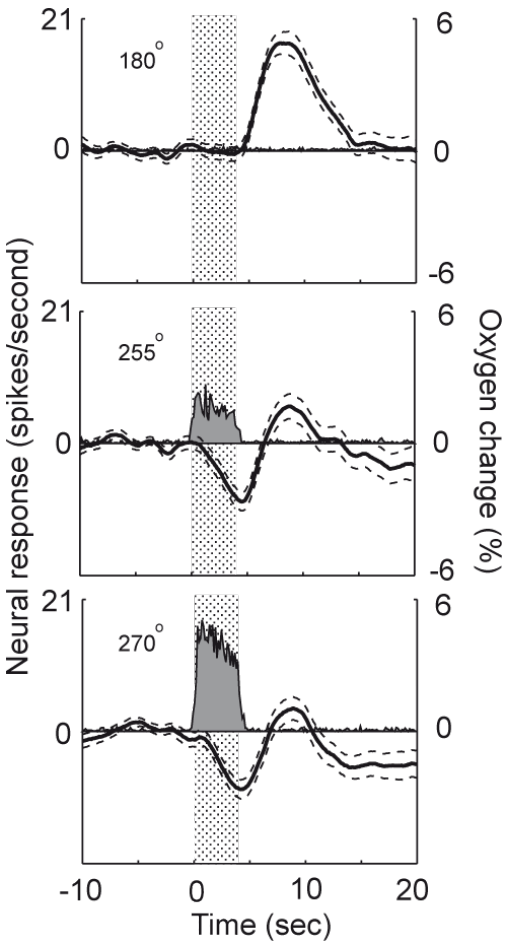

Illustration 33: Oxygen and Field Potential in responses to different visual stimuli (different angles of light bars on the eye of the cat) in the visual cortex (Thompson et al., 2003)

of neuronal activity. This was a particular importance since some groups had suggested that the initial dip in oxygen would be a better indicator of neuronal activity than the large increase in blood flow. Thompson answered this question in two important publications (Thompson, Peterson, and Freeman 2003; Thompson, Peterson, and Freeman 2005). Since Thompson et al. provided direct recordings of oxygen in response to physiological stimulation, they closed the debate on the “elusiveness” of the initial dip (Buxton 2001).

Nevertheless, some questions remained on the precise neuronal origin of this increase in oxidative metabolism. Offenhauser et al. showed in the cerebellum that the postsynaptic compartment of the climbing fiber/purkinje cell synapse was responsible for most of the oxygen consumption triggered by electrical stimulation of the inferior olive (Offenhauser et al. 2005). Viswanathan et al. confirmed this result by showing that changes in oxygen concentration were better correlated with synaptic rather than spiking activity (Viswanathan and Freeman 2007). These results paralleled the distribution of mitochondria in the different neuronal compartments (Wong-Riley 1989).

The synaptic origin of oxygen consumption required confirmation through studies in other areas of the brain. We will see that the olfactory bulb follows the same rule.

2.5.3 Absolute oxygen consumption in the brain

While transient oxygen consumption has been examined through a variety of techniques, most of these techniques have only looked at changes from the baseline consumption.

Hence measuring absolute oxygen consumption is a more difficult task because one needs to record the oxygen level of the tissue and the oxygen content of the blood simultaneously. For this reason, polarographic electrodes, while they give quantitative values of oxygen levels, can't provide direct access to absolute oxygen consumption. Some studies used modeling to fill the lack of data (Caesar, Offenhauser, and M. Lauritzen 2008); other groups have tried to extract the absolute consumption from responses to ischemia (Leniger-Follert 1977).

Some fMRI studies have used modeling combined with CO_2 responses to extract relative change in $CMRO_2$ (Davis et al. 1998). However, no absolute measurements are possible using fMRI in isolation.

PET also relies on an indirect measurement of $CMRO_2$ (M A Mintun et al. 1984) as described previously (see chapter 2.4.4). Nevertheless, as long as the underlying assumptions are correct, PET provides absolutes values.

To date, the most direct method to extract absolute brain oxygen consumption was proposed fifty years ago by Kety and Schmidt (Kety and Schmidt 1945). The principle is to determine cerebral blood flow by using the distribution of an inhaled inert gas between the blood and the brain tissue (Fick principle). If arteriovenous oxygen difference is also measured, $CMRO_2$ can be precisely

measured. The $CMRO_2$ of the rat brain at rest is 7.6 ml $(100g)^{-1}$ min^{-1}, which is about twice the value for the human brain (Nilsson and Siesjö 1976).

2.5.4 Oxygen extraction and diffusion in the brain

Diffusion processes are slow by definition. They rely on the passive movement of molecules across matter. As oxygen is a small molecule, it freely moves across cell membrane without the need of a transporter. A good order of magnitude for the diffusion constant of oxygen in the brain is 2000 µm2 per second (Roh, Goldstick, and Linsenmeier 1990), close to the value for water. So in one second, oxygen migrates over 40 µm. As we have already shown, the brain vascular anatomy is very dense. We will see that the average distance from vessels to neuronal tissues is between 10 and 30 µm. As a result, vasculogenesis and angiogenesis appear to form a network of capillaries which ensures that neurons have access to blood with a mean delay of 0.5 seconds.

Understanding oxygen diffusion in the brain is an important matter. However, due to the complexity of neuronal tissue and the difficulty to extract the required parameters, this undertaking requires extensive modeling. The history of oxygen extraction began nearly one century ago with the work of Krogh (Krogh 1919). Krogh built a simple steady state diffusion model from an infinite cylinder to account for the increase diffusion surface of capillaries upon activation. Much progress has been made since Krogh received his Nobel Prize on capillaries' recruitment in muscles in 1920.

Most insights on oxygen diffusion in microcirculation come from experiments conducted in the periphery, particularly in the cremaster muscle (Tsai, P. C. Johnson, and M. Intaglietta 2003). Its simpler 2D geometry facilitates the examination of radial oxygen gradients. We must remember that oxygen consumption at rest in muscles and in the brain are very different. A typical value for resting skeletal muscle is 0,4 ml $(100g)^{-1}$ min^{-1} which is about ten times less than the resting brain (see chapter 2.5.3). This value can increase substantially upon activation. Hence the brain and muscles must be regulated differently even though it is likely that there are similarities in the properties of their regulation.

- **Arterioles contribution to tissue oxygen level.**

While only capillaries were assumed to deliver oxygen in Krogh studies, Duling et al. showed that arterioles significantly contribute to tissue oxygen level both in muscles (B R Duling and Berne 1970) and in the cat's brain (B. R. Duling, Kuschinsky, and Wahl 1979). The contribution of arterioles to tissue oxygen level can exceed 50% in muscles while, in the brain, the tissue's high metabolic rate reduces it to less than 20% (Sharan et al. 2008).

- **Hemoglobin-Oxygen dissociation curve**

Oxygen in the hemoglobin is in permanent equilibrium with the plasma

according to the famous oxygen dissociation curve of hemoglobin (see Illustration

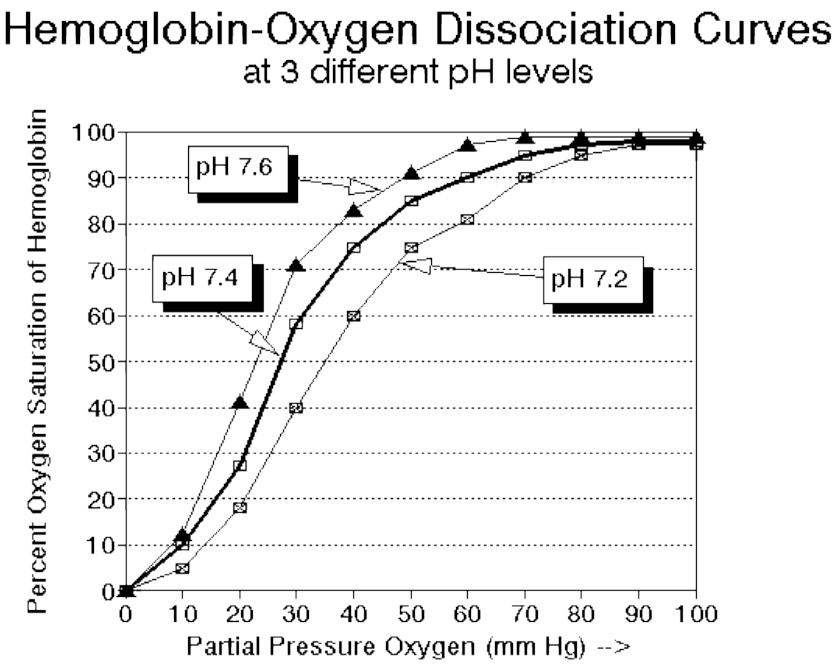

Illustration 34: Oxygen dissociation curve. Increased CO_2 level in the blood decreases pH and favors oxygen release from hemoglobin. (reproduced from http://www.marietta.edu/~mcshaffd/aquatic/sextant/respire.htm)

34) first described by Hill (Barcroft and Hill 1910). The dissociation of oxygen from hemoglobin is very fast, in the order of 50 ms (Sirs 1967) which means that equilibrium is very rapidly reached. This is essential since blood speed in capillaries is about 0.5 mm/s. As a result, an erythrocyte spends about 200 ms in a 100 µm long capillary (typical length in a glomerulus) and has enough time to release its oxygen.

- **Erythrocyte-associated transients**

Capillaries are small vessels whose diameter is around 6 µm. As a result, red blood cells pass through capillaries one by one. Based on this and the fast saturation of hemoglobin, one can predict that oxygen profile along the small vessels is not a continuum but is rather discrete. The term “Erythrocyte-Associated Transients” (EATs) was proposed by Hellums et al. 30 years ago (Hellums 1977). Recording such events requires very fast techniques and it's only recently that the existence of EATs was confirmed in the mesentery, by the use of phosphorescence techniques (Golub and Pittman 2005). In the brain, to my knowledge, no studies have been conducted on EATs so far. This result is of

importance because in a discrete model of oxygen diffusion, the effective capillaries' area is only the surface in contact with erythrocytes.

- **Oxygen diffusion modeling**

Nowadays the trend is to draw models of realistic 3D vascular trees as well as the intra-vascular heterogeneous distribution of oxygen between erythrocyte and plasma. Most modeling on large scale vascular networks have been conducted in steady state conditions (Secomb et al. 2000). Recent models are highly complex and rely on an extensive number of parameters (Tsoukias et al. 2007). In the meantime, very few studies have tried to extract the oxygen diffusion constant in the brain. As a result it has been necessary that models of oxygen diffusion have relied on an estimate of this parameter (Secomb et al. 2000). Moreover, its precise value probably depends on the composition of the tissue (for instance between gray and white matter).

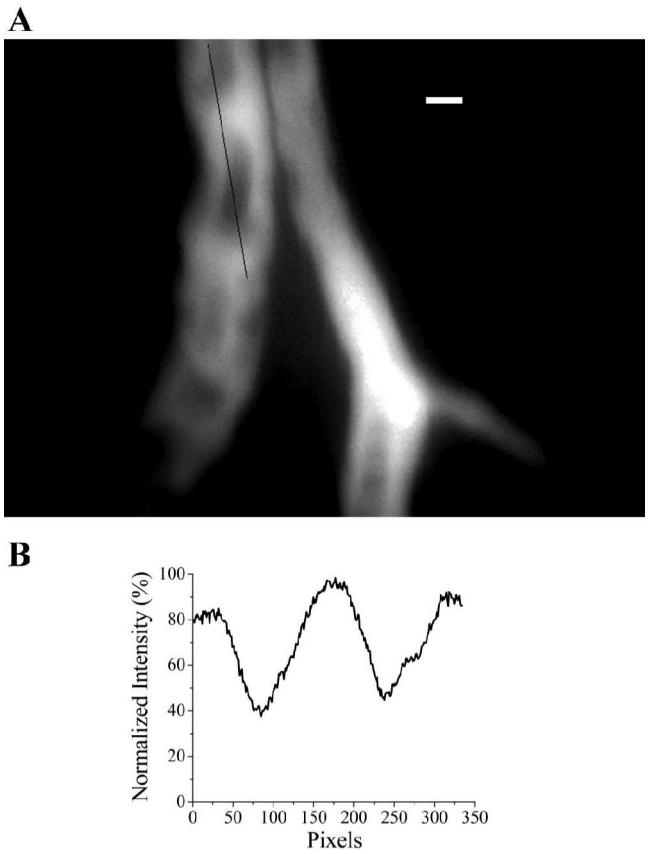

Illustration 35: A. phosphorescence image of a capillary in rat mesentery. Red blood cells (RBCs) appear as dark spots because they contain no phosphor. Bar 5 µm. B. Photometric profile made along the line drawn on the capillary in A. Phosphorescence intensities are expressed as percentages of the maximal value. (Golub and Pittman, 2005)

As a result, there is a clear lack of data on both the precise vascular anatomy and the oxygen diffusion parameters.

Methods & Technical considerations

Chapter 3 : Methods & Technical considerations

Working *in vivo* is a rather technical challenge in many respects. It is therefore essential to take the time to give quite an extensive note on some of the technical constraints we had to face while conducting the experiments. However, I am not going to detail the complete methodology in the thesis. For an extensive description you may consult the methods chapter of my publications. However, I will take the opportunity to introduce some aspects of the experiments which did not lend themselves for inclusion in a paper, but are, nevertheless, crucial pieces of knowledge to pass on. I will also detail some of the technical tools I developed during this thesis.

3.1 Two photon imaging

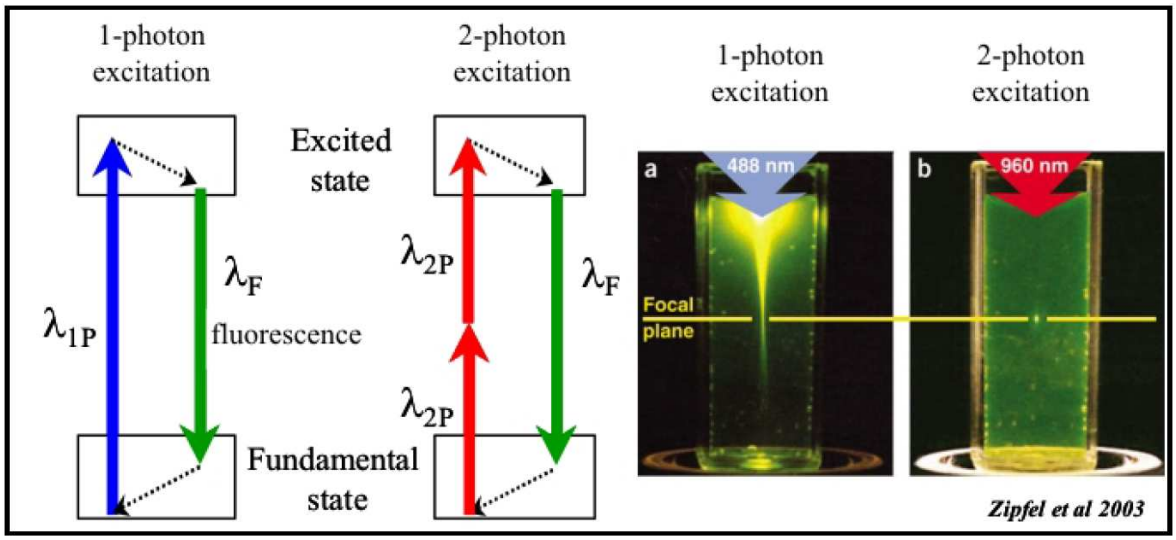

Illustration 36: A comparison of single photon and two-photon excitation (Zipfel, Williams and Webb 2003)

Current technologies to image *in vivo* now give the opportunity to visualize both the local anatomy and follow brain activity. Among the available techniques, two photon imaging was chosen. This technique has now been widely accepted and used in Neuroscience. It is therefore not necessary to give a detailed description. Instead, I will introduce its general principles and point out some of its technical limitations and their consequences for our experiments. For a more extensive description, I would recommend the review by Zipfel (Zipfel, Rebecca M Williams, and Watt W Webb 2003).

3.1.1 Basic principles

Two photon imaging was developed in 1990 by Watt Webb's group (W Denk, Strickler, and W W Webb 1990) as a dramatic improvement to fluorescent microscopy. They took advantage of a non-linear effect of light absorption. When photons from a laser source are sufficiently concentrated (both in time and space), the fluorescent molecule is excited by the simultaneous absorption of two photons (See Illustration 36). This is why in two photon microscopy, in contrast to confocal microscopy, fluorescence only occurs at the focal point of the objective (see Illustration 36). As a result, it allows the experimenter to focus, in depth, on a very precise volume of tissue. This enabled us to follow neuronal activity through calcium imaging using calcium sensitive dyes as well as blood flow.

3.1.2 Imaging the brain

The main limitations of the "two photon imaging" technique relates to the

strong light scattering in superficial tissues, which subsequently causes a reduction in spatial resolution, low contrast, and small penetration depth (Martin Oheim et al. 2001). As a result, we had to gain as much access as possible to the neuronal tissue. This simply means that it was necessary to open the skull.

This had several important consequences. Firstly, we had to use anesthetics to perform the surgery and ensure the animal remained still under the microscope. This is a major point since anesthetics are, by their intrinsic nature, modifying brain activity from its normal state. Secondly, drilling a hole in the rat skull in good conditions takes quite some time and occasionally induce some extensive bleeding, which greatly reduces the success rate of the experiment. This last point is one of the reasons “brain slices” still remains the main technique used today in Neuroscience.

3.1.3 Movements

The neuronal soma has a typical size of approximately 10 µm and brain capillaries are between 2 and 6 µm in internal diameter. Consequently, one of the major issues we had to face was the mechanical stability of the brain, to enable a clear resolution up to the micrometer. Since the brain itself moves with heart beat and breathing, it was necessary to make use of a simple technical trick to ensure the brain remained completely stationary. Agar or agar agar is a gelatinous substance derived from seaweed with a refractive index close to that of glass, when it is dissolved into water. Hence we could stabilize the brain with a 3% agar solution deposit onto the brain and image through. In these conditions, we were able to sufficient stabilize the brain to enable imaging of single capillaries.

However, there was one major drawback with this technique, namely that the brain was no longer accessible to pharmacology once the agar was applied. It was therefore necessary to deliver the drug (or multiple drugs) through a patch pipette by local pressure injection.

3.1.4 Phototoxicity

“Two-photon imaging” *in vivo* requires the use of a minimum level of Laser Power to face with the strong tissue scattering of both laser excitation and fluorescence emission. To circumvent these problems, the imaging apparatus was designed so that, at least, 250 mW of laser power was available at the end of the optical path. We routinely use between 50 and 150 mW at the surface to image blood flow in capillaries or calcium in axons terminals at 100-200 µm depth. Predicting the exact value of light intensity onto the fluorophore is a complex problem, due to the previously mentioned tissue scattering. Over-illumination clearly led to phototoxicity, either through heating of dye bleaching. Phototoxicity is greatly reduced in “two photon imaging” due to the improved specificity in location of the excitation and the higher wavelengths involved. Even so, it still can harm the tissue as pointed out by Zipfel et al. (Zipfel, Rebecca M Williams, and Watt W Webb 2003). Some recent studies decided to use these effects to do some microsurgery on cells (Mejia-Gervacio et al. 2007) but for our experimentation we

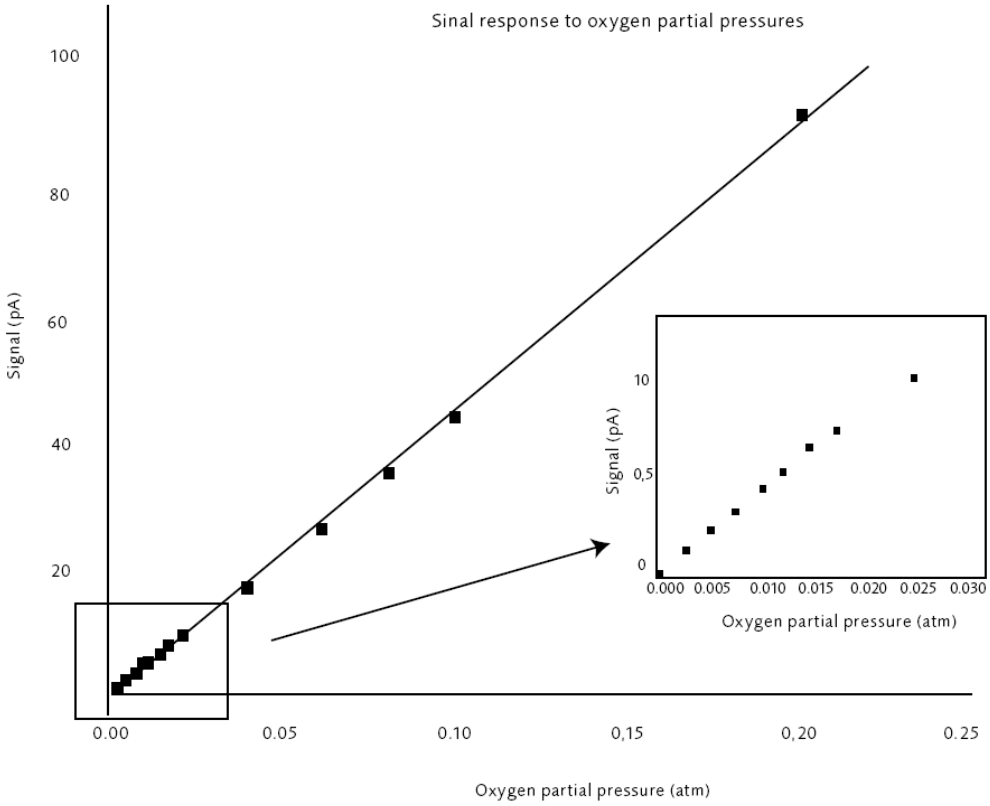

Illustration 37: Oxygen calibration curves (From Unisense)

wanted to avoid this phototoxicity as much as possible. We therefore limited our illumination protocols to 20-30 s maximum per trial with an inter-trial interval of 2 minutes minimum. Under these conditions, risk of phototoxicity was greatly reduced.

3.2 Oxygen recordings

Since we wanted to have both a direct access to neuronal tissue oxygen level as well as a very sharp time resolution, we opted to use Clark oxygen electrodes among all the available techniques (see chapter 2.4).

3.2.1 Theory of oxygen Clark electrodes

Oxygen is an oxidant so it can be readily involved in redox reactions. The underlying reactions involved in the Clark electrodes are the followings:

$$Cathode: O_2 + 2\mathrm{H}_2O + 4e^- \rightarrow 4\mathrm{OH}^- \qquad (2)$$

$$Anode: 4\mathrm{Ag} + 4\mathrm{Cl}^- \rightarrow AgCl + 4\,e^- \quad (3)$$

To facilitate this reaction, it is necessary to maintain a voltage between the anode and the cathode of -0.8 V. If this is done, the current is big enough to be measured using a picoamperometer. This current is proportional to the quantity of oxygen at the electrode tip (see Illustration 37) so that calibrating the electrode prior to every experiment allows the recording of quantitative values of oxygen partial pressure.

3.2.2 Practical considerations

We decided to benefit from the experience of the Danish company called Unisense and bought the electrodes from them with a special request: to add fluorescein within the electrode. This ensured that the electrode tip could be seen under the two photon microscope. However, from my experience, and because the extreme tip of the electrode could be seen in the red channel of our microscope, I suspect the membrane tip to be autofluorescent. This turned out to be advantageous because it helped locate the electrode tip within a stained neuronal tissue.

- **Laser scanning effect**

Combining oxygen recording with two photon microscopy had never been done and we were surprised to see that laser scanning had an effect on the oxygen electrode (see Illustration 38). The effect was variable, but generally, laser scanning onto the electrode introduced high frequency noise correlated with the scanning speed. The closer to the electrode the scan was performed, the bigger the effect was. This effect was direct because it was still present in water and when the electrode polarization was set to 0V (therefore stopping oxygen detection).

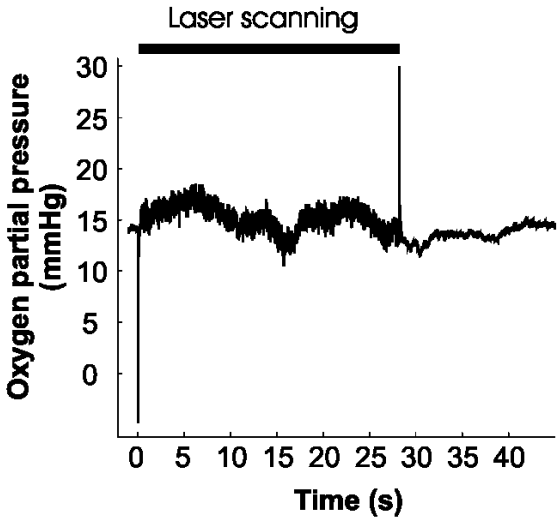

Illustration 38: Two-photon scanning has an effect on the current recorded in the brain by our oxygen electrode. An example of this effect is shown here.

To be sure that we could perform oxygen low frequencies recordings during laser scanning, we measured the oxygen consumption triggered by an odor in the Glomerular Layer before and during laser scanning. As can be seen in the Illustration 39, there was no change in the initial slope of the oxygen responses.

This direct effect could be due to the charging of the cathode via interaction with photons. Evidence of this interaction can be seen through the fact that the cathode is made of gold and Climent et al. recently reported (Climent, Coles, and

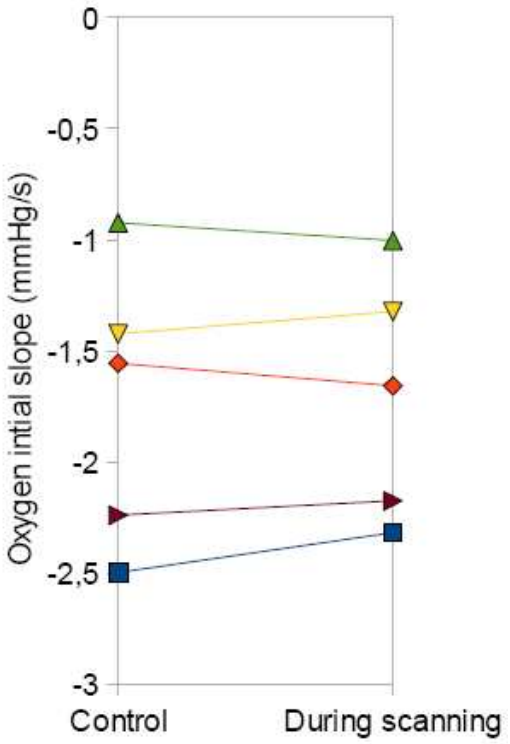

Illustration 39: Control of the effect of laser scanning on the oxygen responses. The initial slope measures the amplitude of the response to odor stimulation.(N=5 rats).

Compton 2001) that a laser could induce current transients when applied to a gold single crystal electrode.

- **Consumption of oxygen by the electrode**

One important point is that these electrodes do consume oxygen. It is therefore important to know whether this could affect our recordings. A typical value for the consumption of these electrodes (obtained from Unisense website) is 2.5 × 10^{-16} moles of oxygen per second. Oxygen basal consumption in the olfactory bulb has already been precisely estimated (Nawroth et al. 2007) to be approximately 100 µmol per liter of tissue per second. For a glomerulus with a diameter of 100 µm, the appropriate conversion will give 10^{-13} moles of oxygen per second. Hence our electrode consumes about 500 times less oxygen than a glomerulus which means we can safely rely on it and that it won't induce hypoxia by itself.

- **Effect of opening the skull**

Because the oxygen level in the air is ten times the level in the brain, we could expect that opening the skull would be a major bias on the basal level of oxygen in the brain. Indeed, a previous study showed that the oxygen level is significantly affected by the size of the craniotomy between 0 and 500 µm depth (Feng et al. 1988). However, thanks to the targeting algorithm, we deposit a thick layer of Agar (approximately 500 µm thick) onto the brain at the very beginning of our experiments. Since oxygen diffusion in agar, in a first approximation, is closed to oxygen diffusion in water (D≈2000 $\mu m^2.s^{-1}$), as well as diffusion in the brain. We can infer that the brain is exposed to the air only briefly during our experiments.

3.3 Targeting pipettes using a two photon microscope

Since we wanted both to image neuronal tissue at the micrometer resolution and bring several electrodes at very precise locations, I had to deal with a thick layer of Agar deposit onto the brain. Both the thick Agar layer and the dense blood

vessel network at the surface of the brain made it impossible to move the electrode laterally within the tissue (which is done routinely in slice preparation). One solution would have been to deposit the Agar after the pipettes but in some experiments the Agar weight was enough to move the brain vertically (therefore

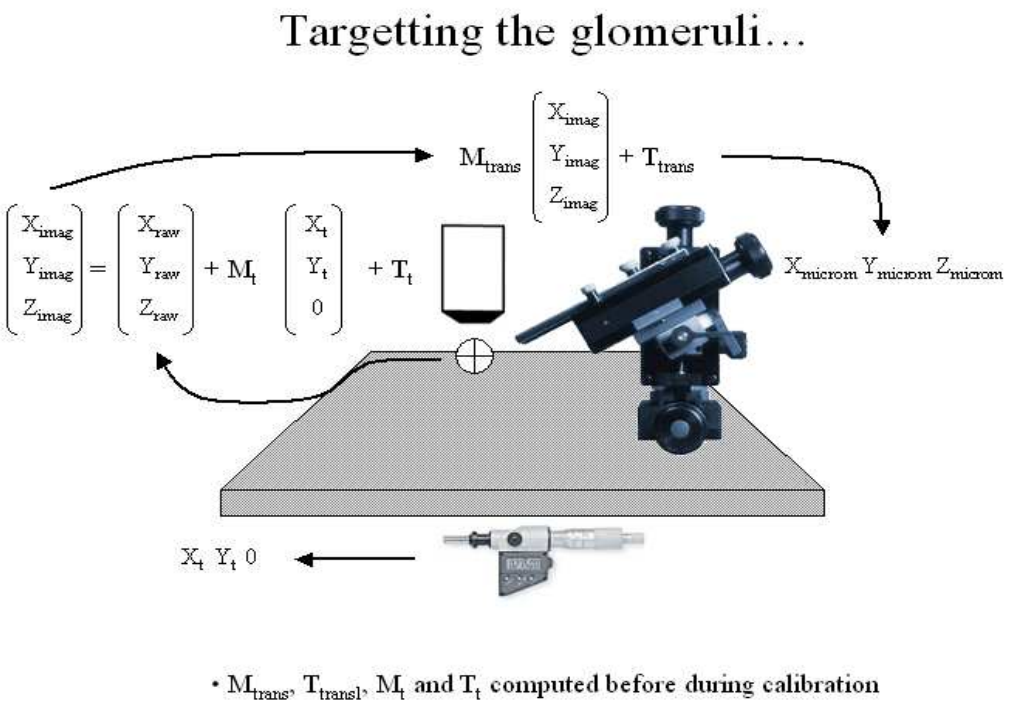

Illustration 40: Mathematical principles underlying the targeting algorithm

ruining several experiments).

Instead I decided to design a targeting algorithm to bring the tips of the electrodes to previously chosen locations in the brain directly, passing through the whole layer of Agar and neuronal tissue. The principle is depicted in the Illustration 40. Briefly, one can relate the chosen target $\begin{pmatrix}X_{raw}\\Y_{raw}\\Z_{raw}\end{pmatrix}$ to the coordinates to apply to the micromanipulator $\begin{pmatrix}X_{microm}\\Y_{microm}\\Z_{microm}\end{pmatrix}$ using simple linear algebra.

Indeed given the coordinates of the moving table $\begin{pmatrix} X_t \\ Y_t \\ 0 \end{pmatrix}$ measured through numerical vernier, we have the following equation:

$$\begin{pmatrix} X_{microm} \\ Y_{microm} \\ Z_{microm} \end{pmatrix} = M_{trans} \times \begin{pmatrix} X_{raw} \\ Y_{raw} \\ Z_{raw} \end{pmatrix} + M_{trans} \times M_t \begin{pmatrix} X_t \\ Y_t \\ 0 \end{pmatrix} + M_{trans} \times T_t + T_{trans} \quad (4)$$

where M_{trans} , T_{trans} , M_t and T_t are the geometric transformations (rotation, scaling and translation) required to change from the imaging $\begin{pmatrix} X_{raw} \\ Y_{raw} \\ Z_{raw} \end{pmatrix}$ to the micromanipulator coordinate system $\begin{pmatrix} X_{microm} \\ Y_{microm} \\ Z_{microm} \end{pmatrix}$.

If we calibrate M_{trans} , T_{trans} , M_t and T_t before the experiments, it is then possible to compute on line the exact coordinates to apply to the micromanipulator. In practice, this proved very practical and greatly enhanced the success rate of the experiments, since we were then able to bring two electrodes directly within few µm without removing the Agar layer.

3.4 Calcium recordings

Recording calcium from olfactory receptors axons was first accomplished by Wachowiak et al. in a very interesting series of publications on the mouse (M. Wachowiak and Shipley 2006; Matt Wachowiak et al. 2005; McGann et al. 2005; Matt Wachowiak and L. B. Cohen 2001; Spors et al. 2006; Pírez and Matt Wachowiak 2008; Matt Wachowiak and Lawrence B. Cohen 2003). However it's only recently that this technology was transferred to the rat (Verhagen et al. 2007) and only on a very small number of animals (n=7). In our hands, during our experimentation, loading the olfactory receptors neurons with Oregon Green BAPTA-1 488 dextran 10000 was highly variable compared to the non BAPTA version. I confirmed this result with Dr. Verhagen during an informal discussion. Moving to Calcium Green-1 reduced this variability drastically and so it may be possible that Oregon Green itself actually had a toxic effect on the olfactory receptor. This could be checked via electron microscopy, as Friedrich did for the zebrafish (Friedrich and Korsching 1997).

3.5 3D reconstruction of blood vessels from two photon stacks

When I started my thesis, there was no easily accessible reconstruction algorithm for two photon stacks to give a very precise reconstruction of a vascular tree. However, intense research is currently ongoing in the field of MRI on this subject and I could benefit from their experience by transferring the technologies developed in MRI to reconstruct vessels.

There is now some software available which performs this task very proficiently, such as Amira from Visage Imaging (http://www.visageimaging.com/).I would therefore recommend for future research to use these solutions instead of starting from the fundamental concepts as I did, due to the complexity of the task.

However, the design of this algorithm within Matlab made it possible to perform some very precise quantification on the anatomy of the vessels and its relation to the glomerular geometry which had never been done. Here, I will briefly introduce the underlying principles of the algorithm and illustrate them with a simple example.

The principle of reconstruction is based on the Fast-Marching Algorithm which was first developed by Sethian (Sethian 1999) and then further improved by Deschamps (Deschamps and L. D. Cohen 2001) during his thesis at Philips MedISys. I had to modify it to account for some two photon particularities. For a full description of the algorithm, which is beyond the scope of this thesis, I would recommend looking at the references mentioned above and at the thesis manuscript of Thomas Deschamps (http://math.lbl.gov/~deschamp/html/phdthesis.html).

3.5.1 Principle

The starting idea is both simple and elegant. Let us consider a pile of pictures as a new material. It is an artificial material in which we can start an artificial

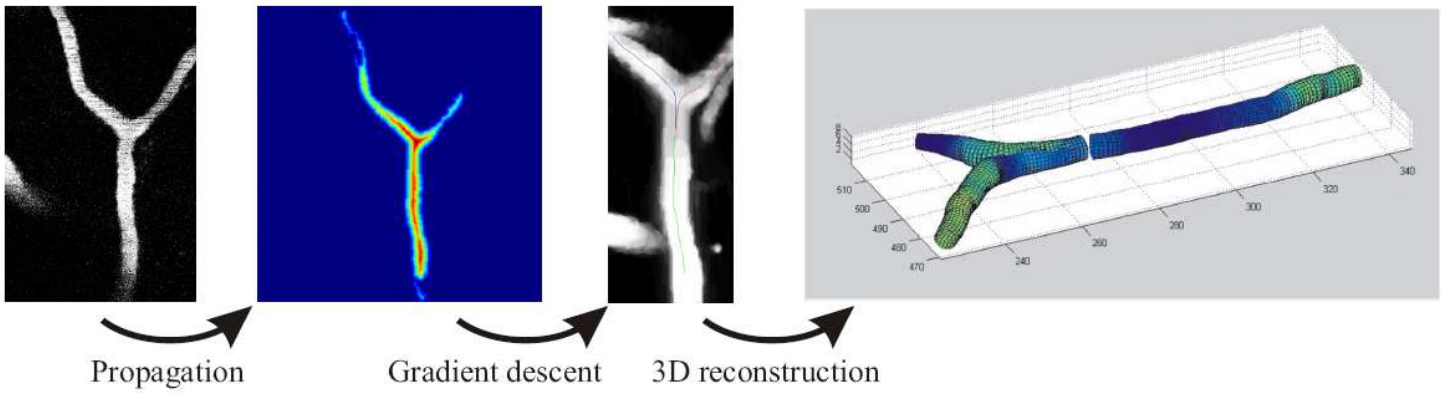

Illustration 41: Steps involved in the Fast-Marching algorithm

electromagnetic waves propagating along the pixels. If we choose the refractive index appropriately then the wave will embrace some of the heterogeneity of our stack. This idea is particularly efficient for blood vessels imaged with the two photon microscope. Evidently, vessels loaded with a dye are highly fluorescent, whereas the rest of the tissue is a dark background (when no fluorescent dyes are present in the cells). Therefore, if we set a low refractive index within the white areas of the vessels, the wave will completely follow the blood vessels anatomy. Due to underlying mathematical properties, electromagnetic waves always follow the shortest path in matter. Consequently, by using the propagation of the artificial wave, one can extract information on the shortest path to go from one part of a vessel to the other, i.e. the capillary's center.

3.5.2 Steps involved

The algorithm can be divided into several steps as follow:

- A two photon stack is acquired directly *in vivo* as shown in the Illustration 41. The stack is converted to a 3D array of refractive indices.
- A starting point is then chosen in the center of a blood vessel to reconstruct the vessels connected to this point.
- The propagation is initiated from this point. After a predefined number of points has been reached, it is stopped and the energy requirement to propagate from the starting point to every point is extracted. This is the second figure in the Illustration 41. From this 3D array, end points of capillaries are automatically segmented and a propagation path is computed. This is the third figure of Illustration 41. For each point of the trajectory, the radius of the vessel is extracted using a simple local binarization which gives the last picture of Illustration 41.

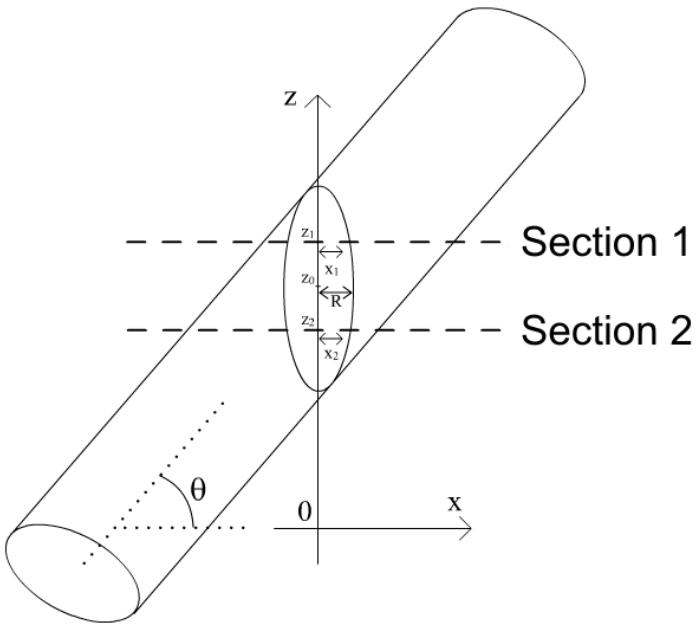

Illustration 42: A schematic to show how it is possible to extract the radius R and the central position z_0 of a vessel imaged at different chapters

3.5.3 Correcting for two photon point spread function

The main difference

between MRI pictures and two-photon stack is due to the difference between the xy resolution (about 0.2-0.3 µm) and the z resolution (about 2 µm). This is due to the fact that the point spread function of two photon imaging is extended along the z direction. In comparison to MRI, where the resolution is the same in every direction, it can raise problems.

To correct for this, it is possible to use a simple trick related to the fact we are looking at blood vessels, which are fundamentally tubes.

As shown in Illustration 42, if we take several images of a tube at different depths (Section 1, 2 and so on), the radius measured at every chapter x_1 and x_2 is related to the true radius R through the angle θ and the true center of the vessels z_0. The involved formula is the following:

$$x^2+(z-z_0)^2\sin^2\theta=R^2 \tag{5}$$

which after the appropriate manipulation leads to:

$$\frac{x_1^2-x_2^2}{z_1-z_2}=-(z_1+z_2)\sin^2\theta+2z_0\sin^2\theta \tag{6}$$

So if we measure x_1,x_2,... at several known depths z_1,z_2,... it is possible to extract the angle θ, the true center z_0 and the radius of the vessel at this particular

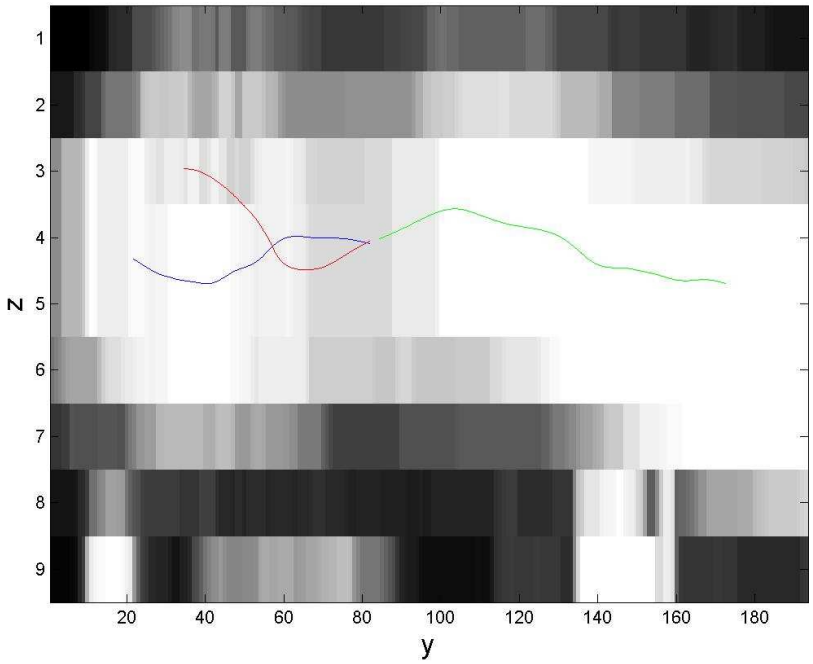

Illustration 43: Reconstruction of the Illustration 41, projected along the YZ planes.

position. As a result we use the very precise resolution along the x,y axis to precisely measure the z position of the vessel. This final step was performed to recenter all the paths along the z direction and to extract the true diameter of blood vessels. The result of this for the Illustration 41 is presented in the Illustration 43, note the significant difference between the precision of the path along z compared to the pixel size.

3.5.4 Large scale reconstruction

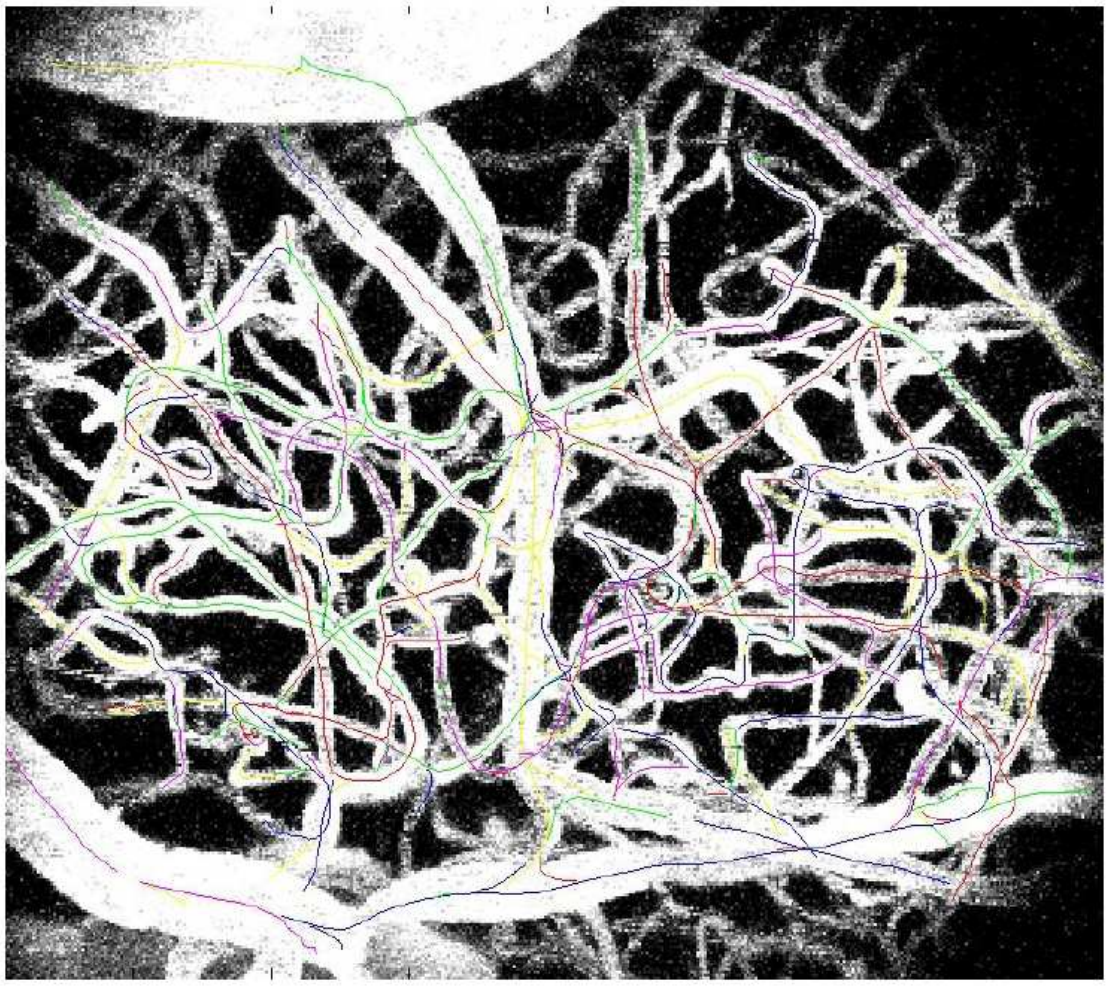

Illustration 44: Partial reconstruction of a network of vessels - The different reconstructed segments are superimposed on a projection of the stack along the z direction.

In Illustration 44, you can see a partial reconstruction of a bigger stack of vessels obtained in vivo. Each color denotes a different branching which has been

automatically segmented. Now, because the Glomerular Layer is also stained, we can also reconstruct the glomeruli volume and compare the densities of vessels in the different neuronal compartments. These results are included in the results chapter of the thesis.

Results

4.1 Oxygen consumption in the olfactory bulb

4.1.1 Introduction

Emmanuelle Chaigneau, previously a PhD student in the lab, has shown that odors elicit blood flow responses in the Glomerular Layer (E. Chaigneau et al. 2003). Using two photon microscopy, she was able to record from single capillaries in the Glomerular Layer and characterize these responses in time and space (see Illustration 45). She also showed qualitatively that the nerve layer was devoid of capillaries as opposed to the Glomerular Layer.

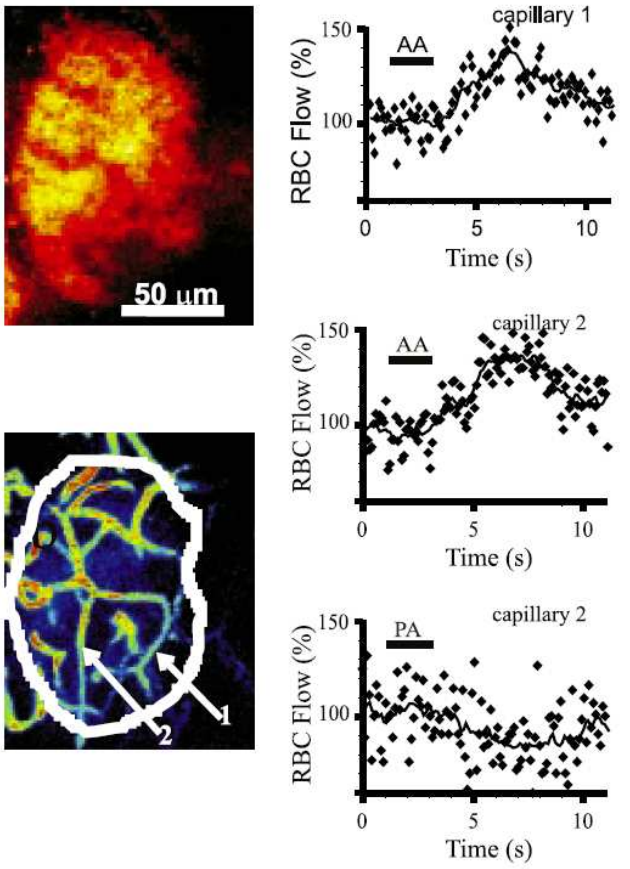

Illustration 45: Odor elicits blood flow responses in single capillaries. The two pictures on the left show the glomerulus boundaries (top) and the vascular anatomy (bottom). Blood flow in capillaries 1 and 2 are shown on the right. (Chaigneau et al., 2003)

When I joined the lab, she was working on the pharmacology of these responses. I participated in these experiments to show that blood flow responses require postsynaptic activation in the Glomerular Layer (E. Chaigneau et al. 2007). This publication is included in the Annex at the end of this thesis manuscript.

My thesis subject was to try to understand why the nerve layer was devoid of capillaries. We decided to perform oxygen recordings in both layers to see whether this difference could be due to different oxygen consumption in response to odors.

I also decided to obtain quantitative measurements of capillaries density in order to compare the energy needs of the olfactory bulb with other brain regions.

Moreover, when we started this project, Thompson had just shown that physiological stimulation triggers a fast transient decrease in oxygen at the location of the increased neuronal activity (Thompson, Peterson, and Freeman 2003). We wanted to see whether this applies to the olfactory bulb and particularly

to the Glomerular Layer.

The results confirmed our expectations and are included in the following publication which is currently submitted to PLoS.

First article

Chapter 4.1 : Oxygen consumption in the olfactory bulb

Contrasting changes in tissue oxygen during action potential propagation and synaptic transmission upon odor stimulation

Abbreviated title: oxygen consumption in the nerve and glomerular layers

Jérôme Lecoq[1], Pascale Tiret[1], Marion Najac[1], Gordon M. Shepherd[2], Charles A. Greer[3] and Serge Charpak[1]

[1]Institut National de la Santé et de la Recherche Médicale (INSERM), U603, Paris 75006, France; Centre National de la Recherche Scientifique (CNRS), UMR 8154, Paris 75006, France; Laboratory of Neurophysiology and New Microscopies, Université Paris Descartes, Paris 75006, France.

[2]Department of Neurobiology, Yale University School of Medicine, 333 Cedar Street, New Haven, CT 06520

[3]Departments of Neurosurgery and Neurobiology, Yale University School of Medicine, 333 Cedar Street, New Haven, CT 06520

Corresponding author: Serge Charpak
INSERM U 603, Laboratory of Neurophysiology
45 rue des St Pères, 75006 Paris, France
Tel 33 1 42 86 41 48
Fax 33 1 42 86 41 51
E-mail: serge.charpak@univ-paris5.fr

Keywords: two-photon microscopy, olfactory bulb, neurovascular coupling, field potential, oxygen consumption, blood flow

Acknowledgments

We thank Etienne Audinat, Didier De Saint Jan and Janna Nawroth for their critical comments. Support was provided by the Institut National de la Santé et de la Recherche Médicale (INSERM), the Ministère de l'Education Nationale de la Recherche et de la Technologie (MENRT, NIC0025), the Centre National de la Recherche Scientifique (CNRS), the Fondation pour la Recherche Médicale (ICP20001222128), the Région Ile de France (Sesame program), the Fondation Bettancourt Schueller, the Human frontier science program organisation (HSFPO) and NIH-NID. Jérôme Lecoq was supported by a fellowship from the Fondation pour la Recherche Médicale (FDT20070910324) and Pascale Tiret by a fellowship from the Association Française contre les Myopathies (12411).

Abstract

The relationship between metabolism of neuronal activity, microvascular organization and blood flow dynamics is critical for interpreting functional brain imaging. Here we used the rat dorsal olfactory bulb as a model to determine *in vivo* the correlation between action potential propagation, synaptic transmission, oxygen consumption and capillary density during odor stimulation. We find that capillary lumen occupies about 3 % of the glomerular volume, where synaptic transmission occurs, and only 0.1 % of the overlying nerve layer. In glomeruli, odor triggers a local early decrease in tissue oxygen partial pressure that results principally from dendritic activation rather than from firing of axon terminals, transmitter release or astrocyte activation. In the nerve layer, action potential propagation does not generate local changes in tissue oxygen partial pressure. We conclude that capillary density is tightly correlated with the oxidative metabolism of synaptic transmission, and suggest that action potential propagation operates mainly anaerobically.

Introduction

The olfactory bulb (OB) is a unique model for investigating *in vivo* the correlation between vascular density, synaptic transmission, metabolism and neurovascular coupling (Shepherd and Charpak, 2008). Dorsal glomeruli can be easily imaged *in vivo* with two-photon laser scanning microscopy (TPLSM), a technique that allows one to characterize vascular architecture with a micrometer spatial resolution and to measure cerebral blood flow (CBF) and neuronal activity (Chaigneau et al., 2003;Chaigneau et al., 2007) with a millisecond time resolution. The olfactory bulb has been well studied with respect to its synaptic organization (Shepherd et al., 2004).The superficial nerve layer is composed of glial cells and unmyelinated axons from olfactory sensory neurons (OSNs). The underlying layer is composed of glomerular modules in which OSN terminals synapse onto juxtaglomerular and principal cell dendrites. These two layers thus sharply differ in their cellular contents and can be expected to show differences in metabolism.

Studies investigating various aspects of metabolism in the two layers have reported contrasting results. Early 2DG studies showed high energy demand in both glomeruli and in the adjacent nerve layer (Greer et al., 1981;Sharp et al., 1975;Sharp et al., 1977;Sokoloff et al., 1977). Early fMRI studies showed BOLD signals in both the glomerular and nerve layers (Xu et al., 2000;Yang et al., 1998). Higher resolution fMRI studies confirmed the presence of BOLD signals in the nerve layer (Kida et al., 2002a;Schafer et al., 2005) that were not attributed to spatial resolution limitations. These results were in good accordance with theoretical calculations that ATP is almost equally consumed during action potential propagation and postsynaptic activation (Attwell and Laughlin, 2001). In contrast, the distribution of cytochrome C oxydase, a key enzyme of oxidative metabolism, suggested that oxidative metabolism differs in the two layers: high

levels of the enzyme were found in glomeruli (Borowsky and Collins, 1989;Hevner et al., 1995;Hevner and Wong-Riley, 1989) and little if any in the nerve layer. In the course of an initial study where we measured CBF responses to odor in the Glomerular Layer, we observed that the nerve layer contained very few capillaries (Chaigneau et al., 2003) (see the comment in (Shepherd, 2003)). Thus, the amount and the nature (i.e. through oxidative versus glycolytic metabolism) of the energy consumed in the nerve and glomerular layers, whether at rest or during sensory stimulation, remain unknown. It was only addressed theoretically by Nawroth et al. (Nawroth et al., 2007) who calculated that, in glomeruli, the density of neuronal elements would be associated with a high resting energy consumption which increases upon firing of OSN axons and subsequent postsynaptic activation.

In the present study, we directly assessed *in vivo* the correlation between capillary density, neuronal activity, cerebral blood flow (CBF) and oxygen consumption, both at rest and during odor stimulation. We combined two-photon laser scanning microscopy (TPLSM) measurements of capillary density and CBF, polarographic measurements of oxygen (for review see (Ndubuizu and LaManna, 2007)), and electrophysiological recording of local neuronal activity. We report that oxygen is principally consumed in glomeruli where capillary and mitochondria densities are very high and not in the nerve layer. Furthermore, glomerular oxygen consumption results mainly from dendritic activation rather than from firing of axon terminals, transmitter release or astrocyte activation.

Methods

• Animal preparation

31 Wistar rats (PN 30–70) were used and anaesthetized with either urethane (I.P., 1.65 g/kg) or ketamine and xylazine (I.P., 90 mg/kg, 10 mg/kg, respectively) and held in a standard stereotaxic apparatus. The posterior cisterna was drained. A craniotomy was performed above the two olfactory bulb hemispheres and the dura was removed. A 100 µm thick glass coverslip was placed over the bulb and fixed on the cranium, and the space below was filled with a 3.25% agar solution. The temperature of the animal was monitored with a rectal thermometer and maintained at 37°C with a feedback-controlled heating blanket (Harvard Apparatus). In several experiments, we monitored breathing frequency through a pneumogram transducer (BIOPAC Systems, Inc., Goleta, CA). Occasionally blood PO_2, PCO_2 and pH were controlled using a RapidLAB 348 analyser from Bayer (Wuppertal, Germany).

• Electrophysiological recordings and application of drugs

To record local field potential, a borosilicate micropipette was filled with a standard extracellular solution and 10µM Oregon green. To record glomerular activity, previously labelled glomeruli were targeted through Agar using the method described below. Electrophysiological signals recorded with a NeuroData amplifier

(Cygnus Technology, Delaware Water Gap, PA) were digitized and stored on a PC (Digidata 1200A, Clampex 9, Axon Instruments, Foster City, CA). Olfactory nerve stimulation was performed using a tungsten microelectrode (TM31A50, World Precision Instruments Inc., Sarasota, FL) which was targeted in the nerve layer approximately 1 mm from (Chaigneau et al., 2007) the recorded glomerulus. Stimulation protocol consisted of 3 trains of 4 pulses (200 µs) at 40 Hz. For local application of drugs, we used Alexa 594 at 13µM as a fluorophore to avoid blurring glomerular boundaries (labelled with Oregon Green) during pressure injection. Laser power was adjusted before injection to follow, as precisely as possible, the spatial diffusion of the fluorescent solution. Of course, the precise extent of the drug effective region is impossible to determine since we are only monitoring the dye and not the drug diffusion. In addition, *in vivo* experiments require to apply drugs at high concentration, conditions that increase the risk of generating non specific actions of drugs. Micromolar concentrations of CNQX and NBQX have been reported to increase GABA release in cerebellum (Brickley et al., 2001) through an unknown mechanism that does not involve AMPA or kainate receptors. In our conditions (see also (Chaigneau et al., 2007)), we used low pressure and brief applications (30-120s) of 250 µM NBQX. The real concentration reaching synapses was certainly much lower, allowing rapid recovery and drug reapplication. Prolonged applications gave similar results (not shown), were more difficult to wash and for this reason avoided. Because we have already demonstrated that 250 µM NBQX blocks the LFP negativities that report EPSPs in mitral cells (Chaigneau et al., 2007), it is unlikely that our approach reveals a non-specific enhancement of GABA release which could modulate oxygen consumption (Caesar et al., 2008).

- **Oxygen Tissue measurements**

Recordings were made with a Clark-style polarographic oxygen sensor (Unisense, Aarhus, Denmark). The oxygen sensor was polarized with respect to an Ag/AgCl internal reference electrode at -0.8 V. The current between the two electrodes is linearly related to the partial pressure of oxygen in the vicinity of the sensor tip. We calibrated at 37°C each sensor prior to experiments, first in saline with 21% oxygen (air-saturated) and then in 0% oxygen (bubbled with nitrogen). In several experiments, we also compared the calibration before and after the experiment without noting any significant difference. Oxygen electrodes are known to have a slow response time (see supplementary Figure 1). To correct for this delay and measure the true oxygen dynamics, we measured for each electrode, the impulse response before the experiment, by differentiating a step change in oxygen concentration: the electrode was rapidly moved from air to 0% oxygen saline. With the presence of fluorescein in the electrolyte, our electrodes showed an exponential decay time of ~ 200 ms (τ = 209 ± 98 ms, n=16 electrodes). We then divided in the Fourier domain the impulse response of the sensor. To avoid high-frequency noise generated by this process, both the impulse response and resulting signal were low-pass filtered (respectively with 5Hz and 1.5Hz cut-off, Butterworth filter, order 4, applied both forward and backward to allow zero-phase

delay). This process simply shifted back in time the curves (about 0.25s) and corrected the oxygen spectrum density to its true low frequency value (Supplementary Figure 1C).All analyses were done on deconvolved oxygen responses. We did not characterize ourselves the volume of tissue detected by the electrode. However, according to the manufacturer (Unisense, Denmark), the steady-state sensing region is a spherical region with a diameter twice that of the tip membrane (1 to 3 µm), the non steady-state being theoretically smaller (Gundersen et al., 1998). Moreover, these electrodes consume a negligible amount of oxygen (10^{-16} moles of oxygen per second) compared to oxygen basal consumption in glomeruli (Nawroth et al., 2007). Altogether, these properties ensure a very good spatial and time resolution for recording oxygen partial pressure.

- **In Vivo Two-Photon Imaging**

Axon terminals from the olfactory nerve (and thus glomeruli) were labeled with Oregon green dextran (MW 10000) 2–8 days before experiments by using the methods developed by Wachowiak and Cohen (Wachowiak and Cohen, 2001). To label vessels, a bolus of 70-kDa Texas Red dextran was injected i.v. through a catheter placed in the femoral vein. We imaged the two fluorophores using a custom-built two-photon laser-scanning microscope. An 890-nm excitation beam from a femtosecond Ti:Sapphire laser (10-W pump; Coherent Radiation, Palo Alto, CA) was focused onto olfactory nerve terminals and capillaries with the use of a 63X Leica (Deerfield, IL) water-immersion objective. Galvanometric scanners (Cambridge Technology, Cambridge, MA) controlled by home-built electronics and software (LABVIEW) were used to produce repetitive single-line scans at ≈ 1-2,000 lines per second or images from subregions of the field of view at rates up to 20 frames per second. We acquired fluorescence simultaneously on two channels separated by a dichroic mirror (cut-off wavelength, 560 nm).

- **Targeting pipettes using a two photon microscope**

In the rat, glomeruli diameter may occasionally be as small as 40 micrometers. It is thus crucial to precisely control, in 3 three dimensions (3D), the recording sites of both oxygen partial pressure and neuronal activity. Therefore, we did not use oxygen sensors with a fixed distance between the oxygen sensor and the local field potential electrode (Offenhauser et al., 2005;Thompson et al., 2003;Thompson et al., 2005). Instead, we used a custom-built technique that enable us to target pipettes in depth using two photon imaging. In brief, the principle was to acquire X, Y and Z positions for one point, in the imaging coordinates system, and to convert it mathematically into the micromanipulator coordinate system. It was then possible to directly position two electrode tips in very close proximity. In our experiments, the distance between the two sensors tips ranged from 6 to 83 µm (the latter in a large glomerulus), ensuring that both electrodes report signals related to the same neuronal population.

• RBC velocity analysis.

Line scans were acquired along the longitudinal capillary axis. Unlabeled RBCs appeared as tilted dark shadows on a bright fluorescent plasma background. The values of the velocities were calculated using algorithms based on (Kleinfeld et al., 1998). The velocities of the RBCs were inversely proportional to the tangent of the shadow angle. Images were pre-treated using 5 by 5 medians, low-pass filters and subdivided into brief images $I(n)$ of 100–200 ms duration. The average velocity $v(n)$ of RBCs in $I(n)$ was then calculated as follows: (1) each image $I(n)$ was rotated by an incremental angle α, (2) a singular value decomposition was performed on each rotated image, (3) the α value for which we obtained the greatest first singular value provided the average angle of the RBC shadow in $I(n)$, (4) $v(n)$ was calculated as $v(n) = 1/\tan(\alpha)$.The onset of the vascular response was defined as the moment when two successive values were larger than twice the resting velocity S.D.

• Electron microscopy protocol

Sprague-Dawley rats, 60-120 days postnatal, were perfused through the heart with phosphate buffer saline (PBS) at 4°C followed by 4% paraformaldehyde and 1% glutaraldhyde in PBS. The treatment of the animals was approved by the Yale Institutional Animal Care and Use Committee. The olfactory bulbs were removed, postfixed overnight in the perfusate at 4°C, and 100µm chapters cut on the Vibratome. Further processing largely followed our established protocols (i.e. Kaswoski et al., 1999; Au et al., 2001). Briefly, the 100µm chapters were washed three times for 10 minutes each with PBS and then osmicated with 2% osmium tetrachloride for 1 hour. After a series of graded alcohol washes with 50% ethanol (EtOH) for 10 minutes and 70% EtOH for 10 minutes, they were stained *en bloc* with 1% uranyl acetate in 70% EtOH for 1 hour. The chapters were further rinsed with 70% EtOH for 10 minutes, 90% EtOH for 20 minutes, and 100% EtOH three times for 15 minutes each. Next, they were rinsed twice with propylene oxide for 5 minutes each. The chapters were then put in a 1:1 propylene oxide/Epon 812 (Epon) mixture on a shaker overnight. The following day, the chapters were infiltrated with fresh Epon for 2 hours, flat embedded in fresh Epon onto quick-release-coated slides (Hobby Time Mold Parting Compound; Electron Microscopy Sciences, Ft. Washington, PA), coverslipped with quick-release-coated coverslips, and polymerized in a 60°C oven overnight. Slides were examined with a light microscope, and areas of the Epon film containing OB tissue with a good stretch of intact ONL were cut out and remounted on Epon blocks and polymerized for 48 hours prior to thin chaptering. Silver chapters (70-100nm) were cut with a Reichert-Jung ultramicrotome, and mounted on slotted grids (2mm x 1mm) covered with Formvar (0.5% in ethylene dichloride). The grids were post-stained with 1% lead citrate for 1.5 minutes, and examined using a JEOL 1200 EXII 120kV transmission electron microscope (Peabody, MA).

Electron micrographs were captured at a primary magnification of 10,000X which provided a working magnification of 24,000X after printing. From electron

micrographs of the Olfactory Nerve Layer totaling 19,375µm^2, we randomly sampled 1,500µm^2 using a template with a 2 X 5µm window. From electron micrographs of the glomerular neuropil totaling 16,300µm^2, we randomly sampled 1,500µm^2 using the same template. Within the template window, all mitochondria were counted.

- **3D vascular anatomy extraction and analysis of the distance to the nearest vessel**

To characterize the 3D vascular architecture from image stacks of labeled vessels, we used a modified version of the Fast-Marching Algorithm (Sethian, 1999), adapted from (Deschamps and Cohen, 2001). The principle of the algorithm was to use a stack of images as a material into which virtual waves could be propagated. As long as these waves respected some of the mathematical properties of electromagnetic waves, their path indicated information on the structure located into the stack. The algorithm was composed of several steps as follows. A starting point was manually chosen in the stack to initiate several waves (Fast-Marching algorithm). A first propagation used a function of gray level as refractive index to create a map of the “energy cost” to propagate from any point to the starting point. Since it propagated faster along the white pixels (ie. inside the vessels), the wave took the shape of the vessels connected to the starting point. One of the mathematical properties of this cost map relates to wave propagation theory, notably with its gradient always pointing in the direction of the shortest path to reach the starting point. Therefore, it was already possible to extract the vessel paths using a gradient descent algorithm. However, these paths didn’t follow the exact center of the vessels since the energy cost to propagate along the border and in the middle of the vessel was the same. To circumvent this problem, we created a new stack from the previous set of propagated points where pixels located in the center of the vessels propagated faster. We therefore obtained a new cost map from which it was possible to extract proper vessel paths. This allowed us to measure the radius of the vessels along the paths radius using a simple local edge detection algorithm. Note that one of the main difference with (Deschamps and Cohen, 2001) relates to TPLSM specificities. Indeed, TPLSM resolution is higher along the x and y axes than in the z direction, in contrary to MRI voxels. To solve this problem, we re-centered all the paths along the z axis using the radius profile of the vessels along the z direction.

To measure the average distance from any point of brain tissue to the nearest cerebral vessel, we extracted from 3D vascular reconstructions the distance from each voxel to the nearest intravascular wall. Calculations of the average distance imposed to fix the voxel values in the lumen of vessels to zero. In order to average several glomerular columns, we took into account the shape of each glomerulus, which was reconstructed in 3D and morphed into a sphere of equivalent volume. To average several columns, 3D distance maps were similarly morphed: each 3D columnar distance map was first averaged on a plane rotating around the central axis of the column. The obtained 2D distance maps were then

averaged and normalised by each glomerular radius (see Figure 1).

- **Data analysis**

All Data were analyzed through a home-made MATLAB program (MathWorks Inc., Natick, MA, USA). 3D Vascular anatomy extraction was partially programmed in C++ to minimize computation time. RBCs flow extraction was performed in LABVIEW (National Instruments, Austin, TX, USA). In the entire study, average values are expressed as mean ± S.E.M.

Results

- **Quantification of capillary density in the nerve and glomerular layers of the dorsal OB**

Using TPLSM and selected volumes in the olfactory nerve and glomerular layers, we have previously shown, *in vivo*, that the capillary network was denser in the glomerular than in the nerve layer (Chaigneau et al., 2003). In another study performed in slices of fixed tissue, Borowsky and Collin (Borowsky and Collins, 1989) reported that the network of small blood vessels (< 10 µm) was denser in the GL than in the external plexiform layer but did not investigate the nerve layer. None of these studies precisely quantified, in mm/mm^3, the density of capillaries in the two superficial layers, a requirement to compare values with those of other brain regions. We thus developed a new 3D algorithm based on a modified version of the Fast-Marching Algorithm (Sethian, 1999) (see Methods) in order to reconstruct the entire vascular structure irrigating the OB layers. The algorithm was able to automatically compute the complete path, radius and angle of all vessels labeled with Texas red and located in TPLSM stacks. Figure 1 illustrates a typical volume of OB in which the density of capillaries (diameter < 6 µm) was more than 10 times higher in glomeruli than in the nerve layer. In glomeruli, the mean capillary density was extremely high (1056 ±72 mm/mm^3, n=7 glomerular columns), the capillary lumen thus filling up ~ 2.98 % of the glomerular volume. Increasing the diameter threshold to 10 µm only slightly increased the glomerular capillary density (1137 ± 61 mm/mm^3). Thus, because the vast majority of glomerular vessels had a diameter < 6 µm in our experimental conditions (urethane anesthesia), we propose that they correspond to true capillaries while vessels with diameter between 6 and 10 µm already include small arterioles. Within glomeruli, capillary density was homogenous (upper half sphere density = 1139 ± 130 mm/mm^3, lower half sphere density = 960 ± 80 mm/mm^3, p=0.3). As a consequence of the high capillary density, the average distance of any point to the nearest capillary (< 6 µm) internal border was 10.78 ± 0.73 µm (Figure 1E, left). This value decreased to 9.96 ± 0.51 µm when including all vessels (Figure 1E, right). In contrast, in the nerve layer the mean capillary density was extremely low (45 ± 26 mm/mm^3, n=7 glomerular columns), the capillary lumen filling up ~ 0.12 % of the glomerular volume). The density remained low when the capillary diameter

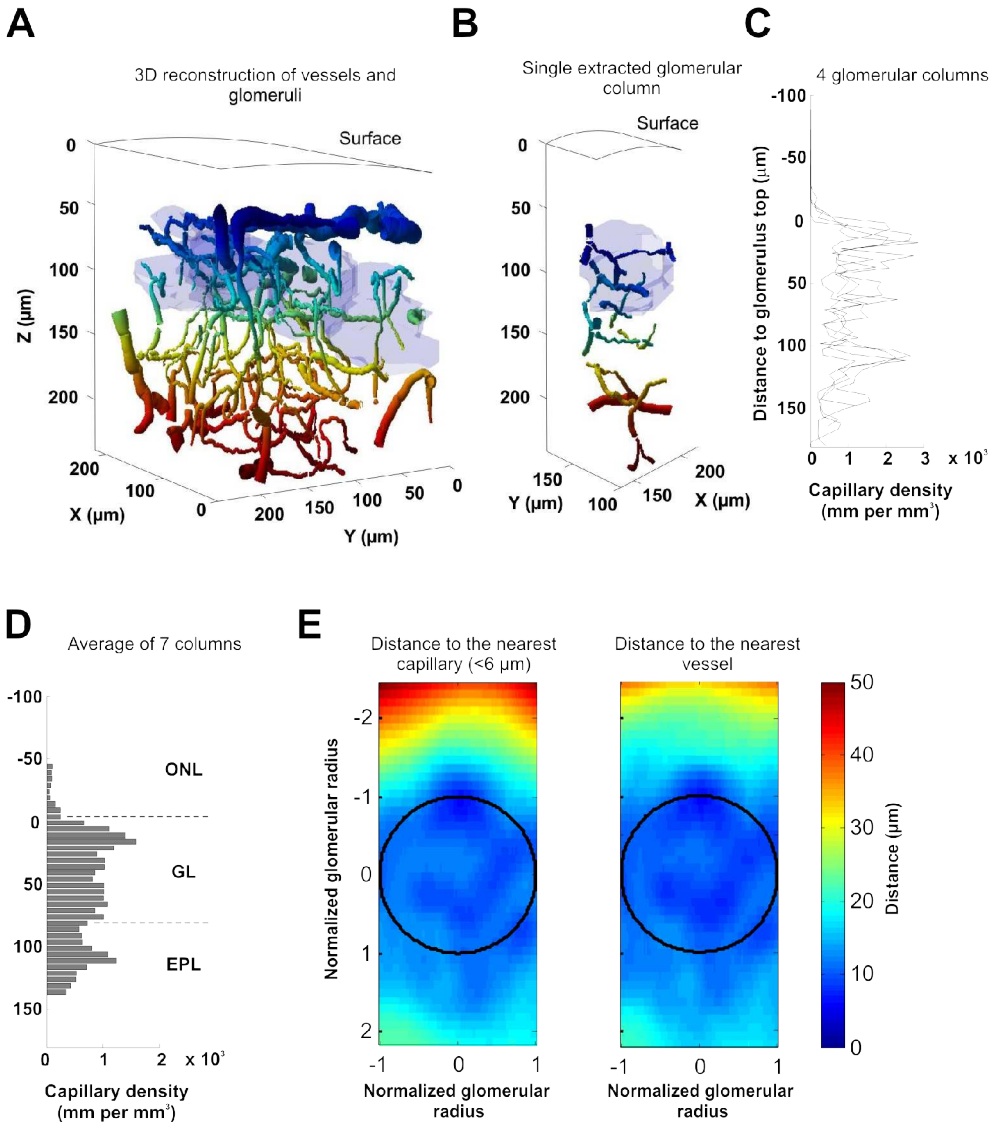

Figure 1 Quantification of capillary density in the olfactory bulb superficial layers

Vessels and glomeruli were reconstructed in 3D from stacks of images obtained with TPSLM *in vivo* and using an original reconstruction algorithm. Glomeruli were labelled with Oregon Green dextran and vessels with Texas red. Vessel colors vary with depth. Glomeruli are indicated in light blue. (B) Each glomerular column can be extracted from the reconstructed olfactory bulb volume. (C) Capillaries density (total length of vessels (diameter < 6 µm) per unit of volume) as a function of depth. Densities were obtained from the 4 glomerular columns extracted from (A). (D) Average of capillary densities from 7 glomerular columns. Note that few capillaries if any were present in the Olfactory Nerve Layer (ONL) as compared to the Glomerular Layer (GL) where the density is extremely high. (E) Average distance from any point of a glomerular column to the nearest capillary (left) or vessel (right) internal border. Data were calculated from the previous glomerular columns (D) (see methods). The color lookup table indicates the distance in µm.

threshold was raised to 10 µm (90 ± 54 mm/mm^3). In fact, the overall "large" (> 10 µm) vessel density was low in the nerve layer (52 ± 28 mm/mm^3). In this layer and for a point located at one glomerular radius above the glomerular border, the average distance to the nearest capillary internal border was 36.55 ± 1.69 µm. This value decreased to 27.97 ± 4.63 µm when including all vessels. Altogether, our vessels' quantification indicate that in the dorsal OB, the glomerular capillary density is one of the highest reported in the brain and confirm that the nerve layer is almost devoid of capillaries (Chaigneau et al., 2003). This contrasting vessel distribution suggests that tissue oxygen partial pressure ($P_{tiss,O2}$) could differ in the two layers, whether at rest or during sensory stimulation.

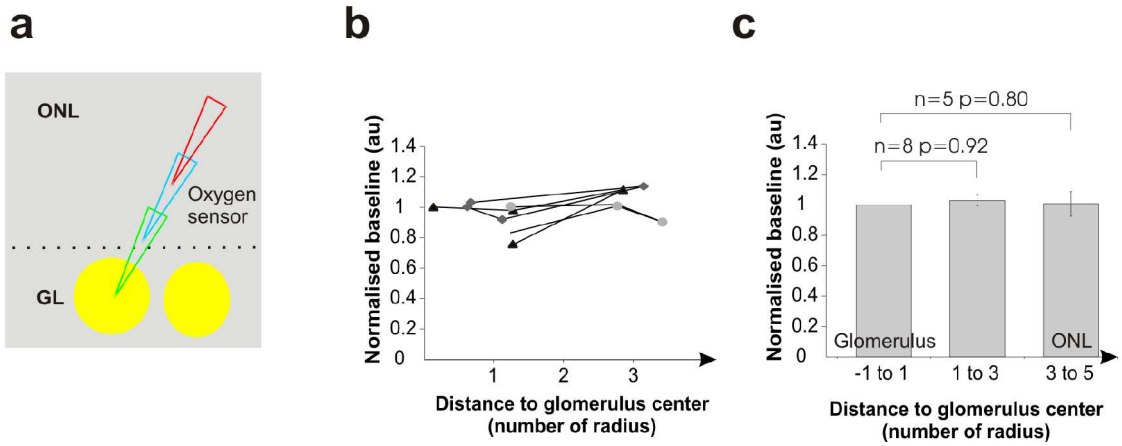

Figure 2 Resting oxygen tension in the ONL and GL
(a) Schematics. A fluorescent oxygen electrode (fluorescein) was placed at several sites in the GL and ONL. (b) Oxygen tension (normalised to the GL value) as a function of distance from the glomerular centre. Each value is an average of 3 to 6 measurements. Note that moving the electrode back and forth (n=3 rats) may slightly affect the oxygen measurements. (c) At resting state, the oxygen tension is similar in both the GL and the ONL.

- **<u>Steady-state $P_{tiss,O2}$ in the nerve and glomerular layers</u>**

In a recent work (Chaigneau et al., 2007), we have shown that we can target fluorescent extracellular recording pipettes in various layers of the rat olfactory bulb. Here, we used a modified version of a "Clark-like" polarographic oxygen sensor that was filled with fluorescein. This enabled us to place the oxygen sensor under TPLSM visual control at various depths and sites in the olfactory bulb In all experiments (n=30 rats), the delays between measured and true $P_{tiss,O2}$ measurements were corrected by deconvoluting the impulse response function of each sensor from the signal measured *in vivo* (see methods and supplementary Figure 1). Considering the diameter of the tip membrane (1 to 3 µm), the steady-state sensing region should be a spherical region with a diameter of about 2-6 µm (Gundersen et al., 1998). Removing the oxygen sensor from the center of

glomeruli to sites in the periglomerular region and above, in the nerve layer (Figure 2), revealed that resting $P_{tiss,O2}$ was maintained in all layers ($P_{tiss,O2}$ in glomeruli = 25.4 ± 2.9 mmHg; $P_{tiss,O2}$ in the nerve layer = 27.1 ± 4.2 mmHg, p=0.36, paired student-t test). A significant portion of oxygen is known to diffuse radially from arteriolar vessel segments (Tsai et al., 1998;Tsai et al., 2003). However, the near absence of capillaries or of any vessels in the nerve layer along with the observation that resting $P_{tiss,O2}$ was similar in both layers suggest that in the steady state, oxygen diffusion from glomerular capillaries participates to $P_{tiss,O2}$ in the nerve layer.

• Odor–evoked $P_{tiss,O2}$ changes in glomeruli

We have recently characterized a component of local field potential (LFP) responses to odor that is generated locally, within a glomerulus (Chaigneau et al., 2007): it consists of respiration-locked rapid negativities that involve mitral cell dendritic synaptic depolarization and are extremely similar within glomerular boundaries. LFP and oxygen electrodes were targeted in the same glomerulus and thus reported signals related to the same neuronal population. The distance between the two sensor tips ranged from 6 to 83 µm (the latter in a large glomerulus). Two types of oxygen responses were observed: the first one (Figure 3B, C) was characterized by a LFP response rapidly (~100 ms) followed by a decrease in $P_{tiss,O2}$ (oxygen "initial dip") and the second one (Figure 3B) by a LFP response associated with a biphasic change in $P_{tiss,O2}$ (a decrease followed by an increase). Both types of response were followed by an increase in CBF. On average, LFP responses preceded oxygen negativities by ~ 0.17 s (± 0.02 s; n=14) and blood flow responses by ~1.91 s (± 0.12 s; n=9). The two types of oxygen responses are reminiscent of what has been observed in the cortex (Thompson et al., 2003) and the lateral geniculate nucleus (LGN) (Thompson et al., 2004;Thompson et al., 2005) where small grating stimuli elicited monophasic responses and large stimuli, involving larger portions of the LGN, evoked biphasic responses. The functional organization of the OB suggests that “specific” odor stimulations activating one to few glomeruli (Chaigneau et al., 2003; Petzold et al., 2008) elicit monophasic oxygen responses while strong odor responses activating several glomeruli (Chaigneau et al., 2007), i.e. a large network of vessels, trigger biphasic responses. However, at the level of a single glomerular capillary, both responses evoke a similar delayed increase in CBF. Still, it is important to note that even the apparent "pure" decrease in $P_{tiss,O2}$ in Figure 3B was also shaped by the delayed CBF increase as it has been shown in the cerebellum (Offenhauser et al., 2005): There, inhibition of nitric oxide synthase blocked CBF responses and uncovered the whole $P_{tiss,O2}$ change evoked by climbing fiber stimulation. In order to circumvent this problem in the rest of our study, i.e. to eliminate the influence of CBF in either mono or biphasic oxygen responses, we only considered the initial slope of $P_{tiss,O2}$ decreases in quantifying $P_{tiss,O2}$ changes. This initial slope can be considered as a marker of local oxygen consumption, at least at the onset of the response to stimulation (see discussion). Its average value was -2,86 ± 0,12 mmHg/s (n=8). Note that moving the sensor by ~10 microns within glomerular

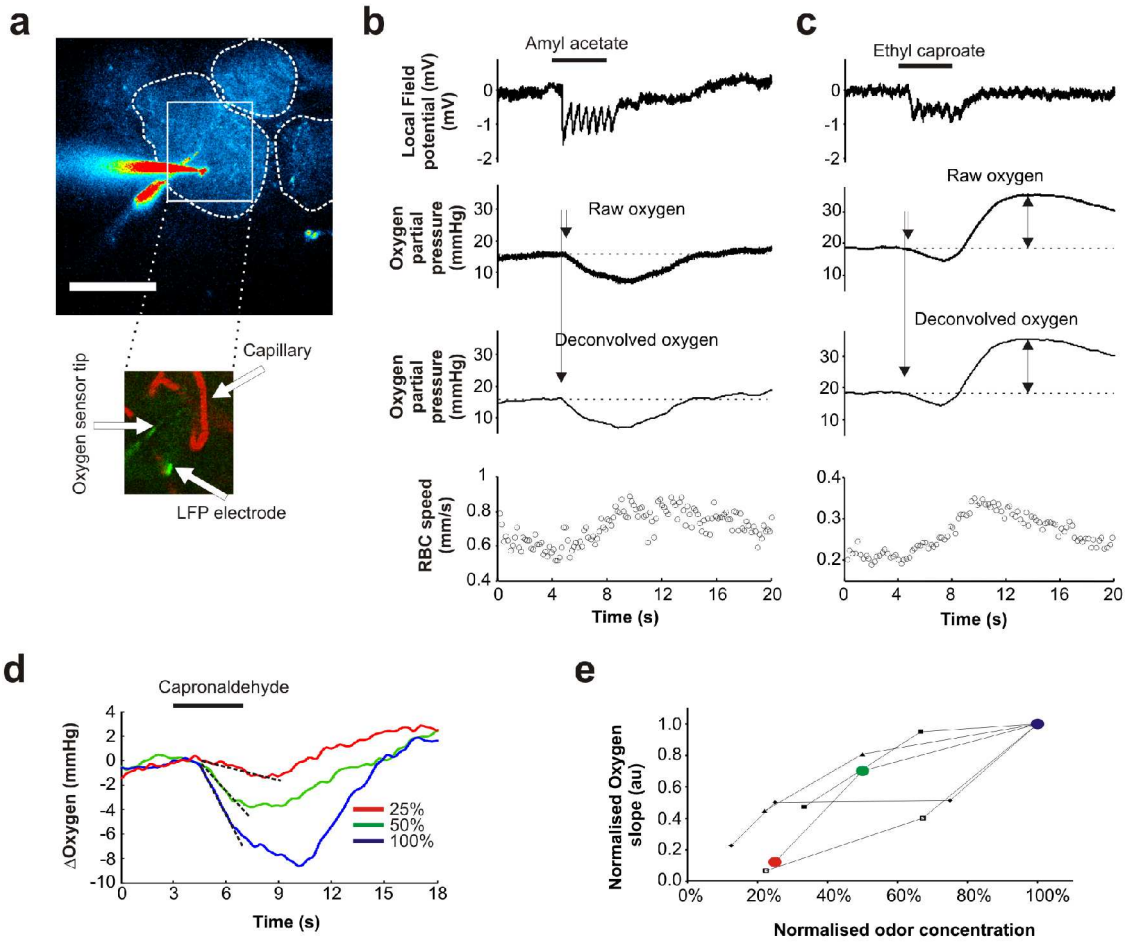

Figure 3 Oxygen tension responses to odor
(a) Top. A labelled (Oregon green dextran) glomerulus was targeted with a fluorecein containing oxygen sensor and an LFP electrode (Oregon green). Bottom, capillaries injected with Texas red were imaged near both electrode tips allowing us to record simultaneously cerebral blood flow (CBF), LFP and oxygen tension responses to odor. (b) A case where odor evoked an LFP response that was followed by a rapid initial oxygen negativity and a delayed RBC flow increase. Note deconvoluting the oxygen tension measurement for the slow impulse response of the oxygen electrode shifts the trace to the left. (c) Another case where odor evoked a biphasic oxygen signal, a rapid initial oxygen dip and a positive rebound that follows the delayed CBF increase. (d-e) Odor and oxygen responses are concentration-dependent. To quantify oxygen responses, the initial slope value of oxygen negativities was used.

boundaries did not affect the initial slope of $P_{tiss,O2}$.changes. As expected, LFP and oxygen responses increased with odor concentration (Figure 3D,E).

- **Role of spontaneous and odor-evoked activity in glomerular $P_{tiss,O2}$**

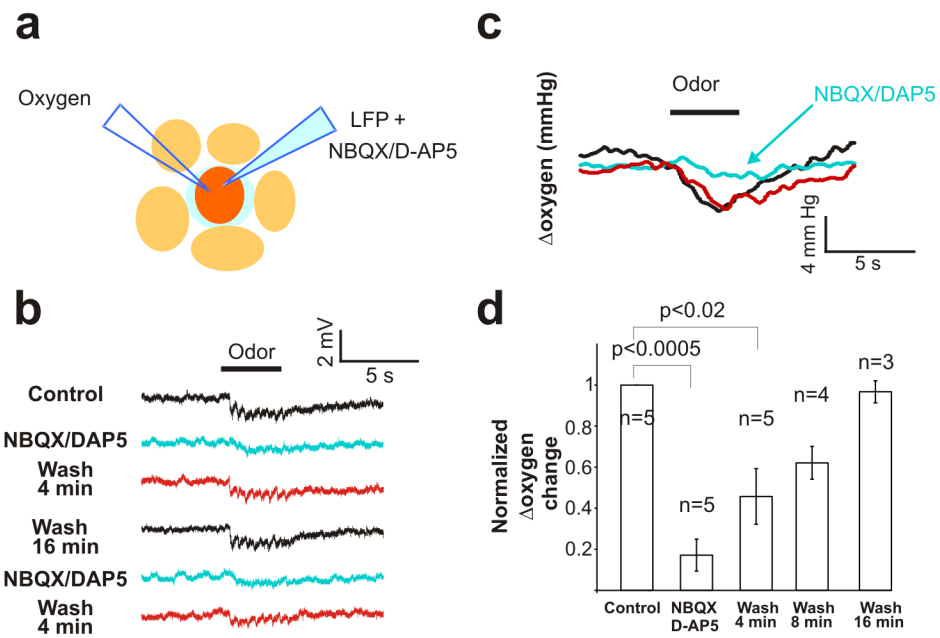

Figure 4 Oxygen consumption requires post-synaptic activation.
(a) Schematics. An LFP electrode containing 250 µM NBQX and 500 µM D-APV was placed near the oxygen sensor tip, within glomerular boundaries. (b) LFP negativities were reproducibly abolished by pressure application of glutamate antagonists (c-d) Glutamate antagonists strongly decreased or abolished oxygen responses. Measurements were performed ~1minute after drug application.

To discriminate the role of presynaptic versus postsynaptic compartments on $P_{tiss,O2}$, we repeated our experiments after focal injections of antagonists of ionotropic glutamate receptors. The effects of such drugs *in vivo* are complex: they block odor-evoked LFP responses (Chaigneau et al., 2007). However, they also enhance OSN presynaptic calcium signals evoked by odors, an effect related to a blockade of tonic presynaptic inhibition (Petzold et al., 2008;Pirez and Wachowiak, 2008). Therefore at rest, a tonic excitatory input onto inhibitory cells causes GABA release and tonic activation of GABAB receptors located on OSN terminals. By blocking this tonic inhibition, glutamate antagonists increase the amount of glutamate released from OSN terminals but also decrease dendritic glutamate and GABA release. Using the same patch pipette to apply antagonists of glutamate ionotropic receptors (250 µM NBQX and 500 µM D-APV, see experimental procedures on the use of high concentration of drugs) and measure LFP responses (Fig. 4), we observed that intraglomerular blockade of synaptic

transmission did not affect resting $P_{tiss,O2}$ ($P_{tiss,O2}$ in control = 22.9 ± 4.0 mmHg; $P_{tiss,O2}$ with antagonists = 25.8 ± 5.3 mmHg, p=0.15, n=6). This indicates that a glomerulus in two very different "states" of spontaneous activity, i.e. at rest and in a condition where the tonic excitatory drive of glomeruli is abolished and CBF remains constant (Petzold et al., 2008), can consume the same amount of oxygen.

In contrast, glutamate antagonists strongly decreased both LFP responses (note the disappearance of the locally generated negativities locked to respiration (Chaigneau et al., 2007)) and the initial slope of $P_{tiss,O2}$ changes. The fact that $P_{tiss,O2}$ changes were largely (16 % of control) if not totally blocked while glutamate release by OSN terminals was enhanced (Pirez and Wachowiak, 2008), suggests that oxygen consumption resulted principally from the activation of glomerular postsynaptic processes, and among those from dendrites and not from astrocyte processes (see discussion). Furthermore, considering that the olfactory receptor terminal compartment occupies an extremely large portion (30 %) of the glomerular volume (Nawroth et al., 2007), our data are really surprising: Restoration of the ionic gradient for such a large glomerular portion should cost energy. Therefore our results suggest that either very few axons fire upon odor stimulation or that the energy required to fire axons and release glutamate may partially operate on an anaerobic metabolism.

- **Comparison of odor-evoked $P_{tiss,O2}$ changes in glomerular and nerve layers**

In their brain energy budget, Attwell and Laughlin estimated that a significant part of ATP is consumed by action potential propagation (Attwell and Laughlin, 2001). Therefore, and in particular in the absence capillaries, large $P_{tiss,O2}$ changes could be expected when ORN unmyelinated axons fire in the nerve layer. We first placed the oxygen sensor and the LFP electrode in a glomerulus and recorded odor responses. We then moved the oxygen sensor in the adjacent juxtaglomerular and nerve layers (Fig. 5A) while the LFP electrode was maintained at its primary location to ensure that neuronal responses remained constant (Fig. 5B, grey traces). $P_{tiss,O2}$ measurements were performed back and forth between glomerular and nerve layer sites, allowing us to ascertain that $P_{tiss,O2}$ changes where independent of whether measurements were first done in the nerve or in the Glomerular Layer. $P_{tiss,O2}$ changes were significantly smaller in the nerve layer (normalized initial slope = 28 ± 6.2%, p=0.0003, n=5) than in glomeruli (Fig. 5C). In addition, the delay between LFP responses and the onset of $P_{tiss,O2}$ negativities increased (Fig. 5D) with distance from the glomerular upper limit (see also the arrow in Fig. 5B). This delay could indicate that $P_{tiss,O2}$ changes recorded in the nerve layer indirectly report glomerular $P_{tiss,O2}$ changes delayed by diffusion. However, 2 other possibilities should be considered, in particular in the ideal condition where an odor activates a single glomerulus: 1) the delay measured in the nerve layer was not correctly determined because $P_{tiss,O2}$ negativities were too small, few axons firing upon odor, 2) due to the functional organization of the nerve layer, the ~10000 axons conveying the information of OSNs expressing the same

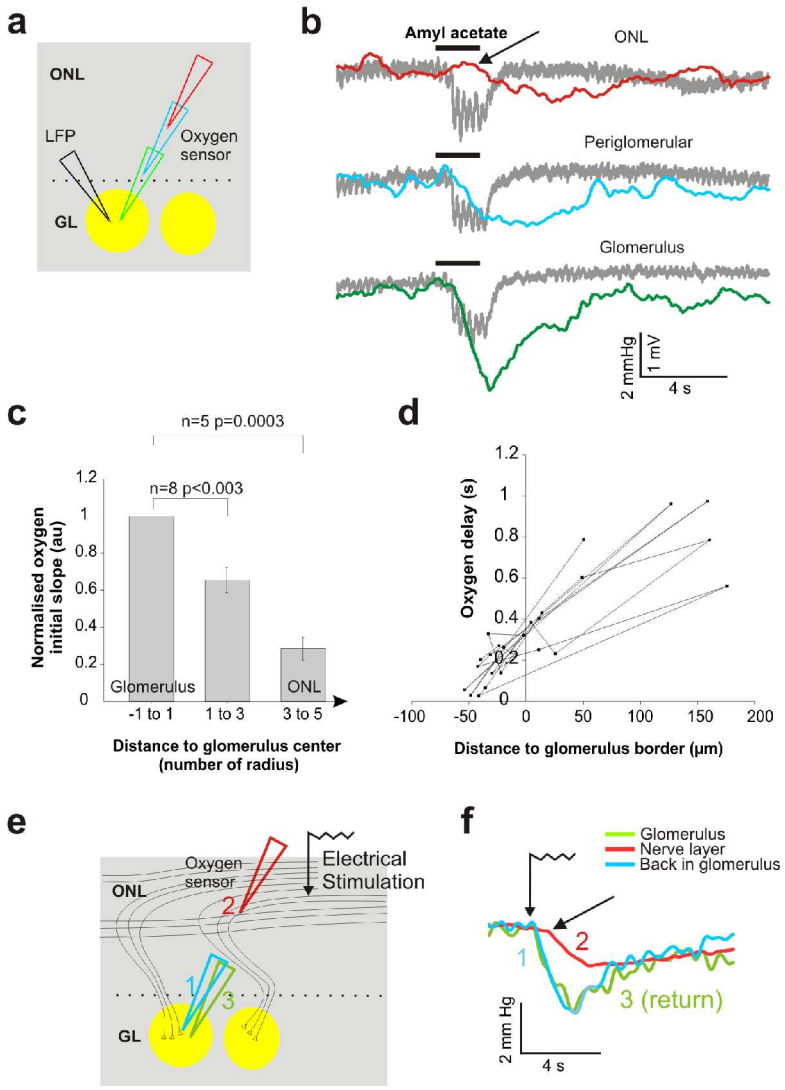

Figure 5 Contrasting odor-evoked oxygen responses in the GL and ONL.
(a) Schematics. Oxygen electrode was moved in different layers while maintaining LFP responses in the glomerulus. (b) Odor evokes stronger consumption in the glomerulus and a delayed response in the ONL. LFP responses were maintained (gray traces). The arrow points to the beginning at the oxygen response in the ONL. (c) Oxygen consumption statistics (8 rats). All oxygen initial slope were normalised the glomerular response. Distance to the glomerulus center were normalised with the average glomerulus radius (average of maximal and minimal radius) to account for glomeruli variability in size. (d) Delay between LFP and oxygen response onsets. Oxygen responses were always delayed in the ONL. The distance to the glomerular boundary was measured by assuming a spherical like shape for the glomerulus, based on its average diameter. (e-f) Electrical stimulation of the ONL similarly evoked a delayed oxygen response. Although a large portion of the ONL was stimulated and the time for synaptic transmission bypassed, the oxygen response was smaller and delayed in the ONL in comparison to glomerular responses.

odorant molecule form small fascicles that converge from several directions in their glomerulus (Kasowski et al., 1999). Thus, by removing the oxygen sensor from the glomerulus in the nerve layer, it was misplaced at a distance from activated axons, inducing a diffusion delay in $P_{tiss,O2}$ measurements.

To circumvent this problem, we modified the stimulation protocol and increased the ratio of axons activated in the nerve layer per axon terminals activated within a given glomerulus. Strong electrical stimulations (3 trains of 4 pulses (100 µs) at 40 Hz, >1 mA) were applied through a monopolar tungsten electrode placed in the nerve layer. The oxygen sensor was placed either in the nerve layer (between the stimulation electrode and a targeted glomerulus) or in a glomerulus. For a glomerular $P_{tiss,O2}$ response of similar amplitude to one evoked by odor, such electrical stimulation is likely to activate a higher proportion of axons in the nerve layer: those projecting to the recorded glomerulus plus those converging to other glomeruli. As expected, electrical stimulation evoked $P_{tiss,O2}$ were still smaller in the nerve layer than in glomeruli (nerve layer = 0.98 ± 0.08 mmHg/s; glomeruli =2.12 ± 0.34 mmHg/s, n=4), but they were proportionally larger (46 % of glomerular responses) then with odor stimulation (28 % of glomerular responses). More importantly, the delay of $P_{tiss,O2}$ responses persisted to be shorter in glomeruli (0.06 ± 0.06 s) than in the nerve layer (0.43 ± 0.06 s).

Altogether, our results show that glomeruli are the main source of odor-evoked $P_{tiss,O2}$ decreases and that $P_{tiss,O2}$ signals detected in the nerve layer mostly reflect “distant” glomerular oxygen consumption. This raises again the possibility that action potential propagation relies less on oxidative metabolism than postsynaptic activation. Could a difference in mitochondria density between OLN and GL layers support such a hypothesis?

- **Differential distribution of mitochondria in the glomerular and nerve layers**

Using electron microscopy, we assessed the density of mitochondria located in glomeruli and in the nerve layer using electron micrographs that totaled 19,375 μm^2 in the nerve layer and 15,300 μm^2 in glomeruli. From these two areas, ~1,500 square microns were randomly sampled using a 10 μm^2 square micron mask/window. In the nerve layer, mitochondria density ranged from 0 – 21/10μm^2 with a mean of 6.06 ± 0.31 (Fig. 6A, B). Importantly, the majority of mitochondria were observed in axons and only occasionally in the processes of the olfactory ensheating cells. In the glomerular neuropil (Fig. 6C), the density of mitochondria ranged from 2 – 28/10μm^2, with a mean of 13.08 ± 0.34, significantly higher than that found in the nerve layer. While the distribution of mitochondria in the dendritic processes and axonal terminals of the glomeruli appeared similar, there was a striking difference in the size of the dendritic mitochondria (compare Fig. 6A, B with Fig. 6C). Mitochondria in the dendritic processes were uniformly larger than those found in axons. Moreover, this seems unlikely to be accounted for simply by the cross-sectional diameter of the dendrites since in longitudinal sections through the Olfactory Nerve Layer (i.e. the oblique sections shown in Fig. 6B) the

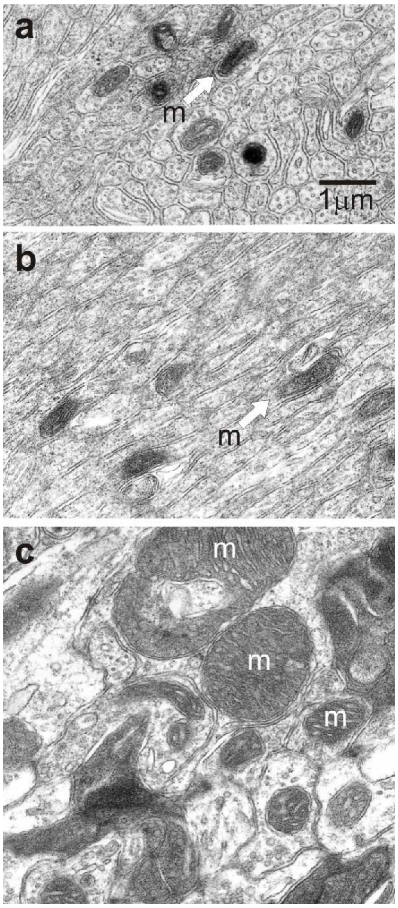

Figure 6 Electron micrographs illustrating the density and properties of mitochondria in the Olfactory Nerve Layer and the glomerular neuropil.
(A) Transverse section through an olfactory nerve fascicle shows many cross sections of the unmyelinated olfactory sensory neuron axons. Only 9 mitochondria are seen (arrow). (B) Oblique section through the olfactory nerve showing semi-longitudinally sectioned olfactory sensory axons. Note that the mitochondria do not conserve a larger volume by extending longitudinally within the axons, but rather maintain a small profile. (C) Transverse section through the neuropil of a glomerulus. Many large mitochondria (i.e. m) are seen in the electron lucent dendrites. Electron dense olfactory sensory axon terminals are seen in the upper right and lower right. Scale bar for (A), (B), and (C) shown in (A).

mitochondria are not particularly long. Such differential distribution of mitochondria density and size has been well described in the monkey visual cortex (Wong-Riley, 1989;Wong-Riley et al., 1989). It supports the hypothesis that, *in vivo*, action

potential propagation and postsynaptic depolarization may be associated with different weights of oxidative/glycolytic metabolism.

Discussion

• Oxygen delivery in glomerular and nerve layers

In the present work, we took advantage of the functional organization of the olfactory bulb to determine the relationship between capillary density and cellular subcompartment metabolism at a fine spatial resolution. Our 3D quantification of vascularity with TPLSM clearly indicates that the nerve layer barely contains any capillaries, although it contains ORN unmyelinated axons and specialized glial cells such as microglial cells and glial ensheating cells. Differences of vascularity within brain regions have been described long ago by Craigie (Craigie, 1920) who observed that “the gray matter was much more richly supplied with capillaries than the white matter”, as well as by Dunning and Wolff (Dunning and Wolff, 1937) who concluded their study by stating that “the nervous tissue involved in synaptic transmission, i.e. containing dendrites and axon terminals, is more richly supplied with blood vessels than nervous tissue involved in conduction only” (for review see (Bar, 1980)). In area 17 of the squirrel monkey (Zheng 1991), capillary density is higher in blobs than in interblobs and much higher in layer IVc than in layer I (by a factor 3-4). However, these numbers are far from those we observed in the OB. In glomeruli, capillary density outnumbers that in the nerve layer by a factor greater than 10. Moreover, with absolute capillary densities > 1000 mm/mm^3, glomeruli appear to have the highest density reported in the brain. Could such density value result from the fact that each vessel acquired in 3D stacks was counted? It is improbable since the recent study by Weber et al. (Weber et al., 2008) revealed that in the macaque visual cortex, absolute and ratio capillary values in and between layers IVc and I are still far from we observed in the OB. Finally, in few extreme cases (not shown), large volumes of nerve layer (e.g. within our 350 µm-350 µm microscope field of view) overlying the glomeruli were even completely devoid of any kind of vessel. Thus although arteries and arterioles, which are known to deliver a significant amount of oxygen to tissue by radial diffusion (Tsai et al., 2003), may participate in oxygenation of the nerve layer, we propose that oxygen is primarily delivered to glomeruli from where a large portion diffuses to the nerve layer and equilibrates at the glomerular $P_{tiss,O2}$. The spatial distribution of the odor-evoked $P_{tiss,O2}$ initial dip also supports this hypothesis. $P_{tiss,O2}$ negativity recorded in the GL clearly preceded that recorded in the ONL. The fact that this delay persisted when using electrical stimulation of the olfactory nerve eliminates the possibility that $P_{tiss,O2}$ negativities in the nerve layer lagged the glomerular ones because the oxygen sensor was not placed at the site of activated axons. In our stimulation conditions (trains of strong shocks), a large portion of the dorsal nerve and glomerular layers were activated and the nerve oxygen response was still delayed while larger. Note that no additional and rapid (as in glomeruli) $P_{tiss,O2}$ negativities appeared. Therefore, it is likely that $P_{tiss,O2}$ negativities observed in the

ONL indirectly reflect oxygen consumed by glomerular processes. This question is discussed further below.

• Oxygen consumption in glomeruli

During odor, activation of OSN terminals (Wachowiak et al., 2004) and postsynaptic responses (Chaigneau et al., 2007) are rather homogeneous within glomerular boundaries. It is thus not surprising that odor systematically induced decreases in $P_{tiss,O2}$ even though our sensor reported $P_{tiss,O2}$ only within a 2-6 µm diameter sphere around the pipette tip. $P_{tiss,O2}$ depends on both neuronal activity and CBF. Because even the early decreases in $P_{tiss,O2}$ changes were partially masked by vascular inflow, we only considered the initial slope and not the integral or the amplitude of $P_{tiss,O2}$ decreases to demonstrate that oxygen is principally consumed by neuronal dendritic activation. We are aware that it is not possible to quantify, in absolute value, oxygen consumption without measuring oxygen released by hemoglobin. However, the initial slope of $P_{tiss,O2}$ decreases can be used to compare oxygen consumption at a given site under 2 different pharmacological conditions (control and NBQX+D-APV), as long as the steady state CBF and $P_{tiss,O2}$ do not change. We found that glutamate antagonists decreased by more than 80 % the $P_{tiss,O2}$ initial slope. Because these drugs enhance glutamate release (Petzold et al., 2008; (Pirez and Wachowiak, 2008), they should also enhance the activation of metabotropic glutamate receptors and the uptake of glutamate by astrocytes. Therefore, our data indicate that firing of OSN terminals, enhanced release of glutamate and enhanced activation of astrocytes consume only 16 % of the oxygen normally consumed during glomerular activation. The resting 84% correspond to oxygen required to restore ionic gradient of juxtaglomerular and mitral cell dendrites.

These percentages provide a new perspective on calculations of the glomerular energy budget (Nawroth et al., 2007) based on the energy demands of neuronal elements from the retina and the cortex. This theoretical study suggests that a third of total glomerular energy demands are due to axonal action potentials. If axonal demands are indeed of this order of magnitude, our results indicate that they are only partially met by aerobic metabolism. Alternatively, it is possible that oxygen consumption in the axonal compartments follows a slower time course than in the dendrites. It is an important consideration that different methods monitor different time courses of energy consumption and use different stimuli. For example, we only quantified what happens within the initial few hundred ms of odor responses (the initial slope of oxygen responses). In addition, our experiments were performed in anesthetized animals using odor stimulations lasting only 1-4 s. In contrast, 2DG accumulation to odor stimulation (Sharp et al., 1977) and olfactory nerve stimulation (Greer et al., 1981) requires prolonged stimulation and occurs over a period of 45 minutes, showing the highest levels of uptake in the olfactory glomeruli but also raised levels in the nerve layer. These high levels of 2DG in the nerve layer may therefore register the slow diffusion of oxygen and glutamate from glomerular capillaries and the slow metabolism

occurring in the mitochondria of the nerve layer (see the discussion on 2DG limitations in (Johnson and Leon, 2007)). Similarly, studies of the BOLD signal with odor stimulation periods of 30 seconds and show the highest BOLD signal in the glomeruli, with also raised levels in the ONL (Kida et al., 2002b). Thus, different methods appear to give critical insights into the time courses of oxygen and glucose diffusion from the glomeruli and rates of energy metabolism in the different layers. The present results provide critical constraints on further experiments to delimit the time dimension of energy metabolism in the glomerular and nerve layers.

These results also confirm the dendritic origin of oxygen consumption reported in the cerebellar cortex upon electrical stimulation (Offenhauser et al., 2005), in good accordance with the dendritic distribution of cytochrome C enzyme expression (Borowsky and Collins, 1989). They also support the predominant role of postsynaptic depolarization onto spiking (Viswanathan and Freeman, 2007). Finally, our study demonstrates for the first time what was proposed theoretically: in our *in vivo* conditions, stimulation of astrocyte consumes little oxygen.

- **Energy consumption by action potential propagation**

Our results also indicate that little oxygen is consumed during action potential propagation. Could action potential propagation then use ATP produced by an anaerobic metabolism? It seems to be the case for a subpopulation of axons of the optic nerve and the corpus callosum (Fern et al., 1998;Tekkok et al., 2003;Tekkok and Ransom, 2004) which are particularly resistant to anoxia but not to aglycemic anoxia. In the OB, this hypothesis is supported by the distribution of cytochrome c oxydase which is absent from the nerve layer and the periglomerular region while it is highly concentrated in the glomerular neuropil (Borowsky and Collins, 1989;Hevner and Wong-Riley, 1989). Also, mitochondria density was lower (~50 %) and mitochondria size smaller in the nerve layer than in glomeruli. Such difference has already been reported in other brain regions (Wong-Riley, 1989) and in our case, the difference in mitochondrial count is smaller than what exists between axonal terminals (~15 %) or myelinated axons (<10 %) and dendrites from the visual cortex (Wong-Riley et al., 1989). Thus, although it is difficult to infer anything quantitative about ATP metabolism from our mitochondrial observation, we believe that the differential distribution of mitochondria supports the hypothesis that action potential propagation and postsynaptic depolarization may be associated with differences in metabolism. We hypothesize that in glomeruli, ATP is produced through oxidative metabolism, whereas in the nerve layer, ATP immediate energy requirements are produced through glycolysis, though not excluding the restitution of ionic equilibrium through slower aerobic processes. The dominant role of glycolysis in axonal excitability would explain the general difference in white and grey matter metabolism, as deduced from 2-DG experiments and cytochrome oxydase histocytochemistry: the 12 fold increase in cytochrome oxydase activity from white to gray (Hevner et al., 1995) matter is only associated with a 3 fold increase in glucose consumption (Sokoloff et al., 1977).

We emphasize that these results may be specific to the organization of the superficial layers of the olfactory bulb, with respect to two special attributes: the high density of unmyelinated axons in the Olfactory Nerve Layer, and the high density of synaptic terminals in the glomeruli. Further experiments will be required to determine the extent to which the mechanisms revealed by the present experiments are unique to these attributes and the extent to which they may reflect general mechanisms that apply to other well-studied regions such as the retina and the cerebral cortex.

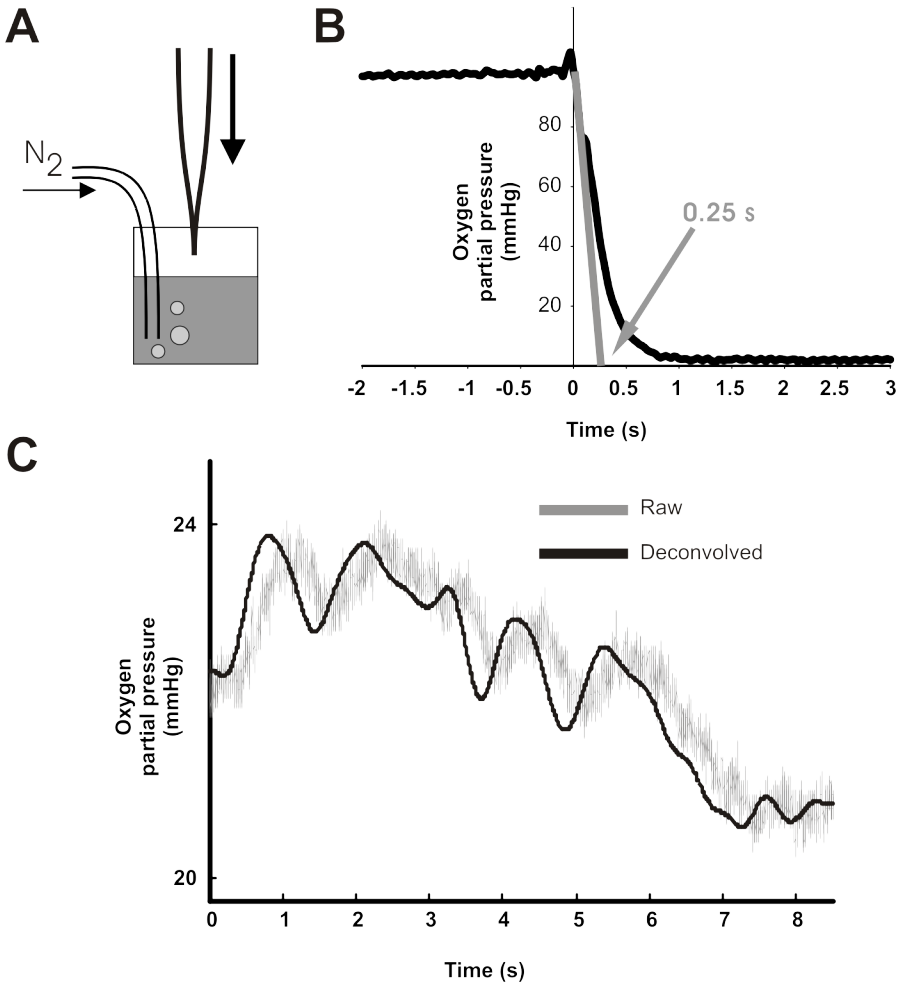

Supplementary Figure 1 Deconvolution of oxygen signals. *(A), The oxygen sensor impulse response was measured by quickly moving the electrode from air to a saline solution with 0 % oxygen concentration. (B), Response of the oxygen sensor to a step change in oxygen. Note the time constant of ~0.2 s. (C), Raw and deconvolved signal for an in vivo experiment. The deconvolved signal is shifted back in time.*

Bibliography

Attwell,D., and Laughlin,S.B. (2001). An energy budget for signaling in the grey matter of the brain. J. Cereb. Blood Flow Metab *21*, 1133-1145.

Bar,T. (1980). The vascular system of the cerebral cortex. Adv. Anat. Embryol. Cell Biol. *59*, I-62.

Borowsky,I.W., and Collins,R.C. (1989). Metabolic anatomy of brain: a comparison of regional capillary density, glucose metabolism, and enzyme activities. J Comp Neurol. *288*, 401-413.

Brickley,S.G., Farrant,M., Swanson,G.T., and Cull-Candy,S.G. (2001). CNQX increases GABA-mediated synaptic transmission in the cerebellum by an AMPA/kainate receptor-independent mechanism. Neuropharmacology *41*, 730-736.

Caesar,K., Offenhauser,N., and Lauritzen,M. (2008). Gamma-aminobutyric acid modulates local brain oxygen consumption and blood flow in rat cerebellar cortex. J. Cereb. Blood Flow Metab *28*, 906-915.

Chaigneau,E., Oheim,M., Audinat,E., and Charpak ,S. (2003). Two-photon imaging of capillary blood flow in olfactory bulb glomeruli. Proc Natl Acad Sci U S A *100*, 13081-13086.

Chaigneau,E., Tiret,P., Lecoq,J., Ducros,M., Knopfel,T., and Charpak,S. (2007). The relationship between blood flow and neuronal activity in the rodent olfactory bulb. J Neurosci *27*, 6452-6460.

Craigie,E.H. (1920). On the relative vascularity of various parts of the central nervous system of the albino rat. The Journal of Comparative Neurology *Volume 31*, 429-464.

Deschamps,T., and Cohen,L.D. (2001). Fast extraction of minimal paths in 3D images and applications to virtual endoscopy. Med. Image Anal. *5*, 281-299.

Dunning,H.S., and Wolff,H.G. (1937). The relative vascularity of various parts of the central and peripheral nervous system of the cat and its relation to function. The Journal of Comparative Neurology *67*, 433-450.

Fern,R., Davis,P., Waxman,S.G., and Ransom,B.R. (1998). Axon conduction and survival in CNS white matter during energy deprivation: a developmental study. J. Neurophysiol. *79*, 95-105.

Greer,C.A., Mori,K., and Shepherd,G.M. (1981). Localization of synaptic responses in the in vitro turtle olfactory bulb using the [14C]2-deoxyglucose method. Brain Res *217*, 295-303.

Gundersen,J.K., Ramsing,N.B., and Ronnie Nīhr Glud,R.N. (1998). Predicting the signal of O2 microsensors from physical dimensions, temperature, salinity, and O2 concentration. Advances in the science of limnology and oceanography *43*, 1932-1937.

Hevner,R.F., Liu,S., and Wong-Riley,M.T. (1995). A metabolic map of cytochrome oxidase in the rat brain: histochemical, densitometric and biochemical studies. Neuroscience *65*, 313-342.

Hevner,R.F., and Wong-Riley,M.T. (1989). Brain cytochrome oxidase: purification, antibody production, and immunohistochemical/histochemical correlations in the CNS. J. Neurosci *9*, 3884-3898.

Johnson,B.A., and Leon,M. (2007). Chemotopic odorant coding in a mammalian olfactory system. J. Comp Neurol. *503*, 1-34.

Kasowski,H.J., Kim,H., and Greer,C.A. (1999). Compartmental organization of the olfactory bulb glomerulus. J. Comp Neurol. *407*, 261-274.

Kida,I., Xu,F., Shulman,R.G., and Hyder,F. (2002a). Mapping at glomerular resolution : fMRI of rat olfactory bulb. Magnetic Resonance in Medecine *48*, 570-6.

Kida,I., Xu,F., Shulman,R.G., and Hyder,F. (2002b). Mapping at glomerular resolution: fMRI of rat olfactory bulb. Magn Reson. Med. *48*, 570-576.

Kleinfeld,D., Mitra,P.P., Helmchen,F., and Denk,W. (1998). Fluctuations and stimulus-induced changes in blood flow observed in individual capillaries in layers 2 through 4 of rat neocortex. Proc Natl Acad Sci U S A *95*, 15741-15746.

Nawroth,J.C., Greer,C.A., Chen,W.R., Laughlin,S.B., and Shepherd,G.M. (2007). An energy budget for the olfactory glomerulus. J Neurosci *27*, 9790-9800.

Ndubuizu,O., and LaManna,J.C. (2007). Brain tissue oxygen concentration measurements. Antioxid. Redox. Signal. *9*, 1207-1219.

Offenhauser,N., Thomsen,K., Caesar,K., and Lauritzen,M. (2005). Activity-induced tissue oxygenation changes in rat cerebellar cortex: interplay of postsynaptic activation and blood flow. J Physiol *565*, 279-294.

Petzold,G.C., Albeanu,D.F., Sato,T.F., and Murthy,V.N. (2008). Coupling of neural activity to blood flow in olfactory glomeruli is mediated by astrocytic pathways. Neuron *58*, 897-910.

Pirez,N., and Wachowiak,M. (2008). In vivo modulation of sensory input to the olfactory bulb by tonic and activity-dependent presynaptic inhibition of receptor neurons. J. Neurosci *28*, 6360-6371.

Schafer,J.R., Kida,I., Rothman,D.L., Hyder,F., and Xu,F. (2005). Adaptation in the rodent olfactory bulb measured by fMRI. Magn Reson. Med. *54*, 443-448.

Sethian,J.A. (1999). Efficient schemes: fast marching methods. In Level set methods and fast marching methods, P.G. ciarlet, A. iserles, R.V. Kohn, and M.H. Wright, eds. Cambridge university press), pp. 86-99.

Sharp,F.R., Kauer,J.S., and Shepherd,G.M. (1975). Local sites of activity-related glucose metabolism in rat olfactory bulb during olfactory stimulation. Brain Res. *98*, 596-600.

Sharp,F.R., Kauer,J.S., and Shepherd,G.M. (1977). Laminar analysis of 2-

deoxyglucose uptake in olfactory bulb and olfactory cortex of rabbit and rat. J Neurophysiol. *40*, 800-813.

Shepherd,G.M. (2003). The single capillary and the active brain. Proc. Natl. Acad. Sci. U. S. A *100*, 12535-12536.

Shepherd,G.M., and Charpak,S. (2008). The olfactory glomerulus: a model for neuro-glio-vascular biology. Neuron *58*, 827-829.

Shepherd,G.M., Chen,W.R., and Greer,C.A. (2004). Olfactory bulb. In The Synaptic Organization of the Brain, G.M. Shepherd , ed. (New York, Oxford: Oxford University Press), pp. 165-216.

Sokoloff,L., Reivich,M., Kennedy,C., Des Rosiers,M.H., Patlak,C.S., Pettigrew,K.D., Sakurada,O., and Shinohara,M. (1977). The [14C]deoxyglucose method for the measurement of local cerebral glucose utilization: theory, procedure, and normal values in the conscious and anesthetized albino rat. J Neurochem. *28*, 897-916.

Tekkok,S.B., Brown,A.M., and Ransom,B.R. (2003). Axon function persists during anoxia in mammalian white matter. J. Cereb. Blood Flow Metab *23*, 1340-1347.

Tekkok,S.B., and Ransom,B.R. (2004). Anoxia effects on CNS function and survival: regional differences. Neurochem. Res. *29*, 2163-2169.

Thompson,J.K., Peterson,M.R., and Freeman,R.D. (2003). Single-neuron activity and tissue oxygenation in the cerebral cortex. Science *299*, 1070-1072.

Thompson,J.K., Peterson,M.R., and Freeman,R.D. (2004). High-resolution neurometabolic coupling revealed by focal activation of visual neurons. Nat Neurosci *7*, 919-920.

Thompson,J.K., Peterson,M.R., and Freeman,R.D. (2005). Separate spatial scales determine neural activity-dependent changes in tissue oxygen within central visual pathways. J Neurosci *25*, 9046-9058.

Tsai,A.G., Friesenecker,B., Mazzoni,M.C., Kerger,H., Buerk,D.G., Johnson,P.C., and Intaglietta,M. (1998). Microvascular and tissue oxygen gradients in the rat mesentery. Proc. Natl. Acad. Sci. U. S. A *95*, 6590-6595.

Tsai,A.G., Johnson,P.C., and Intaglietta,M. (2003). Oxygen gradients in the microcirculation. Physiol Rev. *83*, 933-963.

Viswanathan,A., and Freeman,R.D. (2007). Neurometabolic coupling in cerebral cortex reflects synaptic more than spiking activity. Nat Neurosci *10*, 1308-1312.

Wachowiak,M., and Cohen,L.B. (2001). Representation of odorants by receptor neuron input to the mouse olfactory bulb. Neuron *32*, 723-735.

Wachowiak,M., Denk,W., and Friedrich,R.W. (2004). Functional organization of sensory input to the olfactory bulb glomerulus analyzed by two-photon calcium imaging. Proc Natl Acad Sci U S A *101*, 9097-9102.

Weber,B., Keller,A.L., Reichold,J., and Logothetis,N.K. (2008). The Microvascular

System of the Striate and Extrastriate Visual Cortex of the Macaque. Cereb. Cortex.

Wong-Riley,M.T. (1989). Cytochrome oxidase: an endogenous metabolic marker for neuronal activity. Trends Neurosci *12*, 94-101.

Wong-Riley,M.T., Trusk,T.C., Tripathi,S.C., and Hoppe,D.A. (1989). Effect of retinal impulse blockage on cytochrome oxidase-rich zones in the macaque striate cortex: II. Quantitative electron-microscopic (EM) analysis of neuropil. Vis. Neurosci *2*, 499-514.

Xu,F., Kida,I., Hyder,F., and Shulman,R.G. (2000). Assessment and discrimination of odor stimuli in rat olfactory bulb by dynamic functional MRI. Proc. Natl. Acad. Sci. U. S. A *97*, 10601-10606.

Yang,X., Renken,R., Hyder,F., Siddeek,M., Greer,C.A., Shepherd,G.M., and Shulman,R.G. (1998). Dynamic mapping at the laminar level of odor-elicited responses in rat olfactory bulb by functional MRI. Proc. Natl. Acad. Sci. U. S. A *95*, 7715-7720.

Chapter 4.1 : Oxygen consumption in the olfactory bulb

4.2 Odor adaptation in the olfactory bulb

4.2.1 Introduction

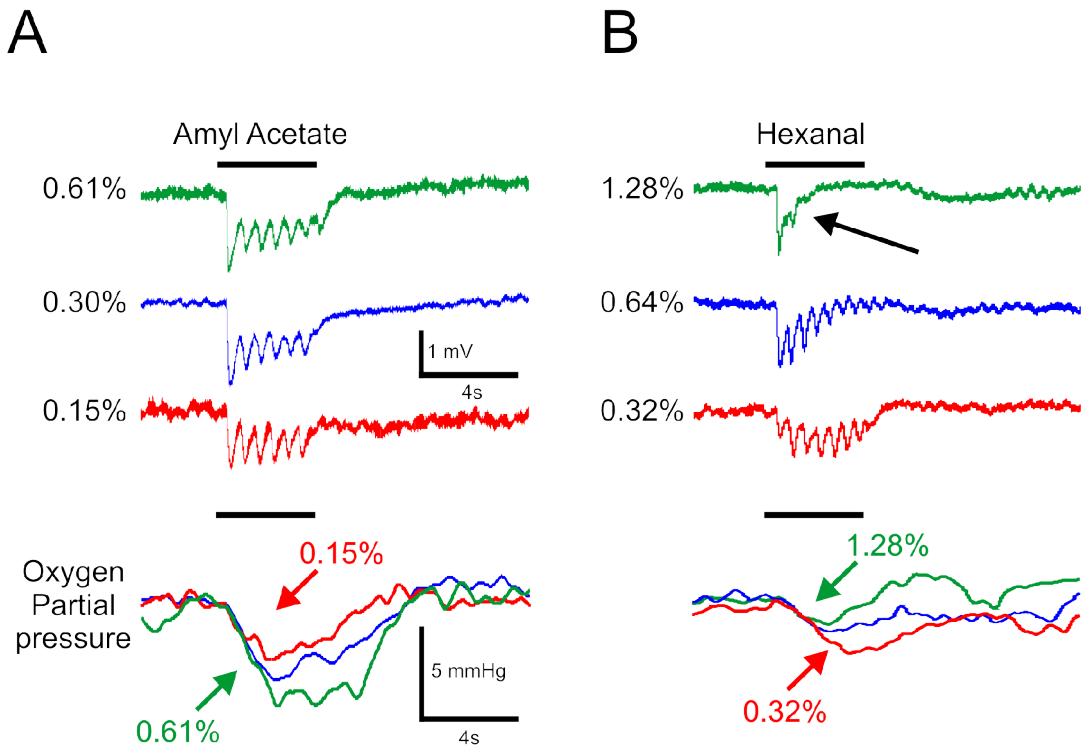

Illustration 46: Varying odor concentration elicits two types of Local Field Potential and oxygen responses in the glomerulus. Odor concentration is indicated as a percentage of air.

In the course of our experiments on oxygen consumption, we discovered a surprising phenomenon. In some cases, increasing odor concentration didn't increase oxygen consumption but decreased it. In the Illustration 46, two examples of the effect of varying odor concentration can be seen. In panel A, increasing odor concentration is accompanied by an increase in oxygen consumption, as would be expected. In panel B, increasing odor concentration strongly shortens the field potential response. As a result, the oxygen consumption is also reduced. We were first very excited by this result because we thought that it could potentially be a local inhibitory mechanism triggered by the odor in the Glomerular Layer. Hence this would have been a way to study oxygen consumption of inhibitory mechanisms as other groups recently did (Caesar, Offenhauser, and M. Lauritzen 2008). However other mechanisms could be responsible for such an effect, like peripheral odor adaptation. This last possibility proved to be right and enabled us to look at the effect of peripheral adaptation on the olfactory bulb. This is the

subject of the following publication, currently submitted.

In the publication on oxygen consumption in the olfactory bulb, we decided to restrict our analysis on responses which were not strongly affected by peripheral adaptation.

Second article

Chapter 4.2 : Odor adaptation in the olfactory bulb

Peripheral adaptation codes for high odor concentration in glomeruli

Jérôme Lecoq[1]*, Pascale Tiret[1]*, and Serge Charpak[1]

[1]Institut National de la Santé et de la Recherche Médicale (INSERM), U603, Paris 75006, France; Centre National de la Recherche Scientifique (CNRS), UMR 8154, Paris 75006, France; Laboratory of Neurophysiology and New Microscopies, Université Paris Descartes, Paris 75006, France.

* J.L. and P.T. contributed equally to the work

Corresponding author: Serge Charpak
INSERM U 603, Laboratory of Neurophysiology
45 rue des St Pères, 75006 Paris, France
Tel 33 1 42 86 41 48
Fax 33 1 42 86 41 51
E-mail: serge.charpak@univ-paris5.fr

Keywords: two-photon microscopy, olfactory bulb, field potential, presynaptic inhibition, odor map, concentration, calcium imaging, *in vivo*

Acknowledgments

Support was provided by the Institut National de la Santé et de la Recherche Médicale (INSERM), the Ministère de l'Education Nationale de la Recherche et de la Technologie (MENRT, NIC0025), the Centre National de la Recherche Scientifique (CNRS), the Fondation pour la Recherche Médicale (ICP20001222128), the Région Ile de France (Sesame program), the Fondation Bettancourt Schueller, the Human frontier science program organisation (HSFPO) and NIH-NID. Jérôme Lecoq was supported by a fellowship from the Fondation pour la Recherche Médicale (FDT20070910324) and Pascale Tiret by a fellowship from the Association Française contre les Myopathies (12411).

Abstract

Adaptation is a general property of sensory receptors which has been extensively studied in olfactory receptor neurons of the vertebrate nasal epithelium. In contrast, little is known about the transform of peripheral adaptation in the central nervous system. Here we used two-photon laser scanning microscopy and targeted extracellular recording to investigate the correlate of peripheral adaptation at the first synapse of the olfactory pathway, in glomeruli of anesthetized, freely breathing rats. We report that at very high concentration, some odorants triggered local field potential postsynaptic responses that rapidly adapted with time, some disappearing within 2 inhalations. Simultaneous measurements of postsynaptic responses and calcium influx in olfactory receptor neuron terminals revealed that this glomerular adaptation results from a decrease in glutamate release (by olfactory receptor neuron terminals). Glomerular adaptation was concentration-dependent and did not change the glomerular input-output curve. In addition, it was not affected by in situ application of antagonists of either glutamate ionotropic receptors or GABA B receptors, discarding the involvement of local presynaptic inhibition. These latter results imply that glomerular adaptation reflects the response decline of olfactory receptor neurons to sustained odor. We postulate that peripheral fast adaptation is a mean by which glomerular output codes for high concentration of odor.

Introduction

In the vertebrate nasal epithelium, volatile odorants bind to odorant receptors (L. Buck et al. 1991) located in the cilia of olfactory receptor neurons (ORNs). It triggers a G-protein-coupled cascade (Jones et al. 1989; Bakalyar et al. 1990) leading to the production of intraciliary cyclic adenosine 3',5'-monophosphate (cAMP). cAMP opens cyclic nucleotide-gated channel (CNG) (Nakamura et al.) permeable to Na+, K+ and Ca2+, leading to ciliary depolarization and firing of ORNs (for review see (Pifferi et al. 2006; Kleene 2008)). Calcium plays a dual excitatory and inhibitory role (Matthews et al. 2003). It depolarizes ORNs and activates Ca2+-sensitive chloride channels which allow an efflux of chloride, and further depolarizes ORNs (Lowe et al. 1993). It also triggers a series of negative feed-backs that underlie adaptation to repeated or prolonged odor activation. Although adaptation has been observed decades ago (Ottoson 1955), the underlying mechanisms are still a matter of debate, their respective contribution depending on the duration and intensity of stimulation (for review see (Bradley et al. 2004; Kleene 2008)). ORN responses already adapt during brief odor exposure (few seconds), Ca^{2+} and Ca^{2+} binding proteins such as Ca^{2+}/calmodulin decreasing the sensitivity of CNG channels (Kurahashi et al. 1997). However, other mechanisms participate to adaptation, e.g. Ca^{2+}/calmodulin triggering the hydrolysis of cAMP by a Ca2+/Calmodulin

dependent phosphodiesterase (Yan et al. 1995; Borisy et al. 1992) or the activation of a Ca2+/Calmodulin kinase II which inhibits the adenylyl cyclase (Wei et al. 1998; Leinders-Zufall et al. 1999).

While ORN adaptation has been extensively studied, few studies have investigated its consequences in the olfactory bulb. ORNs expressing a given odorant receptor type send their axons to the bulb where they converge onto 2 only topographically fixed glomeruli (Nagao et al. 2000; Ressler et al. 1994; Vassar et al. 1994). However, odorants usually activate more than 2 glomeruli, revealing small glomeruli ensembles or maps, as observed with several imaging methods including i) BOLD fMRI (Kida et al. 2002; Schafer et al. 2006; Xu et al. 2000; Yang et al. 1998) ii) optical imaging of calcium (H. Spors et al. 2006; M. Wachowiak et al. 2001; Bozza et al. 2004) voltage (H. Spors et al. 2002) and intrinsic signals (Belluscio et al. 2001; Luo et al. 2001; Meister et al. 2001; Rubin et al. 1999; N Uchida et al. 2000; Yuan et al. 2002), iii) electrophysiological recordings (Imamura et al. 1992; Yokoi et al. 1995; Katoh et al. 1993), and iv) measurements of 2-deoxyglucose consumption (Johnson et al. 1998; Stewart et al. 1979). These spatial maps vary with the odorant concentration and are temporally dynamic (H. Spors and Grinvald 2002, 2006; Schaefer et al. 2007), this variability involving several mechanisms (for review see (Kensaku Mori et al. 2006; M. Wachowiak et al. 2006).

The role of peripheral adaptation in modulation of glomerular maps remains to be established. Using BOLD fMRI, Schaffer et al. (Schafer et al. 2005) recently showed that adaptation to prolonged odor exposure can be detected in glomeruli however, since BOLD signals mostly report changes in blood flow, multiple mechanisms probably underlie the observed adaptation. In the course of a previous study, we have observed that in glomeruli, some odorants induce local field potential (LFP) responses with particular shapes (see figure 4C in (Chaigneau et al. 2007)), postsynaptic responses decreasing within 1 sec under sustained stimulation. Such responses could result from intraglomerular or interglomerular cell interactions as well as from a fast peripheral adaptation. Here, we demonstrate that peripheral adaptation underlies these particular glomerular responses which code for high odor concentration.

Methods

• Animals preparation

28 Wistar rats (PN 30–70) were used, anesthetized with urethane (I.P., 1.65 g/kg) and held in a standard stereotaxic apparatus. The posterior cisterna was drained. A craniotomy was performed above the two olfactory bulb hemispheres and the dura was removed. A 100 µm thick glass coverslip was placed over the bulb, fixed on the cranium, and the space below was filled with a 3.25% agar solution to prevent artifacts due to heart and respiration. The temperature of the animal was monitored with a rectal thermometer and maintained at 37°C with a

feedback-controlled heating blanket (Harvard Apparatus). For all experiments breathing frequency was monitored through a pneumogram transducer (BIOPAC Systems, Inc., Goleta, CA).

• Dyes loading protocol and *In Vivo* Two-Photon Imaging

Olfactory nerve terminals, and thus glomeruli, were labeled with Oregon green 488 BAPTA-1 dextran, 10-kDa (Invitrogen) or with Calcium green 1 dextran, 10-kDa (Invitrogen), 2–8 days before experiments using the methods developed by Wachowiak and Cohen (2001). Fluorophores were imaged using a custom-built two-photon laser-scanning microscope. An 890-nm excitation beam from a femtosecond Ti:Sapphire laser (10-W pump; Coherent Radiation, Palo Alto, CA) was focused onto olfactory nerve terminals by means of a 63X Leica (Deerfield, IL) water-immersion objective. Galvanometric scanners (Cambridge Technology, Cambridge, MA) controlled by home-built electronics and software (LABVIEW) were used to produce images from subregions of the field of view at rates up to 20 frames per second. Fluorescence was simultaneously acquired on two channels separated by a dichroic mirror (cut-off wavelength, 560 nm).

• Electrophysiological recordings and pharmacology

To record local field potential, a borosilicate micropipette was filled with a standard extracellular solution and 10µM Oregon green. To record glomerular activity, the fluorescent electrode was targeted into labeled glomeruli through agar. Electrophysiological signals were recorded with a NeuroData amplifier (Cygnus Technology, Delaware Water Gap, PA) digitized and stored on a PC (Digidata 1200A, Clampex 9, Axon Instruments, Foster City, CA). Pharmacological agents were pressure-applied with the pipette used for LFP recordings, by means of a PM8000 programmable multichannel pressure injection (MicroData Instrument). local pressure application of drugs, we substituted Oregon green with a red fluorophore (Alexa 594, 13µM) to avoid blurring glomerular boundaries (labeled with Oregon Green). Laser power was adjusted before injection to follow, as precisely as possible, the spatial diffusion of the fluorescent solution. The precise extent of drug effective region was impossible to determine since we monitored the dye and not the drug diffusion. NBQX (250 µM), DAPV (500 µM), and CGP35348 (1-10 mM) were obtained from Tocris and dissolved in the fluorescent standard extracellular solution. Osmolarity and pH of the final solution were checked.

• Olfactometer

Odors were applied during 4s with a custom-built olfactometer. The olfactometer delivered a constant flow of humidified air in a small Teflon reservoir surrounding the rat snout. During odor application, this flow was diverted through a glass reservoir of pure odor using electrical valves. All tubes connecting the odor reservoir to the snout were made of Teflon to minimize odor contamination. Odorants used were aldehydes (Benzaldehyde, Heptaldehyde, Octanal, Hexanal)

and esters (Amyl acetate, Ethyl propionate, Ethyl heptanoate, Ethyl caproate, Ethyl caprylate, Ethyl butyrate, Ethyl valerate). Two flow meters (Aalborg, Orangeburg, NY) (one in the clean air path and one before the odor reservoir) allowed to control odor concentration in a reproducible manner. To reveal adaptation, high odor concentrations were used, i.e. from 3%-100% when expressed in percentage of saturated air. However, we indicate in the text the true concentration that takes into account values of saturated vapor pressure.

- **Inter-trial alignments of calcium or LFP responses using respiratory movements**

Respiration monitoring revealed spontaneous variations of inhalation frequency. Although minor, they affected the inter-trial averaged responses, with a progressive decrease of calcium and LFP response amplitudes at each inhalation during sustained odor stimulation (see Supplementary Figure 1A). To take into account this respiration variability, we developed a new averaging algorithm using respiratory movements. For each individual trial, every breathing cycle period was detected and the position of the LFP response onset in the cycle period determined. An averaged breathing signal was then computed from several individuals and each individual trial was stretched to fit with this average. Calcium and LFP responses were then extracted by averaging the trails. Supplementary Figure 1B illustrates that our algorithm allowed to maintain response amplitudes in the averages during prolonged stimulation.

- **Data analysis**

All Data were analyzed through a home-made MATLAB program (MathWorks Inc., Natick, MA, USA). In the entire study, average values are expressed as mean ± S.E.M.

Results

- **High concentration of odor elicits two types of LFP responses in glomeruli**

To record postsynaptic responses in glomeruli, we used TPLSM and targeted a fluorescent extracellular glass pipette in the center of glomeruli. (see methods). As described in a previous study, odor evokes respiration-locked rapid negativities that mirror mitral cell EPSPs (Chaigneau et al. 2007). At high odor concentration (see methods), we observed two types of LFP responses that differed on their level of adaptation. Figure 1A shows a "weakly adapting response": when the odor concentration increased, the first negativity, i.e. the initial EPSP increased and saturated. The following negativities (or peaks) were either maintained or showed a slight decrease in amplitude as the response developed in time. In contrast, some responses strongly adapted upon high concentration (from 10-100% of saturated air). Figure 1B illustrates a LFP "Strongly Adapting Response" (SAR)

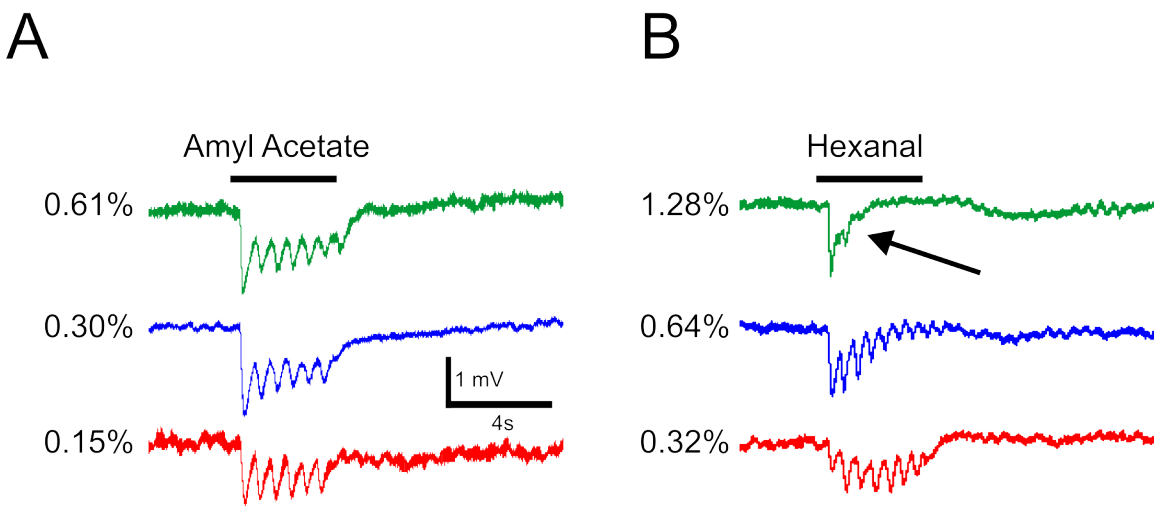

Figure 1 : *Varying odor concentration elicits two types of Field Potential responses*

*Field Potential (FP) was recorded in responding glomeruli (average of 3 to 4 trials). Odor elicits strong respiration-locked FP negativities. Varying odor concentration revealed two types of responses. Poorly adapting glomeruli (**A**) showed an increase of both responses with odor concentration, while strongly adapting glomeruli (**B**) responses were shortened with odor concentration.*

characterized by a large decrease or even an abolition of all the peaks following the initial one. In addition, the slow negative envelop which was crowned by the peaks at low odor concentration also disappeared. Occasionally, even the first peak amplitude slightly decreased (2 out 8 animals). Several mechanisms could underlie the shape of SAR, e.g. a postsynaptic inhibition of mitral cells involving the glomerular network or a progressive decrease in glutamate release by ORN terminals during sustained stimulation.

- **Glomerular recruitment and adaptation of Ca^{2+} influx in olfactory nerve terminals during odor stimulation.**

To analyze glutamate release by ORN terminals, we imaged Ca^{2+} influx in terminals loaded with organic Ca^{2+} sensors (see methods). Labeled terminals outlined glomerular boundaries and allowed to assess the spread and kinetics of odor-evoked calcium signals in several glomeruli of the dorsal olfactory bulb (M. Wachowiak and L. B. Cohen 2001). Animals were tested using TPLSM imaging of large fields of view and low temporal resolution. Figure 2A illustrates an experiment where five neighboring glomeruli were activated by ethyl valerate. At low concentration, the odor evoked a rapid Ca^{2+} response in a single glomerulus, confirming the glomerular specificity of odor stimulation at low concentration. The Ca^{2+}response had a sustained plateau-like shape, showing little attenuation during the 4s stimulation. Increasing the odor concentration (Figure 2B) recruited

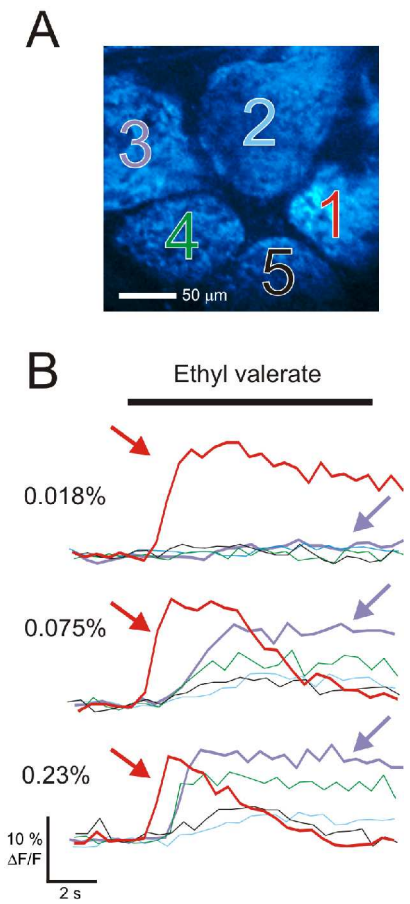

Figure 2 : *Increasing odor concentration reveals two types of odor-evoked presynaptic calcium responses*

*(**A**) Two-photon imaging of a field of view from the Glomerular Layer of the dorsal olfactory bulb, at rest. Glomeruli are visualized by labeling of olfactory receptor neurons with calcium green dextran (10kDa). Each glomerulus is located by a number. (**B**) Glomerular response presents two shapes according to odor concentration. Calcium responses are concentration dependent. Ethyl valerate applied at 0,018% evoked rapid increase in fluorescence in only one glomerulus showing the specificity of odor-evoked calcium signals at this low odor concentration. Glomerular response presents two shapes according to odor concentration. Calcium responses are concentration dependent. Note that the delay increases with odor dilution.*

neighboring glomeruli and shortened response latencies. More importantly, Ca^{2+} responses of the most “sensitive” glomerulus displayed an odor-dependency reminiscent of SARs: the plateau-like response observed at low concentration drastically shortened at high concentration (see the traces in red). Its initial amplitude even slightly decreased. In contrast, neighboring glomeruli presented little Ca^{2+} response adaptation. These results suggest that SARs are associated

with a concentration- and time -dependent adaptation of Ca^{2+} influx in ORN terminals and hence from a decrease in glutamate release. In addition, they show that the relative output of a “sensitive” glomerulus (responsive to low odor concentration) versus its neighbors changes drastically at high odor concentration.

- **The glomerular input-output curve of strongly adapting odor responses**

To further investigate the relation between pre and postsynaptic compartments during odor responses, we simultaneously recorded presynaptic Ca^{2+}, with a higher time resolution, and LFP responses in 8 animals. Figure 3A shows a typical example in which LFP responses were surprisingly similar to presynaptic Ca^{2+} responses. At low odor concentration, the initial Ca^{2+} and LFP peaks were similarly larger than the following ones which maintained their amplitude during the stimulus duration. Note that all peaks were phase-locked to respiration. At high odor concentration, both Ca^{2+} and LFP responses strongly adapted, the third inhalation peaks being barely detectable. In half of the cases (4 of 8 animals), Ca^{2+} concentration decreased below baseline (see arrow). It was not due to photo-bleaching as no run-down was visible prior to odor and as no decay with time was observable in during control experiments (no odor application, not shown). It also did not involve changes in respiration frequency. To quantify adaptation at both pre and postsynaptic levels, we measured on each individual trace the peak amplitude of Ca^{2+} (Figure 3B, top) and LFP (Figure 3B, bottom) signals. At low concentration, Ca^{2+} and LFP peaks decreased after the initial one but then remained similarly constant during most of the odor application (4s). At high concentration, Ca^{2+} and LFP peaks disappeared after the second inhalation but in one single case where they persisted during 5 inhalations. The average delay between the first peak and the first inhalation without any response was 1.04 ± 0.14 s (n=8), indicating that after only 2 inhalations, no output was sent to the cortex. The two graphs in figure 3B indicate that pre and postsynaptic responses were highly correlated. To determine whether this correlation was sensitive to odor concentration, we plotted LFP peaks as a function of presynaptic Ca^{2+} peaks (Figure 3C), i.e. the input-output curve of all recorded glomeruli. At both low and high odor concentration, the linear regression curves were surprisingly overlapping indicating that Ca^{2+} peaks are excellent markers of LFP peaks and hence of EPSPs (Chaigneau et al. 2007) recorded in mitral cells. Overall, SARs result from a decrease in glutamate release. Two mechanisms could underlie this adaptation: presynaptic inhibition of ORN terminals or adaptation of ORNs at the level of the nasal epithelium. Presynaptic inhibition regulates glutamate release at ORN terminals (V Aroniadou-Anderjaska et al. 2000; M. Ennis et al. 2001; Hsia et al. 1999; Olsen et al. 2008; M Wachowiak et al. 1999) by decreasing calcium influx in the terminals (M. Wachowiak et al. 2005; Vucinic et al. 2006; Pírez et al. 2008; M Wachowiak and L B Cohen 1999). To investigate the role of presynaptic

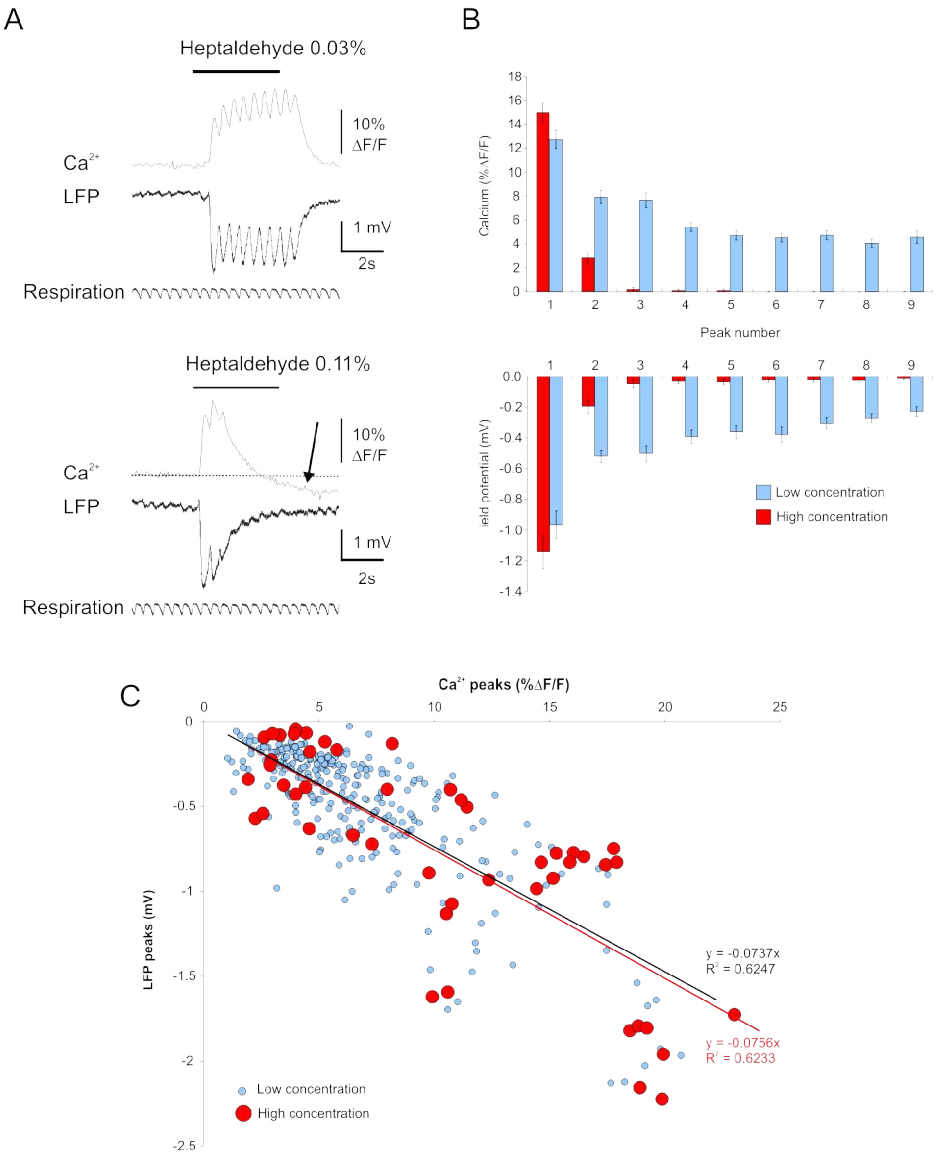

Figure 3 : *Both Calcium and LFP show adaptation*

*(**A**) Pre-synaptic Calcium and LFP were recorded in the same responding glomerulus. Increasing odor concentration (bottom traces) strongly shorten both LFP and Calcium peaks, while respiration was maintained constant. In some cases, strongly adapting responses induces a transient decrease (black arrow) in calcium compare to baseline which was not due to photo-bleaching (not shown). (**B**) Measuring peaks amplitude for calcium (top traces) and LFP (bottom traces) on 8 experiments confirmed this result when low concentration (blue bars) was compared to high concentration odor application (red bars). Note that Calcium and LFP show very similar amplitudes. (**C**) Input (Calcium) - Output (LFP) relationship is not affected by odor concentration as shown by linear regression on high and low concentration set of points.*

inhibition on SARs, we tested the effects of local application of antagonists of ionotropic glutamate receptors and GABA B receptors on ORN terminals Ca^{2+} responses.

- **Fast peripheral adaptation and not presynaptic inhibition underlies glomerular SARs**

We have previously shown that odor-evoked local LFP responses are abolished by focal applications of NBQX and D-APV, antagonists of glutamate AMPA and NMDA receptors, respectively (Chaigneau et al. 2007). Here, we co-applied Alexa Fluor 594 and glutamate antagonists (NBQX 250 µM, D-APV 500 µM) through the LFP recording pipette and maintained the pipette pressure until the drug diffused into the entire glomerular and periglomerular boundaries, ensuring that we blocked all intraglomerular and interglomerular glutamatergic synaptic inputs. Glutamate antagonists reversibly blocked the local LFP response, i.e. the LFP peaks and part of the slow component (Chaigneau et al. 2007). In contrast they reversibly enhanced presynaptic Ca^{2+} responses evoked by both low and high odor concentrations. Figure 4A1-2 illustrates that glutamate antagonists increased the initial Ca^{2+} peak to 126 % of control (Ca2+ peak (% DF/F.): control = 15.30 ± 3.15, NBQX + D-APV = 19.39 ± 3.33, recovery = 15.24 ± 3.26 , n= 8, p=0.013) as well as the overall Ca2+ signal (area) to 116 % of control (Ca2+ area (a.u.): control = 37.341 ± 5.69, NBQX + D-APV = 43.619 ± 6.948, recovery = 36.62 ± 5.77, n= 8, p=0.009). These results confirm, although under different anesthesia conditions, that tonic presynaptic inhibition modulates odor-evoked Ca^{2+} signals in ORN terminals (Pírez and Matt Wachowiak 2008) and in consequence the glomerular output. Similarly, local application of the GABA B receptor antagonist CGP 35348 (1-10 mM, not shown) also increased the overall signal (Ca^{2+} area (a.u.): control 22.86 ± 2.15, CGP 354488 27.97 ± 2.20; n=8 ; p=0.01), indicating that presynaptic tonic inhibition involved GABA B receptors (Pírez and Matt Wachowiak 2008). More importantly, blockade of presynaptic inhibition did seem to significantly affect the glomerular SARs. Ca^{2+} and LFP responses to low odor concentration in control conditions continued to be significantly larger than responses to high odor concentration in the absence of presynaptic inhibition. (see the trace superposition in figure 4A-B). The general shape of Ca^{2+} responses were not modified by glutamate antagonists implying that in urethane anesthetized animals, fast peripheral adaptation of ORNs underlies glomerular SARs that occur during under high odor concentration stimulation.

Discussion

Peripheral adaptation depends on calcium influx in ORNs and in consequence on odor concentration. Spatial maps of glomerular activity vary with odor concentration, however most of the variability is assigned to the low specificity of odorant receptors. Here, we investigated under which conditions odor

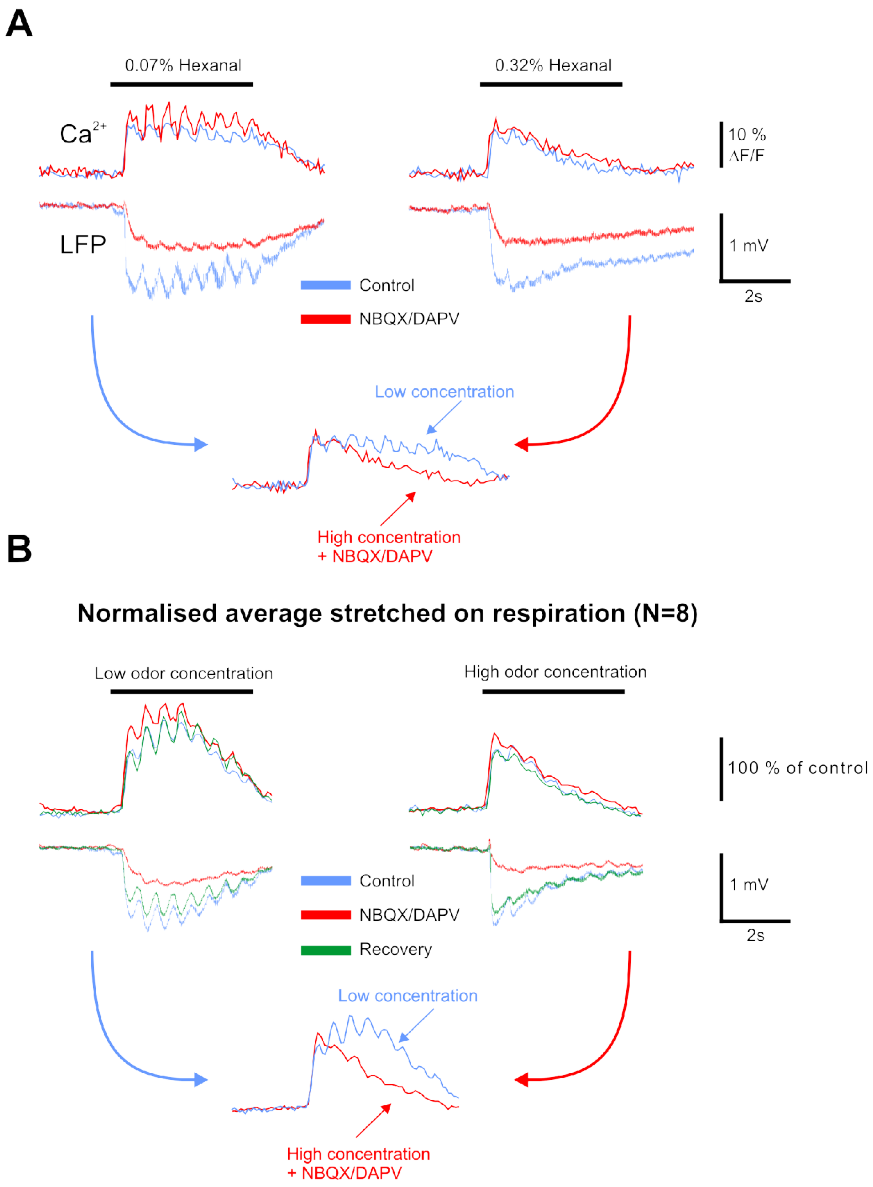

Figure 4 : *In vivo blockade of postsynaptic activity reveals a peripheral adaptation mechanism.*

*(**A**) Simultaneous recordings of pre- and postsynaptic activity in control condition and after NBQX-DAP5 (250 µM - 500 µM) application. An example of averaged traces obtained in one animal at low and high odor concentration. For both concentrations, drugs induced a reversible (not shown here) increase of the amplitude of presynaptic calcium response without affecting the global shape and blocked the LFP response. (**B**) Traces obtained with the same pharmacological protocol by averaging normalized acquisitions of 8 experiments stretched on respiration, in control, after drugs application and after recovery. Summary data showing the effect of NBQX and DAP5 on the area of presynaptic calcium signal are shown on both **A** and **B**.*

could modulate glomerular activation through a mechanism involving peripheral adaptation. We specifically analyzed postsynaptic glomerular responses that expressed strong adaptation under high odor concentration. We found that these glomerular SAR resulted from a decrease in glutamate release by ORN terminals which did not involve local presynaptic inhibition. Our study thus indirectly demonstrated that glomerular SAR result from peripheral adaptation of ORNs. Our pharmacological experiments confirm the existence of a tonic presynaptic inhibition of ORN terminals (Pírez and Matt Wachowiak 2008; Petzold et al. 2008) but also shows that at high concentration, peripheral adaptation largely dominates evoked-presynaptic inhibition.

It is an important consideration that we certainly did not record from glomeruli "specific" of a given odorant. Therefore, the concentrations used to activate glomeruli were probably, by 1-several orders of magnitude, higher than the ones that would activate "specific" glomeruli, in particular in unanesthetized animals. Still, we believe that the observed adaptation is a general mechanism that simply depends on the level of ORN activation, and will thus primarily appears in "specific" glomeruli. In consequence, we postulate that odor stimulation of increasing intensity progressively shortens "specific" glomerular responses. As a

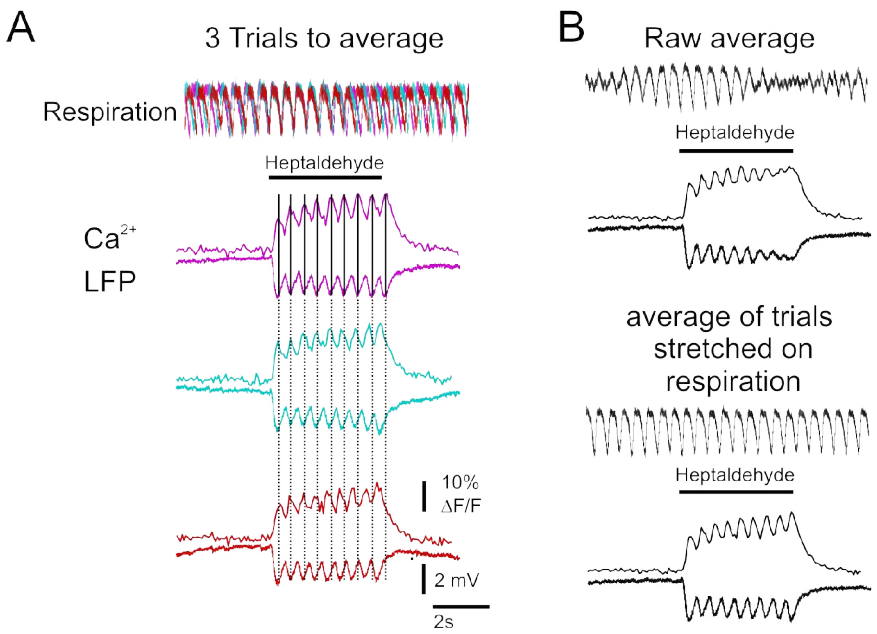

Supplementary Figure 1 : *Synchronized on respiration averaging*

*(**A**) Individuals trials show spontaneous breathing frequency variability (see top breathing traces) which introduce a shift in the calcium and FP responses (see dotted lines on individuals colored bottom traces). (**B**) Raw averaging (top traces) reveals this asynchrony which can be corrected by synchronizing every trials with an average breathing trace (see bottom traces and Methods).*

consequence, at high concentration, only the first inhalation will transmit information to second order neurons, in contrast to what occurs in surrounding less “responsive” but more active glomeruli. The persistence of an odor response during the first inhalation indicates that this glomerular activation state remains compatible with the ability to discriminate odors. Indeed recent studies have demonstrated that discrimination tasks can be achieved within few hundreds milliseconds (Abraham et al. 2004; Naoshige Uchida et al. 2003; Slotnick 2007; Rinberg et al. 2006). In fact the full development of the first inhalation glomerular map is not even required for successful odor discrimination (Wesson et al. 2008). In addition to coding of high odor concentration, the fast peripheral adaptation underlying glomerular adaptation could increase the dynamic range of glomerular activation. Such a role had been proposed for evoked-presynaptic inhibition but couldn't be observed (Pírez and Matt Wachowiak 2008). and is classically reported at the level of ORN transduction (for review see (Kleene et al. 2008)).

Bibliography

Abraham, Nixon M, Hartwig Spors, Alan Carleton, Troy W Margrie, Thomas Kuner, and Andreas T Schaefer. 2004. “Maintaining accuracy at the expense of speed: stimulus similarity defines odor discrimination time in mice.” *Neuron* 44(5):865-76.

Aroniadou-Anderjaska, V, F M Zhou, C A Priest, M Ennis, and M T Shipley. 2000. “Tonic and synaptically evoked presynaptic inhibition of sensory input to the rat olfactory bulb via GABA(B) heteroreceptors.” *Journal of Neurophysiology* 84(3):1194-203.

Bakalyar, H A, and R R Reed. 1990. “Identification of a specialized adenylyl cyclase that may mediate odorant detection.” *Science (New York, N.Y.)* 250(4986):1403-6.

Belluscio, L, and L C Katz. 2001. “Symmetry, stereotypy, and topography of odorant representations in mouse olfactory bulbs.” *The Journal of Neuroscience: The Official Journal of the Society for Neuroscience* 21(6):2113-22.

Borisy, F F, G V Ronnett, A M Cunningham, D Juilfs, J Beavo, and S H Snyder. 1992. “Calcium/calmodulin-activated phosphodiesterase expressed in olfactory receptor neurons.” *The Journal of Neuroscience: The Official Journal of the Society for Neuroscience* 12(3):915-23.

Bozza, Thomas, John P McGann, Peter Mombaerts, and Matt Wachowiak. 2004. “In vivo imaging of neuronal activity by targeted expression of a genetically encoded probe in the mouse.” *Neuron* 42(1):9-21.

Bradley, J., W. Bonigk, K. W. Yau, and S. Frings. 2004. “Calmodulin permanently associates with rat olfactory CNG channels under native conditions.” *Nature neuroscience* 7(7):705-10.

Buck, L., and R. Axel. 1991. “A novel multigene family may encode odorant receptors: a molecular basis for odor recognition.” *Cell* 65(1):175-87.

Chaigneau, E., P. Tiret, J. Lecoq, M. Ducros, T. Knopfel, and S. Charpak. 2007. “The relationship between blood flow and neuronal activity in the rodent olfactory bulb.” *J Neurosci* 27(24):6452-60.

Ennis, M., F. M. Zhou, K. J. Ciombor, V. Aroniadou-Anderjaska, A. Hayar, E. Borrelli, L. A. Zimmer, F. Margolis, and M. T. Shipley. 2001. “Dopamine D2 receptor-mediated presynaptic inhibition of olfactory nerve terminals.” *Journal of neurophysiology* 86(6):2986-97.

Hsia, A Y, J D Vincent, and P M Lledo. 1999. “Dopamine depresses synaptic inputs into the olfactory bulb.” *Journal of Neurophysiology* 82(2):1082-5.

Imamura, K, N Mataga, and K Mori. 1992. “Coding of odor molecules by mitral/tufted cells in rabbit olfactory bulb. I. Aliphatic compounds.” *Journal of Neurophysiology* 68(6):1986-2002.

Johnson, B. A., C. C. Woo, and M. Leon. 1998. “Spatial coding of odorant features in the glomerular layer of the rat olfactory bulb.” *The Journal of comparative neurology* 393(4):457-71.

Jones, D T, and R R Reed. 1989. “Golf: an olfactory neuron specific-G protein involved in odorant signal transduction.” *Science (New York, N.Y.)* 244(4906):790-5.

Katoh, K, H Koshimoto, A Tani, and K Mori. 1993. “Coding of odor molecules by mitral/tufted cells in rabbit olfactory bulb. II. Aromatic compounds.” *Journal of Neurophysiology* 70(5):2161-75.

Kida, I., F. Xu, R. G. Shulman, and F. Hyder. 2002. “Mapping at glomerular resolution: fMRI of rat olfactory bulb.” *Magn Reson Med* 48(3):570-6.

Kleene, Steven J. 2008. “The Electrochemical Basis of Odor Transduction in Vertebrate Olfactory Cilia.” *Chemical Senses*. Available at: http://www.ncbi.nlm.nih.gov/pubmed/18703537 [Accessed August 30, 2008].

Kurahashi, T, and A Menini. 1997. “Mechanism of odorant adaptation in the olfactory receptor cell.” *Nature* 385(6618):725-9.

Leinders-Zufall, T, M Ma, and F Zufall. 1999. “Impaired odor adaptation in olfactory receptor neurons after inhibition of Ca2+/calmodulin kinase II.” *The Journal of Neuroscience: The Official Journal of the Society for Neuroscience* 19(14):RC19.

Lowe, G, and G H Gold. 1993. “Nonlinear amplification by calcium-dependent chloride channels in olfactory receptor cells.” *Nature* 366(6452):283-6.

Luo, M, and L C Katz. 2001. “Response correlation maps of neurons in the mammalian olfactory bulb.” *Neuron* 32(6):1165-79.

Matthews, Hugh R, and Johannes Reisert. 2003. “Calcium, the two-faced messenger of olfactory transduction and adaptation.” *Current Opinion in Neurobiology* 13(4):469-75.

Meister, M., and T. Bonhoeffer. 2001. “Tuning and topography in an odor map on

the rat olfactory bulb." *J Neurosci* 21(4):1351-60.

Mori, Kensaku, Yuji K Takahashi, Kei M Igarashi, and Masahiro Yamaguchi. 2006. "Maps of odorant molecular features in the Mammalian olfactory bulb." *Physiological Reviews* 86(2):409-33.

Nagao, H, Y Yoshihara, S Mitsui, H Fujisawa, and K Mori. 2000. "Two mirror-image sensory maps with domain organization in the mouse main olfactory bulb." *Neuroreport* 11(13):3023-7.

Nakamura, T, and G H Gold. "A cyclic nucleotide-gated conductance in olfactory receptor cilia." *Nature* 325(6103):442-4.

Olsen, Shawn R, and Rachel I Wilson. 2008. "Lateral presynaptic inhibition mediates gain control in an olfactory circuit." *Nature* 452(7190):956-60.

Ottoson, D. 1955. "Analysis of the electrical activity of the olfactory epithelium." *Acta physiologica Scandinavica* 35(122):1-83.

Petzold, Gabor C, Dinu F Albeanu, Tomokazu F Sato, and Venkatesh N Murthy. 2008. "Coupling of neural activity to blood flow in olfactory glomeruli is mediated by astrocytic pathways." *Neuron* 58(6):897-910.

Pifferi, Simone, Anna Boccaccio, and Anna Menini. 2006. "Cyclic nucleotide-gated ion channels in sensory transduction." *FEBS Letters* 580(12):2853-9.

Pírez, Nicolás, and Matt Wachowiak. 2008. "In vivo modulation of sensory input to the olfactory bulb by tonic and activity-dependent presynaptic inhibition of receptor neurons." *The Journal of Neuroscience: The Official Journal of the Society for Neuroscience* 28(25):6360-71.

Ressler, K J, S L Sullivan, and L B Buck. 1994. "Information coding in the olfactory system: evidence for a stereotyped and highly organized epitope map in the olfactory bulb." *Cell* 79(7):1245-55.

Rinberg, Dmitry, Alexei Koulakov, and Alan Gelperin. 2006. "Speed-accuracy tradeoff in olfaction." *Neuron* 51(3):351-8.

Rubin, B D, and L C Katz. 1999. "Optical imaging of odorant representations in the mammalian olfactory bulb." *Neuron* 23(3):499-511.

Schaefer, Andreas T, and Troy W Margrie. 2007. "Spatiotemporal representations in the olfactory system." *Trends in Neurosciences* 30(3):92-100.

Schafer, J. R., I. Kida, D. L. Rothman, F. Hyder, and F. Xu. 2005. "Adaptation in the rodent olfactory bulb measured by fMRI." *Magn Reson Med* 54(2):443-8.

Schafer, J. R., I. Kida, F. Xu, D. L. Rothman, and F. Hyder. 2006. "Reproducibility of odor maps by fMRI in rodents." *NeuroImage* 31(3):1238-46.

Slotnick, Burton. 2007. "Odor-sampling time of mice under different conditions." *Chemical Senses* 32(5):445-54.

Spors, H., and A. Grinvald. 2002. "Spatio-temporal dynamics of odor representations in the mammalian olfactory bulb." *Neuron* 34(2):301-15.

Spors, H., M. Wachowiak, L. B. Cohen, and R. W. Friedrich. 2006. “Temporal dynamics and latency patterns of receptor neuron input to the olfactory bulb.” *J Neurosci* 26(4):1247-59.

Stewart, W B, J S Kauer, and G M Shepherd. 1979. “Functional organization of rat olfactory bulb analysed by the 2-deoxyglucose method.” *The Journal of Comparative Neurology* 185(4):715-34.

Uchida, N, Y K Takahashi, M Tanifuji, and K Mori. 2000. “Odor maps in the mammalian olfactory bulb: domain organization and odorant structural features.” *Nature Neuroscience* 3(10):1035-43.

Uchida, Naoshige, and Zachary F Mainen. 2003. “Speed and accuracy of olfactory discrimination in the rat.” *Nature Neuroscience* 6(11):1224-9.

Vassar, R, S K Chao, R Sitcheran, J M Nuñez, L B Vosshall, and R Axel. 1994. “Topographic organization of sensory projections to the olfactory bulb.” *Cell* 79(6):981-91.

Vucinic, D., L. B. Cohen, and E. K. Kosmidis. 2006. “Interglomerular center-surround inhibition shapes odorant-evoked input to the mouse olfactory bulb in vivo.” *Journal of neurophysiology* 95(3):1881-7.

Wachowiak, M, and L B Cohen. 1999. “Presynaptic inhibition of primary olfactory afferents mediated by different mechanisms in lobster and turtle.” *The Journal of Neuroscience: The Official Journal of the Society for Neuroscience* 19(20):8808-17.

Wachowiak, M., and L. B. Cohen. 2001. “Representation of odorants by receptor neuron input to the mouse olfactory bulb.” *Neuron* 32(4):723-35.

Wachowiak, M., J. P. McGann, P. M. Heyward, Z. Shao, A. C. Puche, and M. T. Shipley. 2005. “Inhibition [corrected] of olfactory receptor neuron input to olfactory bulb glomeruli mediated by suppression of presynaptic calcium influx.” *Journal of neurophysiology* 94(4):2700-12.

Wachowiak, M., and M. T. Shipley. 2006. “Coding and synaptic processing of sensory information in the glomerular layer of the olfactory bulb.” *Seminars in cell & developmental biology* 17(4):411-23.

Wei, J, A Z Zhao, G C Chan, L P Baker, S Impey, J A Beavo, and D R Storm. 1998. “Phosphorylation and inhibition of olfactory adenylyl cyclase by CaM kinase II in Neurons: a mechanism for attenuation of olfactory signals.” *Neuron* 21(3):495-504.

Wesson, Daniel W, Ryan M Carey, Justus V Verhagen, and Matt Wachowiak. 2008. “Rapid encoding and perception of novel odors in the rat.” *PLoS Biology* 6(4):e82.

Xu, F., I. Kida, F. Hyder, and R. G. Shulman. 2000. “Assessment and discrimination of odor stimuli in rat olfactory bulb by dynamic functional MRI.” *Proceedings of the National Academy of Sciences of the United States of America* 97(19):10601-6.

Yan, C, A Z Zhao, J K Bentley, K Loughney, K Ferguson, and J A Beavo. 1995. “Molecular cloning and characterization of a calmodulin-dependent phosphodiesterase enriched in olfactory sensory neurons.” *Proceedings of the National Academy of Sciences of the United States of America* 92(21):9677-81.

Yang, X, R Renken, F Hyder, M Siddeek, C A Greer, G M Shepherd, and R G Shulman. 1998. “Dynamic mapping at the laminar level of odor-elicited responses in rat olfactory bulb by functional MRI.” *Proceedings of the National Academy of Sciences of the United States of America* 95(13):7715-20.

Yokoi, M, K Mori, and S Nakanishi. 1995. “Refinement of odor molecule tuning by dendrodendritic synaptic inhibition in the olfactory bulb.” *Proceedings of the National Academy of Sciences of the United States of America* 92(8):3371-5.

Yuan, Qi, Carolyn W Harley, John H McLean, and Thomas Knöpfel. 2002. “Optical imaging of odor preference memory in the rat olfactory bulb.” *Journal of Neurophysiology* 87(6):3156-9.

Chapter 4.2 : Odor adaptation in the olfactory bulb

4.3 Oxygen diffusion in the olfactory bulb

4.3.1 Introduction

Oxygen gradients in the vicinity of brain capillaries have already been studied but at a limited depth and in steady-state (E Vovenko 1999). In the meantime, recordings from single capillaries have shown that blood flow is highly variable in time (Kleinfeld et al. 1998). Some spontaneous oscillations occur at a frequency of around 0.1 Hz and were termed “vasomotion”. They are due to variation in the arterial supply and were described using a variety of techniques. Some of these fluctuations were particularly sensitive to anesthesia. As early as 1958, Clark using chronically implanted oxygen electrodes described similar oscillations in oxygen level in the cat cortex (Clark, Misrahy, and R. P. Fox 1958). Both events obviously relates to the same phenomenon.

Diffusion processes are slow as we have already mentioned (see chapter 2.5.4). Hence oxygen fluctuations can be expected to follow blood fluctuations with a delay related to oxygen diffusion in the parenchymal tissue. This lag would provide a direct way to look at diffusion processes in the neuronal tissue and how these processes are modulated.

A recent study, using simultaneous oxygen and blood flow recordings (through polarographic electrodes and laser Doppler flowmetry) showed a delay of ~1.2 second between the two signals (Masamoto et al. 2007). These delays were quite variable (from 0.6 to 2.3 second for individual animals). Laser Doppler flowmetry, even if it is a very efficient technique to record fast transients in flow can't give access to variations in individual capillaries. As a result they couldn't analyze in more detail the origin of these variations. A more precise technique to measure blood flow is required to study in detail the effect of oxygen diffusion on the oxygen supply to the brain.

4.3.2 Methods

- **Principle**

Two photon imaging provides a way to look at blood flow in depth at the level of single capillaries (E. Chaigneau et al. 2003; Kleinfeld et al. 1998). Oxygen clark electrodes also gives access to oxygen levels in a very confined region of a few μm^3. Therefore both techniques can record these two parameters in depth at a very good spatial and time resolution.

As we have already developed a dedicated algorithm (see chapter 3.5), we can reconstruct directly in vivo the 3D local vascular environment of the recording electrode. This is a very good base to look at how the local oxygen tension is regulated by the microcirculation at the level of single capillaries.

Single capillaries were targeted according to the method already described

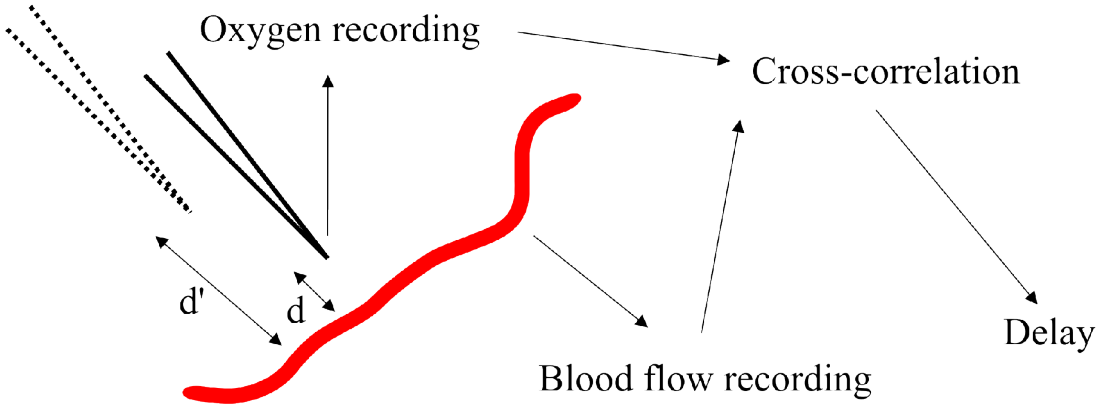

Illustration 47: Principle of the experiment. Oxygen and blood flow are recorded simultaneously for different distance d and d' . The diffusion delay is extracted using a cross-correlation algorithm.

(see chapter 3.3). We could therefore bring directly the oxygen electrode to individual chosen capillaries. The accuracy of the targeting algorithm was good enough to bring the electrode tip very close to the capillary wall (from 5 to 10 µm).

The method used to record blood flow from single capillaries has already been described before (see chapter 4.1.2). It relies on the intravenous injection of a fluorescent dye in the blood. Two photon longitudinal line-scans give access to the speed of individual red blood cells.

The principle of the experiment is depicted in the Illustration 47. Briefly, simultaneous flow and oxygen recordings are done at several known distance d and d' from the capillary wall. A cross-correlation diagram is then computed off-line to extract the delay between the two signals.

An example of such a dual recording is shown in the Illustration 48. Note how both signals are strikingly correlated. Both slow and fast events in blood flow modify oxygen tissue level. While we corrected for the delay induced by the oxygen electrode itself through deconvolution (see chapter 4.1.2), our time resolution was insufficient to look at Erythrocyte Associated Transients (see chapter 2.5.4). A faster technique, like phosphorescence quenching (see chapter 2.4.3) would be required as it has previously been done in the periphery (Golub and Pittman 2005).

- **Cross correlation algorithm between single capillary red blood cells' speed and oxygen level in the tissue.**

Extracting correlation between oxygen level and single capillary red blood cells' speed is a difficult task. Indeed, if in some cases, the correlation is obvious (see Illustration 48), in some other cases (not shown), these correlated oscillations were blurred by a fluctuating baseline. In fact, every capillary in the local area contributes with a different delay to the local oxygen level. As a consequence,

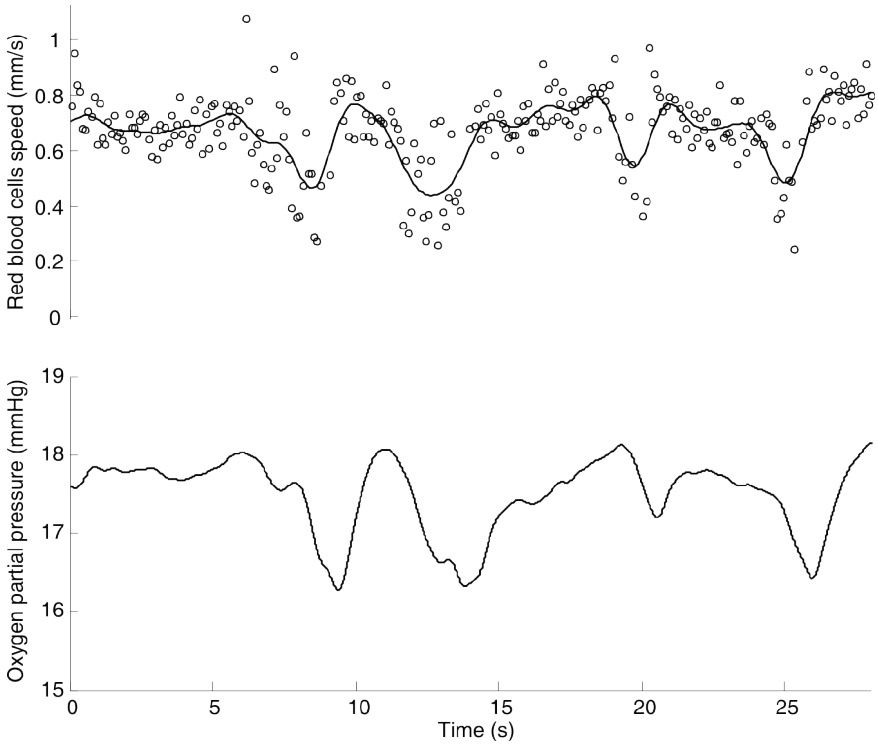

Illustration 48: Single capillary red blood cell speed and oxygen level in the neuronal tissue are highly correlated. In this example, the distance between the electrode tip and the vessel was 27 µm.

even if a human eye is able to see that both signals are correlated, the fluctuation in the baseline makes it difficult to use a simple correlation scheme.

Another difficulty arises from the fact that both signals are acquired at different time frequencies. Most available cross-correlation algorithm assumes that they are measured at the same time points.

I had therefore to design a specific correlation algorithm dedicated to this task.

To relate two signals f and g measured at the points t_i, the classical approach is to use the normalized cross correlation:

$$C_{orr}(t)=\frac{\sum_i (f(t_i)-\bar{f})(g(t_i-t)-\bar{g})}{\sqrt{\sum_i (f(t_i)-\bar{f})^2}\times\sqrt{\sum_i (g(t_i)-\bar{g})^2}} \quad (7)$$

Where $\bar{f}$ and $\bar{g}$ are the mean of f and g over the whole time interval.

In this formula, C_{orr} gives values close to 1 when the fluctuation of f and g, around the baseline $\bar{f}$ and $\bar{g}$, are correlated. When they are anti-correlated, C_{orr} is close to -1 and when they are not correlated, it is close to 0.

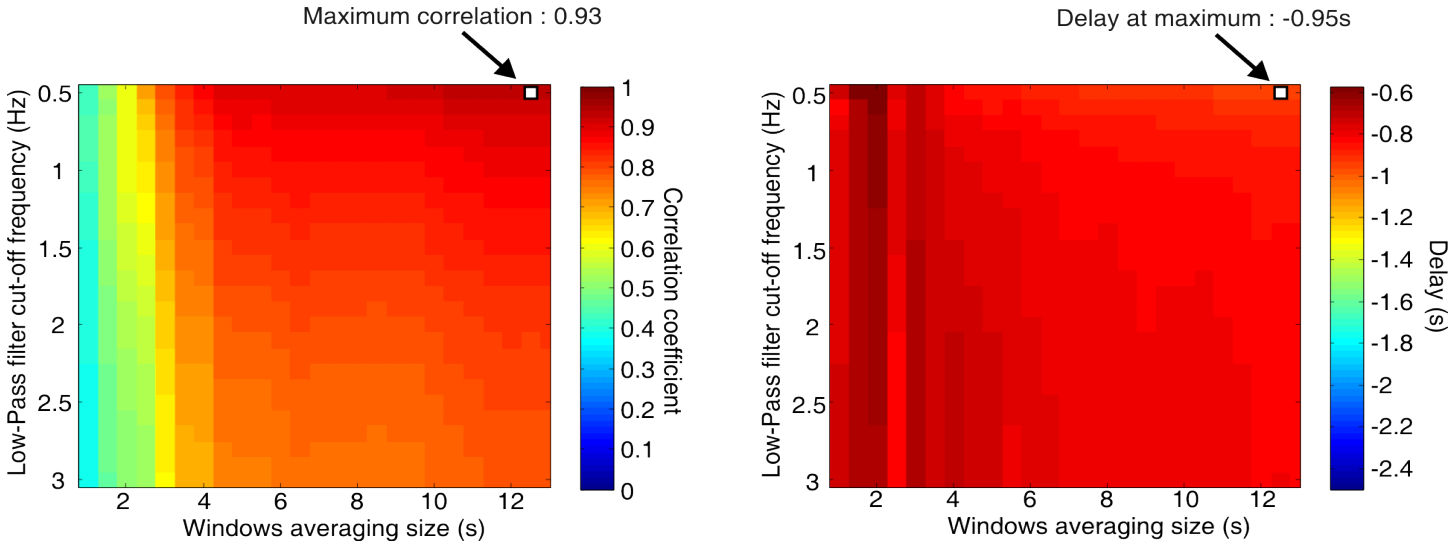

Illustration 49: Correlation map between red blood cell speed and oxygen tissue level for the Illustration 48.

Obviously C_{orr} can only be measured at discrete time points t.

Now, I used this formula and modified it in a few ways.

- f is chosen to be the blood flow because it is acquired unevenly (when red blood cells passes). As a result g is the oxygen tissue level. The reason is that, as we saw, both signals are not acquired at the same acquisition speed. So we need to interpolate to bring the two signals back on the same time points. Oxygen is acquired at a faster speed (around 10kHz) than blood speed (10Hz). Moreover a linear interpolation on the oxygen signal will be more relevant because its fluctuations are slower (see Illustration 48).

- The main problem in the formula 7 for our particular application is the value of $\bar{f}$ and $\bar{g}$. If the oxygen tissue level is influenced by another capillary, $\bar{g}$ can be very different from $\bar{f}$, even if some correlations are clearly shared. As a result, we can't measure $\bar{g}$ and $\bar{f}$ on a long period (more than 10 seconds). To account for this, we decided to measure the value of C_{orr} on different time periods T and compare the correlation of the two signals on these periods. This time window is then slided along the signals to select a subregion to look for correlations.

- To filter out irrelevant fluctuations, we used a low-pass filter. One must remember that most low-pass filters induce a phase shift which would affect our measurements of the delay. We avoided this problem using zero-phase digital filtering. The principle is to process the data in both the forward and reverse directions. After filtering in the forward direction, it reverses the filtered sequence and runs it back through the filter. The resulting sequence has precisely zero-phase distortion and doubles the filter order. We also evaluated the influence of the cut-off frequency of the filter on the amplitude

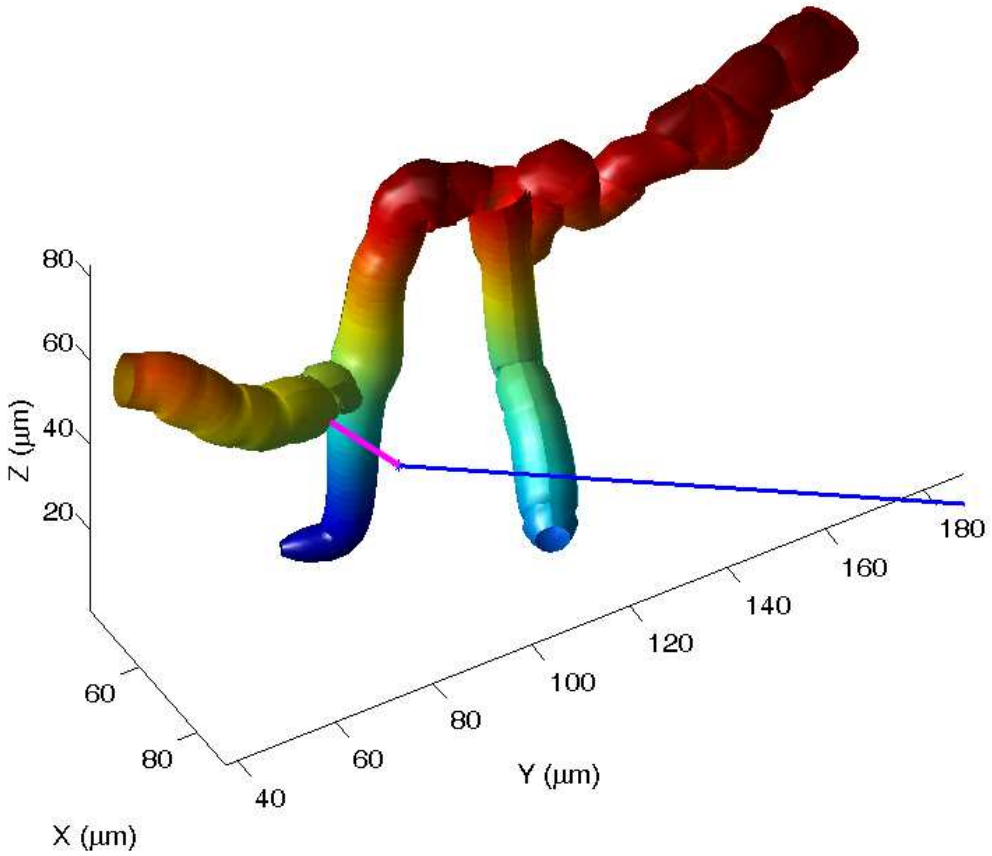

Illustration 50: 3D reconstruction of the vascular environment around the oxygen electrode (indicated in blue). The pink line (15 µm long) connects the electrode tip to the closest capillary segment.

of the correlation. We used a Butterworth filter as a base. Its order (after zero-phase filtering) was 8.

The result of the algorithm is shown in the Illustration 49 for the example of the Illustration 48. For each low-pass filter cut-off frequency and windows averaging size, the value of the maximum correlation and its corresponding delay is extracted. These values are color coded on the two graphs.

Note that a minimal windows size of 4 seconds is required. Filtering high frequency fluctuations also improves the extracted correlation. This is pretty much expected regarding the time resolution of our oxygen electrodes. All the following results were deduced from the computations of these two maps. The maximal correlation with its corresponding time lag is always extracted. These points always correspond to time windows between 8 and 12 seconds and cut-

frequencies between 1.5 and 0.5 Hz.

- **3D reconstruction of the local microvasculature**

Regarding the 3D reconstruction, the same algorithm than for the analysis of the olfactory bulb's glomerular columns was used (see chapter 3.5 for a detailed description).

For each electrode location, a two-photon stack of the area is performed (typical volume 100µm x 100µm x 100µm) and the vascular anatomy is reconstructed. The electrode's tip is manually located.

A typical reconstruction is shown in the Illustration 50. We must keep in mind that the dye injected in the blood (Texas Red Dextran 70.000) only stains the intravascular compartment. We have no information on the local thickness of the endothelial cells. For this reason, we decided to measure the distance between the electrode tip and the capillary center.

The distance to every local capillary segment is computed. Therefore we could control that our electrode doesn't get too close to another capillary.

- **Data analysis**

All Data were analyzed through a home-made MATLAB program (MathWorks Inc., Natick, MA, USA). In the entire study, average values are expressed as mean ± S.D.

4.3.3 Results and discussion

We could extract correlations out of 6 capillaries. While additional experiments are required to complete the following results, this was sufficient to draw some interesting conclusions.

The average correlation coefficient in the 6 experiments was 0.66 ± 0.06. Recordings with a correlation coefficient inferior to 0,5 were discarded. The average closest distance from the capillary center to the electrode's tip was 10.4 ± 4.9 µm. The furthest distance was 28.5 ± 11,8 µm. The average depth of the 6 capillaries was 151 ± 78 µm. In these experiments, the Glomerular Layer was not labeled. However we can infer from the depth of our recordings and the distribution of capillaries in between the nerve and the Glomerular Layer that our capillaries are located in the Glomerular Layer.

- **Oxygen gradients near capillaries**

The first thing we look at is the existence of local gradients in oxygen. Indeed oxygen gradients in the microcirculation have been extensively studied (for a review see (Tsai, P. C. Johnson, and M. Intaglietta 2003)) Surprisingly, only one out of 6 capillary showed a marked increase of oxygen baseline level in the vicinity of the capillary (light blue in the Illustration 51). Moreover, the value of oxygen

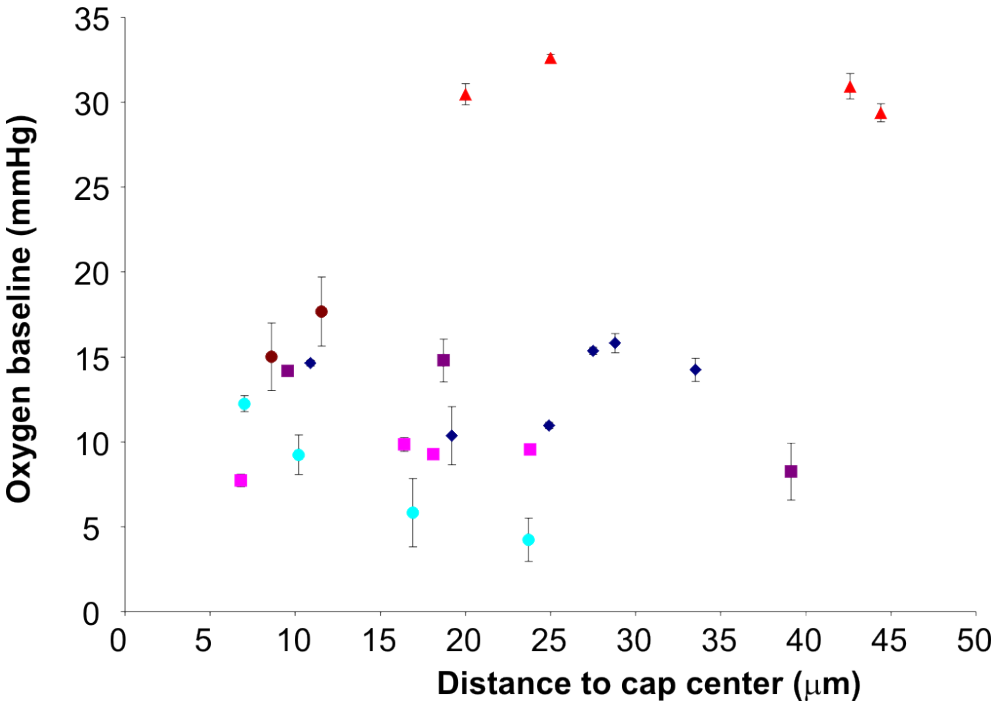

Illustration 51: Oxygen gradients near olfactory bulb capillaries. Each color denotes a different capillary (N=6).

partial pressure for this particular experiment were particularly low. Intaglietta already reported uniform values between arterioles in the periphery (M Intaglietta, P C Johnson, and Winslow 1996). We have already seen that the density of capillaries in the Glomerular Layer is seemingly one of the highest in the brain (see Chapter 4.1.2). The very dense capillary network in the Glomerular Layer probably explains such a result.

- **Delay gradient near capillaries**

If oxygen baseline doesn't vary with distance to the capillary center at distance superior to 6 µm, we could question whether the delay between red blood cell speed and oxygen would change. Nevertheless, our first assumption proved to be right. In the Illustration 52, you can see that, even if the delay varies between capillaries, its value increases with distance to the capillary center.

To make this result clearer, we normalized distance and delay with the value of the closest location. In the Illustration 53,you can see the results of such a process.

Interestingly we find similar values of delays than Masamoto (Masamoto et al. 2007). They assumed that their delay resulted from diffusion between the closest capillary and the electrode's tip. Our study confirms their hypothesis. However it also raises new questions. Indeed we know the exact distance between our electrodes and the capillary. You can note that, at a distance of 20

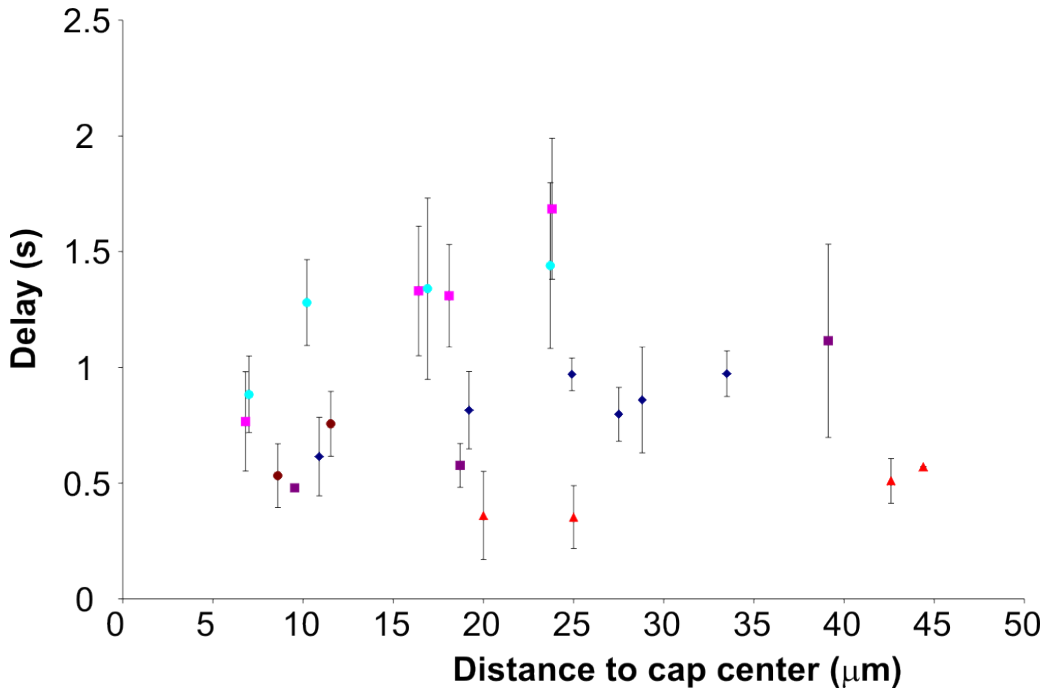

Illustration 52: Delay gradient near olfactory bulb capillaries. Although the absolute value of the delay varies between capillaries, this delay increases with distance to the capillary. Each color is a different capillary (N=6).

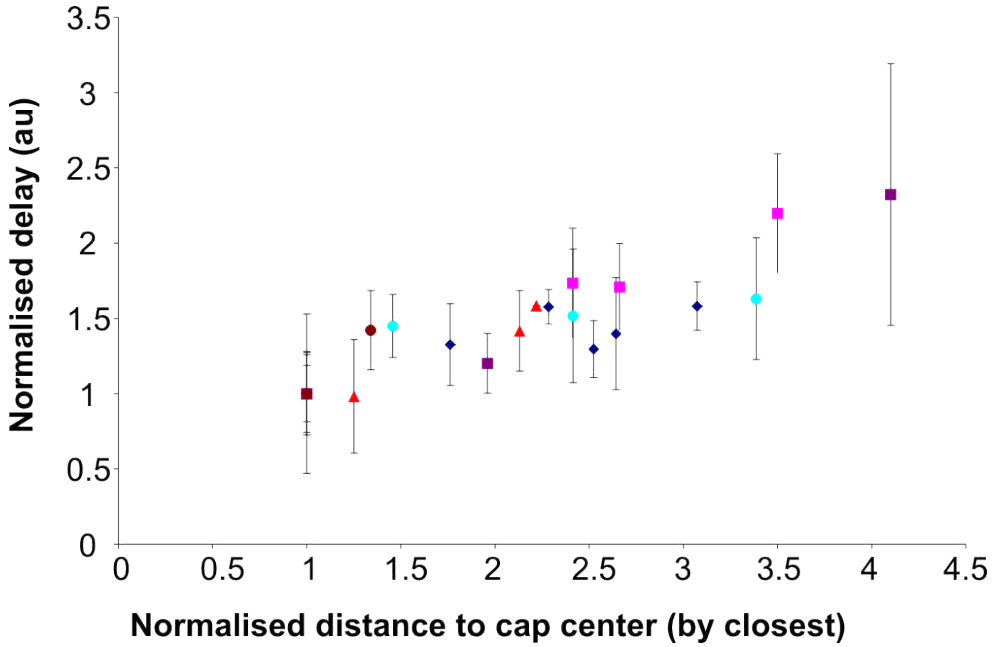

Illustration 53: Normalizing the values in the Illustration 53 reveals that the delay increases with distance to the capillary center.

µm, the delay varies between 0,4 and 1,3 seconds. It came as a surprise to us because we wanted to use the delay gradient to extract the exact diffusion coefficient in the tissue. The variability of this delay made it impossible to use a simple oxygen diffusion model as Masamoto did (Masamoto et al. 2007).

- **Influence of oxygen baseline on the delay**

To try to understand this variability, we look at the effect of oxygen baseline on the absolute value of the delay. To do so, we segmented our data in groups of locations. For instance, all the points located between 10 and 20 µm were grouped together. The result of such segmentation are shown in the Illustration 54. We were surprised to see that the absolute value of the delay was highly correlated with the oxygen baseline level. Highest level in oxygen baseline had smaller delay values.

Such an effect is unexpected from a simple diffusion phenomenon. We contacted Professor Timothy Secomb who has been working in the field of oxygen diffusion for decades (Secomb et al. 2000) and he couldn't come out with a simple explanation. One possibility would be that, as it has been proposed many times

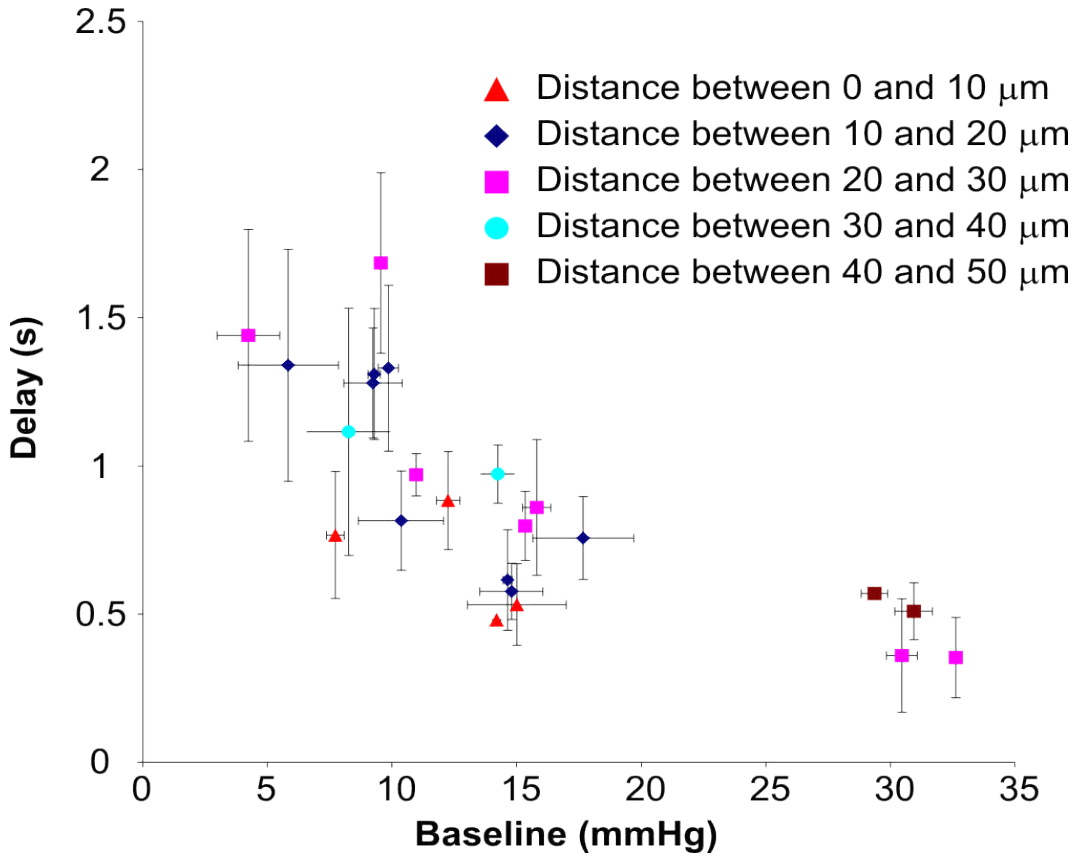

Illustration 54: Effect of oxygen baseline level on the absolute value of the delay. Values were grouped by range of distance to the capillary center.

before (Buxton 2001; Offenhauser et al. 2005), we are dealing with a buffer of oxygen.

When the tissue oxygen level is low, the buffer is empty and oxygen needs to fill the buffer, slowing down the diffusion process. When the tissue level is high, the buffer is full and oxygen can diffuse directly to our electrode.

4.3.4 Conclusion

We have demonstrated that the fluctuations in the oxygen level are due to variations in blood flow in the local microcirculation. The dense network of capillary in the Glomerular Layer prevents the existence of strong oxygen gradients. Moreover the time lags that exist between blood flow and oxygen tissue level are not solely due to diffusion processes. The existence of an oxygen buffer in the parenchymal tissue could explain the variability of this delay.

Discussion & Perspective

I won't discuss here in detail all the results presented in this thesis. This has already been done in the previous publications. However I wanted to point out some aspects that did not lend themselves to being published.

5.1 Oxygen consumption in the olfactory bulb

We have shown that the Glomerular Layer consumes a substantial amount of oxygen compared to the Nerve Layer. The density of synapses in the glomerulus compartment explains both the high energy need and the local capillaries' density. We now know that upon odor stimulation, a very fast and transient decrease in oxygen occurs in activated glomeruli.

We report that a typical value for the rate of consumption during odor stimulation in the glomerulus is 2.5mmHg per second. Brain oxygen solubility is around 3.10^{-5} liter of oxygen per liter of brain per mmHg (Leniger-Follert 1977). This leads to the consumption rate of 3.3 $\mu M.s^{-1}$ oxygen upon stimulation using a molar volume of 22.4 L for oxygen. We know, that when this slope is measured, blood flow has not increased yet. So it measures the increase in consumption exclusively due to odor stimulation.

This number must be considered carefully since oxygen uptake from blood vessels can increase upon stimulation due to desaturation of hemoglobin. In addition ATP consumption is not necessarily directly converted into oxygen consumption, there can be a transient increase in glycolysis.

However, the recent model designed by Nawroth et al on the consumption of the glomerulus compartment at rest and during stimulation(Nawroth et al. 2007), proposed two ranges of consumption: a low and high range. The two possibilities corresponded to whether all the axons coming in the glomerulus were activated or not during odor stimulation. Our results remarkably fit with the low range hypothesis. In these conditions, they showed that the energy budget of the glomerulus compartment was dominated by the consumption at rest. In our experiments, local blockade of postsynaptic activity didn't affect the basal oxygen level. This last result confirms the domination of oxygen consumption at rest over consumption induced by odor stimulation. However, looking in more detail at the consumption at rest would be an interesting future line of research.

In the meantime, an extension of the model of ATP consumption by Nawroth et al to the nerve layer would be interesting to precisely assess the consumption induced by action potentials in this layer.

Deeper layers like the Granule Cell Layer are not easily accessed using two-photon microscopy. However oxygen electrodes can reach these depths. Moreover, both transient gene expression (see Chapter 2.1.4) and 2DG uptake experiments (B. A. Johnson, Woo, and M. Leon 1998) have shown that deeper layers are more broadly activated than the Glomeruli Layer upon odor stimulation. As a consequence, we could expect a large decrease in oxygen across the whole Granule Cell Layer.

5.2 NO is everywhere

We have already mentioned that NO is involved in one of the pathway of neurovascular coupling (see 2.3.5). A very recent study in the olfactory bulb showed that, at low odor concentration, only the presynaptic compartment was involved in neurovascular coupling in the Glomerular Layer (Petzold et al. 2008). This result is not in agreement with our own results for high odor concentration (E. Chaigneau et al. 2007). Indeed, we showed that the postsynaptic compartment was required. Petzold et al demonstrated that astrocytes were involved through two simultaneous pathways: mGluR and Glutamate transporters. It is likely that a third pathway may also be involved : Nitric Oxide.

Strong stimuli would activate NO synthesis in the postsynaptic compartment which would explain the discrepancies between our own results and results from Petzold et al (G. M. Shepherd and Serge Charpak 2008).

There are several other reasons why NO recordings through polarographic electrodes would be required.

NO and oxygen are brothers in the law of brain metabolism :

- NO inhibits mitochondria oxygen consumption (G C Brown 1999). This inhibition is probably involved in oxygen diffusion. Several models have shown that higher levels of NO shunt down cells' respiration and can increase oxygen diffusion (Lamkin-Kennard, Donald G Buerk, and Jaron 2004).

- NO is transiently synthesized and is converted to NO_2^- through a reaction with oxygen (Nagano and Yoshimura 2002). As a consequence, the values for the half-life of NO under physiological conditions range from 0.1 to 5 s.

- NO stimulates glycogen storage (Nancy F Cruz and Gerald A Dienel 2002)

In the light of these last statements, I would like to propose the following hypothesis to finish my thesis :

Upon odor stimulation, a transient increase in NO is triggered in the Glomerular Layer from the postsynaptic compartment. The rise in NO locally inhibits oxidative metabolism in both the neuronal and the astrocytic compartment. However due to the fact that the ATP sink is probably much stronger in the postsynaptic compartment than in the astrocytic compartment, oxidative metabolism pertains in this particular neuronal compartment. As a result, oxygen level decreases locally due to postsynaptic consumption. This is in favor of NO diffusion, as we have already seen. When NO reaches a blood vessel, it triggers a vascular response. The subsequent increase in blood flow brings a great quantity of oxygen which diffuses easily thanks to NO action. NO mitochondria inhibition is relieved when the oxygen level goes up and reacts with NO to form NO_2^-.

Such a mechanism could account for both a transient increase in glycolysis

and explain the shunt of oxidative phosphorylation in the astrocytic compartment.

A recent *in vitro* and *in vivo* study has shown the first NO recordings in the olfactory bulb (Lowe et al. 2008). They recorded these transients in the Granule Cell Layer *in vivo*.

To confirm such a mechanism, dual NO and oxygen recordings would be required with inhibitors of neuronal NO synthase (nNOS). The size of the NO sensor used by Lowe et al. (5 to 10 µm tip) would allow to perform such experiments in the same glomerulus.

Chapter 5.2 : NO is everywhere

Annex

Chapter 6 : Annex

Cellular/Molecular

The Relationship between Blood Flow and Neuronal Activity in the Rodent Olfactory Bulb

Emmanuelle Chaigneau,[1,2] Pascale Tiret,[1,2]* Jérôme Lecoq,[1,2]* Mathieu Ducros,[1,2] Thomas Knöpfel,[3] and Serge Charpak[1,2]

[1]Institut National de la Santé et de la Recherche Médicale U603, 75006 Paris, France, [2]Laboratory of Neurophysiology, Université Paris Descartes, 75006 Paris, France, and [3]Laboratory for Neural Circuit Dynamics, Riken Brain Science Institute, 2-1 Hirosawa, Wako-shi, Saitama 351-0198, Japan

In the brain, neuronal activation triggers an increase in cerebral blood flow (CBF). Here, we use two animal models and several techniques (two-photon imaging of CBF and neuronal calcium dynamics, intracellular and extracellular recordings, local pharmacology) to analyze the relationship between neuronal activity and local CBF during odor stimulation in the rodent olfactory bulb. Application of glutamate receptor antagonists or tetrodotoxin directly into single rat olfactory glomeruli blocked postsynaptic responses but did not affect the local odor-evoked CBF increases. This suggests that in our experimental conditions, odor always activates more than one glomerulus and that silencing one of a few clustered glomeruli does not affect the vascular response. To block synaptic transmission more widely, we then superfused glutamate antagonists over the surface of the olfactory bulb in transgenic G-CaMP2 mice. This was for two reasons: (1) mice have a thin olfactory nerve layer compared to rats and this will favor drug access to the glomerular layer, and (2) transgenic G-CaMP2 mice express the fluorescent calcium sensor protein G-CaMP2 in mitral cells. In G-CaMP2 mice, odor-evoked, odor-specific, and concentration-dependent calcium increases in glomeruli. Superfusion of glutamate receptor antagonists blocked odor-evoked postsynaptic calcium signals and CBF responses. We conclude that activation of postsynaptic glutamate receptors and rises in dendritic calcium are major steps for neurovascular coupling in olfactory bulb glomeruli.

Key words: **two-photon microscopy; olfactory bulb; neurovascular coupling; field potential; mitral cell; blood flow**

Introduction

In humans, most noninvasive brain imaging techniques assess neuronal activation from measurement of hemodynamic changes. However, the molecular and cellular mechanisms underlying the neurovascular coupling are not fully understood (for review, see Villringer and Dirnagl, 1995; Magistretti et al., 1999; Attwell and Iadecola, 2002; Logothetis and Pfeuffer, 2004; Lauritzen, 2005). Although there is a general consensus that neuronal activation is tightly correlated to cerebral blood flow (CBF) responses, the requirement for postsynaptic activation in the generation of vascular responses is still under debate (Mathiesen et al., 1998;Yang and Iadecola, 1998; Nielsen and Lauritzen, 2001; Gsell et al., 2006; Gurden et al., 2006, Hoffmeyer et al., 2006) (for review, see Logothetis, 2003; Lauritzen, 2005).

We have previously investigated neurovascular coupling in the rat olfactory bulb using two-photon laser scanning microscopy (TPLSM) (Denk et al., 1990), a technique that allows simultaneous measurements of capillary red blood cell (RBC) flow (Kleinfeld et al., 1998; Chaigneau et al., 2003) and neuronal/glial cell activity (Svoboda et al., 1999; Helmchen et al., 1999; Charpak et al., 2001; Debarbieux et al., 2003; Hirase et al., 2004; Wang et al., 2006). We found that odor stimulation evoked odor-specific CBF increases in glomerular capillaries (Chaigneau et al., 2003). In addition, we observed vascular responses that apparently were confined to single glomeruli. However, in these TPLSM experiments, only a few glomeruli could be imaged, and because optical functional imaging of calcium (Wachowiak and Cohen, 2001; Spors et al., 2006), voltage (Spors and Grinvald, 2002), and intrinsic signals (Rubin and Katz, 1999; Uchida et al., 2000; Belluscio and Katz, 2001; Luo and Katz, 2001; Meister and Bonhoeffer, 2001; Yuan et al., 2002) have demonstrated that several glomeruli are often coactivated by a given odor, it remains unclear whether neurovascular coupling is regulated strictly at the level of a single glomerulus.

Here, we used calcium imaging, RBC flow measurements, and local field potential (LFP) recordings in rats and G-CaMP-expressing mice (Diez-Garcia et al., 2005) to investigate the glomerular specificity and the role of postsynaptic activity in neurovascular coupling. We show that RBC flow and local neuronal activity uncouple with repetitive stimulation and local blockade of glutamatergic synaptic transmission. Furthermore, we also demonstrate that glutamatergic synaptic transmission and rises in dendritic intracellular calcium ($[Ca^{2+}]_i$) are required to trigger blood flow responses.

Received July 24, 2006; revised May 2, 2007; accepted May 4, 2007.

This work was supported by the Institut National de la Santé et de la Recherche Médicale, the Ministère de l'Education Nationale de la Recherche et de la Technologie (NIC0025), the Centre National de la Recherche Scientifique (CNRS), the Fondation pour la Recherche Médicale (ICP20001222128), and the Région Ile de France (Sesame program). Emmanuelle Chaigneau, Jérôme Lecoq, and Pascale Tiret were supported by fellowships from the Fondation pour la Recherche Médicale, the CNRS-Bourse de Doctorat pour Ingenieur and the Association Française contre les Myopathies, respectively. We thank Etienne Audinat, Jason Rothman, and Laurent Moreaux for their critical comments.

*P.T. and J.L. contributed equally to this work.

Correspondence should be addressed to Serge Charpak, Institut National de la Santé et de la Recherche Médicale U603, Laboratory of Neurophysiology, 45 rue des St Pères, 75006 Paris, France. E-mail: serge.charpak@univ-paris5.fr.

DOI:10.1523/JNEUROSCI.3141-06.2007

 0270-6474/07/276452-09$15.00/0

Materials and Methods

In vivo *electrophysiology and odor stimulations.* Wistar rats, postnatal days 30–60 (P30–P60), were anesthetized with 1.5 g/kg urethane intraperitoneally and held in a standard stereotaxic apparatus with ear bars. A craniotomy was performed above the two olfactory bulb hemispheres, the posterior cisterna drained, and the dura removed. G-CaMP mice (Diez-Garcia et al., 2005), P30–P90, were anesthetized with a mixture of ketamine (100 mg/kg) and xylazin (16 mg/Kg) intraperitoneally and held in a custom-built apparatus by a screw fixed on the cranium. A craniotomy was performed above approximately half of one olfactory bulb. To record field potentials, a borosilicate patch pipette with a single or double barrel was filled with a standard extracellular solution containing 10 μM Oregon Green and placed under visual control in labeled glomeruli using TPLSM imaging (see below). Intracellular recordings were performed using 50–100 Mohm borosilicate glass micropipettes filled with a solution of 3 mM Oregon Green-BAPTA-1 in 2 M K-acetate, pH 7.2. The dye was injected with a continuous hyperpolarizing current of ~0.2–0.5 nA for 10–30 min. In most recordings, a 100-μm-thick glass coverslip was placed over the bulb, fixed on the cranium, and the space below filled with a 3% agar solution. A hole in the agar was created and the coverslip omitted during experiments in which the dorsal bulb was superfused with drugs. Electrophysiological signals recorded with a Neurodata amplifier (Cygnus Technology, Delaware Water Gap, PA) were digitized and stored on a personal computer (Digidata 1322 A, Clampex 9; Molecular Devices, Menlo Park, CA). These signals were simultaneously acquired and synchronized to images. Odors were applied for 1–4 s with a custom-built olfactometer. The olfactometer delivered a constant flow of humidified air on the rat nose. For odor application, this flow was diverted through the glass odor reservoirs by electrically triggered electrovalves. Teflon tubing was used from the odor reservoir to the nose to minimize odor contamination. C2–8 aldehydes, ketones, esters, alcohols, and carboxylic acids were used as odorants. Odor concentrations that ranged from 0.002–5% (taking into account values of saturated vapor pressure) are indicated in the figures when different odors or odor concentrations are compared. The temperature of the animal was monitored with a rectal thermometer and maintained at 37°C with a feedback controlled heating blanket (Harvard Apparatus, Holliston, MA). Occasionally blood PO_2, PCO_2, pH, and electrolytes were controlled using a RapidLAB 348 analyzer from Bayer (Wuppertal, Germany).

In vivo *TPLSM imaging.* Axon terminals from the olfactory nerve were labeled with Oregon Green dextran with a molecular weight (MW) of 10 kDa using the method developed by Wachowiak and Cohen (2001). To label vessels, a bolus of 70 kDa Texas Red dextran was injected intravenously through a catheter placed in the femoral vein. Dyes were excited and imaged using a custom two-photon laser scanning microscope (Charpak et al., 2001). Images of neurons (Oregon Green-BAPTA-1), olfactory nerve terminals (Oregon Green dextran; MW, 10 kDa), extracellular pipettes (Oregon Green) and blood plasma (Texas Red dextran; MW, 70 kDa) were simultaneously acquired on two channels separated using a dichroic mirror (cutoff wavelength, 560 nm). An 880 nm excitation beam from a femtosecond Ti:Sapphir laser (10 W pump; Coherent, Santa Clara, CA) was focused onto neurons and capillaries using a 63× Leica (Nussloch, Germany) water-immersion objective. Galvanometric scanners (Cambridge Technology, Cambridge, MA) controlled by home-built electronics and software (LabView) were used to acquire repetitive single-line scans at ~2000 lines/s or images from subregions of the field of view at rates up to 20 frames/s. For $[Ca^{2+}]_i$ measurements, normalized fluorescence changes were calculated as follows: $\Delta F/F = (F_n - F_0)/(F_0)$, where F_n is the background corrected average fluorescence intensity within the measurement box in frame n, and F_0 is the background corrected intensity averaged over 3–5 frames at the start of a sequence. In experiments in which 6-nitro-7-sulfamoylbenzo(f)-quinoxaline-2,3-dione (NBQX) was applied, only ΔF was measured because NBQX modified the basal level of fluorescence. Fluorescent signals were acquired using a 12 bit analog-to-digital converter.

Applications of drugs. For local applications, one barrel of a borosilicate double barrel patch pipette was used to record the local field potential whereas the other one was filled with a standard extracellular solution containing drugs and 10 μM Oregon Green. Two-dimensional projections of three-dimensional imaging stacks acquired through the glomerular layer (GL) were used to estimate glomerular boundaries (Chaigneau et al., 2003). During pressure injections, the laser power was increased to follow, as best as possible, the spatial diffusion of the fluorescent solution. The extent of drug diffusion was impossible to determine because we detected diffusion of the dye and not that of the drug.

Superfusion of glutamate antagonists over the dorsal bulb was achieved as follows: in rat experiments, agar was omitted from one part of the olfactory bulb surface uncovered by the craniotomy. In mouse experiments, agar was completely omitted. To block synaptic transmission, a 250 μl drop of concentrated drugs (see text) diluted in saline was applied on the bulb surface.

RBC velocity analysis. Line scans were acquired along the longitudinal capillary axis. Unlabeled RBCs appeared as tilted dark shadows on a bright fluorescent plasma background. The values of the velocities were calculated using algorithms based on Kleinfeld et al. (1998). The velocities of the RBCs were inversely proportional to the tangent of the shadow angle. Images were pretreated using 5 × 5 median and low-pass filters and subdivided into brief images $I(n)$ of 100–200 ms duration. The average velocity $v(n)$ of RBCs in $I(n)$ was then calculated as follows: (1) each image $I(n)$ was rotated by an incremental angle α, (2) a singular value decomposition was performed on each rotated image, (3) the α value for which we obtained the greatest first singular value provided the average angle of the RBC shadow in $I(n)$, (4) $v(n)$ was calculated as $v(n) = 1/\tan(\alpha)$. To measure changes in RBC velocity, the value at rest was determined as the mean RBC velocity before odor inhalation (5 s) and the value during stimulation as the mean RBC velocity at the response maximum (3 s). The onset of the vascular response was defined as the moment when two successive values were larger than twice the resting velocity SD. In the entire study, average values are expressed as mean ± SEM.

Results

Odor-evoked LFP responses in single rat glomeruli

Previous studies have shown that LFP signals are correlated to blood flow responses. Hence, we first investigated in the rat (n = 25) which component of the odor-evoked LFP response was generated locally, within single glomerulus boundaries. Extracellular recording pipettes filled with a fluorescent marker (10 μM Oregon Green) were placed under visual control at various depths in olfactory bulb superficial layers (see Materials and Methods), after which ~15–20 odorants per experiment were screened to obtain an odor response in the recorded glomerulus. In glomeruli, odors evoked various types of LFP responses (Fig. 1*A*,*B*,*D*,*E*). Figure 1*A* shows the most common case in which odor inhalation induced repetitive rapid negativities locked to the 2 Hz respiration frequency. The LFP response was strongly reproducible from trial to trial (Fig. 1*A*). Furthermore, once the recording electrode was lowered a few tens of micrometers into the external plexiform layer (EPL), the LFP response drastically changed, and exhibited a long-lasting negativity that had no rapid repetitive negativities (Fig. 1*B*). Sharp transitions of LFP responses between the GL and EPL were observed with all types of odor responses (see inset): the initial rapid negativity and part of the slow negative component systematically disappeared in the upper part of the EPL. Note that such LFP response profiles strongly differed from those previously observed with olfactory nerve stimulation (Fig. 1*C*) (Martinez and Freeman, 1984; Aroniadou-Anderjaska et al., 1999), in which the main component of the negativity was present in both the GL and most of the EPL, fully reversed below the mitral cell layer, and involved granule cell activation. The depth profiles of odor-evoked LFP responses thus suggest that respiration-locked rapid negativities were generated in the glomerular layer.

To investigate the lateral spread of LFP responses, we used two

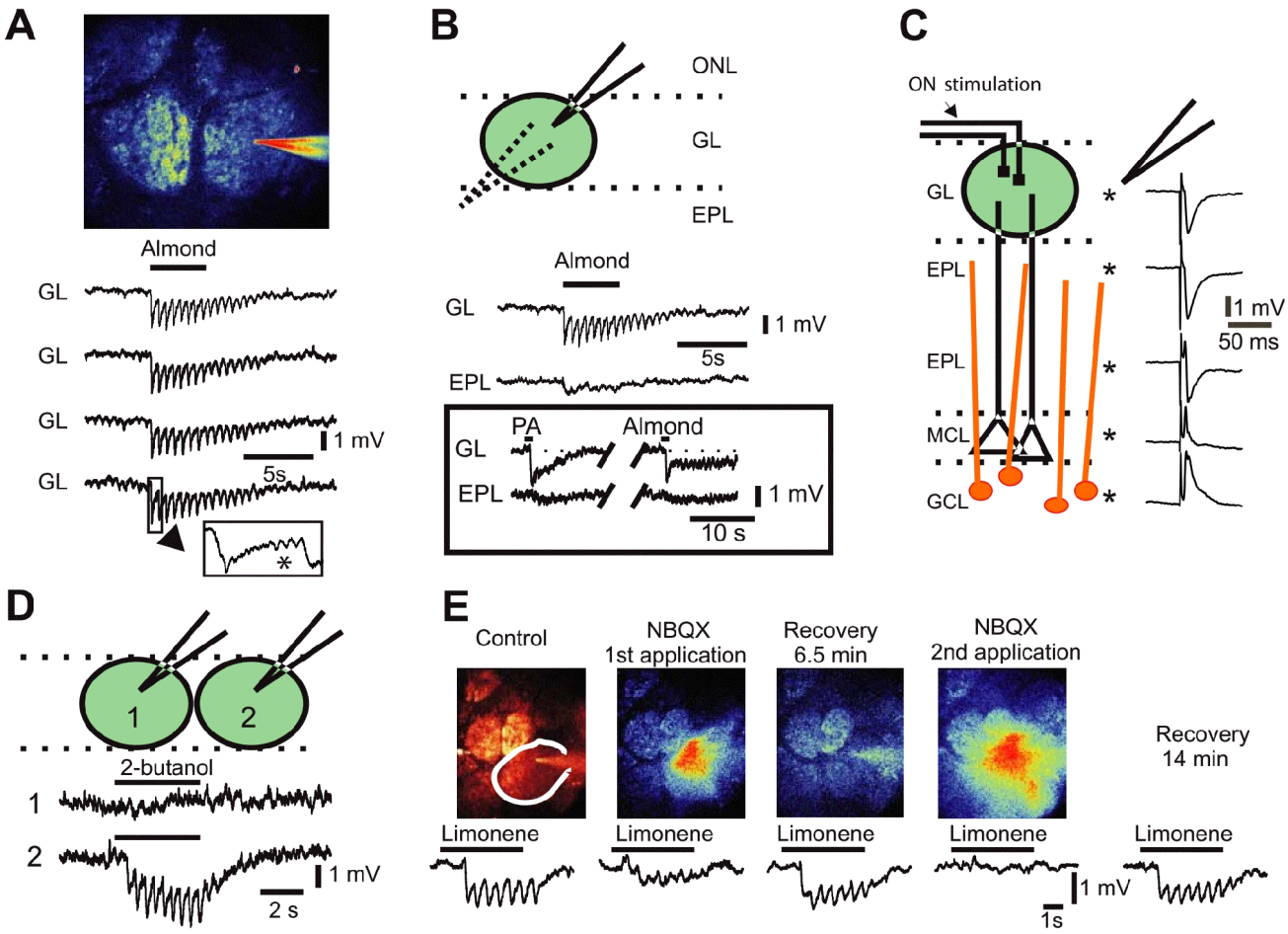

Figure 1. Odor stimulation evokes an LFP response specific to a single glomerulus. ***A***, The field potential recording pipette (filled with Oregon Green), was precisely placed in the center of the labeled glomerulus under visual control using TPLSM. In the GL, odor- evoked LFP responses that consisted of rapid and repetitive negativities locked to respiration. Note that LFP responses evoked by four successive applications of benzaldehyde (0.5%) were very similar. Occasionally β oscillations were recorded (inset, star). ***B***, Odor-evoked fast negativities were exclusive to the glomerular volume. Unlike the field potential negativity evoked by nerve stimulation (***C***), odor-evoked fast negativities (same as in ***A***) disappeared in the EPL a few tens of micrometers below the GL, leaving a slow and long-lasting negativity. Inset shows another recording in which brief application of two different odors [almond, 0.5% and propionic acid (PA), 0.3%] evoked rapid negativities followed by slower ones of various shapes. Rapid negativities also disappeared, and the slower ones diminished in the EPL. ***C***, Depth profile of LFP responses to olfactory nerve stimulation. ***D***, LFP responses to 2-butanol (0.5%) were glomerular-specific and showed little volume conduction. ***E***, Glutamate receptor antagonist NBQX (250 μM dissolved in fluorescent saline) blocked LFP responses to limonene (0.4%). TPLSM was used to image drug diffusion within glomerulus boundaries. Partial (first application) and full block (second application) occurred within seconds after application. ONL, Olfactory nerve layer; MCL, mitral cell layer; GCL, granule cell layer.

other approaches. First, the recording electrode was successively placed in two neighboring glomeruli, and LFP responses were tested for the same odor ($n = 12$ animals). Figure 1*D* illustrates that 2-butanol evoked rapid negativities in one glomerulus, but had no effect in the next glomerulus, indicating that volume transmission of LFP responses was limited when a single glomerulus was activated. Second, we recorded odor responses using double barrel recording electrodes (one barrel to record the LFP and one to pressure-apply NBQX and D-AP5, antagonists of glutamate AMPA, and NMDA receptors, respectively). Localized application of NBQX alone, or with D-AP5 (250 and 500 μM respectively, 15–30 s, $n = 11$ animals) fully, reversibly, and reproducibly blocked odor-evoked LFP rapid negativities (Fig. 1*E*, see Fig. 4*A–C*). Note that although our methods ensured that drugs diffused within glomerular boundaries, they did not eliminate a possible diffusion outside these boundaries (see Materials and Methods). Together, these results suggest that LFP negativities are good indicators of local neuronal postsynaptic activation.

Odor-evoked LFP negativities are correlated to mitral/tufted cell dendritic tuft depolarization and accompanied by a capillary increase in blood flow

We further examined the nature of the cells generating the odor-evoked LFP in glomeruli. Postsynaptic activation after an odor involves two types of postsynaptic cells in glomeruli: mitral/tufted cells and periglomerular cells. Although mitral/tufted cells are outnumbered by a factor of ~20 by juxtaglomerular cells within a glomerulus, they are more likely to participate in the generation of odor-evoked LFP negativities because they are organized in a "vertical open field" configuration, as opposed to juxtaglomerular cells (Rall and Shepherd, 1968). The rapid LFP transition observed during odor stimulation would then be explained by the fact that our recordings were performed in the lateral or the medial dorsal olfactory bulb and the recording electrode axis was nearly perpendicular to the direction of activated apical dendrites and thus perpendicular to the dipole axis. To investigate the role of mitral/tufted cells in the generation of

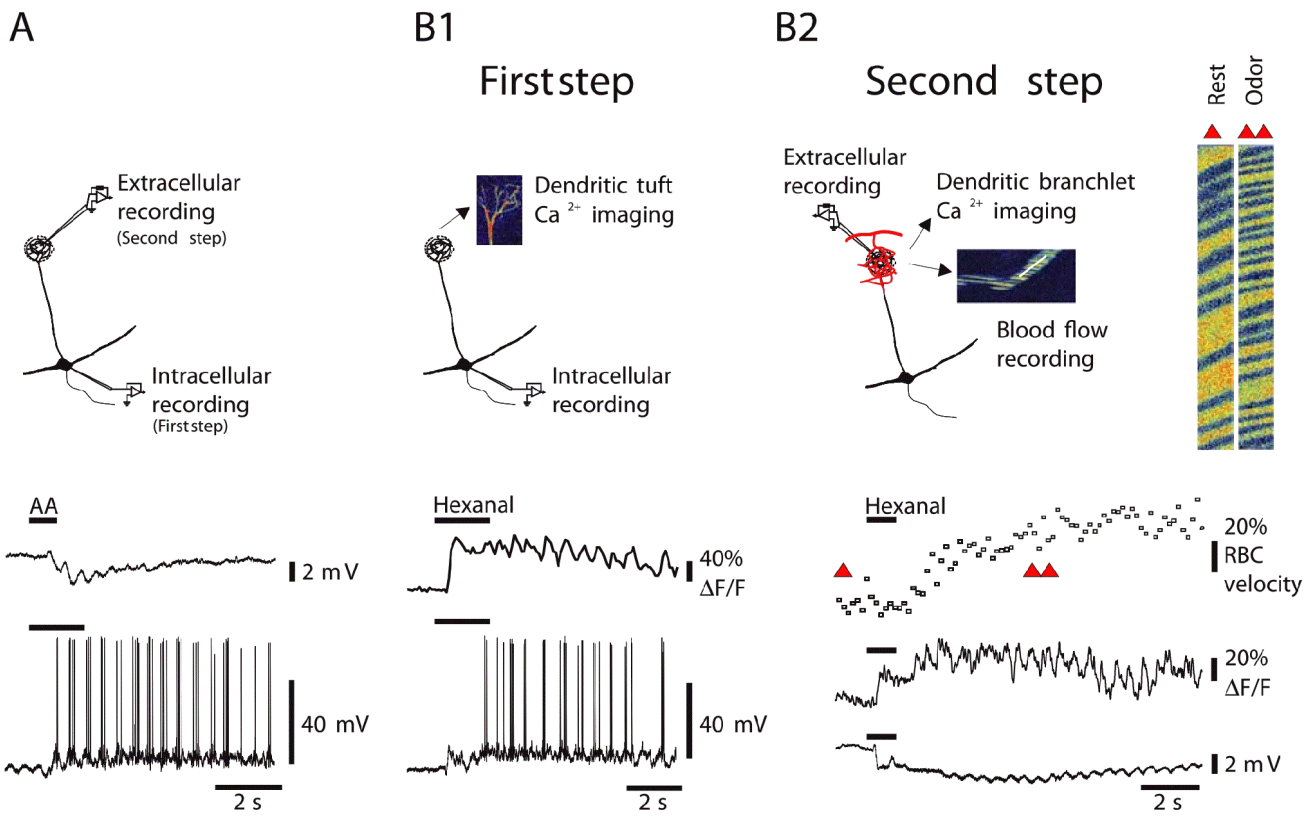

Figure 2. LFP responses are correlated to principal cell activation and associated with a local increase in blood flow. ***A***, A mitral cell that was impaled in the soma, labeled with Oregon Green BAPTA-1, and imaged with TPLSM. This cell fired a burst of action potentials on odor inhalation [isoamyl acetate (AA) at 0.6%]. After the micropipette was withdrawn, an extracellular pipette was placed in the labeled glomerulus and used to record the LFP response. LFP negativities were locked to respiration as action potential bursts. ***B1***, In another cell, odor (hexanal 1.2%) evoked a large EPSP crowned with action potential firing. Both the EPSP and the action potentials generated calcium ($[Ca^{2+}]_i$) increases in the dendritic tuft. ***B2***, Left, Subsequent and simultaneous recordings of tuft $[Ca^{2+}]_i$, LFP, and RBC velocity revealed that mitral cell activity underlies LFP responses and is associated with an increase in RBC velocity. Right, Raw data of blood flow recordings at the time indicated by red triangles in the graphs. Note that $[Ca^{2+}]_i$ measurements were performed using movie acquisition (***B1***) or with line-scan acquisition, allowing simultaneous measurement of RBC velocity (***B2***).

LFPs, we successively recorded mitral/tufted cells and LFP responses to odor (Fig. 2). In the first step of the experiment, four principal cells were intracellularly recorded with micropipettes containing Ca^{2+}-sensitive dye (Oregon Green BAPTA-1) and their responses to odor stimulation recorded during the time necessary for the dye to diffuse to the apical dendritic tuft. TPLSM was then used to determine the location of the tuft and measure its $[Ca^{2+}]_i$ dynamics in response to odor stimulation. In the second step of the experiment, the intracellular pipette was withdrawn and an extracellular recording micropipette was placed in the glomerulus containing the labeled tuft. As Figure 2 shows, LFP responses perfectly mirrored the activation of principal cells: odor stimulation evoked synaptic depolarizations and action potential discharges locked to the respiration frequency; mitral cell membrane depolarizations also corresponded to LFP negativities. Both excitatory postsynaptic potentials and back-propagating action potentials (data not shown, but see Charpak et al., 2001; Debarbieux et al., 2003) generated calcium ($[Ca^{2+}]_i$) increases in the dendritic tuft. Dendritic $[Ca^{2+}]_i$ recordings allowed for monitoring the stability of odor response, and similar $[Ca^{2+}]_i$ increases were observed when the electrical responses were recorded with intracellular (Fig. 2*B1*) or later with extracellular recording electrodes (Fig. 2*B2*). Overall, these results demonstrate that glomerular odor-evoked LFP responses are correlated to the activity of principal cells projecting to the glomerulus. However, the precise weight of their contribution to LFPs as opposed to the juxtaglomerular contribution (Karnup et al., 2006) remains to be established.

We also found that local neuronal activation was associated with vascular responses. RBC flow increase followed LFP response (64 rats), and, in five rats in which intracellular recordings were combined with flow measurements, vascular responses lagged behind EPSP onset by a mean delay of 1.9 ± 0.1 s (mean ΔRBC increase, 39 ± 5%; 27 odor applications; measurements were performed in capillaries that were intermingled with tuft dendritic branchlets). Finally, by combining LFP and RBC velocity measurements, we verified that both neuronal responses [quantified as the summation of LFP rapid negativities (Σ LFP)] and vascular responses increased accordingly when the duration of odor stimulation was doubled (Σ LFP increased from 2.0 ± 0.3 to 3.9 ± 0.9 mV and RBC velocity from 29 ± 7 to 55 ± 10%; $n = 7$; $p < 0.03$ and $p < 0.02$, respectively; interstimulus interval, 4 min).

Vascular and neuronal responses on repetitive odor stimulation

Having characterized LFPs as indicators of glomerulus-specific neuronal activity, we examined the reproducibility of vascular responses, a necessary step before the application of drugs that modulate synaptic transmission. LFP and vascular responses were simultaneously measured when odor was repetitively applied at first every 4 min and then every minute. In six of six rats,

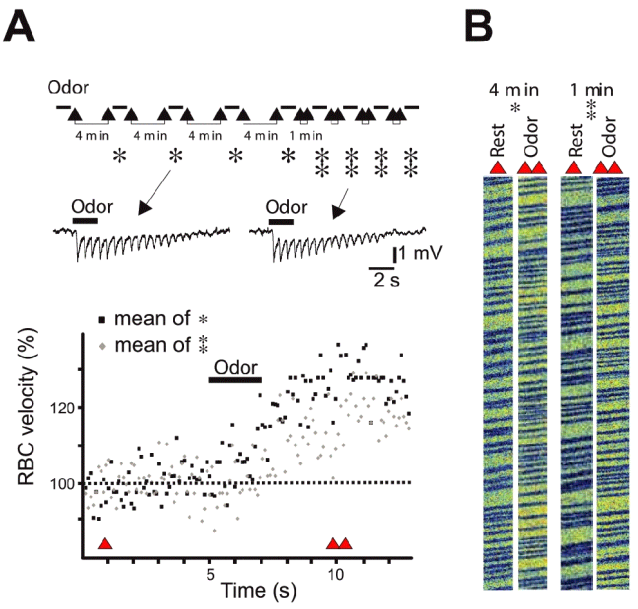

Figure 3. LFP and vascular responses uncouple on repetitive odor stimulation. ***A***, Top, Experimental protocol: benzaldehyde (0.5%) was repetitively applied every 4 min (single star) and every 1 min (double stars). LFP responses remained stable with both interstimulus intervals (single traces are illustrated). In contrast, vascular responses decreased with 1 min interstimulus intervals. Averages of four vascular responses recorded with 4 (in black) and 1 (in gray) min interstimulus intervals are illustrated. Bottom, Single and double triangles indicate the times at which raw data in ***B*** are extracted. ***B***, Raw data of RBC flow recordings obtained before odor (single triangle) and during odor (double triangle).

vascular responses significantly decreased when the frequency of odor stimulation increased: odor-evoked RBC velocity changes decreased from 31 ± 7 to 22 ± 6% when interstimulus intervals decreased from 4 to 1 min, respectively ($n = 6$; $p < 0.05$). In contrast, LFP responses, quantified as the summation of rapid negativities, were the same for both frequencies of odor stimulation (Σ LFP, 7 ± 1.7 to 6.9 ± 1.4 mV) (interstimulus intervals of 4 and 1 min, respectively; $n = 6$; $p = 0.7$). A detailed example is shown in Figure 3. These results prompted us to use interstimulus intervals of 4 min to trigger maximal vascular responses.

Regulation of blood flow involves several glomeruli

We first investigated the role of postsynaptic activation in neurovascular coupling by using double-barrel micropipettes to focally apply antagonists of glutamatergic synaptic transmission while measuring both LFP and vascular responses (Fig. 4*A*,*B*). Focal application of antagonists of glutamate ionotropic receptors either alone (250 μM NBQX and 500 μM D-APV diluted in fluorescent saline), or combined with an antagonist of group I glutamate metabotropic receptors (mGluRs) [250 μM 2-methyl-4-carboxyphenylglycine (LY367385)], reversibly and reproducibly blocked synaptic transmission, but left vascular responses unchanged: odor-evoked RBC velocity increase was 29 ± 5% in the presence of NBQX and D-APV versus 30 ± 4% in control conditions ($n = 5$) and 41 ± 14% in the presence of NBQX, D-APV, and LY367385 versus 38 ± 13% in control conditions ($n = 3$). Because olfactory nerve stimulation (Heinbockel et al., 2004; Saint Jan and Westbrook, 2005) activates ionotropic and mGluR1 glutamate receptors of principal cells, these results demonstrate that neurovascular coupling within a glomerulus is independent of the activation of the related mitral/tufted cells. Note that application of NBQX, D-APV, and LY367385 at such concentrations also blocked most of the excitatory synaptic activation of the periglomerular cells. Two mechanisms could explain these results: first, within a single glomerulus, vascular responses are independent of postsynaptic activation of neurons and are instead triggered by glutamate release and activation of astrocytes (Takano et al., 2005). Second, and more likely, vascular responses are not perfectly glomerular-specific, and the local RBC velocity changes observed during local inhibition of synaptic transmission are triggered by the coactivation of neighboring glomeruli (Rubin and Katz, 1999; Uchida et al., 2000; Belluscio and Katz, 2001; Luo and Katz, 2001; Meister and Bonhoeffer, 2001; Wachowiak and Cohen, 2001; Spors and Grinvald, 2002; Yuan et al., 2002; Spors et al., 2006). To investigate whether local activation of astrocytes by glutamate was sufficient to trigger vascular responses, we blocked glutamate release with local injections of tetrodotoxin (TTX). As expected (Fig. 4*C*,*D*), intraglomerular applications of 1 μM TTX fully blocked the LFP responses. However, they neither blocked nor affected vascular responses (RBC velocity increased by 28 ± 4% in control and by 33 ± 7% in the presence of TTX; $n = 6$; $p > 0.4$). In contrast, we observed a clear depression of vascular responses when TTX was applied at a higher concentration (5 μM) and with spatially larger applications (i.e., the dye diffusing outside single glomerular boundaries) (RBC velocity increased by 27 ± 4% in control and by 6 ± 3% in the presence of TTX; $n = 3$; $p < 0.01$). These results are consistent with the idea that in our experimental conditions, vascular responses are controlled by cooperation of several glomeruli. Therefore, the role of postsynaptic activation in triggering neurovascular coupling cannot be definitely established using local blockade of synaptic transmission.

Postsynaptic activation modulates vascular responses

To interfere with synaptic transmission more widely, we only partially covered the dorsal bulb with agar and superfused glutamate antagonists onto the bulb surface. Removing agar decreased the preparation stability. For this reason, we were only able to obtain stable two-photon measurements of CBF in four of 11 rats. In these four cases, high concentrations of glutamate ionotropic receptor antagonists (NBQX, 250–500 μM; D-AP5, 0.5–1 mM) induced a modest but significant decrease of odor-evoked LFP and RBC flow responses (Σ LFP decreased from 1.68 ± 0.3 to 0.96 ± 0.38 mV, $p = 0.038$; and changes in RBC velocity decreased from 0.36 ± 0.02 to 0.19 ± 0.02 mm/s, $p = 0.022$). Although these results clearly indicate that postsynaptic activation modulates vascular responses, we looked for a more reliable model for the following reasons: (1) because of movement problems, these imaging experiments were extremely difficult to perform, (2) the blockade of LFPs by glutamate antagonists was not complete and in some cases rapidly reversible, probably resulting from drug washout by blood flow, (3) higher NBQX concentrations decreased the signal-to-noise ratio of fluorescent signals and thus could not be used. We thus further investigated the role of postsynaptic activation in the mouse where the olfactory nerve layer is thin and glutamate receptor antagonists, applied on the bulb surface, can be expected to reach the glomerular layer more readily than in the rat and thus block synaptic transmission over a larger portion of the dorsal olfactory bulb.

Odor induces Ca^{2+} fluorescence increases in the glomerular layer from G-CaMP2 mice

To facilitate the detection of responsive glomeruli, we recorded odor responses in the G-CaMP2 transgenic mouse (Diez-Garcia et al., 2005, 2007). This mouse has been successfully used to re-

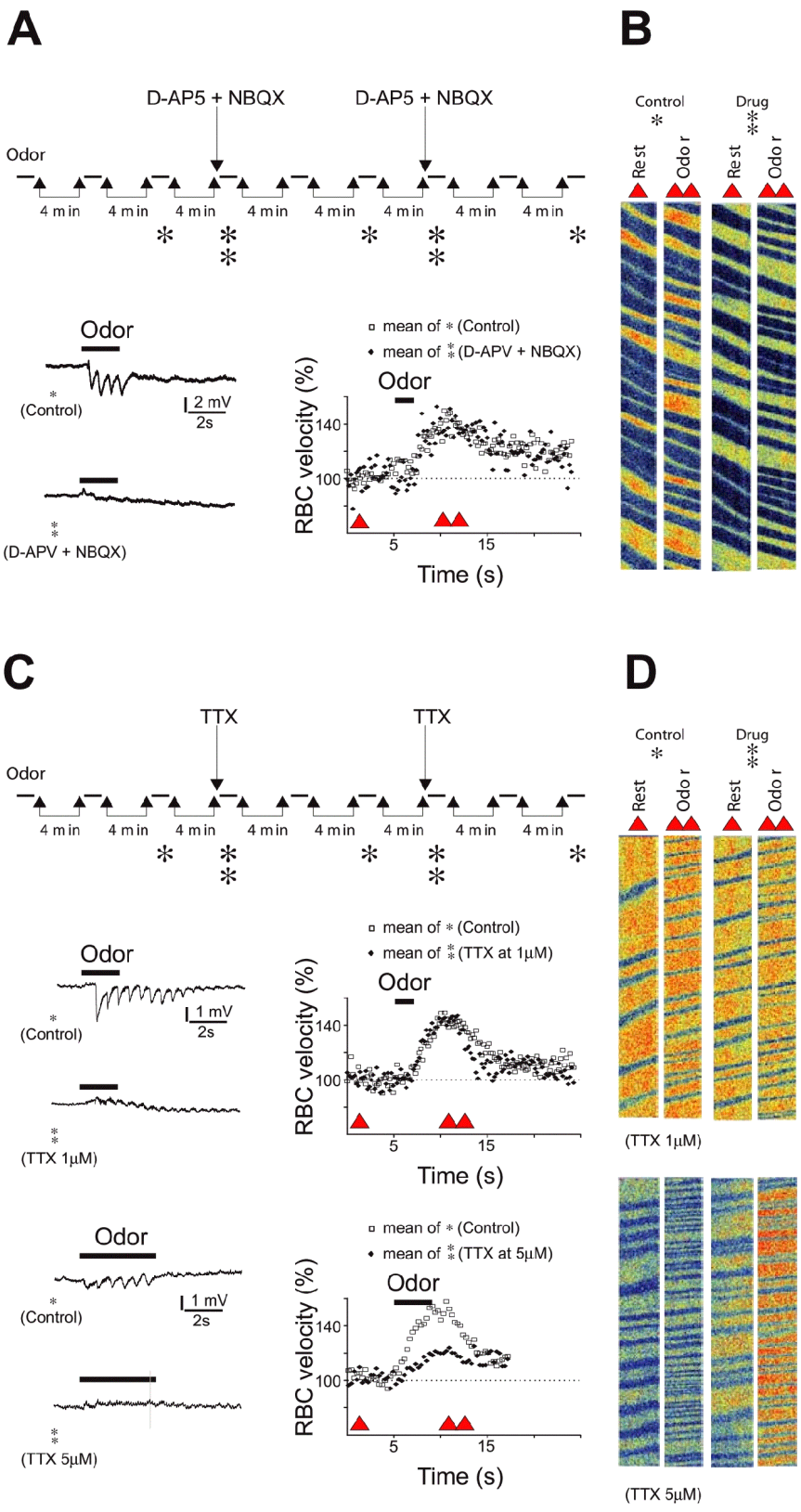

port neuronal activity in granule cells from the cerebellum, where G-CaMP2 fluorescence increases with neuronal $[Ca^{2+}]_i$. We first tested whether this mouse could be used to report glomerular activation. In 12 of 12 mice, we observed that G-CaMP2 was expressed in mitral cells (Fig. 5*AI*, arrows point to two activated mitral cell apical dendrites) and in some periglomerular cells (Fig. 5*AII*,*AIII*, arrowheads). In each mouse, odor triggered odorant-specific increases in glomerular fluorescence, reflecting a Ca^{2+} increase in activated postsynaptic cells (for the effect of glutamate antagonists, see below). Responses to high odor concentrations were first investigated in several fields of view from the dorsal bulb, until fluorescence signals were reliably obtained. Odors were then compared at diluted concentrations (0.01–1.3%). Figure 5*B* shows different Ca^{2+}-signal increases of three neighboring glomeruli in response to three odorants. Note that in these examples, as well as in Figure 5*C*, Ca^{2+} responses were locked to respiration, a rhythmic activity reminiscent of what is observed in LFP (see above) and mitral cell responses (Charpak et al., 2001; Debarbieux et al., 2003). Dilution of the odor concentration decreased the number of activated neighboring glomeruli (Fig. 5*C*) and increased the response delay, a phenomenon that was also observed in LFP responses (data not shown). The properties of these odor-evoked fluorescence responses suggest that G-CaMP2 mice can be used to study the role of postsynaptic activity in neurovascular coupling. In the rest of the study, we used odor concentrations that activated one to three glomeruli in a 400 × 400 μm field of view and in this way mimicked the experimental conditions previously seen in the rat.

Figure 4. ***A***, Blockade of local postsynaptic activity does not affect the vascular responses. Top, Experimental protocol: Hexanal (1.2%) was repetitively applied every 4 min in the control condition and 30 – 60 s after intraglomerular applications of glutamate ionotropic receptor antagonists (250 μM NBQX, 500 μM D-APV diluted in fluorescent saline). TPLSM was used to image drug diffusion within glomerulus boundaries. Glutamate antagonists reversibly and reproducibly blocked LFP negativities but left vascular responses to hexanal unchanged. Single trial LFPs and average vascular responses are illustrated. Single and double triangles indicate the times at which raw data in ***B*** are extracted. ***B***, Raw data of RBC flow recordings obtained before odor (single triangle) and during odor (double triangle) in control condition (single star) and in the presence of glutamate antagonists (double star). ***C***, Blockade of local glutamate release does not affect vascular responses. Top, Local application of 1 μM TTX (diluted in fluorescent saline) fully blocked LFP responses but did not affect vascular responses to ethyl propionate (0.005%). Bottom, Application of a higher concentration of TTX (5 μM) outside glomerular boundaries decreased vascular responses to hexanal (1.2%). In each case, single trial LFPs and average vascular responses are illustrated. Single and double triangles indicate the times at which raw data in ***D*** are extracted. ***D***, Raw data of RBC flow recordings obtained before odor (single triangle) and during odor (double triangle) in control condition (single triangle) and in the presence of 1 μM TTX (top) and 5 μM TTX (bottom).

Postsynaptic activation of glomerular dendrites is required to trigger vascular responses in G-CaMP2 mice

In seven of 10 mice (no agar), we were able to measure CBF in a single capillary while simultaneously recording G-CaMP2 fluorescence in the nearby glomerular neuropil. To do this, long line scans with an angle were acquired (Fig. 6*A*), drawing the first part of the line along the capillary, and the second part through the neuropil (fluorescence of CBF and Ca^{2+} were recorded in two separate detector channels). Results of these experiments show that odor triggered a $[Ca^{2+}]_i$ increase that preceded the vascular response by 1–2 s. Furthermore, high concentrations of glutamate ionotropic receptor antagonists applied to the surface of the bulb (NBQX, 0.25–0.5 mM; D-AP5, 0.5–1 mM) decreased both odor-evoked $[Ca^{2+}]_i$ and RBC responses ($n = 6$ capillaries): Ca^{2+} responses, measured as ΔF (see Materials and Methods), decreased from 306 ± 121 to 47 ± 26 arbitrary units (a.u.), $p = 0.03$ and ΔRBC velocity decreased from 0.18 ± 0.05 to 0.05 ± 0.01 mm/s, $p = 0.03$. Notably, although the blocking effects of glutamate antagonists on ΔRBC velocity and Ca^{2+} responses were correlated, they were also highly variable, ranging from 37 to 95% for ΔRBC velocity and from 52 to 100% for Ca^{2+} responses. Coapplication of LY367385 (500 μM) with ionotropic receptor antagonists had a similar effect on CBF (in three capillaries, ΔRBC velocity decreased from 0.16 ± 0.03 to 0.08 ± 0.02 mm/s; $p = 0.05$). Hence, we conclude that if glutamate ionotropic receptors are principally located on glomerular dendrites (see Discussion), their activation and the subsequent dendritic $[Ca^{2+}]_i$ increase are likely to play a major role in triggering the vascular response.

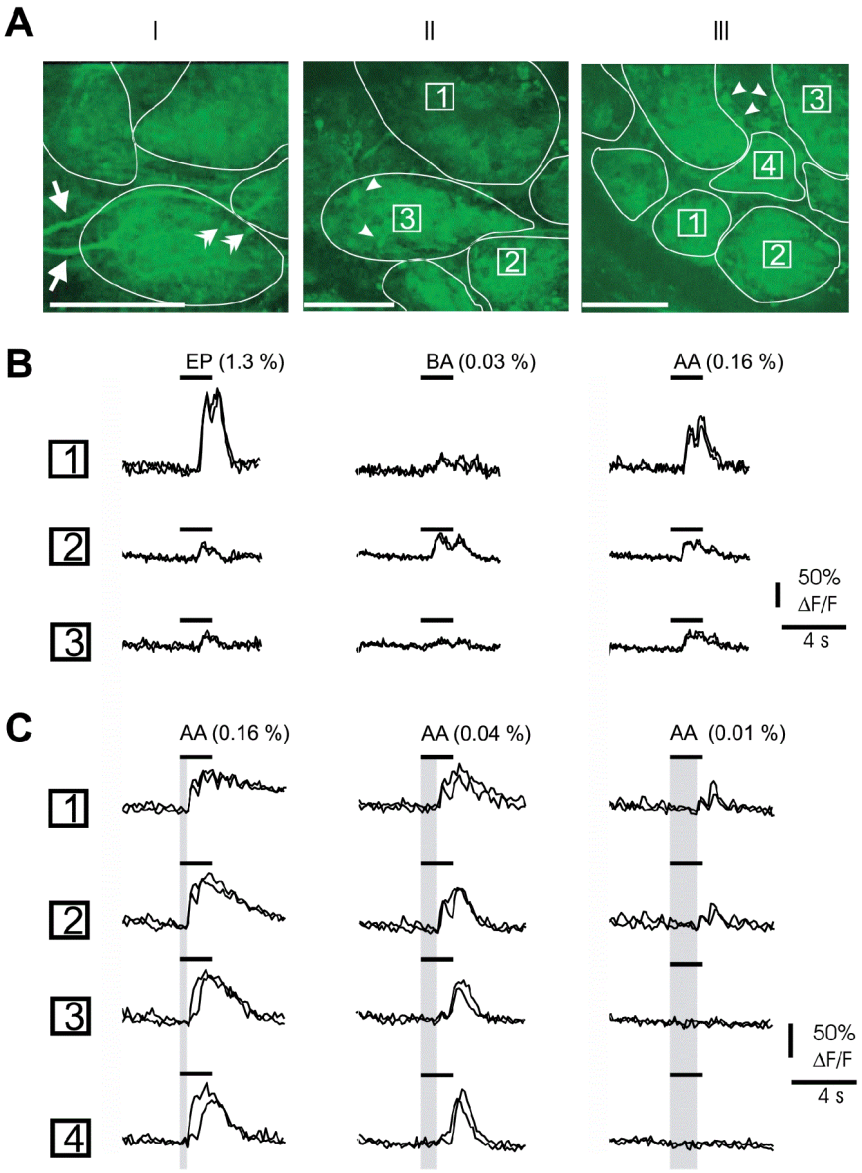

Figure 5. Odor induces Ca^{2+} signals in glomeruli from G-CaMP2 mice. ***A***, Two-photon imaging of three fields of view obtained in the glomerular layer (glomerular contours are outlined). G-CaMP2 fluorescence is expressed in mitral cells and in some periglomerular cells: arrows point to two longitudinal mitral cell apical dendrites and double arrowheads to two apical dendrite sections (***AI***); arrowheads point at several periglomerular cells (***AII***, ***AIII***). Scale bars, 100 μm. ***B***, Odorant-dependent increases in Ca^{2+} fluorescence. Movies were acquired over the field of view illustrated in ***AII*** with a lower spatial and higher time resolution. Responses to ethylpropionate (EP), benzaldehyde (BA), and isoamylacetate (AA) varied according to each glomerulus. For each glomerulus, responses to two odor applications are overlaid. As odor-evoked LFP responses, Ca^{2+} responses were occasionally locked to respiration, in particular at low odor concentration. ***C***, Ca^{2+} responses are concentration dependent. Movies were acquired over the field of view illustrated in ***AIII***. At a high concentration, isoamylacetate (AA) activated all glomeruli in the field of view. Only two of them responded when the odor was diluted. For each glomerulus, responses to two odor applications are overlaid. Note the increasing delay (in gray) of Ca^{2+} responses with odor dilution.

Discussion

In the olfactory bulb, methods for detecting hemodynamic changes (e.g., blood oxygenation level-dependent functional magnetic resonance imaging (Yang et al., 1998; Xu et al., 2000; Kida et al., 2002) and TPLSM (Chaigneau et al., 2003) have clearly demonstrated that odor stimulation reproducibly activates small glomerular ensembles. However, the nature of the coupling between neuronal activation and the local glomerular vascular response has been unknown until a recent study, using intrinsic optical signals, suggested that local metabolic processing and blood flow responses are independent of postsynaptic activation (Gurden et al., 2006). Our local pharmacological results seemed initially to support this hypothesis: intraglomerular blockade of glutamate ionotropic receptors abolished odor-evoked postsynaptic responses, whether measured as LFP responses or as increases in dendritic $[Ca^{2+}]_i$, but it did not affect vascular responses. However, intraglomerular blockade of neuronal activity with TTX (i.e., glutamate release from terminals) did not block vascular responses either. These results suggest that in our experimental conditions, several clustered glomeruli were activated by the odor, and silencing one of them did not affect neurovascular coupling. They also point to the fact that when spatially distinct neuronal populations are activated (i.e., several glomeruli) single-site measurements of LFP can be misleading when quantifying neurovascular coupling.

mechanism. Magn Reson Imaging 22:1517–1531. dynamic control of brain microcirculation. Nat Neurosci 6:43–50.

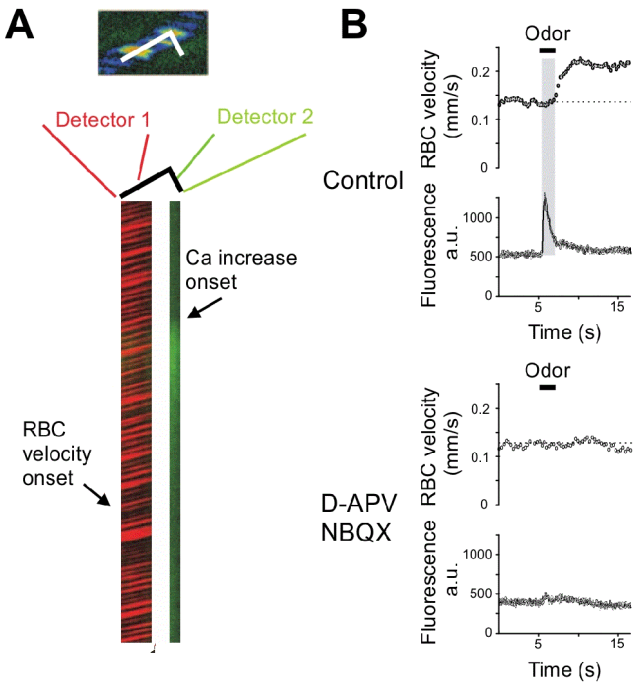

Figure 6. Postsynaptic activation of glomerular dendrites is required to trigger blood flow responses in G-CaMP2 expressing mice. ***A***, Left, Odor (ethyl butyrate at 0.004%) triggers a Ca^{2+} signal followed by an increase in CBF. Line scans were acquired on a segment going along the longitudinal axis of the capillary for its first part and through the neighboring neuropil for its second part. RBC velocity measurements (the first part of the line scan) were acquired on one detector and Ca^{2+} fluorescence (the last part of the line scan) on the second one. Right, Both neuronal and vascular responses were blocked in the presence of 250 μM NBQX and 500 μM D-APV. Note the delay (in gray) between neuronal and vascular responses.

Because our initial experiments did not allow us to assess the role of postsynaptic activation in neurovascular coupling, we used another paradigm that allowed us to block synaptic transmission in a large portion of the dorsal bulb. Experiments using superfusion of glutamate antagonists over the olfactory bulb in rats and particularly in mice strongly supported the hypothesis that neurovascular coupling requires postsynaptic activation. G-CaMP2 mice have been previously used to report neuronal activity in the cerebellar cortex where they are exclusively expressed in granule cells: activation of parallel fibers induced Ca^{2+} transients that could be observed using one- or two-photon excitation imaging (Diez-Garcia et al., 2007). Here, because G-CaMP2 fluorescence was expressed mostly in mitral cells, but also in a few periglomerular cells, odorant molecules induced Ca^{2+} responses that principally reflected postsynaptic activation of mitral cells and shared the properties of LFP responses: Ca^{2+} response amplitudes were correlated to the odor concentration and to respiration frequency. Glutamate receptor antagonists either strongly reduced or fully blocked both postsynaptic Ca^{2+} and vascular responses in G-CaMP2 mice.

Although this set of experiments clearly showed that vascular responses required the activation of glutamate ionotropic receptors, it did not exclude the possibility that the relevant receptors are located on glial cells (for review, see Lalo, 2005, 2006). However, this is unlikely because in glomerular astrocytes, synaptically released glutamate activates only an indirect K^+ current resulting from the glutamatergic activation of mitral cells and a direct glutamate transporter current (Saint Jan and Westbrook, 2005). We thus propose that postsynaptic activation of glomerular neurons is required to trigger vascular responses, because it has been shown in the cerebellum and the cortex (Mathiesen et al., 1998; Yang and Iadecola, 1998; Nielsen and Lauritzen, 2001; Gsell et al., 2006; Hoffmeyer et al., 2006). As mentioned by Gurden et al. (2006), it is likely that certain intrinsic optical signals maintained in the presence of glutamate antagonists may reflect changes in light scattering involving either olfactory nerve terminals or astrocytes.

In vitro brain preparations have shown several molecular mechanisms involved in the regulation of arteriolar diameter by glial cells and neurons (Zonta et al., 2003; Cauli et al., 2004; Mulligan and MacVicar, 2004; Filosa et al., 2004, 2006; Metea and Newman, 2006; Rancillac et al., 2006). Yet, the results from these *in vitro* preparations also raised issues, such as the absence of adequate smooth muscle resting tone and the disruption of cellular networks, which certainly will affect neurovascular coupling. Our study and that by Wang et al. (2006) show that TPLSM allows for adequate spatial and temporal resolution while studying neurovascular coupling *in vivo* and so demonstrates that the vascular response is tightly coupled to neuronal and glial $[Ca^{2+}]_i$. It thus becomes possible to link *in vivo* cellular $[Ca^{2+}]_i$ rises to the production of several compounds involved in the regulation of vessel diameters (e.g., nitric oxide or prostaglandins) (Yang and Iadecola, 1998; Lauritzen, 2005; Hoffmeyer et al., 2006; Stefanovic et al., 2007). However, our study stresses that responses to drugs, applied on the brain surface, are extremely variable and reversible, indicating the need to permanently and simultaneously control neuronal activity and blood flow at the same site. We attribute the difficulty to fully block the responses to the efficiency of drug clearance by blood flow as well as to the variability of glomeruli location in depth.

What components of odor-evoked LFP responses are generated locally? LFP rapid negativities reflect neuronal activation restricted to a single glomerular volume: over the study, hundreds of odor presentations did not evoke any LFP responses in many glomeruli. When tested between two neighboring glomeruli, odor-evoked LFP responses were clearly glomerular specific, and their transitions in space (laterally and in depth) were sharp and abolished with intraglomerular TTX application. Odor-evoked LFP rapid negativities thus constitute a reliable and reproducible measure of glomerular activity. It should be noted that LFPs contained a slow component that we did not use for our analysis and that appeared to reflect only partially local activity. Which cell type generates local LFP responses? As suggested by Rall and Shepherd (1968) decades ago, LFPs are most likely generated by mitral/tufted cells that are organized in a "vertical open field" configuration as opposed to juxtaglomerular cells. In favor of this hypothesis, in this study, LFPs were tightly correlated to mitral cell activity and varied little when the recording electrode was moved within glomerulus boundaries (data not shown). Note that an LFP transition and reversal should have been observed at the border of the glomerulus if a subpopulation of juxtaglomerular cells had been activated. These results raise the general issue that physiological stimuli involve completely different neuronal networks from those activated during nerve stimulation or those occurring spontaneously in isolated glomerular layer slices (Karnup et al., 2006). For example, olfactory nerve stimulation activates a large portion of the glomerular layer, triggering a very powerful granule cell excitation that generates almost entirely the first rapid LFP negativity. In contrast, odorants usually activate only a few glomeruli, and granule cells do not participate in the glomerular fast LFP negativities. This should be

Bibliography

Chapter 7 : Bibliography

Attwell, D. & Laughlin, S.B., 2001. An energy budget for signaling in the grey matter of the brain. *J Cereb Blood Flow Metab*, 21(10), 1133-45.

Baba, K. et al., 1997. Odor exposure reveals non-uniform expression profiles of c-Jun protein in rat olfactory bulb neurons. *Brain Research*, 774(1-2), 142-148.

Bar, T., 1980. The vascular system of the cerebral cortex. *Advances in anatomy, embryology, and cell biology*, 59, I-VI,1-62.

Barcroft, J. & Hill, A.V., 1910. The nature of oxyhaemoglobin, with a note on its molecular weight. *The Journal of Physiology*, 39(6), 411-28.

Baron, J.C. et al., 1982. Noninvasive measurement of blood flow, oxygen consumption, and glucose utilization in the same brain regions in man by positron emission tomography: concise communication. *Journal of Nuclear Medicine: Official Publication, Society of Nuclear Medicine*, 23(5), 391-9.

Biagiotti, E. et al., 2000. Posttranslational regulation of glucose-6-phosphate dehydrogenase activity in tongue epithelium. *The Journal of Histochemistry and Cytochemistry: Official Journal of the Histochemistry Society*, 48(7), 971-7.

Biagiotti, E. et al., 2005. Glucose-6-phosphate dehydrogenase and NADPH-consuming enzymes in the rat olfactory bulb. *Journal of Neuroscience Research*, 80(3), 434-41.

Borowsky, I.W. & Collins, R.C., 1989. Metabolic anatomy of brain: a comparison of regional capillary density, glucose metabolism, and enzyme activities. *The Journal of comparative neurology*, 288(3), 401-13.

Bradley, J. et al., 2004. Calmodulin permanently associates with rat olfactory CNG channels under native conditions. *Nature neuroscience*, 7(7), 705-10.

Brown, A.M. & Ransom, B.R., 2007. Astrocyte glycogen and brain energy metabolism. *Glia*, 55(12), 1263-71.

Brown, G.C., 1999. Nitric oxide and mitochondrial respiration. *Biochimica Et Biophysica Acta*, 1411(2-3), 351-69.

Buck, L. & Axel, R., 1991. A novel multigene family may encode odorant receptors: a molecular basis for odor recognition. *Cell*, 65(1), 175-87.

Buxton, R.B., 2001. The elusive initial dip. *NeuroImage*, 13(6 Pt 1), 953-8.

Caesar, K., Offenhauser, N. & Lauritzen, M., 2008. Gamma-aminobutyric acid modulates local brain oxygen consumption and blood flow in rat cerebellar cortex. *Journal of Cerebral Blood Flow and Metabolism: Official Journal of the International Society of Cerebral Blood Flow and Metabolism*, 28(5), 906-15.

Chaigneau, E. et al., 2003. Two-photon imaging of capillary blood flow in olfactory bulb glomeruli. *Proceedings of the National Academy of Sciences of the United States of America*, 100(22), 13081-6.

Chaigneau, E. et al., 2007. The relationship between blood flow and neuronal activity in the rodent olfactory bulb. *J Neurosci*, 27(24), 6452-60.

Chih, C.P., Lipton, P. & Roberts, E.L., 2001. Do active cerebral neurons really use lactate rather than glucose? *Trends in Neurosciences*, 24(10), 573-8.

Chih, C.P. & Roberts Jr, E.L., 2003. Energy substrates for neurons during neural activity: a critical review of the astrocyte-neuron lactate shuttle hypothesis. *J Cereb Blood Flow Metab*, 23(11), 1263-81.

Clark, L.C., Misrahy, G. & Fox, R.P., 1958. Chronically implanted polarographic electrodes. *Journal of applied physiology*, 13(1), 85-91.

Clark, L.C. et al., 1953. Continuous recording of blood oxygen tensions by polarography. *Journal of applied physiology*, 6(3), 189-93.

Cleland, T.A. et al., 2007. Relational representation in the olfactory system. *Proceedings of the National Academy of Sciences of the United States of America*, 104(6), 1953-8.

Climent, V., Coles, B.A. & Compton, R.G., 2001. Laser induced current transients applied to a Au(111) single crystal electrode. A general method for the measurement of potentials of zero charge of solid electrodes. *Journal of Physical Chemistry B*, 105(43), 10669-10673.

Coopersmith, R. & Leon, M., 1987. Glycogen phosphorylase activity in the olfactory bulb of the young rat. *The Journal of Comparative Neurology*, 261(1), 148-54.

Coopersmith, R. & Leon, M., 1995. Olfactory bulb glycogen metabolism: noradrenergic modulation in the young rat. *Brain Research*, 674(2), 230-237.

Craigie, E.H., 1920. On the relative vascularity of various parts of the central nervous system of the albino rat. *The Journal of Comparative Neurology*, 31(5), 429-464.

Cruz, N.F. & Dienel, G.A., 2002. High glycogen levels in brains of rats with minimal environmental stimuli: implications for metabolic contributions of working astrocytes. *Journal of Cerebral Blood Flow and Metabolism: Official Journal of the International Society of Cerebral Blood Flow and Metabolism*, 22(12), 1476-89.

Dalsgaard, M.K., 2005. Fuelling cerebral activity in exercising man. *J Cereb Blood Flow Metab*, 26(6), 731-750.

Davies, P.W. & Bronk, D.W., 1957. Oxygen tension in mammalian brain. *Federation proceedings*, 16(3), 689-92.

Davis, T.L. et al., 1998. Calibrated functional MRI: mapping the dynamics of oxidative metabolism. *Proceedings of the National Academy of Sciences of the United States of America*, 95(4), 1834-9.

Denk, W., Strickler, J.H. & Webb, W.W., 1990. Two-photon laser scanning fluorescence microscopy. *Science (New York, N.Y.)*, 248(4951), 73-6.

Deschamps, T. & Cohen, L.D., 2001. Fast extraction of minimal paths in 3D images and applications to virtual endoscopy. *Medical Image Analysis*, 5(4),

281-299.

Dienel, G.A., Wang, R.Y. & Cruz, N.F., 2002. Generalized sensory stimulation of conscious rats increases labeling of oxidative pathways of glucose metabolism when the brain glucose-oxygen uptake ratio rises. *Journal of Cerebral Blood Flow and Metabolism: Official Journal of the International Society of Cerebral Blood Flow and Metabolism*, 22(12), 1490-502.

Duchamp-Viret, P., Chaput, M.A. & Duchamp, A., 1999. Odor response properties of rat olfactory receptor neurons. *Science (New York, N.Y*, 284(5423), 2171-4.

Duchamp-Viret, P., Duchamp, A. & Chaput, M.A., 2000. Peripheral odor coding in the rat and frog: quality and intensity specification. *J Neurosci*, 20(6), 2383-90.

Duling, B.R. & Berne, R.M., 1970. Longitudinal gradients in periarteriolar oxygen tension. A possible mechanism for the participation of oxygen in local regulation of blood flow. *Circulation Research*, 27(5), 669-78.

Duling, B.R., Kuschinsky, W. & Wahl, M., 1979. Measurements of the perivascular PO2 in the vicinity of the pial vessels of the cat. *Pflugers Arch*, 383(1), 29-34.

Dunn, J.F. & Swartz, H.M., 2003. In vivo electron paramagnetic resonance oximetry with particulate materials. *Methods*, 30(2), 159-166.

Dunning, H.S. & Wolff, H.G., 1937. The relative vascularity of various parts of the central and peripheral nervous system of the cat and its relation to function. *J Comp Neurol*, 67(3), 433-450.

Edvinsson, L. & Krause, D.N., 2001. *Cerebral Blood Flow and Metabolism* 2 ed., Lippincott Williams & Wilkins.

Elas, M. et al., 2003. Quantitative tumor oxymetric images from 4D electron paramagnetic resonance imaging (EPRI): methodology and comparison with blood oxygen level-dependent (BOLD) MRI. *Magnetic Resonance in Medicine: Official Journal of the Society of Magnetic Resonance in Medicine / Society of Magnetic Resonance in Medicine*, 49(4), 682-91.

Ernst, T. & Hennig, J., 1994. Observation of a fast response in functional MR. *Magnetic Resonance in Medicine: Official Journal of the Society of Magnetic Resonance in Medicine / Society of Magnetic Resonance in Medicine*, 32(1), 146-9.

Estrada, A.D. et al., 2008. Microvascular oxygen quantification using two-photon microscopy. *Optics Letters*, 33(10), 1038-40.

Feng, Z.C. et al., 1988. Depth profile of local oxygen tension and blood flow in rat cerebral cortex, white matter and hippocampus. *Brain Research*, 445(2), 280-8.

Fox, P.T. & Raichle, M.E., 1986. Focal physiological uncoupling of cerebral blood flow and oxidative metabolism during somatosensory stimulation in human subjects. *Proceedings of the National Academy of Sciences of the United States of America*, 83(4), 1140-4.

Fox, P.T. et al., 1988. Nonoxidative glucose consumption during focal physiologic neural activity. *Science (New York, N.Y.)*, 241(4864), 462-4.

Frahm, J. et al., 1996. Dynamic uncoupling and recoupling of perfusion and oxidative metabolism during focal brain activation in man. *Magnetic Resonance in Medicine: Official Journal of the Society of Magnetic Resonance in Medicine / Society of Magnetic Resonance in Medicine*, 35(2), 143-8.

Friedrich, R.W. & Korsching, S.I., 1997. Combinatorial and chemotopic odorant coding in the zebrafish olfactory bulb visualized by optical imaging. *Neuron*, 18(5), 737-52.

Frings, S., 2001. Chemoelectrical signal transduction in olfactory sensory neurons of air-breathing vertebrates. *Cell Mol Life Sci*, 58(4), 510-9.

Frostig, R.D. et al., 1990. Cortical functional architecture and local coupling between neuronal activity and the microcirculation revealed by in vivo high-resolution optical imaging of intrinsic signals. *Proceedings of the National Academy of Sciences of the United States of America*, 87(16), 6082-6.

Fujita, H. et al., 1999. Oxygen Consumption of Cerebral Cortex Fails to Increase During Continued Vibrotactile Stimulation. *J Cereb Blood Flow Metab*, 19(3), 266-271.

Gally, J.A. et al., 1990. The NO hypothesis: possible effects of a short-lived, rapidly diffusible signal in the development and function of the nervous system. *Proceedings of the National Academy of Sciences of the United States of America*, 87(9), 3547-51.

Gjedde, A. & Marrett, S., 2001. Glycolysis in neurons, not astrocytes, delays oxidative metabolism of human visual cortex during sustained checkerboard stimulation in vivo. *Journal of Cerebral Blood Flow and Metabolism: Official Journal of the International Society of Cerebral Blood Flow and Metabolism*, 21(12), 1384-92.

Golub, A.S. & Pittman, R.N., 2005. Erythrocyte-associated transients in PO2 revealed in capillaries of rat mesentery. *American Journal of Physiology. Heart and Circulatory Physiology*, 288(6), H2735-43.

Greer, C.A. et al., 1981. Topographical and laminar localization of 2-deoxyglucose uptake in rat olfactory bulb induced by electrical stimulation of olfactory nerves. *Brain research*, 217(2), 279-93.

Grinvald, A. et al., 1986. Functional architecture of cortex revealed by optical imaging of intrinsic signals. *Nature*, 324(6095), 361-364.

Gurden, H., Uchida, N. & Mainen, Z.F., 2006. Sensory-evoked intrinsic optical signals in the olfactory bulb are coupled to glutamate release and uptake. *Neuron*, 52(2), 335-45.

Guthrie, K.M. et al., 1993. Odor-induced increases in c-fos mRNA expression reveal an anatomical "unit" for odor processing in olfactory bulb. *Proceedings of*

the National Academy of Sciences of the United States of America, 90(8), 3329-33.

Hamel, E., 2006. Perivascular nerves and the regulation of cerebrovascular tone. *J Appl Physiol*, 100(3), 1059-64.

Hellums, J.D., 1977. The resistance to oxygen transport in the capillaries relative to that in the surrounding tissue. *Microvascular Research*, 13(1), 131-6.

Herscovitch, P., Markham, J. & Raichle, M.E., 1983. Brain blood flow measured with intravenous H2(15)O. I. Theory and error analysis. *Journal of Nuclear Medicine: Official Publication, Society of Nuclear Medicine*, 24(9), 782-9.

Hertz, L., Peng, L. & Dienel, G.A., 2006. Energy metabolism in astrocytes: high rate of oxidative metabolism and spatiotemporal dependence on glycolysis//glycogenolysis. *J Cereb Blood Flow Metab*, 27(2), 219-249.

Hevner, R.F., Liu, S. & Wong-Riley, M.T., 1995. A metabolic map of cytochrome oxidase in the rat brain: histochemical, densitometric and biochemical studies. *Neuroscience*, 65(2), 313-42.

Hevner, R.F. & Wong-Riley, M.T., 1989. Brain cytochrome oxidase: purification, antibody production, and immunohistochemical/histochemical correlations in the CNS. *J Neurosci*, 9(11), 3884-98.

Hinds, J.W. & McNelly, N.A., 1982. Capillaries in aging rat olfactory bulb: a quantitative light and electron microscopic analysis. *Neurobiology of Aging*, 3(3), 197-207.

Hoge, R.D. & Pike, G.B., 2001. Oxidative metabolism and the detection of neuronal activation via imaging. *Journal of Chemical Neuroanatomy*, 22(1-2), 43-52.

Hou, H. et al., 2003. Electron paramagnetic resonance assessment of brain tissue oxygen tension in anesthetized rats. *Anesthesia and Analgesia*, 96(5), 1467-72, table of contents.

Iadecola, C. & Nedergaard, M., 2007. Glial regulation of the cerebral microvasculature. *Nature Neuroscience*, 10(11), 1369-76.

Intaglietta, M., Johnson, P.C. & Winslow, R.M., 1996. Microvascular and tissue oxygen distribution. *Cardiovascular Research*, 32(4), 632-43.

Jöbsis, F.F., 1977. Noninvasive, infrared monitoring of cerebral and myocardial oxygen sufficiency and circulatory parameters. *Science (New York, N.Y.)*, 198(4323), 1264-7.

Johnson, B.A. & Leon, M., 2000. Modular representations of odorants in the glomerular layer of the rat olfactory bulb and the effects of stimulus concentration. *The Journal of Comparative Neurology*, 422(4), 496-509.

Johnson, B.A. et al., 2002. Functional mapping of the rat olfactory bulb using diverse odorants reveals modular responses to functional groups and hydrocarbon

structural features. *The Journal of comparative neurology*, 449(2), 180-94.

Johnson, B.A., Woo, C.C. & Leon, M., 1998. Spatial coding of odorant features in the glomerular layer of the rat olfactory bulb. *The Journal of comparative neurology*, 393(4), 457-71.

Jourdan, F. et al., 1980. Spatial distribution of [14C]2-deoxyglucose uptake in the olfactory bulbs of rats stimulated with two different odours. *Brain Research*, 188(1), 139-54.

Kacem, K. et al., 1998. Structural organization of the perivascular astrocyte endfeet and their relationship with the endothelial glucose transporter: a confocal microscopy study. *Glia*, 23(1), 1-10.

Kasischke, K.A. et al., 2004. Neural Activity Triggers Neuronal Oxidative Metabolism Followed by Astrocytic Glycolysis. *Science*, 305(5680), 99-103.

Kety, S.S. & Schmidt, C.F., 1945. The determination of cerebral blood flow in man by the use of nitrous oxide in low concentrations. *American Journal of Physiology*, 143(1), 53-66.

Kida, I. et al., 2002. Mapping at glomerular resolution: fMRI of rat olfactory bulb. *Magn Reson Med*, 48(3), 570-6.

Kimelberg, H.K., 2004. The role of hypotheses in current research, illustrated by hypotheses on the possible role of astrocytes in energy metabolism and cerebral blood flow: from Newton to now. *Journal of Cerebral Blood Flow and Metabolism: Official Journal of the International Society of Cerebral Blood Flow and Metabolism*, 24(11), 1235-9.

Kleinfeld, D. et al., 1998. Fluctuations and stimulus-induced changes in blood flow observed in individual capillaries in layers 2 through 4 of rat neocortex. *Proceedings of the National Academy of Sciences of the United States of America*, 95(26), 15741-6.

Kontos, H.A. et al., 1978. Responses of cerebral arteries and arterioles to acute hypotension and hypertension. *The American Journal of Physiology*, 234(4), H371-83.

Korf, J., 2006. Is brain lactate metabolized immediately after neuronal activity through the oxidative pathway? *J Cereb Blood Flow Metab*, 26(12), 1584-6.

Korol, D.L. & Brunjes, P.C., 1992. Unilateral naris closure and vascular development in the rat olfactory bulb. *Neuroscience*, 46(3), 631-41.

Krogh, A., 1919. The number and distribution of capillaries in muscles with calculations of the oxygen pressure head necessary for supplying the tissue. *J Physiol*, 52(6), 409-415.

Kurahashi, T. & Menini, A., 1997. Mechanism of odorant adaptation in the olfactory receptor cell. *Nature*, 385(6618), 725-9.

Lamkin-Kennard, K.A., Buerk, D.G. & Jaron, D., 2004. Interactions between NO

and O2 in the microcirculation: a mathematical analysis. *Microvascular Research*, 68(1), 38-50.

Lauritzen, M. & Gold, L., 2003. Brain function and neurophysiological correlates of signals used in functional neuroimaging. *The Journal of Neuroscience: The Official Journal of the Society for Neuroscience*, 23(10), 3972-80.

Leniger-Follert, E., 1977. Direct determination of local oxygen consumption of the brain cortex in vivo. *Pflugers Arch*, 372(2), 175-9.

Leniger-Follert, E., Wrabetz, W. & Lubbers, D.W., 1976. Local tissue PO2 and microflow of the brain cortex under varying arterial oxygen pressure. *Advances in experimental medicine and biology*, 75, 361-7.

Lindauer, U. et al., 2001. No evidence for early decrease in blood oxygenation in rat whisker cortex in response to functional activation. *NeuroImage*, 13(6 Pt 1), 988-1001.

Linster, C. et al., 2002. Spontaneous versus reinforced olfactory discriminations. *J Neurosci*, 22(16), 6842-5.

Liu, S. et al., 2004. Application of in vivo EPR in brain research: monitoring tissue oxygenation, blood flow, and oxidative stress. *NMR in Biomedicine*, 17(5), 327-34.

Logothetis, N.K. et al., 2001. Neurophysiological investigation of the basis of the fMRI signal. *Nature*, 412(6843), 150-7.

Lowe, G. et al., 2008. Tonic and stimulus-evoked nitric oxide production in the mouse olfactory bulb. *Neuroscience*, 153(3), 842-50.

Madsen, P.L. et al., 1995. Persistent resetting of the cerebral oxygen/glucose uptake ratio by brain activation: evidence obtained with the Kety-Schmidt technique. *Journal of Cerebral Blood Flow and Metabolism: Official Journal of the International Society of Cerebral Blood Flow and Metabolism*, 15(3), 485-91.

Madsen, P.L. & Secher, N.H., 1999. Near-infrared oximetry of the brain. *Progress in Neurobiology*, 58(6), 541-60.

Madsen, P.L. et al., 1999. Cerebral oxygen/glucose ratio is low during sensory stimulation and rises above normal during recovery: excess glucose consumption during stimulation is not accounted for by lactate efflux from or accumulation in brain tissue. *J Cereb Blood Flow Metab*, 19(4), 393-400.

Madsen, P.L. et al., 1998. Activation-Induced Resetting of Cerebral Oxygen and Glucose Uptake in the Rat. *J Cereb Blood Flow Metab*, 18(7), 742-748.

Magistretti, P.J. & Allaman, I., 2007. Glycogen: a Trojan horse for neurons. *Nat Neurosci*, 10(11), 1341-1342.

Malnic, B. et al., 1999. Combinatorial receptor codes for odors. *Cell*, 96(5), 713-23.

Malonek, D. & Grinvald, A., 1996. Interactions between electrical activity and cortical microcirculation revealed by imaging spectroscopy: implications for functional brain mapping. *Science (New York, N.Y*, 272(5261), 551-4.

Martin, C. et al., 2007. fMRI visualization of transient activations in the rat olfactory bulb using short odor stimulations. *NeuroImage*, 36(4), 1288-1293.

Masamoto, K. et al., 2007. Apparent Diffusion Time of Oxygen from Blood to Tissue in Rat Cerebral Cortex: Implication for Tissue Oxygen Dynamics during Brain Functions. *J Appl Physiol*.

McGann, J.P. et al., 2005. Odorant representations are modulated by intra- but not interglomerular presynaptic inhibition of olfactory sensory neurons. *Neuron*, 48(6), 1039-53.

Mejia-Gervacio, S. et al., 2007. Axonal speeding: shaping synaptic potentials in small neurons by the axonal membrane compartment. *Neuron*, 53(6), 843-55.

Mik, E.G. et al., 2004. Quantitative determination of localized tissue oxygen concentration in vivo by two-photon excitation phosphorescence lifetime measurements. *Journal of Applied Physiology (Bethesda, Md.: 1985)*, 97(5), 1962-9.

Miller, S., Coopersmith, R. & Leon, M., 1991. Biochemical quantitation and histochemical localization of glucose-6-phosphate dehydrogenase activity in the olfactory system of adult and aged rats. *Neurochemical Research*, 16(4), 475-481.

Mintun, M.A. et al., 1984. Brain oxygen utilization measured with O-15 radiotracers and positron emission tomography. *Journal of Nuclear Medicine: Official Publication, Society of Nuclear Medicine*, 25(2), 177-87.

Mombaerts, P. et al., 1996. Visualizing an olfactory sensory map. *Cell*, 87(4), 675-86.

Nagano, T. & Yoshimura, T., 2002. Bioimaging of nitric oxide. *Chemical reviews*, 102(4), 1235-70.

Nagao, H. et al., 2002. Grouping and representation of odorant receptors in domains of the olfactory bulb sensory map. *Microscopy Research and Technique*, 58(3), 168-75.

Nawroth, J.C. et al., 2007. An energy budget for the olfactory glomerulus. *J Neurosci*, 27(36), 9790-800.

Ndubuizu, O. & LaManna, J.C., 2007. Brain tissue oxygen concentration measurements. *Antioxidants & redox signaling*, 9(8), 1207-19.

Nilsson, B. & Siesjö, B.K., 1976. A method for determining blood flow and oxygen consumption in the rat brain. *Acta Physiologica Scandinavica*, 96(1), 72-82.

Offenhauser, N. et al., 2005. Activity-induced tissue oxygenation changes in rat cerebellar cortex: interplay of postsynaptic activation and blood flow. *The Journal of physiology*, 565(Pt 1), 279-94.

Ogawa, S. et al., 1990. Brain magnetic resonance imaging with contrast dependent on blood oxygenation. *Proceedings of the National Academy of Sciences of the United States of America*, 87(24), 9868-72.

Oheim, M. et al., 2001. Two-photon microscopy in brain tissue: parameters influencing the imaging depth. *Journal of Neuroscience Methods*, 111(1), 29-37.

Ottoson, D., 1955. Analysis of the electrical activity of the olfactory epithelium. *Acta physiologica Scandinavica*, 35(122), 1-83.

Pellegri, G. et al., 1996. Cloning, localization and induction of mouse brain glycogen synthase. *Brain Research. Molecular Brain Research*, 38(2), 191-9.

Pellerin, L. & Magistretti, P.J., 1994. Glutamate uptake into astrocytes stimulates aerobic glycolysis: a mechanism coupling neuronal activity to glucose utilization. *Proceedings of the National Academy of Sciences of the United States of America*, 91(22), 10625-9.

Pellerin, L. & Magistretti, P.J., 2004. Empiricism and rationalism: two paths toward the same goal. *Journal of Cerebral Blood Flow and Metabolism: Official Journal of the International Society of Cerebral Blood Flow and Metabolism*, 24(11), 1240-1.

Pellerin, L. & Magistretti, P.J., 2003. Food for thought: challenging the dogmas. *Journal of Cerebral Blood Flow and Metabolism: Official Journal of the International Society of Cerebral Blood Flow and Metabolism*, 23(11), 1282-6.

Pellerin, L. & Magistretti, P.J., 2004. NEUROSCIENCE: Let There Be (NADH) Light. *Science*, 305(5680), 50-52.

Petzold, G.C. et al., 2008. Coupling of neural activity to blood flow in olfactory glomeruli is mediated by astrocytic pathways. *Neuron*, 58(6), 897-910.

Phelps, C.H., 1972. Barbiturate-induced glycogen accumulation in brain. An electron microscopic study. *Brain Research*, 39(1), 225-234.

Phelps, M.E. et al., 1979. Validation of tomographic measurement of cerebral blood volume with C-11-labeled carboxyhemoglobin. *Journal of Nuclear Medicine: Official Publication, Society of Nuclear Medicine*, 20(4), 328-34.

Pierre, K. & Pellerin, L., 2005. Monocarboxylate transporters in the central nervous system: distribution, regulation and function. *Journal of Neurochemistry*, 94(1), 1-14.

Pírez, N. & Wachowiak, M., 2008. In vivo modulation of sensory input to the olfactory bulb by tonic and activity-dependent presynaptic inhibition of receptor neurons. *The Journal of Neuroscience: The Official Journal of the Society for Neuroscience*, 28(25), 6360-71.

Raichle, M.E., 1998. Behind the scenes of functional brain imaging: a historical and physiological perspective. *Proceedings of the National Academy of Sciences of the United States of America*, 95(3), 765-72.

Raichle, M.E. & Mintun, M.A., 2006. Brain work and brain imaging. *Annual review of neuroscience*, 29, 449-76.

Ressler, K.J., Sullivan, S.L. & Buck, L.B., 1993. A zonal organization of odorant receptor gene expression in the olfactory epithelium. *Cell*, 73(3), 597-609.

Reuter, D. et al., 1998. A depolarizing chloride current contributes to chemoelectrical transduction in olfactory sensory neurons in situ. *The Journal of Neuroscience: The Official Journal of the Society for Neuroscience*, 18(17), 6623-30.

Roh, H.D., Goldstick, T.K. & Linsenmeier, R.A., 1990. Spatial variation of the local tissue oxygen diffusion coefficient measured in situ in the cat retina and cornea. *Advances in Experimental Medicine and Biology*, 277, 127-36.

Rossi, D.J., Oshima, T. & Attwell, D., 2000. Glutamate release in severe brain ischaemia is mainly by reversed uptake. *Nature*, 403(6767), 316-21.

Rubin, B.D. & Katz, L.C., 1999. Optical imaging of odorant representations in the mammalian olfactory bulb. *Neuron*, 23(3), 499-511.

Sá et al., 2004. Positron flight in human tissues and its influence on PET image spatial resolution. *European Journal of Nuclear Medicine and Molecular Imaging*, 31, 44-51.

Schaefer, M.L., Finger, T.E. & Restrepo, D., 2001. Variability of position of the P2 glomerulus within a map of the mouse olfactory bulb. *The Journal of Comparative Neurology*, 436(3), 351-62.

Schafer, J.R. et al., 2005. Adaptation in the rodent olfactory bulb measured by fMRI. *Magn Reson Med*, 54(2), 443-8.

Schafer, J.R. et al., 2006. Reproducibility of odor maps by fMRI in rodents. *NeuroImage*, 31(3), 1238-46.

Schurr, A., West, C.A. & Rigor, B.M., 1988. Lactate-supported synaptic function in the rat hippocampal slice preparation. *Science (New York, N.Y.)*, 240(4857), 1326-8.

Schurr, A., 2006. Lactate: the ultimate cerebral oxidative energy substrate? *J Cereb Blood Flow Metab*, 26(1), 142-52.

Secomb, T.W. et al., 2000. Theoretical simulation of oxygen transport to brain by networks of microvessels: effects of oxygen supply and demand on tissue hypoxia. *Microcirculation*, 7(4), 237-47.

Sethian, J.A., 1999. *Level Set Methods and Fast Marching Methods: Evolving Interfaces in Computational Geometry, Fluid Mechanics, Computer Vision, and Materials Science* 2 ed., Cambridge University Press.

Sharan, M. et al., 2008. Experimental and theoretical studies of oxygen gradients in rat pial microvessels. *Journal of Cerebral Blood Flow and Metabolism: Official Journal of the International Society of Cerebral Blood Flow and Metabolism*. Available at: http://www.ncbi.nlm.nih.gov/pubmed/18506196 [Accessed August 24, 2008].

Sharp, F.R., Kauer, J.S. & Shepherd, G.M., 1977. Laminar analysis of 2-deoxyglucose uptake in olfactory bulb and olfactory cortex of rabbit and rat. *Journal of Neurophysiology*, 40(4), 800-13.

Sharp, F.R., Kauer, J.S. & Shepherd, G.M., 1975. Local sites of activity-related glucose metabolism in rat olfactory bulb during olfactory stimulation. *Brain research*, 98(3), 596-600.

Shepherd, G.M., 2003. *The Synaptic Organization of the Brain* 5 ed., Oxford University Press, USA.

Shepherd, G.M. & Charpak, S., 2008. The olfactory glomerulus: a model for neuro-glio-vascular biology. *Neuron*, 58(6), 827-9.

Sirs, J.A., 1967. The egress of oxygen from human HbO(2) in solution and in the erythrocyte. *The Journal of Physiology*, 189(3), 461-473.

Sokoloff, L., 1977. Relation between physiological function and energy metabolism in the central nervous system. *Journal of neurochemistry*, 29(1), 13-26.

Spors, H. & Grinvald, A., 2002. Spatio-temporal dynamics of odor representations in the mammalian olfactory bulb. *Neuron*, 34(2), 301-15.

Spors, H. et al., 2006. Temporal dynamics and latency patterns of receptor neuron input to the olfactory bulb. *J Neurosci*, 26(4), 1247-59.

Thompson, J.K., Peterson, M.R. & Freeman, R.D., 2005. Separate spatial scales determine neural activity-dependent changes in tissue oxygen within central visual pathways. *J Neurosci*, 25(39), 9046-58.

Thompson, J.K., Peterson, M.R. & Freeman, R.D., 2003. Single-neuron activity and tissue oxygenation in the cerebral cortex. *Science*, 299(5609), 1070-2.

Tsai, A.G., Johnson, P.C. & Intaglietta, M., 2003. Oxygen gradients in the microcirculation. *Physiological reviews*, 83(3), 933-63.

Tsoukias, N.M. et al., 2007. A computational model of oxygen delivery by hemoglobin-based oxygen carriers in three-dimensional microvascular networks. *Journal of Theoretical Biology*, 248(4), 657-74.

Vanzetta, I. & Grinvald, A., 1999. Increased cortical oxidative metabolism due to sensory stimulation: implications for functional brain imaging. *Science (New York, N.Y.)*, 286(5444), 1555-8.

Verhagen, J.V. et al., 2007. Sniffing controls an adaptive filter of sensory input to the olfactory bulb. *Nature neuroscience*, 10(5), 631-9.

Vilchez, D. et al., 2007. Mechanism suppressing glycogen synthesis in neurons and its demise in progressive myoclonus epilepsy. *Nature Neuroscience*, 10(11), 1407-13.

Viswanathan, A. & Freeman, R.D., 2007. Neurometabolic coupling in cerebral cortex reflects synaptic more than spiking activity. *Nature neuroscience*, 10(10), 1308-12.

Vovenko, E., 1999. Distribution of oxygen tension on the surface of arterioles, capillaries and venules of brain cortex and in tissue in normoxia: an experimental study on rats. *Pflügers Archiv: European Journal of Physiology*, 437(4), 617-23.

Wachowiak, M. & Shipley, M.T., 2006. Coding and synaptic processing of sensory information in the glomerular layer of the olfactory bulb. *Seminars in cell & developmental biology*, 17(4), 411-23.

Wachowiak, M. & Cohen, L.B., 2001. Representation of odorants by receptor neuron input to the mouse olfactory bulb. *Neuron*, 32(4), 723-35.

Wachowiak, M. & Cohen, L.B., 2003. Correspondence Between Odorant-Evoked Patterns of Receptor Neuron Input and Intrinsic Optical Signals in the Mouse Olfactory Bulb. *J Neurophysiol*, 89(3), 1623-1639.

Wachowiak, M. et al., 2005. Inhibition [corrected] of olfactory receptor neuron input to olfactory bulb glomeruli mediated by suppression of presynaptic calcium influx. *Journal of neurophysiology*, 94(4), 2700-12.

Wei, J. et al., 1998. Phosphorylation and inhibition of olfactory adenylyl cyclase by CaM kinase II in Neurons: a mechanism for attenuation of olfactory signals. *Neuron*, 21(3), 495-504.

Wong-Riley, M.T., 1989. Cytochrome oxidase: an endogenous metabolic marker for neuronal activity. *Trends in neurosciences*, 12(3), 94-101.

Yan, C. et al., 1995. Molecular cloning and characterization of a calmodulin-dependent phosphodiesterase enriched in olfactory sensory neurons. *Proceedings of the National Academy of Sciences of the United States of America*, 92(21), 9677-81.

Yang, X. et al., 1998. Dynamic mapping at the laminar level of odor-elicited responses in rat olfactory bulb by functional MRI. *Proceedings of the National Academy of Sciences of the United States of America*, 95(13), 7715-20.

Zipfel, W.R., Williams, R.M. & Webb, W.W., 2003. Nonlinear magic: multiphoton microscopy in the biosciences. *Nature Biotechnology*, 21(11), 1369-77.

Titre: Métabolisme cérébral et olfaction : Étude des réponses olfactives et leur consommation d'énergie dans le bulbe olfactif du rat anesthésié

Résumé: Les techniques modernes d'imagerie fonctionnelle du cerveau utilisent le métabolisme cérébral comme marqueur d'activité neuronale. En effet le cerveau dépend intimement des apports sanguins en métabolites pour son fonctionnement. Cependant les mécanismes de régulation du métabolisme sont encore mal connus. Dans cette étude nous avons utilisé le modèle du bulbe olfactif chez le rat anesthésié pour caractériser la consommation d'oxygène en réponse à une stimulation physiologique. La quantification précise de la vascularisation du bulbe olfactif a pu mettre en évidence que la couche glomérulaire, très dense en synapses, est l'une des zones les plus vascularisées du cerveau. Cette couche est aussi le lieu d'une intense consommation d'oxygène lors du traitement de l'information olfactive. Par contraste, la couche du nerf, complètement dénuée d'interactions synaptiques et très peu vascularisée, consomme peu d'oxygène. L'étude pharmacologique de ces réponses métaboliques nous a permis de montrer que le compartiment post-synaptique du glomérule est le siège de cette intense activité métabolique. Cette dernière est aussi dépendante du traitement de l'information olfactive qui est effectué à la fois dans le bulbe olfactif et à la périphérie, dans la cavité nasale. Ceci nous a permis de caractériser l'effet de l'adaptation périphérique sur la consommation d'oxygène et le traitement local de l'information olfactive. Enfin, nous avons décrit en détail l'importance des phénomènes de diffusion au niveau du réseau microvasculaire dans le rééquilibrage transitoire du taux d'oxygène local.

Mots-clés: Olfaction, métabolisme cérébral, couplage neurovasculaire, oxygène, in vivo, deux photon, imagerie, diffusion, microcirculation

Laboratoire: Laboratoire de Neurophysiologie et Nouvelles Microscopies - INSERM U603 - CNRS UMR 8154 - 45 rue des Saints Pères - 75006 Paris - France

Title: Brain metabolism and olfaction : a study on olfactory responses and their energy usage in the olfactory bulb of anesthetized rats.

Abstract: The relationship between metabolism of neuronal activity, microvascular organization and blood flow dynamics is critical for interpreting functional brain imaging. Here we used the rat dorsal olfactory bulb as a model to determine in vivo the correlation between action potential propagation, synaptic transmission, oxygen consumption and capillary density during odor stimulation. We find that capillaries are extremely dense in layers of intense synaptic interactions like the glomerular layer while it is very low in the overlying nerve layer, devoid of capillaries. In glomeruli, odor triggers a local early decrease in tissue oxygen partial pressure that results principally from dendritic activation rather than from firing of axon terminals, transmitter release or astrocyte activation. In the nerve layer, action potential propagation does not generate local changes in tissue oxygen partial pressure. We also show that under strong peripheral stimulation, i.e. high odor concentration, glomerular neuronal and metabolic responses are shaped by peripheral adaptation of olfactory sensory neurons. Eventually, we show the importance of oxygen diffusion processes from brain capillaries to neuronal tissue. We characterize how transient changes in blood flow are precisely influencing the oxygen tissue level.

Keywords: Olfaction, brain metabolism, neurovascular coupling, oxygen, in vivo, two photon, imaging, diffusion, microcirculation

Laboratory: Neurophysiology and New Microscopies Laboratory - INSERM U603 - CNRS UMR 8154 - 45 rue des Saints Pères - 75006 Paris - France